THE UNIVERSITY
of EDINBURGH

The Effect of Unicompartmental Knee Replacement Tibial Component Design on Proximal Tibial Strain and Ongoing Pain

---

A study of clinical and radiological outcomes and finite element modelling

Chloe E H Scott

MBChB BSc MSc FRCSEd (Tr&Orth)

Thesis Submitted for the Degree of Doctor of Medicine (MD)

University of Edinburgh

Abstract

Introduction:

Unicompartmental knee replacements (UKRs) are an alternative to total knee replacements (TKRs) for treating isolated medial compartment knee osteoarthritis. However, revision rates are consistently higher than for TKR and UKRs are commonly revised for "unexplained" pain, a possible cause of which is elevated proximal tibial bone strain. The influence of implant design on this strain has not been previously investigated.

Aims:

The aims of this thesis are to determine the effect of medial UKR tibial component design on proximal tibial strain and ongoing pain.

Methods:

A retrospective clinical cohort study was performed comparing patient reported outcome and implant survival of a metal backed mobile bearing UKR implant (n=289) and an all-polyethylene (AP) fixed bearing UKR implant (n=111) with minimum 5 year follow up. A method of digital radiological densitometry, the greyscale ratio b (GSRb), was developed, validated and applied to plain radiographs to measure changes in bone density over 5 years in both the metal backed (n=173) and all-polyethylene (n=72) UKR patients. A finite element model (FEM) was validated against previous mechanical testing data and was used to analyse the effect of metal backing and implant thickness on proximal tibial cancellous bone strain in fixed bearing UKR implants.

Results:

There were no significant differences in patient reported outcomes between implants throughout follow up. Ten year all cause survival was 90.2 (95%CI 86-94) for the metal backed implant and 79.9 (60.7 to 99) for the all-polyethylene. Revision for unexplained pain was significantly greater in the AP implant where revisions were performed significantly earlier. Overall, the mean GSRb reduced following medial UKR with no difference between implants. In those patients where GSRb increased, patient reported outcomes were worse with an association with ongoing pain.

A finite element model was successfully validated using acoustic emission and digital image correlation data. This model confirmed that the volume of cancellous bone exposed to compressive and tensile strains in excess of 3000 (pathological overloading) and 7000 (fracture) microstrain were higher in the AP implants, as were peak tensile and compressive strains. Varying polyethylene insert thickness did not affect these strain parameters in the metal backed implant, but varying polyethylene thickness in the AP implants had significant effects at all loads with elevated strains in thinner implants. Increasing the AP thickness to 10mm did not reduce strains to the levels found under metal backed implants, and imminent cancellous bone failure was implied when AP thickness was reduced to 6mm.

Conclusion:

UKRs with all-polyethylene tibial components are associated with greater proximal tibial strains than metal backed implants and this is exacerbated in thinner implants. The clinical consequences of this are uncertain. Medial UKR implantation does alter proximal tibial GSRb, though this is not uniform and is independent of implant type. When GSRb increases it is associated with ongoing pain.

Lay Summary of Thesis

Unicompartmental knee replacements (UKRs) are an alternative to total knee replacements (TKRs) for treating arthritis confined to the inside edge (medial compartment) of the knee. They are partial knee replacements where only one part of the knee is replaced and the remaining two compartments with no arthritis are left intact. Unfortunately, many UKRs fail due to ongoing "unexplained" pain and are revised to total knee replacements. A possible cause of "unexplained" pain is high strain in the bone underlying the implant on the tibial (shin bone) side. The influence of implant design on this strain has not been previously investigated.

Aims:

The aims of this thesis are to determine the effect of medial UKR tibial component design on proximal tibial strain and ongoing pain. The designs investigated were 1. metal backed with a polyethylene (plastic) insert as the load bearing surface and 2. All-polyethylene (made entirely from plastic).

Methods:

A clinical cohort study was performed comparing patient reported outcome and implant survival of a metal backed UKR implant (n=289) and an all-polyethylene (AP) UKR implant (n=111) with minimum 5 year follow up. A method of measuring the bone density from plain x-rays was developed – the greyscale ratio GSRb - validated and applied to plain radiographs to measure changes in bone density over 5 years in both the metal backed (n=173) and all-polyethylene (n=72) UKR patients. A computer simulation of these UKR implants cemented in bone (a finite element model) was created and validated against previous mechanical testing data and was used to analyse the effect of metal backing and implant thickness on bone strain in UKR implants.

Results:

There were no significant differences in patient reported outcomes between implants throughout follow up. Ten year survival was 90.2 (95% Confidence Interval 86-94) for the metal backed implant and 79.9 (60.7 to 99) for the all-polyethylene. Failure for unexplained pain was significantly greater in the AP implant where revision surgeries were performed significantly earlier. Overall, the mean tibial GSRb reduced following medial UKR with no difference between implants. In those patients where GSRb increased, patient reported outcomes were worse with an association with ongoing pain.

A finite element model (computer simulation model) was successfully validated using mechanical testing measurements of bone strain. This model confirmed that the volume of cancellous (internal bone) bone exposed to compressive and tensile strains in excess of 3000 (dangerous overloading) and 7000 (at risk of fracturing) microstrain were higher in the AP implants, as were peak bone strains. Varying polyethylene (plastic) insert thickness did not affect these strain parameters in the metal backed implant, but varying polyethylene thickness in the AP implants had significant effects at all loads with higher strains in thinner implants. Increasing the AP thickness to 10mm did not reduce strains to the levels found under metal backed implants, and imminent bone failure was implied when AP thickness was reduced to 6mm.

Conclusion:

UKRs with all-polyethylene tibial components are associated with greater strains in the underlying bone than metal backed implants and this is exacerbated in thinner implants. Medial UKR implantation alters tibial bone density, though this is not uniform and is independent of implant type. When bone density increases it is associated with ongoing pain.

Acknowledgements

A number of individuals from the Royal Infirmary of Edinburgh, the University of Edinburgh and Cardiff University, have been instrumental to the completion of this project.

In Edinburgh I would like to thank Mr Richard Nutton and Mr Frazer Wade for first suggesting proximal tibial strain as an issue in UKRs and for all of their help with the clinical elements of this thesis and in obtaining prostheses for mechanical testing; Dr Pankaj Pankaj for supervision and engineering advice throughout; Dr Tom McGillvray for advice on image analysis; Professor Hamish Simpson, Professor Colin Howie, and Dr Rob Wallace for the use of the Edinburgh Orthopaedic Engineering Centre; Deborah MacDonald for assistance with patient reported outcomes; and to Noel Conlisk, Ali MacLeod and Krishna Manda for help navigating ABAQUS software.

From Cardiff I would like to thank Prof Sam Evans for supervising the mechanical testing study used to validate the model here; and Dr Mark Eaton for giving up his time to help with the DIC and AE experiments.

I would like to thank the British Association for Surgery of the Knee and Joint Action, without whose financial support this work would not have been possible.

This work was made possible by Research Grants provided by Joint Action and the British Association for Surgery of the Knee

Declarations

I hereby declare that this thesis is composed entirely of my own work. Contributions and help from other members of the associated research group are acknowledged. I have not submitted this thesis in candidature for any other degree, diploma or professional qualification.

Chloe E H Scott

MBChB BSc MSc FRCSEd (Tr&Orth)

May 2016

Contents

Abstract i
Acknowledgements iii
Declarations vi
Figures and Tables xii
Figures xii
Tables xvi
1 Introduction 1
1.1 Knee Osteoarthritis Epidemiology 1
1.2 Medial Compartment Osteoarthritis Aetiology 2
1.2.1 Loading and Alignment 2
1.2.2 Tibial and Meniscal Anatomy 3
1.2.3 Kinematics and Gait 7
1.2.4 Location of Wear 9
1.3 Management of End-Stage Medial Compartment Osteoarthritis 9
1.4 Unicompartmental Knee Replacements 13
1.4.1 UKR Implant Design 13
1.4.2 UKR Kinematics 15
1.4.3 Modes of Failure and Survivorship 16
1.4.4 Pain as a Mode of Failure 17
1.5 Bone Strain and Remodelling 19
1.5.1 Measuring Bone Strain 20
1.6 Implant Biomechanics and Bone Strain 23
1.6.1 Component Material 24
1.6.2 Component Geometry 25
1.6.3 Tibial Coverage 27

1.6.4 Cement 28

1.7 Aims and Objectives 29

2 Methods 30

2.1 Clinical Outcome Study 30

2.1.1 Aims and Objectives 30

2.1.2 Patient Identification 31

2.1.3 UKR Implants 32

2.1.4 Patient Reported Outcome Measures (PROMs) 34

2.1.5 Survivorship 36

2.2 Radiological Study 37

2.2.1 Aims and Objectives 37

2.2.2 Developing a Quantitative measure of BMD 37

2.3 Statistical Analysis 46

2.4 Experimental Mechanical Testing 47

2.4.1 Aims and Objectives 47

2.4.2 Mechanical Testing Set Up 47

2.4.3 Digital Image Correlation 50

2.4.4 Acoustic Emission 51

2.4.5 Statistical Analysis 52

2.4.6 Results: DIC 52

2.4.7 Results: Acoustic Emission 53

2.5 Finite Element Model Creation and Validation 56

2.5.1 Aims and Objectives 56

2.5.2 Parts 56

2.5.3 Material Properties 60

2.5.4 Mesh 60

2.5.5 Assembly and Boundary Conditions 62
2.5.6 Loading 64
2.5.7 Data collection 65
2.6 Model Validation 66
2.6.1 Aims and Objectives 66
2.6.2 Validation Method 66
2.6.3 Validation Statistics 67
2.6.4 Model Validation: Cancellous Bone Compressive Strain 68
2.6.5 Model Validation: Cancellous Bone Tensile Strain 71
2.6.6 Model Validation: Digital Image Correlation Experimental Data 72
2.6.7 Model Validation: Acoustic Emission Experimental Data 73
2.7 Finite Element Analyses 79
2.7.1 Aims and Objectives 79
2.7.2 Altering the Loading Environment 79
2.7.3 Altering Implant Thickness 81
3 Clinical Outcomes 84
3.1 Aims and Objectives 84
3.1.1 Research Question 84
3.2 Chapter Summary 85
3.3 Introduction 86
3.4 Results 87
3.4.1 UKR Patient Identification 87
3.4.2 PROMs Study 88
3.4.3 Implant Survivorship 106
3.5 Chapter Discussion 118
4 Radiological Analysis 122

4.1 Aims and Objectives 122
4.1.1 Research Questions 122
4.2 Chapter Summary 123
4.3 Introduction 124
4.4 Results 125
4.4.1 Developing the BMD Quantitative Measure 125
4.4.2 Applying Image Analysis to the Clinical Cohort 136
4.4.3 Correlating Clinical Outcomes with Radiological Analysis 146
4.5 Chapter Discussion 154
5 Finite Element Analysis 158
5.1 Aims and Objectives 158
5.1.1 Research Questions 158
5.2 Chapter Summary 159
5.3 Introduction 161
5.4 Results 165
5.4.1 Loading Both Plateaus 165
5.4.2 Comparing All-Polyethylene and Metal-Backed Implants 172
5.4.3 Altering Implant Thickness 181
5.5 Discussion 190
6 Discussion 201
6.1 Implant Factors 201
6.2 Strain Magnification and Bone Remodelling 204
6.3 Loading 206
6.4 Conclusion 207
7 Future Work 208
7.1 Patient Factors 208

7.2 Implant Factors 208

Bibliography 211

Appendices 222

7.3 Appendix 1 - Publications 222

7.4 Appendix 2 – CAD Design Drawings 224

7.5 Appendix 3 – Published Papers 228

Figures and Tables

Figures

Chapter 1 Introduction

Figure 1.1 Medial compartment osteoarthritis. 1

Figure 1.2 Bony anatomy of the proximal tibia. 4

Figure 1.3 Tibial plateaus with menisci. 5

Figure 1.4. Sagittal plane proximal tibial anatomy. 6

Figure 1.5. Knee Kinematics. 7

Figure 1.6 . Cruciate function and femoral roll-back. 8

Figure 1.7 Frontal plane moments at the knee during gait. 9

Figure 1.8 Knee arthroplasty options. 12

Figure 1.9 All-polyethylene and metal backed designs of UKR. 14

Figure 1.10 Reasons for UKR revision - Norwegian Arthroplasty Register. 18

Figure 1.11 Proportions of UKRs and TKRs revised for pain - NZealand Registry 18

Figure 1.12 Strain gauges. 21

Figure 1.13 DIC using a speckle pattern 22

Figure 1.14 Tibial component deformation in TKR. 24

Figure 1.15 UKR designs and manufacturers. 27

Chapter 2 Methods

Figure 2.1 The Oxford (MB) and the Preservation (AP) UKRs 30

Figure 2.2 The Preservation UKR with an all-polyethylene tibial component.. 32

Figure 2.3 The Oxford UKR with a metal backed tibial component. 33

Figure 2.4 Preoperative alignment measures 40

Figure 2.5 Postoperative coronal alignment 41

Figure 2.6 Postoperative sagittal alignment 42

Figure 2.7 Delineating the ROIs 43

Figure 2.8 Preoperative radiograph analysis.. 45

Figure 2.9 Postoperative radiograph analysis.. 45

Figure 2.10 Experimental set up. 50
Figure 2.11 Mean vertical surface microstrain measured by DIC. 53
Figure 2.12 Continuous AE output graphs. 54
Figure 2.13 AE activity on a) loading to and b) unloading. 55
Figure 2.14 Drawn CAD models of the Sigma Partial UKR. 57
Figure 2.15 Cortical tibia with cut made for UKR tibial implant. 58
Figure 2.16 Cancellous tibial parts with cut surfaces for implantation 59
Figure 2.17 Creating the cement mantles for each tibial component. 59
Figure 2.18 All-polyethylene tibial component. 61
Figure 2.19 Metal backed tibial component 61
Figure 2.20 FEM with metal backed tibia. 63
Figure 2.21 FE model proximal constraint 63
Figure 2.22 Using datum planes to identify the central node. 65
Figure 2.23 Applying the load via a 6mm radius coupling constraint. 65
Figure 2.24 a) DIC vertical strain map and b) an anteromedial line of FEM nodes. 67
Figure 2.25 Mid-coronal plane contours of the entire model 69
Figure 2.26 Mid-coronal plane oblique contours: cancellous bone, medial load. 69
Figure 2.27 Compressive strain (minimum principal strain) 8mm AP and MB 70
Figure 2.28 Tensile strain (maximum principal strain) 8mm AP and MB 71
Figure 2.29 Cortical bone vertical strain: DIC Vs. predicted FEM data 72
Figure 2.30 Cortical bone strain along an anteromedial line for the MB 8mm implant 72
Figure 2.31 Scatter graphs: AE hits compared to compressive strain FE data. 75
Figure 2.32 Scatter graphs: AE hits on loading compared to tensile strain FE data 76
Figure 2.33 Axial views of the tibial plateaus 80
Figure 2.34 AP tibias of different thickness created from the original 8mm implant. 81
Figure 2.35 MB tibias of different thickness created from the original 8mm implant. 82

Chapter 3 Results: Clinical Outcomes

Figure 3.1 Patient age by UKR implant. 88
Figure 3.2 PROMs study cohort. 89
Figure 3.3 Physical component score trend over >5 years in all UKRs 92

Figure 3.4 Mental component score trend over >5 years in all UKRs 92
Figure 3.5 Scatter graph of length of follow-up and >5 year PCS..... 93
Figure 3.6 Scatter graph of length of follow-up and change in PCS. 94
Figure 3.7 OKS trend over >5 years for all UKRs. 95
Figure 3.8 OKS trend over >5 years by implant. 95
Figure 3.9 Scatter graph of length of follow-up and >5 year OKS..... 96
Figure 3.10 Scatter graph of length of follow-up and change in >5 year OKS..... 96
Figure 3.11 Changes in OKS by BMI grades for all UKRs. 98
Figure 3.12 Changes in OKS by age groups for all UKRs. 99
Figure 3.13 Trends in OKS for UKR patients with and without depression..... 100
Figure 3.14 Patient satisfaction at >5 years by UKR implant..... 101
Figure 3.15 The location of pain at 5 years by implant. 104
Figure 3.16 Expectation fulfilment at 5 years by UKR implant..... 105
Figure 3.17 The UKR survivorship cohort. 107
Figure 3.18Kaplan Meier survival curve for both UKR implants (all cause failures). 110
Figure 3.19 Kaplan-Meier survival curve for revisions due to unexplained pain..... 111
Figure 3.20 Modes of failure of UKR by implant. 114
Figure 3.21 Modes of failure of UKR by implant (percentage of revisions)..... 114
Figure 3.22 Revision components required at first revision by UKR implant. 115
Figure 3.23 Mean BMI in revised and unrevised implants (all UKRs). 116
Figure 3.24 Mean BMI in revised and unrevised Preservation UKRs..... 117
Figure 3.25 Mean age in revised and unrevised Preservation UKRs. 117

Chapter 4 Results: Radiological Analysis

Figure 4.1 The UKR image analysis cohort. 126
Figure 4.2 Modality of analysed radiographs..... 127
Figure 4.3 ROI areas at each time point by implant. 129
Figure 4.4 Histograms of each ROI preop and at 1 year 131
Figure 4.5 Histograms of GSRa and GSRb for all UKRs 133
Figure 4.6 GSRa in patients with and without qualitative sclerosis..... 134
Figure 4.7 GSRb in patients with and without qualitative sclerosis 134

Figure 4.8 Trend in GSRa and GSRb over time for all UKRs. 135
Figure 4.9 Distribution of overhang and underhang by UKR implant..... 140
Figure 4.10 Trends in a) GSRa and b) GSRb over time by UKR implant..... 141
Figure 4.11 GSRa and GSRb by sex and UKR implant..... 142
Figure 4.12 GSRa and GSRb by BMI and UKR implant..... 144
Figure 4.13 UKR implant overhang and GSRb change. 145
Figure 4.14 Change in GSRb and improvement in OKS by UKR implant 146
Figure 4.15 GSRa and GSRb in UKRs revised for pain and those not revised for pain. . 147
Figure 4.16 Mean age in painful and not painful UKRs by implant 148
Figure 4.17 Mean BMI in painful and not painful UKRs by implant..... 149
Figure 4.18 Trends in GSRa and GSRb in painful and not painful UKRs by implant. 149
Figure 4.19 Tibial component alignment in revised and unrevised UKRs by implant ... 152
Figure 4.20 Femoral component alignment in revised and unrevised UKRs 153

Chapter 5 Results: Finite Element Analysis

Figure 5.1 An acoustic signal wave form and its parameters 164
Figure 5.2 Mid-coronal plane contours, entire model, AP 8mm, medial load..... 167
Figure 5.3 Mid-coronal plane contours, entire model, MB 8mm, medial load. 168
Figure 5.4 The effect of loading the medial plateau only (MP) and both plateaus (BP).. 170
Figure 5.5 The effect of loading the medial plateau only (MP) and both plateaus (BP).. 171
Figure 5.6 Cancellous bone compressive strain shielding 172
Figure 5.7 Contours of cancellous bone outer surface for each implant..... 173
Figure 5.8 Mid-coronal oblique contours of the upper surface of cancellous bone. 174
Figure 5.9 Contours at the upper surface of cancellous bone for each 8mm implant..... 175
Figure 5.10 Cancellous bone compressive strain (minimum principal strain) 176
Figure 5.11 Cancellous bone tensile strain (maximum principal strain). 177
Figure 5.12 Medial aspect contour of the outer surface of cancellous bone..... 178
Figure 5.13 Peak compressive strain element location 179
Figure 5.14 Peak tensile strain element location. 179
Figure 5.15 Coronal plane contours showing implant deformation. 180
Figure 5.16 Sagittal plane contours showing implant deformation. 180

Figure 5.17 Cancellous elements compressive strain MB and AP 6-10mm thickness. 184
Figure 5.18 Cancellous elements tensile strain MB and AP 6-10mm thickness. 187
Figure 5.19 Axial compressive contours of the tibial upper surface. 188
Figure 5.20 Compressive contours of the upper surface of cancellous bone 189
Figure 5.21 A sigmoid curve 193

Chapter 6 Discussion

Figure 6.1 UKR tibial component bending on loading. 203

Chapter 7 Future Work

Figure 7.1 Altering the AP implant undersurface projections. 209
Figure 7.2 Altering the MB implant undersurface projections....209
Figure 7.3 Rescaling the AP implant. 210
Figure 7.4 Rescaling the MB implant. 210

Tables

Chapter 1 Introduction

Table 1.1 Contraindications to valgising osteotomy at the knee 10

Chapter 2 Methods

Table 2.1 ROI standardisation method. 43
Table 2.2 Material properties assigned to FEM parts 60
Table 2.3 Finite element model: elements. 60
Table 2.4 FEM part interactions. 62
Table 2.5 Element volume with compressive strain below defined microstrain limits....70
Table 2.6 Pearson's correlation of acoustic emission and finite element parameters. 73
Table 2.7 AE hits on loading Vs FE data: Measuring linearity....77
Table 2.8 Linear regression analyses of AE hits against FEM parameters 78

Table 2.9 Loading of both plateaus in a 60:40 medial:lateral division 80

Chapter 3 Results: Clinical Outcomes

Table 3.1 Unrevised UKR patient preoperative characteristics by implant. 87
Table 3.2. Demographics of PROMs responders and non-responders. 90
Table 3.3 Preoperative patient characteristics in the PROMs study by implant. 90
Table 3.4 Changes in postoperative PROMs by implant 93
Table 3.5 Correlations with >5year OKS..... 97
Table 3.6 Preoperative predictors of satisfaction at >5years..... 102
Table 3.7 Associations with satisfaction at >5years. 102
Table 3.8 Correlations with pain VAS at >5 years by implant. 103
Table 3.9 Preservation UKR revisions. 106
Table 3.10 Oxford UKR revisions. 108
Table 3.11 Reoperations (excluding revisions) for both UKR implants. 109
Table 3.12 Kaplan-Meier UKR implant survival up to 15 years 111
Table 3.13 Preoperative characteristics of intact and revised Oxford UKRs..... 112
Table 3.14 Preoperative characteristics of intact and revised Preservation UKRs. 112
Table 3.15 Comparison of Oxford and Preservation UKR revisions..... 113

Chapter 4 Results: Radiological Analysis

Table 4.1 Timing of radiographs (months). 125
Table 4.2 Intra and inter-observer agreement of qualitative sclerosis. 128
Table 4.3 The quantitative proxy measures of BMD 132
Table 4.4 Power analysis..... 136
Table 4.5 Characteristics of patients included and excluded for radiographic analysis. 137
Table 4.6 Baseline characteristics of radiographic analysis cohort by UKR implant. 138
Table 4.7 Postoperative UKR alignment by implant. 139
Table 4.8 Change in GSRb and OKS over time by UKR implant..... 146
Table 4.9 Preoperative variables in ultimately painful and not painful UKRs. 148
Table 4.10 Radiographic analysis parameters: revised and unrevised UKRs..... 150

Table 4.11 Tibial component implant alignment with GSR changes. 151

Chapter 5 Results: Finite Element Analysis

Table 5.1 UKR finite element model validation studies..... 162
Table 5.2 Finite Element Analyses of UKRs in the literature 162
Table 5.3 Compressive (minimum principal) strain: medial Vs both plateaus 169
Table 5.4. Tensile (maximum principal) strain: medial Vs both plateaus. 169
Table 5.5 Peak strains (compressive and tensile) for AP and MB implants 6-10mm..... 182
Table 5.6 Compressive strain parameters for both AP and MB implants 6-10mm..... 183
Table 5.7 Tensile strain parameters for both AP and MB implants 6-10mm 186
Table 5.8 Quoted polyethylene thickness and minimal polyethylene thickness..... 197

1 Introduction

1.1 Knee Osteoarthritis Epidemiology

Knee osteoarthritis (OA) is a common degenerative joint disease affecting 37% of those over 60 years of age radiographically, and 12% symptomatically (Dillon, et al., 2006). In 20-30% symptomatic knee OA is isolated to the medial compartment (Figure 1.1) (Khan, et al., 2008; Wise, et al., 2012). In a recent radiographic study of 608 patients, OA confined to the medial compartment was found in 9% of patients with an additional 13% having medial compartment OA plus some patellofemoral joint involvement (Khan, et al., 2008). The aetiology of medial compartment OA is multifactorial, but mechanical alignment, loading, and local meniscal and cartilage integrity are fundamental to its development.

Figure 1.1 Medial compartment osteoarthritis. Joint space narrowing and sclerosis are present medially with a well preserved lateral compartment and a resultant varus deformity.

1.2 Medial Compartment Osteoarthritis Aetiology

Loading of the knee joint is a function of the three-dimensional morphology of the articulating surfaces and the mechanical axis of the lower limb. The pattern of loading is therefore influenced by local knee joint anatomy and by the lower limb alignment resultant of ipsilateral hip, femur, tibia, ankle joint, and hindfoot anatomy.

1.2.1 Loading and Alignment

Anatomical axes and mechanical axes are both used to describe lower limb alignment. MRI analysis has shown that in normally aligned knees, the femoral condyles are at a mean of 83.3° to the coronal plane anatomic femoral axis, i.e. in 6.7° of valgus (Matsuda, et al., 2004). The proximal tibia has a mean medial proximal tibial angle (MPTA) of 87°, i.e. 3° of varus (Matsuda, et al., 2004). Any deformity that shifts the mechanical axis medially increases the proportion of load passing through the medial compartment. In the coronal plane this includes increased femoral offset (Weidow, et al., 2005), coxa vara, distal femoral varus, proximal tibial varus, internal tibia torsion (Weidow, et al., 2006), and hindfoot varus.

There is a clear relationship between coronal plane lower limb alignment and medial compartment knee OA development and progression. Varus alignment is associated with a 3 fold increase in the risk of progression measured by joint space narrowing (Sharma, et al., 2001). For each 1° increase in varus alignment, Khan et al (Khan, et al., 2008) found a 40% increase in the chance of having predominantly medial compartment OA and a 52% increase in the chance of having severe rather than mild/moderate disease. In normal alignment and double limb support, 60% of load is reported to pass through the medial compartment and 40% to the lateral (Haddad and Bentley, 2000; Marti, et al., 2001). Malalignment overloads one compartment relative to the other, with subsequent OA worsening the malalignment as cartilage and bone are lost.

In conjunction with lower limb alignment, body weight is a key determinant of the load across the knee. Obesity is a well-recognised risk factor for the development of knee OA (McAlindon, et al., 1996; Weidow, 2006) and its progression (Yusuf, et al., 2011). A BMI of 25-30 (overweight) is associated with a relative risk of OA progression of 2.4 (95% Confidence Interval (CI) 1.0-3.6) increasing to 2.9 (95%CI 1.7-4.1) with BMI>30 (obese) (Yusuf, et al., 2011). Becoming overweight earlier in adulthood further increases the risk of knee OA (Holliday, et al., 2011). Weight loss has been shown to increase proteoglycan content and reduce cartilage thickness losses in the medial compartment (Anandacoomarasamy, et al., 2012).

1.2.2 Tibial and Meniscal Anatomy

The proximal tibial metaphysis consists of two dense bone platforms across medial and lateral plateaus supported peripherally by relatively thin cortical bone and inferiorly by cancellous bone trabeculae (Figure 1.2) (Reilly, et al., 1982). The medial platform is excised for insertion of a medial UKR, and both are excised for total knee replacement (TKR). The tibial implant is therefore supported by cortical rim and trabecular bone, the strength of which reduces as the resection depth increases (Hvid, 1988). The rim of cortex thickens distally as the metaphyseal flare narrows into the diaphysis. Tibial implants are variably supported by the cortical rim dependent upon their size and the position in which they are inserted.

Figure 1.2 Bony anatomy of the proximal tibia. Coronal plane CT arthrogram image showing varus proximal tibia with dense subchondral platforms, epiphyseal scar and cortical bone thickening at the metaphyseal flare.

The proximal tibia is normally in 3° of varus (Matsuda, et al., 2004) and thus the medial plateau is subjected to a greater proportion of axial load than the lateral plateau. Wolff's Law (Wolf, 1892) states that bone remodels, altering its external and internal architecture, in response to stress and strain resulting from load. When bone is loaded deposition occurs, with absorption when not loaded. Alignment variation therefore affects local bone mineral density, cancellous bone strength and ultimately the pattern of wear.

Finite element models (FEM) of intact tibias have shown proximal tibial stresses to be maximal medially, and least anterolaterally (Completo, et al., 2009). These models also indicate that intact tibial stresses are maximal just under the joint surface and at the proximal diaphysis, corresponding to areas of increased bone density anatomically. Experimental studies have found the medial tibial condyle to be strongest in varus aligned knees (Hvid, 1988) with the highest bone mineral density (Li and Nilsson, 2000). Similarly, the amplitude of the adduction moment across the knee during gait has been found to be the

single best predictor of the medial-lateral ratio of bone mineral content (Hurwitz, et al., 1998). The distribution of bone strength also varies in the sagittal plane. The medial tibial condyle bone strength is maximal centrally, intermediate anteriorly and is weakest posteriorly, reflecting the loading of these sections of the articular surface during gait. In contrast, lateral condyle bone strength is maximal posteriorly, intermediate centrally and is weakest anteriorly (Hvid, 1988).

Medial (37.2%) and lateral (36.7%) tibial plateaus represent similar percentages of the transverse plane proximal tibia, but are of different geometries with significantly different anteroposterior dimensions (Figure 1.3 and 1.4) (Servien, et al., 2008).

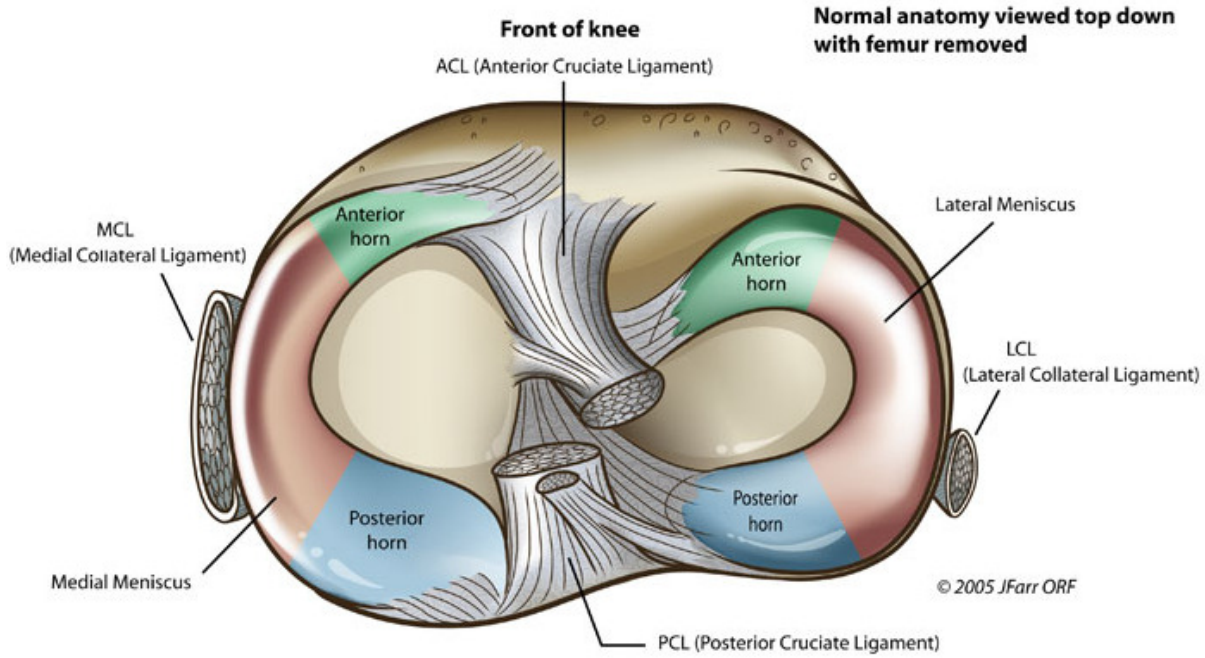

Figure 1.3 Tibial plateaus with menisci. Note the different dimensions of medial and lateral plateaus in this plane (Farr, 2005).

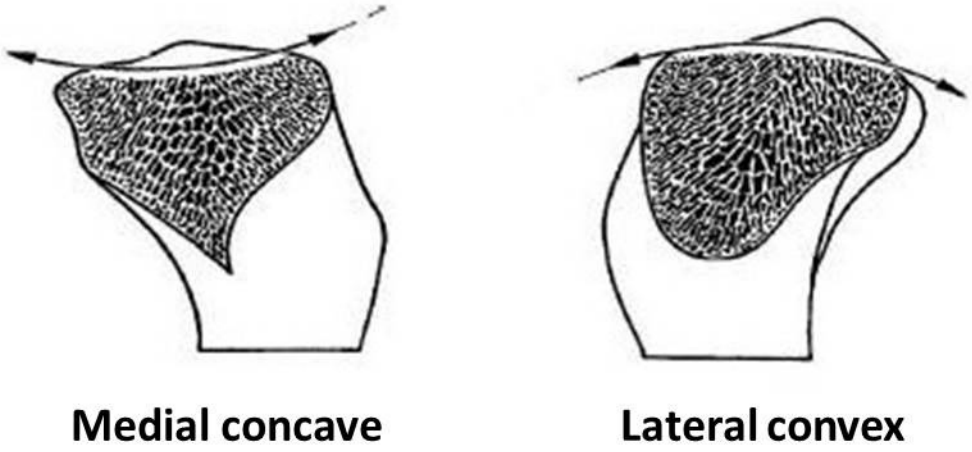

Figure 1.4. Sagittal plane proximal tibial anatomy. The medial plateau is concave and the lateral more convex. The overlying menisci help to conform these geometrically different plateaus with the articulating femoral condyles (Kapandli, 1970).

The medial meniscus functions to improve load distribution across the knee by increasing the contact area of the medial compartment from ~2cm^2 to ~6cm^2 thus reducing contact stresses (Walker and Erkman, 1975). The concavity of the medial tibial plateau is made more conforming by the medial meniscus which also contributes to the stability in an anteroposterior direction. The medial meniscus is well anchored with firm attachments to the posterior intercondylar fossa and an anterior insertion anterior to the anterior cruciate ligament (ACL) footprint. It is also anchored peripherally where it is continuous with the capsular condensation of the deep medial collateral ligament. The meniscus functions as a shock-absorber with 80% of the load across the knee passing through the menisci, ~30% through the medial meniscus (Pena, et al., 2006). Total medial menisectomy is associated with a 27-30% incidence of symptomatic radiographic degenerative changes at long term follow-up of >14years, most commonly isolated to the medial compartment (Englund and Lohmander, 2004; Jorgensen, et al., 1987). Radiographic asymptomatic OA incidence is higher still, occurring in 114/251 (45%) patients at 15-22 years following medial meniscectomy (Englund and Lohmander, 2004).

1.2.3 Kinematics and Gait

During native knee flexion, the medial femoral condyle remains relatively static in the anteroposterior direction with ~1.5mm of motion when the knee flexes (Hill, et al., 2000; Iwaki, et al., 2000; Nakagawa, et al., 2000). This is due in part to the concave plateau and in part to the conforming, stable, medial meniscus. The tibia internally rotates causing the lateral femoral condyle to posteriorly translate by up to 9-15mm on the lateral tibial plateau. This posterior translation increases with deep flexion and is demonstrated in figure 1.5 below (Iwaki, et al., 2000). As the knee extends, the reverse occurs with the "screw home" mechanism at the terminal 10° of extension. These kinematics are facilitated by the four-bar-linkage mechanism of the intact anterior (ACL) and posterior (PCL) cruciate ligaments (Figure 1.6).

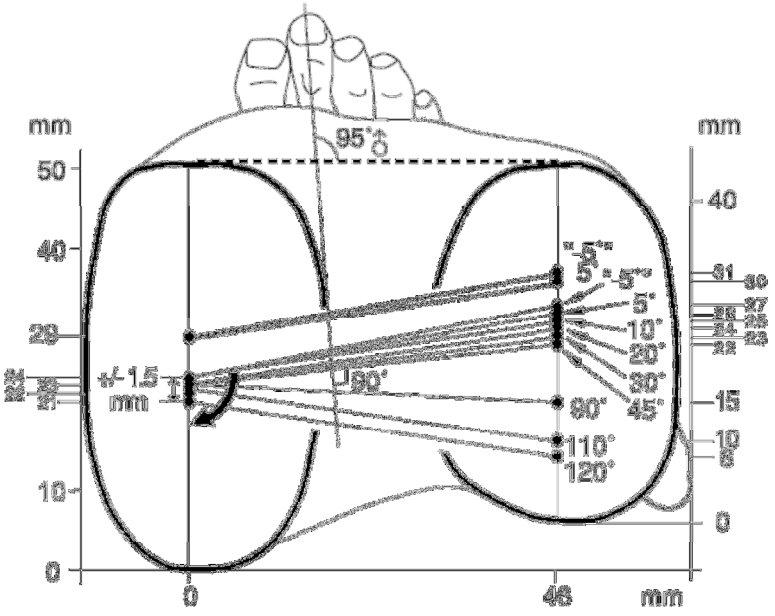

Figure 1.5. Knee Kinematics. Diagram showing the AP translation of the lateral and medial femoral condyles across the tibial plateaus during flexion. The lateral femoral condyle moves posteriorly throughout flexion as it rolls-back in addition to sliding. This does not occur on the medial side causing internal tibia rotation as the knee flexes. Reproduced from Iwaki et al (Iwaki, et al., 2000).

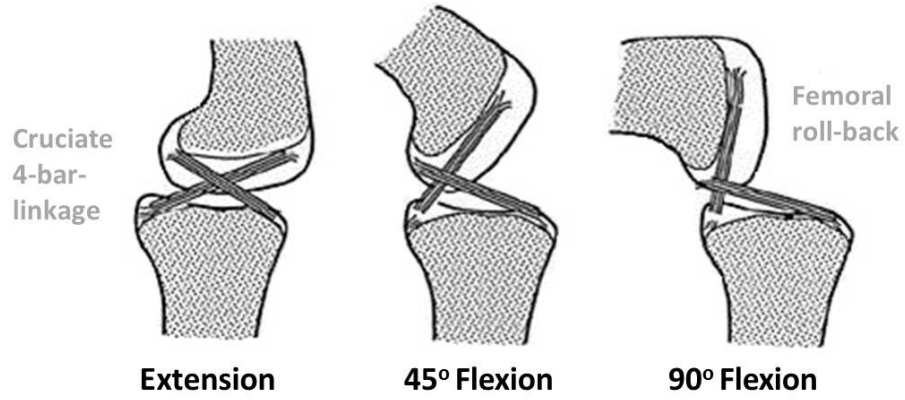

Figure 1.6 . Cruciate function and femoral roll-back. During flexion, the pair of cruciate ligaments function as a 4-bar linkage system to facilitate femoral roll-back and enable deep flexion (Burgess, 1999).

During normal gait, a varus adduction moment is present at the knee for 85% of stance (Figure 1.7). A valgus abduction moment exists for the first 10% and final 5% of stance only (Yang, et al., 2010). This stance phase adduction moment is described as the primary factor in the distribution of load to the medial compartment of the knee, which receives 70-75% of the load across the normal knee during the gait cycle (Chang, et al., 2011). While significant differences exist in gait between lateral and medial OA (Weidow, et al., 2006), medial OA is primarily a disease of gait, particularly heel strike, whereas lateral OA is a disease of high flexion activities such as squatting. The patterns of wear appear to confirm this.

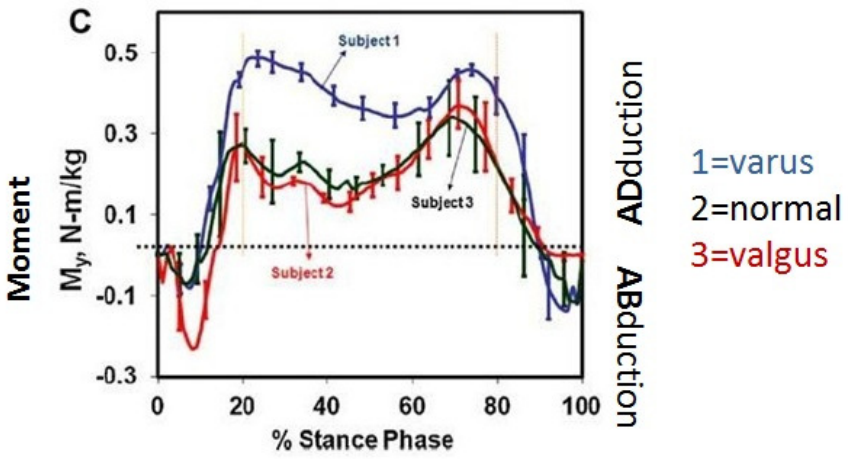

Figure 1.7 Frontal plane moments at the knee during gait. In individuals with varus, normal and valgus lower limb alignment. An adduction moment predominates for 90% of the stance phase even in valgus aligned individuals. Taken from Yang et al (Yang, et al., 2010).

1.2.4 Location of Wear

Studies (Gulati, et al., 2009; Harman, et al., 1998; Weidow, 2006) have consistently shown medial compartment wear to be central and anterior on both tibia and femur. Absence of the anterior cruciate ligament (ACL) alters this pattern of medial wear, translating tibial wear posteriorly (Harman, et al., 1998). Lesions of the medial compartment engage maximally in 11° of flexion and subtend a 25° arc, compared to lateral compartment lesions maximal at 40° of flexion subtending a 65° arc (Gulati, et al., 2009). This supports the concept of medial OA as a disease of extension and lateral OA as a disease of flexion.

1.3 Management of End-Stage Medial Compartment Osteoarthritis

When conservative management of established symptomatic medial compartment OA has failed, surgical options include realignment osteotomy, unicompartmental knee replacement (UKR) or total knee replacement (TKR).

Lateralising the mechanical axis of the lower limb to off-load the medial compartment can provide symptomatic relief in medial OA and curtail disease progression in some patients. To achieve the best possible correction and to avoid secondary deformities and joint line obliquity, the correction should be performed at the level of the deformity (Gugenheim and Brinker, 2003). As the deformity is most commonly located in the tibia, realignment is most commonly achieved via a proximal (high) tibial osteotomy (HTO – medial opening wedge or lateral closing wedge), though a distal femoral osteotomy (DFO – lateral closing wedge, medial opening wedge) can be used in rare cases of femorally based deformities. Physiologically young patients with isolated medial compartment OA and a desire to continue to participate in high-impact activities or manual work are candidates for realignment. It is a stop-gap to total knee replacement, not a long-term alternative, and patient expectations must be managed as such (Gardiner, et al., 2010). Table 1.1 lists absolute and relative contraindications to valgising realignment osteotomy at the knee.

Table 1.1 Contraindications to valgising osteotomy at the knee (Gardiner, et al., 2010). FFD = fixed flexion deformity.

ABSOLUTE CONTRAINDICATIONS	***RELATIVE CONTRAINDICATIONS***
Inflammatory arthropathy	*Large deformity >20° (coronal instability)*
Lateral compartment degeneration	*Previous lateral menisectomy*
Symptomatic PFJ degeneration	*AP instability*
FFD >20°	*Medial femoral condyle osteonecrosis*
Flexion <90°	*Excessive bone loss*
>1cm subluxation	
Coronal instability	

When realignment is not appropriate, or is contraindicated (Table 1.1), arthroplasty options must be considered (Figure 1.8). Total knee replacement (TKR) is a proven procedure that is cost-effective and successful in improving pain and function in OA (Scott, et al., 2010). Condylar resurfacing implants were introduced in 1976 (Insall, et al., 1976; Insall, et al., 1979) and numerous biomechanical, kinematic (Churchill, et al., 1998; Hill, et al., 2000; Hollister, et al., 1993; Howell, et al., 2010; Iwaki, et al., 2000; Nakagawa, et al., 2000) and finite element studies (Bartel, et al., 1986; Bartel, et al., 1982; Conlisk, et al., 2015; Reilly,

et al., 1982) have informed modern TKR prosthesis design since. The incidence of serious complications in TKR is low and National Joint Registries demonstrate 10 year revision rates of <5% in a number of implants (NJR, 2012; Norwegian, 2010; Swedish, 2011; Zealand, 2010). However, up to 20% of patients are not satisfied with their TKR (Scott, et al., 2010) and this is in part due to on-going pain and functional impairment (Baker, et al., 2007), in addition to psychosocial issues and a failure of the TKR to meet some patients' expectations (Scott, et al., 2012). Real time *in vivo* fluoroscopy studies have shown that modern TKRs do not restore normal knee kinematics (Catani, et al., 2010; D'Lima, et al., 2011). This is due in large part to the excision of the ACL in TKR and the defunctioning of the four-bar-linkage cruciate mechanism, for which even posterior stabilised TKRs do not fully compensate (Catani, et al., 2010). This failure to reproduce normal knee kinematics, even in well-balanced, well-aligned TKRs, undoubtedly contributes to difficulties performing deep flexion activities such as squatting, kneeling, and stair climbing. Studies have shown that it is these activities that are of particular importance to patients (Noble, et al., 2005) and where expectation/outcome mismatch (Scott, et al., 2012) is maximal contributing significantly to patient dissatisfaction (Scott, et al., 2010).

In the 25% of patients with isolated medial compartment OA, medial unicompartmental knee replacement (UKR) can provide an arthroplasty alternative to TKR. UKR facilitates retention of the cruciate ligaments, in fact it necessitates it. It requires less exposure and smaller incisions with less disruption to the soft-tissue envelope. UKR is thus associated with reduced peri-operative analgesic requirements and immobility and shorter length of hospital stay.

Figure 1.8 Knee arthroplasty options. Total knee replacement (TKR) or Unicompartmental knee replacement (UKR) if single compartment disease.

1.4 Unicompartmental Knee Replacements

UKRs represent 8.7% of the primary knee arthroplasties performed in England and Wales in the last 10 years (NJR, 2012). Indications include medial compartment OA in the presence of an intact ACL with a flexible varus deformity and a fixed flexion deformity of less than 15°. Inflammatory arthropathy, lateral compartment involvement and patellofemoral joint OA (if advanced or symptomatic) are contraindications. Joint registries consistently quote 10 year survivorships of ~90% across all UKR implants (NJR, 2012; Norwegian, 2010; Swedish, 2011), but only the Swedish register distinguishes between medial and lateral UKRs. It reports that 91% of UKRs implanted in Sweden from 1975-1996 were medial (Lewold, et al., 1998; Swedish, 2011) and this figure is supported by other case series (Scott, 2005). Across the orthopaedic literature, 10 year UKR survival varies considerably between implants and institutions ranging from 80-96% in published series (Argenson, et al., 2002; Bhattacharya, et al., 2012; Furnes, et al., 2007; Lewold, et al., 1998; Newman, et al., 2009; Pandit, et al., 2010; Squire, et al., 1999; Svärd and Price, 2001). Explanations offered for these differences have included patient selection and expectations, surgeon volume and operative technique, and a high revision rate secondary to perceived ease of revision to TKR. An issue as yet unresolved is that of optimal implant design and there is a paucity of biomechanical evidence to inform decisions between implants of different material or geometry.

1.4.1 UKR Implant Design

Unicompartmental knee arthroplasties are available in fixed and mobile bearing designs (Figure 1.9). While mobile bearing tibias are by necessity metal backed, fixed bearing implants are available with both all-polyethylene (UHMWPE – ultra high molecular weight polyethylene) and metal backed tibial components. All-polyethylene tibial components have the perceived advantages of reduced cost, reduced backside wear, reduced bone resection and reduced edge loading and metallosis that can occur in the presence of

instability/malalignment. Their disadvantages include a lack of modularity and increased stress/strain in the underlying cancellous bone. The perceived advantages of metal backing are the option of polyethylene exchange in infection, and reduced compressive loads at the bone-implant interface (Bartel, et al., 1982). Disadvantages include a larger bone resection or compromised thinner polyethylene associated with higher wear (Bartel, et al., 1982) and backside wear. A randomized controlled trial comparing all-polyethylene and metal backed tibias in TKRs, found no difference in 10 year survivorship (Bettinson, et al., 2009), and so for the real advantages in terms of cost, all-polyethylene tibias have gained popularity in both TKR and UKR.

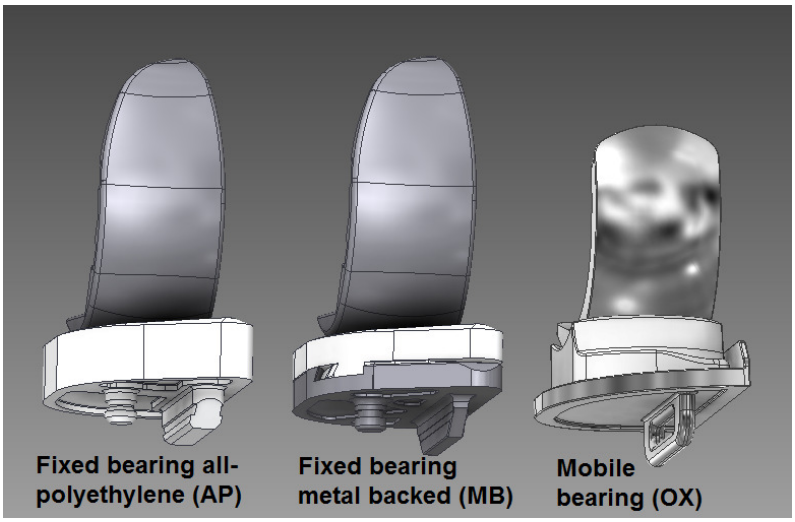

Figure 1.9 All-polyethylene and metal backed designs of UKR. Computer assisted design (CAD) models of the fixed bearing Sigma Partial UKR (DePuy) and the mobile bearing Oxford UKR (Biomet).

Mobile bearing, or meniscal bearing, devices typically have a polyethylene insert that conforms fully to the femoral component thus reducing contact stresses (Simpson, et al., 2008) and providing some AP stability. They do however, come with the risk of bearing dislocation as a mode of failure. Reducing contact stresses reduces interface shear in mobile bearing implants and thus reduces the need for undersurface projections such as pegs in addition to keels. Despite having two bearing surfaces from which to wear, *in vitro* studies have not shown increased wear rates in mobile bearing compared to fixed bearing UKRs

(Taddei, et al., 2011). This appears to be borne out clinically with low-wear rates in mobile bearing UKRs reported at 20 years (Kendrick, et al., 2011).

Clinical evidence has not proven one design to be favourable over the other. Li et al (Li, et al., 2006) performed a randomised trial on 56 knees comparing fixed and mobile bearing implants finding a lower incidence of radiolucencies in the mobile group at 2 years, but no difference in function. Whittaker et al (Whittaker, et al., 2010) retrospectively examined the midterm survivorship and functional outcome in 79 mobile bearing compared to 150 fixed bearing UKRs and report no significant differences. Similarly, data published from our own unit (Bhattacharya, et al., 2012) has failed to show significant differences in survivorship between implant types clinically. These series all contain small numbers, especially in arthroplasty terms, and it is difficult to draw firm conclusions from them.

1.4.2 UKR Kinematics

The *in vivo* kinematics of both fixed and mobile bearing UKRs have been reported by studies using 3 dimensional fluoroscopy or radiostereometric analysis (RSA) during gait (Argenson, et al., 2002; Azikuzi, et al., 2009; Li, et al., 2006). Various weight-bearing activities at different degrees of flexion have been examined, but weight-bearing kinematics have been reported most frequently in 0°, 30° and 90° of flexion to replicate that needed for the stance phase of gait (0-20°) (Nordin and Frankel, 2001) and for stair ascent and descent (0-90°) (Nordin and Frankel, 2001).

In fixed bearing UKRs, when weight-bearing in full extension, the point of contact of the femur on the tibia has been found to be at the midline in anteroposterior and medial-lateral (ML) directions (Argenson, et al., 2002; Li, et al., 2006), or just posterior to it (Azikuzi, et al., 2009). In this position, 1.5^{o} of external rotation was also found (Argenson, et al., 2002). In deep knee flexion, the medial femoral condyle has been found to translate more than in a

normal cruciate-intact knees, but less than in TKR. That is, fixed bearing UKR does not restore normal knee kinematics, but is closer to doing so than TKR.

At 30° flexion, mean posterior translations range from 2-6.7mm (Argenson, et al., 2002; Azikuzi, et al., 2009; Li, et al., 2006) with mean internal rotation of the tibia of 0.75° to 3° (Argenson, et al., 2002; Li, et al., 2006). At 90°, posterior translation is more variable with 0.8mm (Argenson, et al., 2002) and 6.4mm (Azikuzi, et al., 2009) reported whilst weight-bearing. Li et al (Li, et al., 2006) report anterior translation of 4.2mm, but this was non-weightbearing measured via RSA on plain radiographs. At 90°, mean tibial internal rotation ranges from 1.5° to 4° (Argenson, et al., 2002; Li, et al., 2006).

In mobile bearing UKRs, Li et al (Li, et al., 2006) report less than 2mm anterior or posterior translation from the midsagittal line from extension to 90° flexion. They report greater internal rotation of the tibia than in fixed bearings, rotating from neutral in extension to 4.3° at 30° flexion and 9.5° at 90°. Mobile bearing UKRs appear to be better than fixed bearing at restoring normal knee kinematics based on these *in vivo* studies.

1.4.3 Modes of Failure and Survivorship

National joint registries (NJRs) do not report medial and lateral UKRs separately, and whilst some do present data for individual implants (Swedish, 2011), they do not distinguish between all-polyethylene and metal backed options amongst fixed bearing designs. Series within the literature have reported the survivorship of metal backed and all-polyethylene implants, reporting both favourable and adverse survivorships in both designs. From the current clinical literature base, it is impossible to draw firm conclusions on many of the implants currently available.

1.4.4 Pain as a Mode of Failure

Unexplained pain is among the commonest reasons for revision of UKR across the joint registry data (Figure 1.10). The Norwegian Arthroplasty Register from 1994-2004 reported that 23.5% of revised UKRs were done so for pain alone across different implants, compared to 3.65% of TKRs over the same period ($p<0.001$) (Furnes, et al., 2007). In the Australian Joint Registry the figure is 12% (Australian, 2012) , in England and Wales 23% (Baker, et al., 2012), and in New Zealand up to 48% (Zealand, 2010). Whilst the New Zealand register does not give mutually exclusive reasons for revision, pain is its commonest reason and peaks at 2 years postoperatively when it is the mode of failure identified in 35% of UKR revisions (Zealand, 2010). The perceived ease of revision of UKRs contributes to the difference in approach to painful UKRs and painful TKRs and thus the worse reported survivorship of UKRs (Baker, et al., 2012) (Figure 1.11). It has been suggested that an increase in proximal tibial strain may be a cause of on-going pain (Simpson, et al., 2009). This relationship has not been previously investigated and the hypothesis that pain results from adaptive remodelling under the tibial component due to increased strain remains unproven.

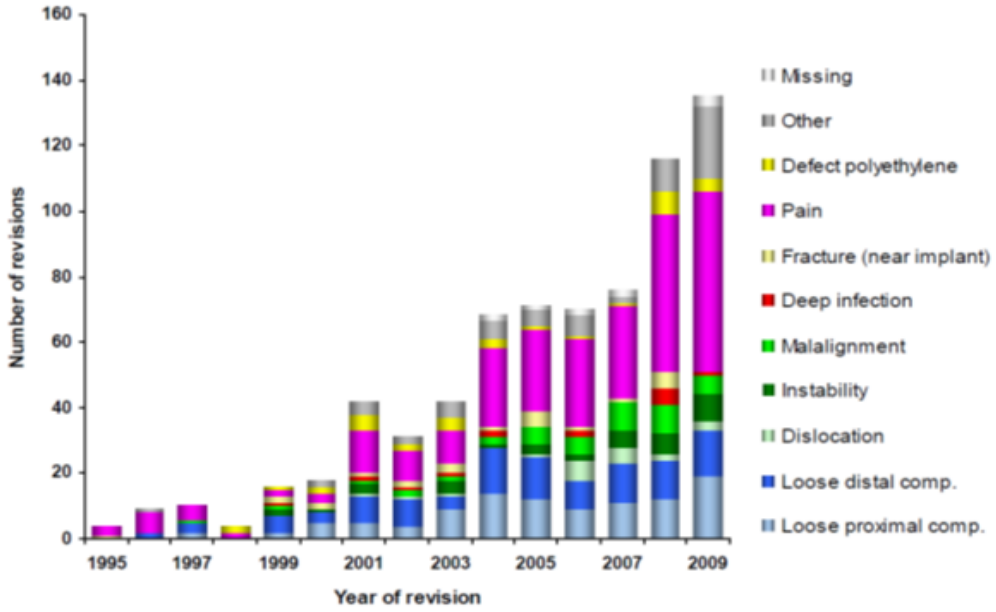

Figure 1.10 Reasons for UKR revision - Norwegian Arthroplasty Register. The mode of failure of 520 UKRs from 1994-2009 (Norwegian, 2010). Pain is the commonest mode of failure in all years.

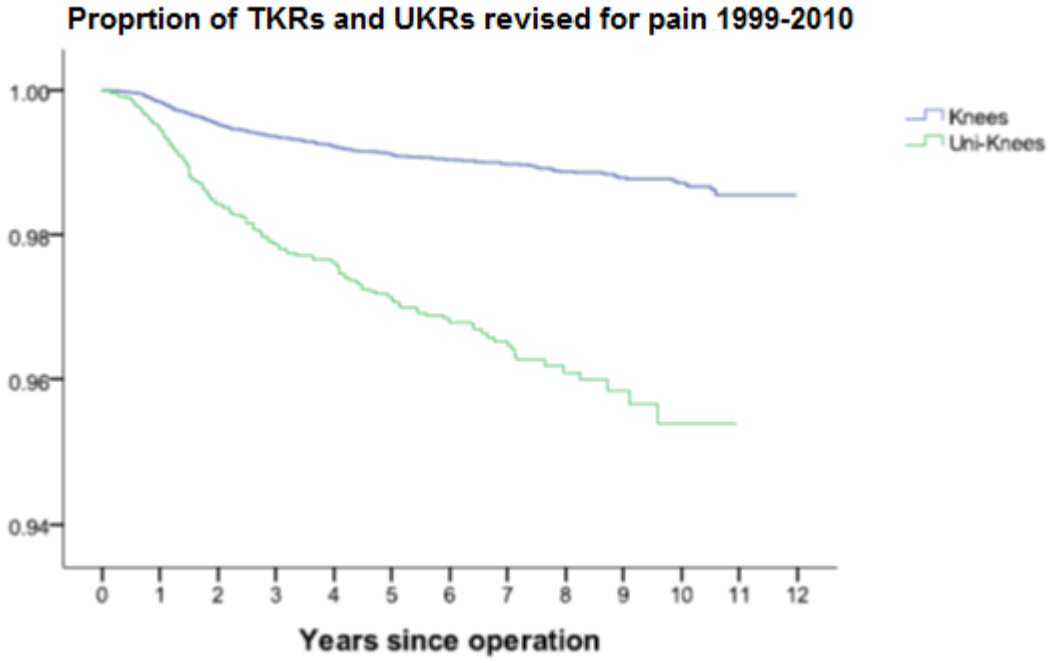

Figure 1.11 Proportions of UKRs and TKRs revised for pain - New Zealand Joint Registry. Data from 1999-2010 showing the proportions of TKRs revised for pain (blue) compared to UKRs revised for pain (green) (Zealand, 2010).

1.5 Bone Strain and Remodelling

Bone displays mechanotransduction, altering its biologic and biochemical activity in response to mechanical demand (Nicolella, et al., 2005). As per Wolff's Law (Wolf, 1892), this results in net bone formation when mechanical demands (stress and strain) are increased, and resorption when bone is unloaded or shielded. Due to their position within the microarchitecture of bone, osteocytes are thought to be the cells responsible for the reception of mechanical stimuli (Lanyon, 1993) via stress-generated fluid flow forces or bone matrix deformation itself (Nicolella, et al., 2005), mediating a remodelling response via the coordinated action of osteoblasts and osteoclasts.

For physiologic remodelling to occur, proximal tibial strain must be within a physiologic range, suggested as 50-1500με (microstrains) (Frost, 1983; Frost, 1991; Frost, 1997). Below 50με, bone is shielded and resorption takes place. Above 1500με there is a risk of microdamage within the cancellous bone microstructure with microfracture, above 3000με the pathological overloading is occurring with risk of collapse, and above 7000με cancellous bone fails (Frost, 1983; Frost, 1991; Frost, 1997). Both over- and under-loading are therefore risk factors for bone loss and subsidence of tibial implants (Lewis, et al., 1998). This physiologic window of remodelling varies with age, bone mass, and with the presence of OA. The quantity of bone tissue and collagen density increase with early OA (Ding, et al., 2001). However, the mechanical properties of osteoarthritic bone are inferior to normal bone with a reduction in Young's modulus of up to 60%, reduction in ultimate stress and in failure energy (Day, et al., 2001; Ding, et al., 2001)

Local microdamage may initiate remodelling in a number of ways. Microcracks initiating at lacunae (Burr, et al., 1996) may injure the associated osteocyte, or cause it to apoptose signalling osteoclast activity. Alternatively, it may be the sudden relief of strain as a result of microcracking that signals remodelling (Prendergast and Huiskes, 1996).

Regardless of the exact mechanism of mechanotransduction, there is no doubt that bone remodels in response to its strain environment, and that both microstructure and bone mineral content are important determinants of local strain in cortical bone (Hoc, et al., 2006). Microscopic stress risers that occur as part of the normal structure of cortical bone, concentrate subsurface microstructural strain to levels that far exceed that which is measured macroscopically on the bone surface.

1.5.1 Measuring Bone Strain

Strain is defined as change in length per unit length of a material in response to stress and is therefore unitless, and is normally expressed as a percentage. It can be measured experimentally in a number of ways: directly via strain gauges, indirectly via digital image correlation (DIC) or acoustic emission (AE), or it can be predicted using finite element modelling (FEM).

1.5.1.1 Strain Gauges

Strain gauges are conductive metal foil devices that are affixed to a surface (Figure 1.12). Electrical current is passed across the foil and any change in its length alters proportionally its resistance to electricity and is thus represented as a voltage output. Foils are sensitive to strain in one direction only, so 3 foils in different orientations are typically combined to form a rosette (Figure 1.12a) which can detect strain in 3 directions. Their output is therefore very dependent upon the orientation in which they are affixed and they measure surface strain only.

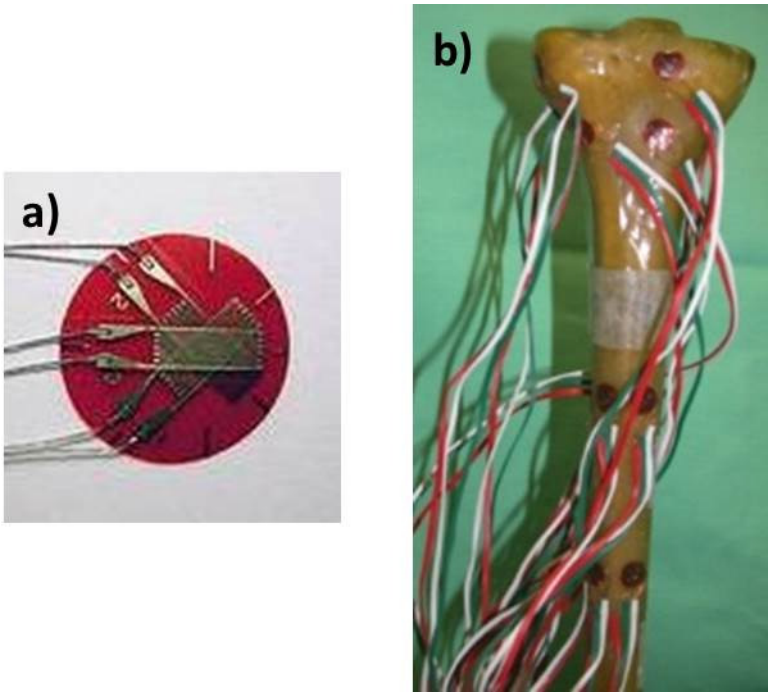

Figure 1.12 Strain gauges a) a single rosette combining 3 foils and b) as applied to a synthetic tibia.

1.5.1.2 Digital Image Correlation

Digital Image Correlation (DIC) is an optical, non-destructive, surface strain measurement technique involving applying a high-contrast speckle pattern to a sample and observing pattern deformation on loading with cameras. The displacement of pixel regions relative to surrounding regions is analysed using computer software to represent the magnitude, gradient and distribution of strain across a surface (Figure 1.13). The displacement of each speckle relative to surrounding speckles is analysed and rigid body motion is accounted for and excluded. The entire field of view is recorded, which can subsequently be divided into subsets as regions of interest or "facets" to aid analysis. If a small, well defined facet was selected, the average strain over the facet would be equivalent to that obtained from a strain gauge rosette at that location (Sztefek, et al., 2010). Surface strain can therefore be expressed as mean strain over the entire surface, or can be examined in specific regions.

DIC has been used for a number of applications within orthopaedic research to examine both cortical and cancellous bone strain at microscopic and macroscopic levels, using both cadaveric and synthetic bone models in two and three dimensions (Hoc, et al., 2006).

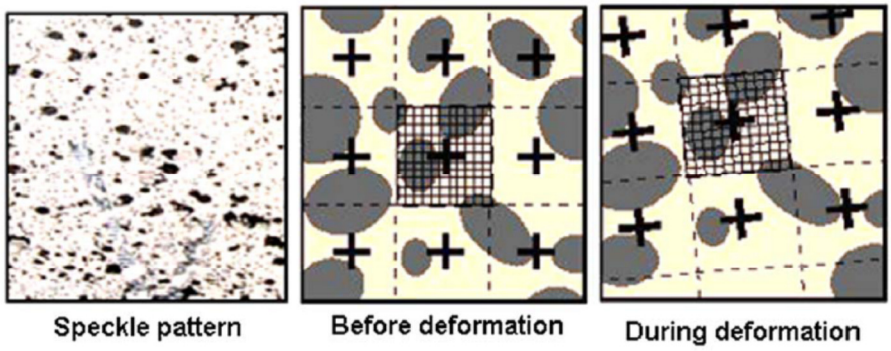

Figure 1.13 DIC using a speckle pattern. The deformation of the speckle pattern is tracked here using a facet (grid) containing a defined subset of image pixels. Taken from Sztefek (Sztefek, et al., 2010).

1.5.1.3 Acoustic Emission

Acoustic Emission (AE) is an engineering technique for measuring structural microdamage. Damage in response to stress creates elastic sound waves that conduct through material and can be detected at the material's surface by piezoelectric sensors, transforming the signal into voltage and enabling real time detection and quantification of microfracture (Hirasawa, et al., 2002; Leung, et al., 2009). It is used in a number of mechanical and structural engineering applications for the early detection of crack formation in pipelines, concrete structures, and in the aerospace industry. It has been used to investigate cortical and cancellous bone properties (Nicholls and Berg, 1981; Wells and Rawlings, 1985) including fracture healing and callus formation (Hirasawa, et al., 2002); cement fatigue crack location and propagation ; bone-cement interface integrity (Leung, et al., 2009); and hip prosthesis loosening (Mavrogordato, et al., 2011). This method was used, in conjunction with DIC, in the experimental mechanical testing of UKR implants performed by the author prior to this thesis. The resulting paper can be found in Appendix 3.

1.5.1.4 Finite Element Analysis

Finite element modelling (FEM) is a mathematical computer modelling technique used in engineering to simulate the loading of structures to predict stresses, strains and construct failure. It divides complex problems into multiple smaller problems and uses mathematical techniques to solve them. This negates the need for complex, expensive, impractical and unrepeatable mechanical testing experiments that would often be impossible to perform.

It consists of creating a model out of parts, each of which is divided into a number of smaller elements, much like three dimensional pixels. Each part, and therefore group of elements, is assigned material properties. Interactions between parts are designated and any constraints on the structure are imposed as boundary conditions. Load is then applied to the structure and the output displays patterns of stress and strain in the structure resultant of the load and the environment that you have created. The key variables in this form of analysis are therefore component geometry, material properties, boundary conditions and load application. The FE method depends upon making certain assumptions as it is often impossible to accurately model all variables in a system. Finite element models therefore require validation against experimental results to ensure that results are meaningful and representative and that the assumptions within the model are appropriate and have not voided the results.

1.6 Implant Biomechanics and Bone Strain

The transfer of load through tibial implants and resultant shielding or overload is influenced by implant material and geometry, tibial coverage and the use of cement.

1.6.1 Component Material

In total knee replacement (TKR) the material properties of tibial prostheses influence how stress is conveyed to the underlying bone. The stiffer the material, the more stress shielding occurs (Rawlinson, et al., 2008). More shielding is therefore expected under a cobalt-chrome tray (E= 210GPa) than an all-polyethylene (AP) one (E = 0.69GPa) (Abraham, et al., 2007). Conversely, the more flexible the material, the more it axially deforms with load and the greater the strain in the supporting bone (Figure 1.14). In TKR, stress shielding or overloading is further influenced by the thickness of the component, metal backing thickness, and the presence or absence of undersurface projections.

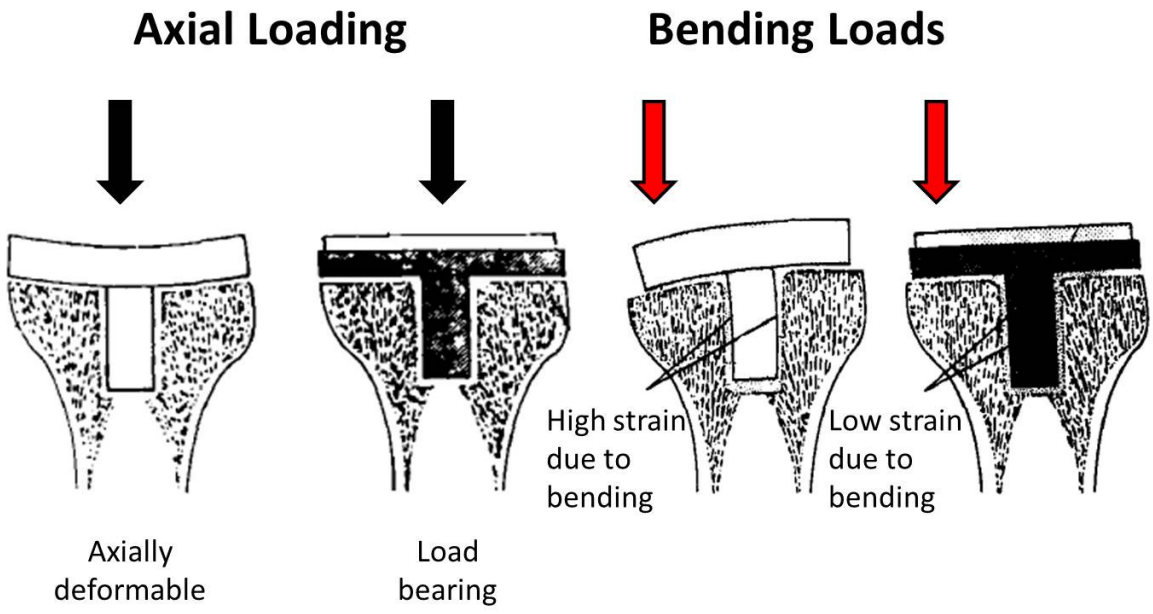

Figure 1.14 Tibial component deformation in TKR. Diagram of deformation and strain in all-polyethylene (white) and metal backed (black) TKRs (Adapted from Reilly (Reilly, et al., 1982)).

Finite element analysis of the Oxford metal backed, mobile bearing congruent tibial implant, has shown a 40% increase in proximal tibial bone strain (Simpson, et al., 2009). This

particular implant currently has the most favourable and consistent results reported in the literature. In addition to the mechanical testing study in Appendix 3 there is one further mechanical testing study of UKRs in the literature (Small, et al., 2011). Small et al 2011 used DIC with photoelastic paint to compare proximal tibial cortical strain in the Oxford metal backed mobile bearing implant with that occurring in a fixed bearing all-polyethylene implant. Surface shear strain appeared to be significantly greater in the all-polyethylene implant. Cancellous strain was not measured. As a pilot study for this thesis, both DIC and acoustic emission were used to measure strain and microdamage under all-polyethylene and metal backed UKR tibial components of fixed and mobile bearing designs in 20 composite tibias (Appendix 3). Elevated microdamage was found in the all-polyethylene implants even at low loads. Adaptive changes in the proximal tibia, both resorptive and depository, have been reported in UKRs of different designs and this may reflect changes in proximal tibial strain (Gillies, et al., 2007).

1.6.2 Component Geometry

During knee motion flexion, extension and femoral roll-back occur in the sagittal plane, and internal rotation of the tibia on the femur occurs in the transverse plane (Iwaki, et al., 2000). These movements result in forces of compression, tension, axial torque, varus/valgus moments and shear that must be resisted by knee prostheses to achieve mechanical stability. To reduce shear at the interface between the tibial component and proximal tibia, projections in the form of stems, pegs or keels/fins can be added to the under surface of tibial components. In addition to reducing shear, these projections reduce axial displacement (lift-off) which can result from varus-valgus moments (Lonner, et al., 2001). In TKR, micromotion and see-sawing at the bone/cement interface is limited by stems, thus reducing aseptic loosening (Rawlinson, et al., 2008). Micromotion is further reduced by the use of cement. The presence of any undersurface projection however, introduces additional shear forces between it and the proximal tibia (Murase, et al., 1983).

The length of undersurface projections is proportional to the amount of stress-shielding that will occur around it. Different designs of UKR tibial components include solid keels, fenestrated keels, vertical and oblique pegs (Figure 1.15). Pegs have been associated with stress shielding, though this is more localised than that occurring with stems in TKR (Au, et al., 2005). Finite element analysis in TKRs has found that the highest stresses occur when load is applied to only one plateau (Bartel, et al., 1982). It may be that in all-polyethylene UKRs, with no post, no metal backing, and different materials for medial and lateral compartments (i.e. bone and polyethylene), that strain within the cancellous bone is persistently high with resultant adaptive remodelling and pain. Conversely, unloaded bone under metal backed implants may cause a bone density reduction increasing the risk of implant subsidence (tibial migration), loosening and periprosthetic fracture.

Figure 1.15 UKR designs and manufacturers. All of these UKRs are available on the market today. Tibial design is very variable. Many are available with all-polyethylene tibias though predominantly metal backed implants are shown here.

1.6.3 Tibial Coverage

In TKR, cancellous bone stress is influenced by the presence or absence cortical rim support to the implant. Strain gauge experiments and FEM of TKR consistently report lower stress with cortical rim coverage in metal backed implants, but not in all-polyethylene tibial components (Hvid, 1988; Lonner, et al., 2001). In UKRs where the straight edge of the tibial component will never have cortical support, the strain pattern is undoubtedly less balanced underneath the surface area of the implant.

1.6.4 Cement

Cemented and uncemented implants create different boundary conditions and convey load to the proximal tibia differently. In TKR, cemented components have been found experimentally to exhibit the greatest strain shielding (Rawlinson, et al., 2008) with strain reduction 4 times that of an uncemented press fit device. Cement reduces implant micromotion, migration and subsidence when compared to press-fit uncemented implants both clinically and in FEM (Au, et al., 2005). The surface covering on uncemented implants also affects load distribution with hydroxyapatite ongrowth coating significantly reducing micromotion in RSA studies compared to porous ingrowth type implants (Au, et al., 2005).

1.7 Aims and Objectives

The aims of this thesis are to determine the effect of medial UKR tibial component design on proximal tibial strain and pain using 3 different approaches:

1. An observational clinical study of patient reported outcome measures and implant survivorship of cemented UKRs of two different designs:
    a. A mobile bearing UKR implant with a metal backed tibial component
    b. A fixed bearing UKR implant with an all-polyethylene tibial component

2. To develop a radiographic analysis tool to measure proximal tibial bone density using digital radiological densitometry and apply this to the clinical study patient cohort.

3. A Finite Element Analysis study, validated by mechanical testing, to investigate the effect of the following design variables upon proximal tibial strain in medial UKRs:
    a. Metal backing
    b. Polyethylene thickness

2 Methods

2.1 Clinical Outcome Study

2.1.1 Aims and Objectives

The aims of this study were:

1. To identify all patients who had undergone medial UKR from 1999-2007
2. To examine differences in patient reported outcome measures (PROMs) for patients treated with medial UKR of two designs (Figure 2.1):
    a. a mobile bearing metal backed implant (Oxford)
    b. a fixed bearing all-polyethylene implant (Preservation).

The primary outcome measure was the Oxford Knee Score. Secondary outcome measures included patient satisfaction and measures of pain.

Figure 2.1 The Oxford (metal backed) and the Preservation (all-polyethylene) UKRs (CAD models).

2.1.2 Patient Identification

All orthopaedic notes in our department are stored electronically and are searchable. This database was searched in March 2012 for the terms "unicompartmental knee replacement" and "unicompartmental knee arthroplasty" yielding 1051 files. These notes were examined manually to identify all patients who had undergone UKRs during the study period of 1999-2007. Patients were cross referenced with our prospectively collected department Arthroplasty Database to ensure no omissions. Medical notes and operation notes were examined for all patients who had undergone UKR and for those who had undergone revision. Data recorded included age, sex, weight (kg), Body Mass Index (BMI), indication for surgery, side of surgery, responsible Consultant, implant type and implant sizes. In those who were revised, the pre-operative mode of failure and the intra-operative findings were recorded. Contact details were recorded to facilitate postal questionnaire follow-up.

2.1.3 UKR Implants

2.1.3.1 Fixed Bearing All-Polyethylene UKR

The Preservation UKR (DePuy, Johnson and Johnson, Raynham, Massachusetts, USA) was released in 2000 and was available until 2009. It offered mobile and fixed bearing options, with the fixed bearing device available with either a metal backed or an all-polyethylene tibial component (Figure 2.2). The femoral component was cobalt-chrome, poly-radial with a single peg, and was available in 5 sizes. The all-polyethylene tibial component consisted of gamma irradiated UHMWPE (ultra-high molecular weight polyethylene) with a single non-fenestrated keel. It was non-conforming and available in 5 sizes with minimum thickness 7.5mm and was used in our unit from 2003 to 2007. It has since been replaced by the Sigma Partial UKR, which was the second most commonly implanted UKR in the NJR in 2011 (NJR, 2012).

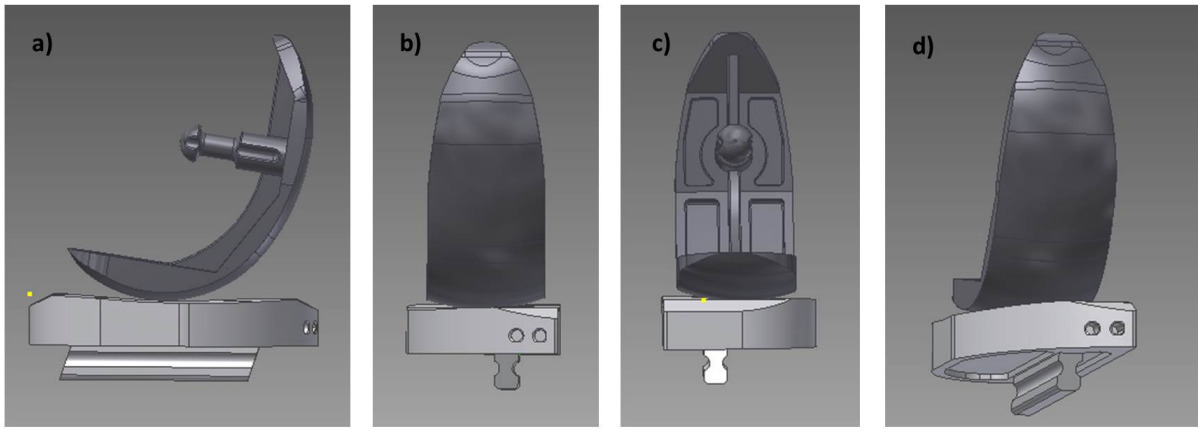

Figure 2.2 The Preservation UKR with an all-polyethylene tibial component. CAD model viewed from a) lateral b) anterior c) posterior and d) oblique aspects.

2.1.3.2 Mobile Bearing Metal-Backed UKR

The Oxford Partial Knee UKR (Figure 2.3) (Biomet, Swindon, UK) is a mobile bearing implant and is the market leader in the UK, Scandinavia and Australasia where implant usage is reported by National Joint Registries. The Phase III version of the Oxford UKR has been implanted in our unit since 1999. The Phase III femoral component has a single radius of curvature in 2 planes and comes in 4 size options with a single fixation peg. The polyethylene bearing is fully conforming to the femur and is available in 3-8mm thicknesses, with 4 and 5mm bearings being the commonest used. The tibial component is made of cobalt-chrome and has 5 size options all of which are 2.5mm thick incorporating a fenestrated keel. In the UK, 4648 Oxford Partial UKRs were implanted in 2011 constituting 68% of the UKR market (NJR, 2012).

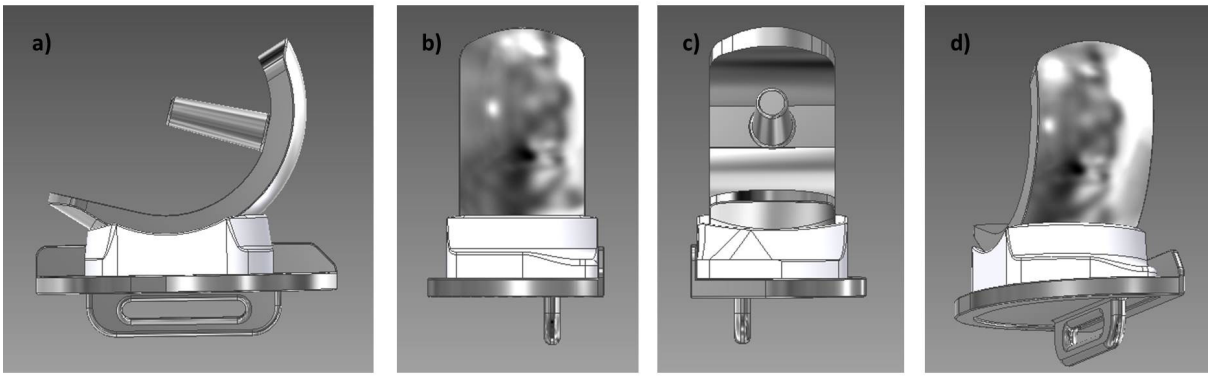

Figure 2.3 The Oxford UKR with a metal backed tibial component. CAD model viewed from a) lateral b) anterior c) posterior and d) oblique aspects.

2.1.4 Patient Reported Outcome Measures (PROMs)

Prior to surgery, a postal questionnaire was sent to all patients undergoing a medial UKR from 1999-2007. This consisted of the Short-form (SF-12) health questionnaire (Dunbar, et al., 2001) which includes physical and mental components, the Oxford Knee Score (OKS) (Dawson, et al., 2010; Murray, et al., 2007) and detailed comorbidity questions (Scott, et al., 2010). Specifically, patients were asked if they suffered from heart disease, high blood pressure, lung disease, vascular disease, neurological problems, diabetes, stomach ulcer, kidney disease, liver disease, anaemia, depression, back pain or pain in other joints. Completed questionnaires were collected at a pre-assessment clinic.

The OKS is a reliable and validated knee specific outcome measure designed to minimise the influence of comorbidities (Murray, et al., 2007). It consists of 12 questions, each with five possible answers. The OKS was originally designed to be represented as a score 12-60 with lower scores representing better knee pain and function, i.e. 12 is the best possible score, 60 the worst. Subsequently, though the questions remain the same, the score representation has been adjusted to be a score from 0-48 with higher scores representing better function. In this report, the OKS is used in its original format with 12 as the best score and 60 the worst as this was the convention at the time of data collection.

Post-operatively questionnaires were sent to patients prior to their attendance at a 12 month follow up appointment. Again, these contained the SF-12 general health score, comorbidity questions and the OKS and were collected at the clinic. Any patients who did not bring completed questionnaires to the clinic appointments were asked to complete one while waiting to be seen. All questionnaires were completed in the absence of medical and nursing staff. Collection of data was independent of the routine clinical care of the patient.

In April 2012 a similar questionnaire was sent out by post to patients who had undergone an Oxford or a Preservation UKR which was thought not to have been revised. In

addition to the SF-12 and OKS these included measures of patient satisfaction, expectation fulfilment and knee specific pain questions. To assess satisfaction, patients were asked, 'How satisfied are you with your operated knee?' with tick box answers for 'very satisfied', 'satisfied', 'unsure' or 'dissatisfied' (Scott, et al., 2010). They were also asked how well the surgery had relieved pain in the affected joint; how it had increased their ability to perform regular activities; how it enabled the performance of heavy work/sporting activity and how it met their expectations. Responses were indicated on a 6 point Likert scale as "excellently", "very well", "well", "fairly", "poorly" or "don't know".

The expectation questionnaire was based upon the validated Knee Surgery Expectation questionnaire developed by the Hospital for Special Surgery (Mancuso, et al., 2001). This was altered to reflect an arthroplasty population by removing the sports knee questions as has previously been done to assess expectation fulfilment in TKR (Scott, et al., 2012). Patients were asked how well their UKR had met their expectations of 17 parameters with fulfilment level indicated on a Likert scale as "Greatly", "a lot", "a little", 'I do not expect this' or 'this does not apply to me'. For further analysis, an expectation was deemed to have been fulfilled if it had been met "greatly" or "a lot", and was deemed to be unfulfilled if met only "a little".

To specifically assess pain following UKR, patients were asked to indicate the level of pain they experience from their knee with a visual analogue pain scale (VAS) ranging from no pain (0) to the worst pain imaginable (100). If pain was present at the knee they were asked to indicate the location of this pain by ticking as many boxes as applied from "at the front of the knee", "at the back of the knee", "on the inside edge of the knee", "on the outside edge of the knee", "at the top of the shinbone", "all over the knee" and "other". If other they were asked to specify.

2.1.5 Survivorship

In addition to PROMs, the postal questionnaire sent in April 2012 included 2 questions regarding reoperations to the knee with tick box answers of yes and no: firstly "since your initial unicompartmental knee replacement, have you had any further surgery to the same knee?"; and secondly "if 'yes', have you had the unicompartmental knee replacement revised or redone for any reason?". A third question regarding the reason for the revision followed with tick box answers of "arthritis in the rest of the knee", "pain", "infection", "worn out implant", "loose implant", "instability" and "I don't know". A free text box was available for any other comments.

Any patient giving positive responses to either of these questions and all non-responders were further investigated by examination of the medical and orthopaedic notes. Attempts were made by telephone to contact non-responders who had not been reviewed by musculoskeletal services within the preceding year. The National PACS radiographic archive was examined for all patients to identify any revision surgery that may have been undertaken elsewhere in Scotland. Deceased patients were identified via medical records and the Scottish deaths register, from which the date of death was also determined.

In patients who had undergone revision surgery, the operative note and radiographs were examined. The mode of implant failure, confirmed at revision surgery, was noted in addition to the revision implant and any requirement for stems and augments.

2.2 Radiological Study

2.2.1 Aims and Objectives

The aims of this study were:

1. To develop a quantitative method of measuring tibial bone mineral density (BMD) from plain radiographs
2. To use this method to examine changes in tibial BMD in patients treated with medial UKR of two designs:
    a. a mobile bearing metal backed implant (Oxford)
    b. a fixed bearing all-polyethylene implant (Preservation).

Secondary aims included correlating these changes with patient reported outcome measures and pain.

2.2.2 Developing a Quantitative measure of BMD

2.2.2.1 Qualitative BMD Measurement

All patients identified as having an Oxford or a Preservation UKR in situ, were included in this element of the study. The second of bilateral UKRs were excluded. Those who had subsequently undergone revision of their UKR were included prior to revision.

Preoperatively, all patients underwent short standing knee radiographs. These are anteroposterior weightbearing radiographs including both knees, the distal half of the femur and proximal half of the tibia. Lateral knee radiographs were also taken. These were performed again postoperatively and at routine follow up appointments at 1, 2 and 5 years.

Additional radiographs were taken if clinically indicated at additional appointments but were not used for the purposes of this study.

Prior to 2008, radiographs taken in our department were produced on x-ray film and were not digitised. All pre-operative radiographs were of this type and all were indexed and stored. Digital radiography was introduced in 2008 with all subsequent radiographs viewable as DICOM (Digital Imaging and Communications in Medicine) images using Kodak Carestream PACS software (Kodak Carestream, Rochester, NY, USA).

All hard copy radiographs were digitised using a UMAX Power Look 2100XL (RSA Biomedical, Umea, Sweden) flatbed scanner. Manual control settings were used in transmissive mode scanning at 256 grey scale with 300dpi with no descreen and auto-contrast. All were scanned in the correct orientation at 100% size. Only the affected knee was scanned to improve contrast. Files were stored as TIFF files to maximise resolution and enable onward analysis. This was performed for all hard copy radiographs at the 5 time points under investigation (pre-operative, immediate post-operative, and 1, 2 and 5 year follow up).

All pre-operative and 1 year radiographs were examined independently by 2 observers (CEHS and FAW) for the presence or absence of sclerosis in the medial tibial condyle. Observers were instructed to assess medial condylar sclerosis, but to disregard sclerosis occurring immediately under the articular surface, normal in osteoarthritis. Sclerosis was graded as present or absent. All images were evaluated at the same magnification (50%) using the same screen and the same ambient conditions. This was repeated by Observer 1 (CEHS) 1 month following this and was also repeated with unrestricted magnification at the time of image analysis. Observers were blinded as to the identity of the patient and in the case of the pre-operative radiographs, observers were also blinded as to the prosthesis subsequently implanted

2.2.2.2 Quantitative BMD Measurement

All patients identified as having an Oxford or a Preservation UKR in situ from the qualitative BMD study were included. All available radiographs were analysed.

All digitised radiographs and PACS system digital radiographs were exported as TIFF files. Image analysis was performed using ImageJ 1.45m, a public domain Java based scientific image processing and analysis package (Image J). Implant alignment and pixel value statistics were measured as described below.

2.2.2.2.1 Implant Alignment

Alignment was measured both preoperatively and on immediate postoperative radiographs. Where the immediate postoperative radiograph was absent, the first available postoperative radiograph was used. Femorotibial angle (FTA) was measured for both pre and postoperative radiographs. On preoperative radiographs the tibial plateau angle (TPA) and posterior tibial slope (PTS) were measured. On postoperative radiographs, tibial component alignment was measured coronally using the medial proximal tibial angle (MPTA) and sagittally using the PTS. Femoral component alignment was measured in both coronal and sagittal planes as per Sarmah et al (Sarmah, et al., 2012).

2.2.2.2.1.1 Preoperative Alignment

The local anatomical axes of the femur and tibia were determined using the method described by Khan and Bruni (Bruni, et al., 2010; Khan, et al., 2008) which is applicable to short weight-bearing knee radiographs. The femoral anatomical axis (AA) was identified by bisecting the shaft at a point approximately 10cm proximal to the joint line and at a second point at least 30mm proximal to this, joining these to a point and extending this distally to the deepest part of the intercondylar notch (Figure 2.4a). Similarly, the tibial AA was defined by bisecting the tibial shaft 10cm distal to the joint line, at a second point distal to this and joining these points to the intercondylar eminences. The FTA was defined as the angle between the two AAs at the lateral aspect (Varus >180°). The TPA was defined as the medial angle between the tibial AA and a line drawn across the tibial plateau just distal to the articular surface (Varus <90°). The PTS was measured on both pre and postoperative radiographs relative to the posterior cortex of the tibia and is represented as degrees from the perpendicular (positive posterior slope, negative anterior slope) (Figure 2.4b).

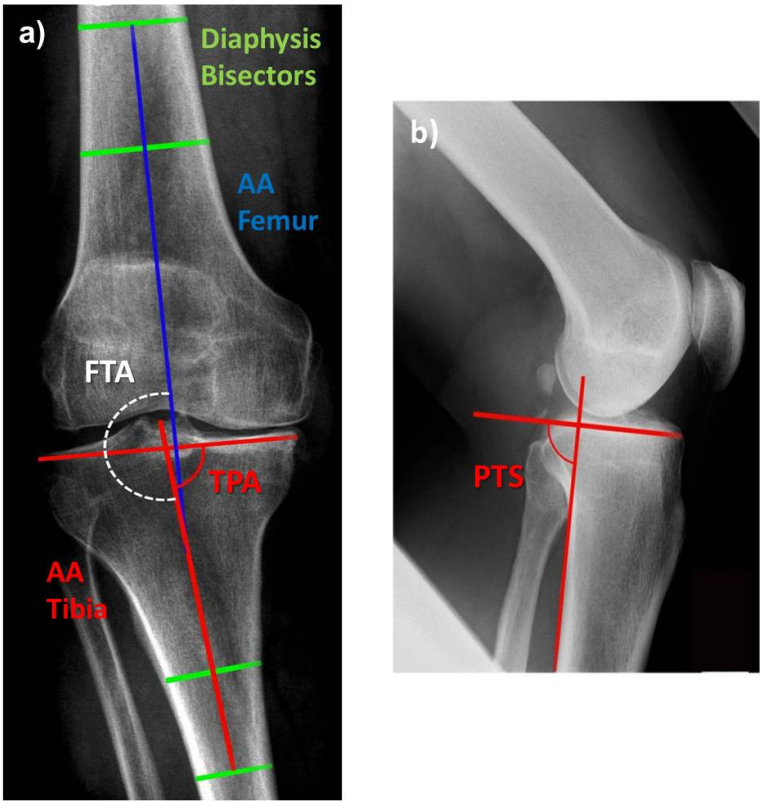

Figure 2.4 Preoperative alignment measures in a) coronal plane and b) sagittal plane.

2.2.2.2.1.2 Postoperative Alignment

On the postoperative radiographs, coronal tibial component alignment was measured as the medial proximal tibial angle (MPTA) (Varus <90°) (Figure 2.5). Femoral component alignment in this plane was measured as the angle between the femoral AA and a line perpendicular to the long axis of the implant (relative valgus <90°). This is equal to the lateral distal femoral angle (LDFA). This was done according to the method described by Sarmah et al (Sarmah, et al., 2012). PTS was measured as described above. Femoral component flexion/extension was measured relative to the posterior cortex (positive flexion, negative extension) (Figure 2.6).

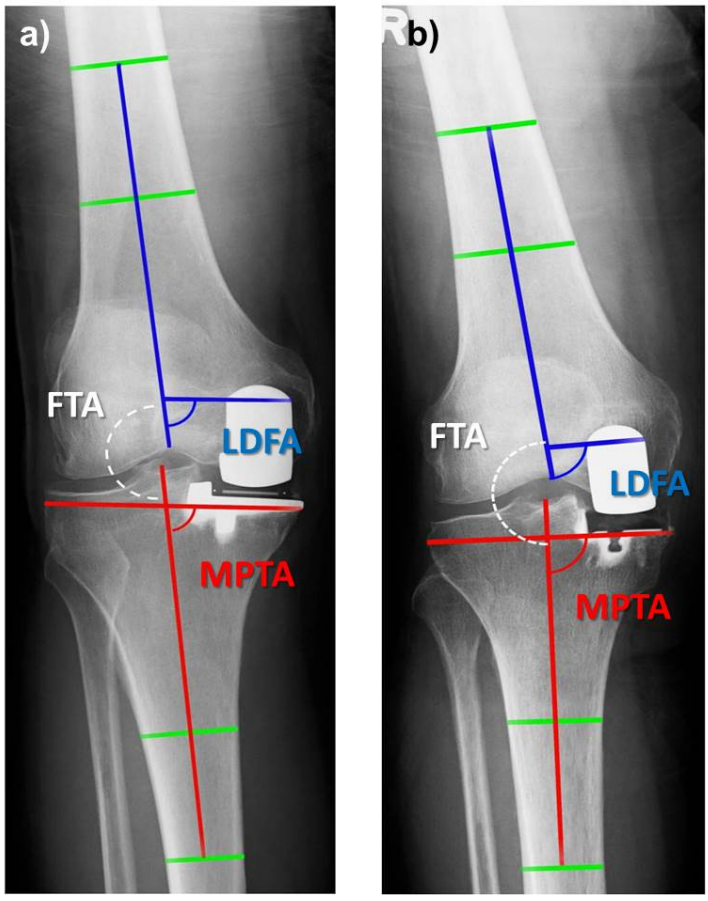

Figure 2.5 Postoperative coronal alignment of a) Oxford and b) Preservation implants. (FTA=femorotibial angle, LDFA=lateral distal femoral angle, MPTA=medial proximal tibial angle).

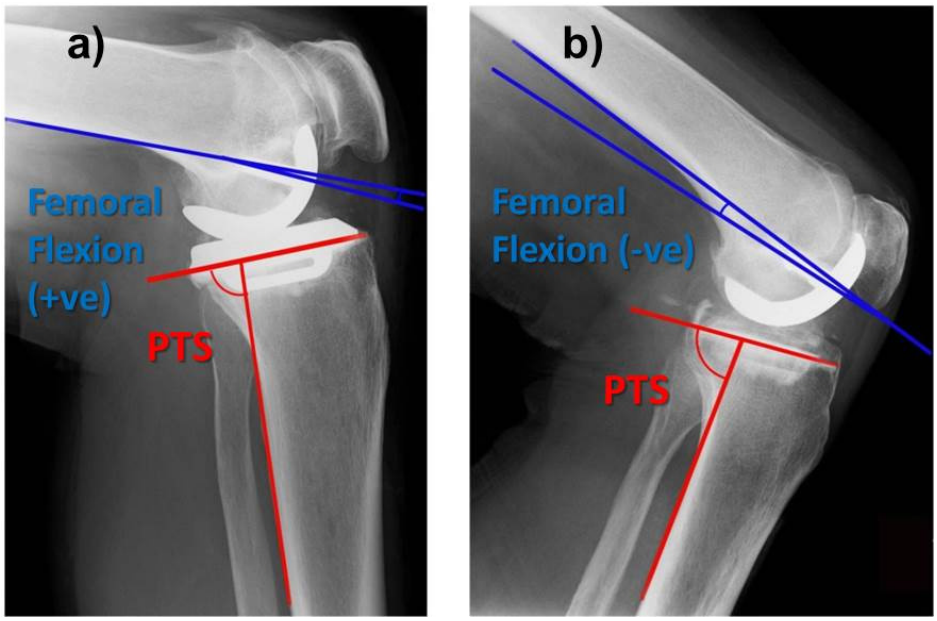

Figure 2.6 Postoperative sagittal alignment of a) Oxford and b) Preservation implants.

(PTS=posterior tibial slope, +ve=positive, -ve=negative)

2.2.2.2.2 BMD Measurement

To assess BMD, anteroposterior weight-bearing knee radiographs were examined at 5 time-points for each patient: pre-operative, immediate postoperative, and at 1, 2 and 5 years post-operatively. Regions of interest (ROIs) were defined using the anatomical axes described above and standardised measurements (Table 2.1) to create 4 ROIs: 2 medial (A1 and A2) and 2 lateral (A3 and A4) (Figure 2.7).

Table 2.1 ROI standardisation method.

Step	Figure 2.7	Description
1	a	Tibial diaphysis measured at 2 points (green lines)
2	a	Tibial anatomical axis (AA, red line) drawn by bisecting green lines
3	a	Line D1 drawn through lateral corner of implant perpendicular to AA
4	a	Vertical distance from lateral tibial spine to D1 measured as D4. This is a proxy measure of tibial resection depth and is represented as a % of D1
5	b	D4 used to transpose D1 on to a preoperative radiograph
6	b	Line D2 drawn parallel to D1 at a distance 0.5D1 to mark distal boundary
7	b	2 vertical lines (D3s) drawn where D2 intersects the cortices
8	c	4 ROIs thus created: A1, A2, A3, A4.

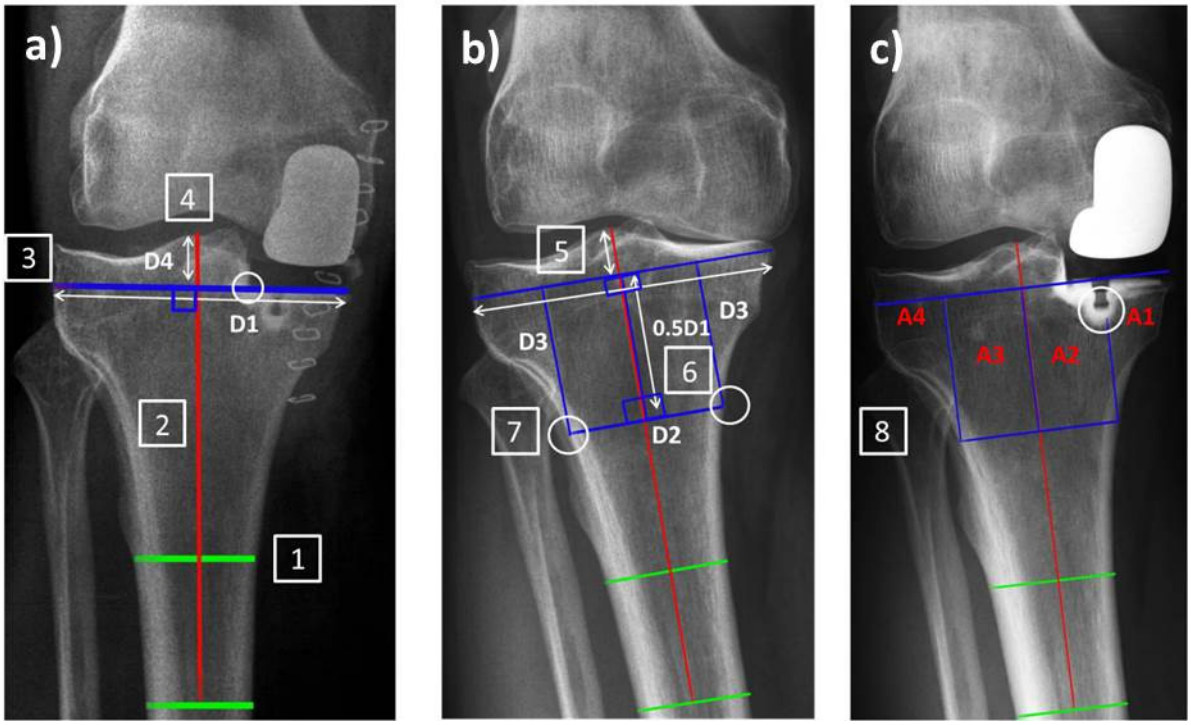

Figure 2.7 Delineating the ROIs.

Following the definition of the four ROIs A1-4, each region was analysed to obtain a quantitative measure of the greyscale within it. All radiographs were magnified to the same size (full screen) prior to analysis using Image J. The polygon function tool was used to create regional boundaries to maximise trabecular bone content and exclude artefact from

fibular head, cement, pin radiolucencies and peripheral cortical bone as per Small et al (2013) (Figure 2.8).

Image J was used to measure pixel value statistics producing a range of greyscale values from 0-255 for each pixel. Each image was calibrated such that air (black pixels) had a value of 0 and the femoral component (white pixels) a value of 255 (Small, et al., 2013). The histogram function was used to measure the number of pixels within each ROI, their mean grey scale, standard deviation, mode and range. Figures 2.8 and 2.9 show this analysis being performed. Data were collected on a pro-forma created using Formic 3.0 (Formic Solutions, Heathrow, UK) and scanned to obtain data in spreadsheet form for ongoing statistical analysis.

The ROIs were transposed to all radiographs of a given patient to ensure the same areas were measured at each time. Hence the mean measurements of density were recorded for each of the four ROIs in each patient at each follow up. To further facilitate the quantitative comparison of different radiographs taken at different times, the mean grey scale was represented as a ratio, the greyscale ratio (GSR). This compared the density of medial to lateral ROIs (GSRa, equation 1) and the most medial ROI to the remainder of the proximal tibia (GSRb, equation 2) corrected for area. All measurements were taken by a single observer (CEHS). A GSR>1 reflected a relative medial sclerosis.

Equation1:

$$GSRa = \frac{\overline{(A1}(A1pix) + \overline{A2}(A2pix))}{(A1pix + A2pix)} \Big/ \frac{\overline{(A3}(A3pix) + \overline{A4}(A4pix))}{(A3pix + A4pix)}$$

Equation 2:

$$GSRb = \overline{A1} \Big/ \frac{\overline{\overline{A2}(A2pix) + (A3}(A3pix) + \overline{A4}(A4pix))}{(A2pix + A3pix + A4pix)}$$

$$Where\ \bar{A} = mean\ greyscale\ of\ ROI \quad pix = area\ in\ pixels\ of\ ROI$$

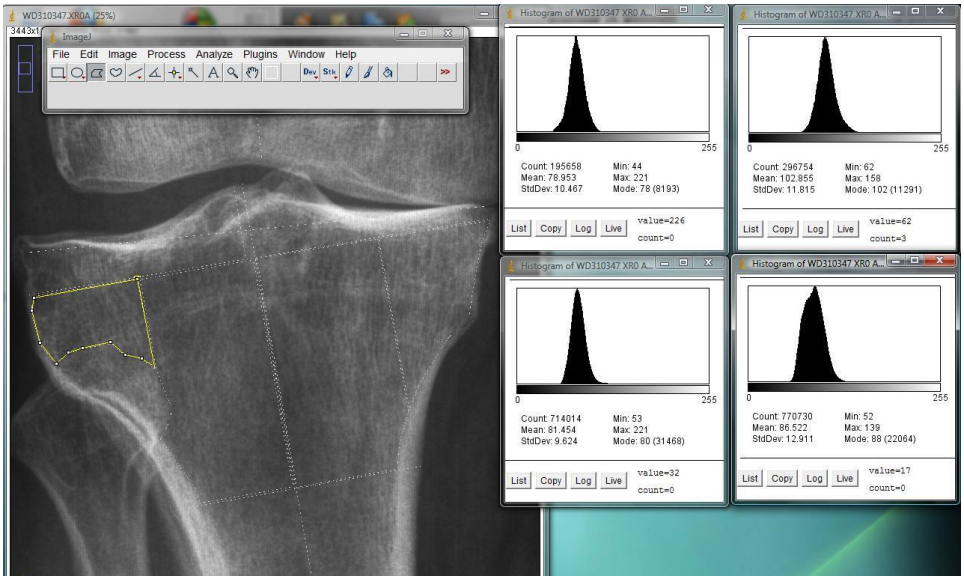

Figure 2.8 Preoperative radiograph analysis. The 4 ROIs have been delineated with exclusion of the fibular head and cortical condensations using Image J. The measurement D4 has been used to ensure the ROIs are at the same depth as in the postoperative radiograph in Figure 2.9. Adjacent histograms indicate the greyscale measures for each ROI.

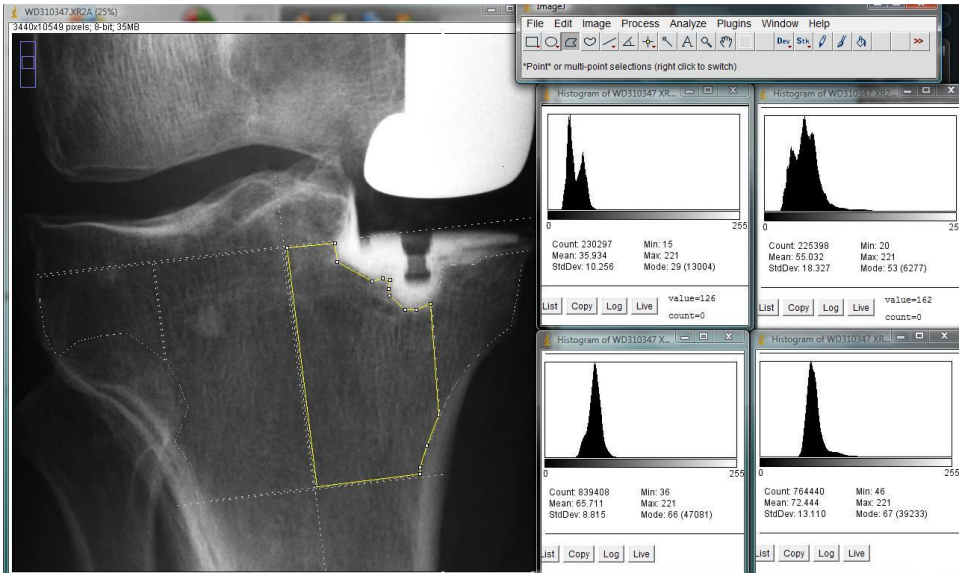

Figure 2.9 Postoperative radiograph analysis. The 4 ROIs have been delineated with exclusion of the fibular head, cortical condensations and cement. This is the same patient as figure 2.8.

2.3 Statistical Analysis

Statistical analysis was performed using Statistical Package for Social Sciences version 19.0 (SPSS Inc., Chicago, IL, USA). In patients who had undergone bilateral UKRs, PROMs and radiographic data pertaining to the second UKR was excluded to avoid bias. One way ANOVA was used to compare continuous variables with multiple groups. Parametric (unpaired T-tests, paired T-tests) and non-parametric (Mann-Whitney U, Wilcoxon rank) tests were used as appropriate to assess differences in continuous variables. Nominal categorical variables were assessed using a Chi square or Fisher's exact test. Repeated measures ANOVA was used to examine changes in parametric variables over the 5 year study period. A p value of <0.05 was considered to be statistically significant. In repeated measures analysis, post hoc analysis was performed using paired t-tests with significance set at $p<0.0125$ incorporating a Bonferroni correction to correct for multiple testing. Survival analysis was undertaken using Kaplan Meier analysis and Log Rank statistics using different endpoints. Inter and intra-observer agreement was calculated using Cohen's Kappa statistic.

2.4 Experimental Mechanical Testing

Mechanical testing was performed as part of another degree (MSc in Orthopaedic Engineering, Cardiff University) and so should not be considered as part of this degree. Details of the methodology used are included here for clarity as requested by the examiners of this MD thesis. The full published paper can be found as appendix 3.

2.4.1 Aims and Objectives

To determine the effect of medial UKR metal-backing and bearing design on proximal tibial strain in an experimental model using two techniques:

1. Digital Image Correlation (DIC) to measure cortical surface strain
2. Acoustic Emission (AE) to measure cancellous bone microdamage.

2.4.2 Mechanical Testing Set Up

Twenty 4th generation, left sided, medium composite Sawbone tibias (Pacific Research Laboratories, Vashon, Washington, USA) were obtained. These display <10% interspecimen variability with material properties and biomechanical behaviour similar to human cadaveric bone (Christofolini and Viceconti, 2000). Rigid polyurethane foam (Young's modulus E =0.155GPa) simulates cancellous bone and short fibre filled epoxy composite (E = 16.7GPa) simulates cortical bone. The medial proximal tibial angle (MPTA) measures 87^{o} with posterior tibial slope (PTS) 7^{o}.

The Sigma Partial (DePuy, Johnson & Johnson Professional Inc, Raynham, Massachusetts, USA) medial UKR in metal backed and all-polyethylene tibial designs and the Oxford Partial Knee (Biomet, Swindon, UK) were used for this part of the study. A single

size 3 Sigma Partial femur, 5x size 3 MB tibias with 5x 8mm tibial inserts and 5x size 3 8mm AP tibias were obtained, as were a single medium Oxford femoral component, with 5 size C tibias and a 4mm polyethylene bearing. Five tibias were allocated to each implant group and 5 were used as controls (TIB).

To ensure specimen uniformity, horizontal and vertical proximal tibial cuts were measured using anatomical axes and landmarks and cut without using implant specific instrumentation. Both implants define an optimal frontal plane alignment as MPTA of 90^{o} and sagittal alignment reproducing native PTS (here 7^{o}). Tibial coronal and sagittal plane anatomic axes were defined as per Paley (2002) and were drawn onto the tibias proximally. All cuts were referenced from these axes. Six millimetres of tibia were resected to restore the joint line with MPTA 90^{o} and PTS 7^{o}. The depth of the resected tibia was measured, in addition to MPTA and PTS to monitor specimen uniformity. Cut tibias were randomly assigned to receive either a mobile bearing Oxford (OX), a fixed bearing metal backed Sigma Partial (MB) or a fixed bearing all-polyethylene (AP) implant. Implant specific instrumentation was used for subsequent preparation and implants were cemented using Smart-Set High Viscosity PMMA bone cement (DePuy, Warsaw, IN, USA) with a cement mantle of 1-1.5mm. Mantle thickness was measured at 3 locations in each specimen: the anterior corner of the implant; the posterior corner; and medial line present on all tibias from manufacturing.

Femoral components were cemented onto custom designed blocks made of hard wood and steel to facilitate loading directly over the point of contact in 30^{o} of flexion. For the control tibias, the distal 30mm of a Sawbone composite femur was cut to represent a 30^{o} articulation. To simulate intervening articular cartilage and meniscus in controls, a 6mm thick piece of Sorbothane 75 durometer polyurethane (Sorbothane Inc, Kent, OH, USA) was interposed between femoral and tibial surfaces prior to loading. Sorbothane is a viscoelastic, polymeric solid with E=0.83 to 2.07MPa (cartilage E=0.31 to 1.13MPa (Korhonena, et al., 2002).

The line of loading was drawn on the femoral component assembly and was aligned with the tibial component midpoint in the sagittal plane to reproduce 30^{o} kinematics (Li, et al., 2006). In the mobile bearing implant the bearing was aligned with the centre of the tibial base plate.

Distally, coronal and sagittal mechanical axes were drawn onto tibias to aid alignment of the experimental set-up. A steel coupling cylinder was inserted vertically into the tibial plafond and the tibia was mounted on a ball bearing as a simply supported construct. When correct tibial alignment was achieved in all planes under the femoral component and loading machine, a cage was constructed around the midpoint of the tibia to restrict anterior and lateral translation and external tibial rotation on loading. The cage was not altered between specimens. Figure 2.10 shows the experimental set up.

Load was applied to the medial plateau via the corresponding femoral component. Loading was performed using a servohydraulic 5kN loading machine (Losenhausen Maschinenbau, Dusseldorf). A preload of 100N was applied to check the set-up. Loading was then undertaken in 500N increments to a maximum load of 2500N, unloading between increments to 100N. The loading rate was 5mm/minute and load data was recorded every 0.1seconds.

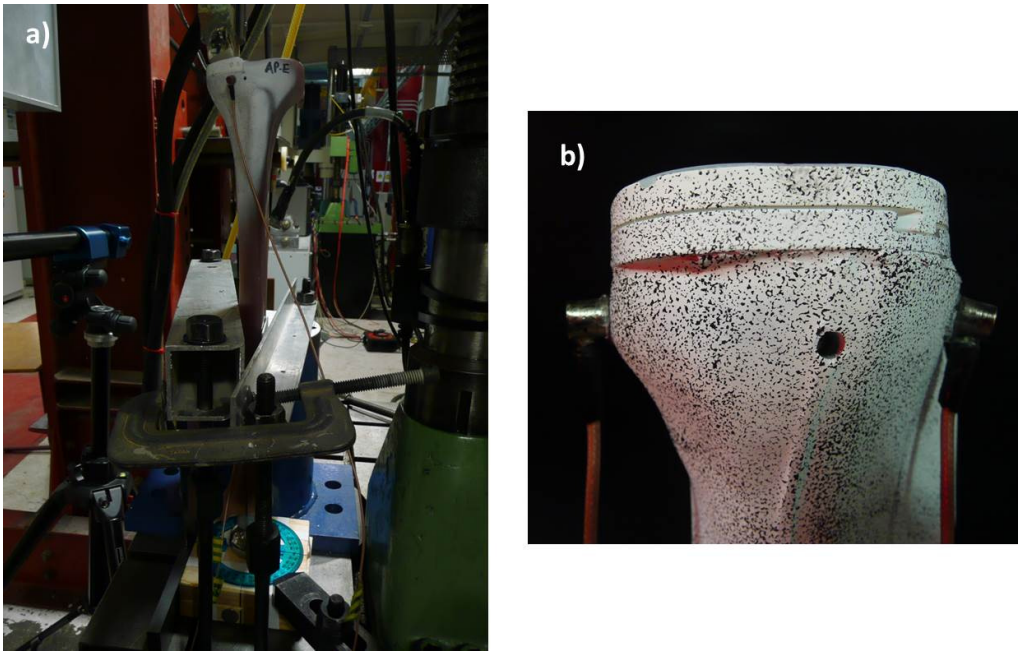

Figure 2.10 Experimental set up showing a) the tibial constraint and loading via the tensiometer and b) the preparation of the proximal tibias with UKR implanted and AE piezoelectric sensors affixed anteriorly and posteriorly with a speckle covering for DIC.

2.4.3 Digital Image Correlation

Digital Image Correlation (DIC) is an optical, non-destructive, surface strain measurement technique involving applying a high-contrast speckle pattern to a sample and observing pattern deformation on loading with cameras. The displacement of pixel regions relative to surrounding regions is analysed using computer software to represent the magnitude, gradient and distribution of strain across a surface. Rigid body motion is accounted for and excluded.

The proximal tibia was coated with matt white paint and a black speckle pattern applied (Figure 2.10b). Paint was removed at two locations on the anterior and posterior surface and 2 AE sensors were attachment with cyanoacrylate adhesive. Two charge-coupled DIC cameras (Limess, Messtechnik und Software GmbH, Krefeld, Germany) were positioned to view the anteromedial tibia. Positions were locked onto a tripod (Figure 2.10a). A red light

source was used to maximise speckle contrast. Cameras were calibrated and images were taken at zero load, 100N pre-load and at each 500N load and unload giving a total of 12 images for each specimen loaded up to 2500N. Analysis was performed using Istra 4D 3.1 software (Dantec Dynamics, Skovlunde, Denmark). A contour statistical error radius map of the pre-load image was used to apply a mask over the area where resolution was <0.001mm. Strain was visualized as vertical strain in the y-direction from -5000 to +5000με (microstrain). For quantitative analysis, a line was drawn from the cut surface of the tibia (or equivalent depth in controls) down the anteromedial cortex 5mm anterior to the standard hole present in each tibia using the camera 1 view. This was divided into 5mm depth zones to a maximum of 30mm. This 30mm length contained microstrain data at ≥80 consecutive points with each 5mm increment containing ~12 consecutive data points. Data was exported to Excel 2010 (Microsoft) for onward analysis.

2.4.4 Acoustic Emission

Acoustic Emission (AE) is an engineering technique for measuring construct microdamage. Microdamage events in response to stress create elastic sound waves that conduct through material and can be detected at its surface by piezoelectric sensors, transforming the signal into voltage and enabling real time detection and quantification of microdamage.

Two piezoelectric Pancom Pico-z AE sensors (125-750kHz, Pancom, Huntingdon, UK) (Eaton, et al., 2012) were affixed with cyanoacrylate adhesive in equivalent positions on each tibia (Figure 2.10b). Sensors were connected to IL40S preamplifiers (Physical Acoustics Corporation, Princeton, USA) with 40dB gain and 20-1200kHz bandwidth. A Physical Acoustics Corporation processor was used with AEWin 3.5 software for computer analysis. Sensor coupling was assessed using a Hsu-Nielson (H-N) source (Hsu and Breckenridge, 1981) and the response of all sensors was seen to be greater than 97dB. Test parameters

included a fixed threshold of 45dB, pre-amplitude of 40dB and an analogue filter of 20kHz to 2MHz. AE data was recorded continuously throughout the loading cycle. The AE data was marked at the start of each loading phase, at load hold and at the start of each unload. For each acoustic hit above 45dB the following parameters were recorded: peak amplitude, duration, rise time, ring-down counts (number of threshold crossings) and absolute energy (atto Joules (aJ)). Data so obtained was exported to Excel 2010 for onward analysis.

2.4.5 Statistical Analysis

Statistical analysis was performed using SPSS version 19.0. Continuous parametric data (quantitative DIC data) was analysed using one way ANOVA to compare implant types, and 2-tailed independent Student's T-test to compare implant and control. Non-parametric data (AE data) was analysed using Kruskall-Wallace to compare means between implants and Mann-Whitney U tests to compare implant and control. A p-value of <0.05 was deemed significant and the null hypothesis that no differences existed between implants, was thus rejected at the 5% level.

2.4.6 Results: DIC

The implantation method produced standardised tibial resections, prosthesis alignment and cement mantles. The mean contact area of the fixed bearing implants was 116mm^2 (SD 20.0, range 68-144). There was no significant difference in contact area between AP (Mean 114.4, SD 28.9) and MB implants (mean 117.6, SD 7.8) ($p=0.752$, Mann-Whitney U). The contact area of the fully conforming mobile-bearing implant is ~665mm^2.

Macroscopically, there was little difference in vertical surface strain between implants and controls. At 1500N, one-way ANOVA showed significant differences in surface strain between the implant groups at depths of 0-5mm ($p<0.001$), 5-10mm ($p<0.001$) and 25-30mm ($p=0.037$). At 2500N, one-way ANOVA showed significant differences between implant

groups at depths of 0-5mm ($p<0.001$), 5-10mm ($p<0.001$), 10-15mm ($p=0.041$), 20-25mm ($p=0.026$) and 25-30mm ($p=0.011$). Significant differences existed between all implants and controls at loads of 1500N and 2500N for the proximal 5mm only.

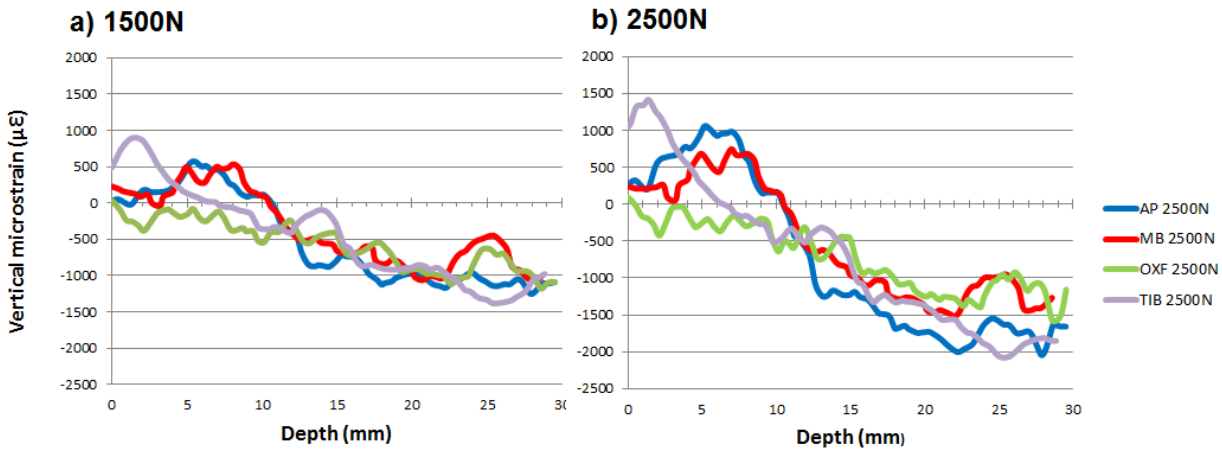

Figure 2.11 Mean vertical surface microstrain measured by DIC for all specimens of each implant type at loads of a)1500N and b)2500N.

2.4.7 Results: Acoustic Emission

60-70% of AE hits were detected at the posterior sensor in all groups. Hit amplitude and number for each implant type throughout the loading cycle are demonstrated in Figure 2.12. The cumulative number of AE hits up to a 2500N load differed significantly between implants ($p=0.001$ Kruskall-Wallis): AP 352 mean cumulative hits (SD 74.3); MB 140 (SD 19.9); OX 63 (SD 29.4); and controls 23 (SD 11.6).

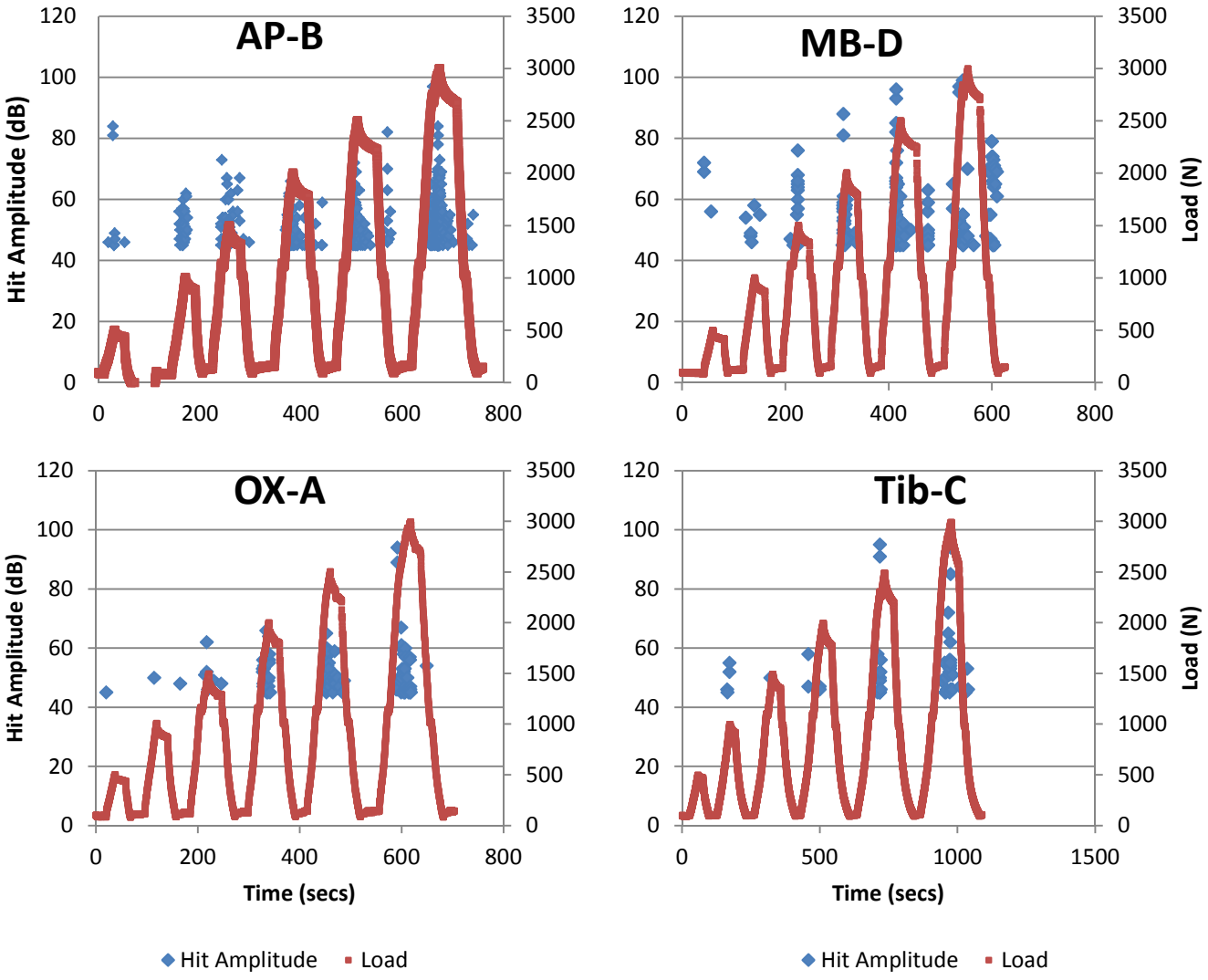

Figure 2.12 Continuous AE output graphs showing hit amplitude and load against time. Each AE hit is represented by a single blue point and load every 0.1 seconds by a single red point.

A graph for each implant type is shown.

On loading, there were significant differences in the number of AE hits between implants at every load (500-2500N) (Figure 2.13a). Compared to controls (TIB), AP implants had significantly more hits at all loads, the MB implants at loads ≥1500N, and the OX at 1500N and 2000N loads only ($p<0.001$ Mann-Whitney-U). AP implants had significantly more hits than the metal backed implants (MB and OX) at loads ≥1500N ($p<0.001$ Mann-Whitney-U). There were no significant differences in AE hit number between MB and OX implants at any load. Significant differences in AE activity were found on unloading from 2000N ($p=0.010$, Kruskall-Wallis) and 2500N ($p=0.011$, Kruskall-Wallis) (Figure 2.13b). AP

implants displayed significantly more AE hits than controls on unloading from 2000N ($p<0.001$, Mann-Whitney-U) and more than the OX on unloading from 2500N ($p<0.001$ Mann-Whitney-U). AE hits on unloading the MB implant from 2500N were significantly greater than in OX implants ($p<0.001$ Mann-Whitney-U).

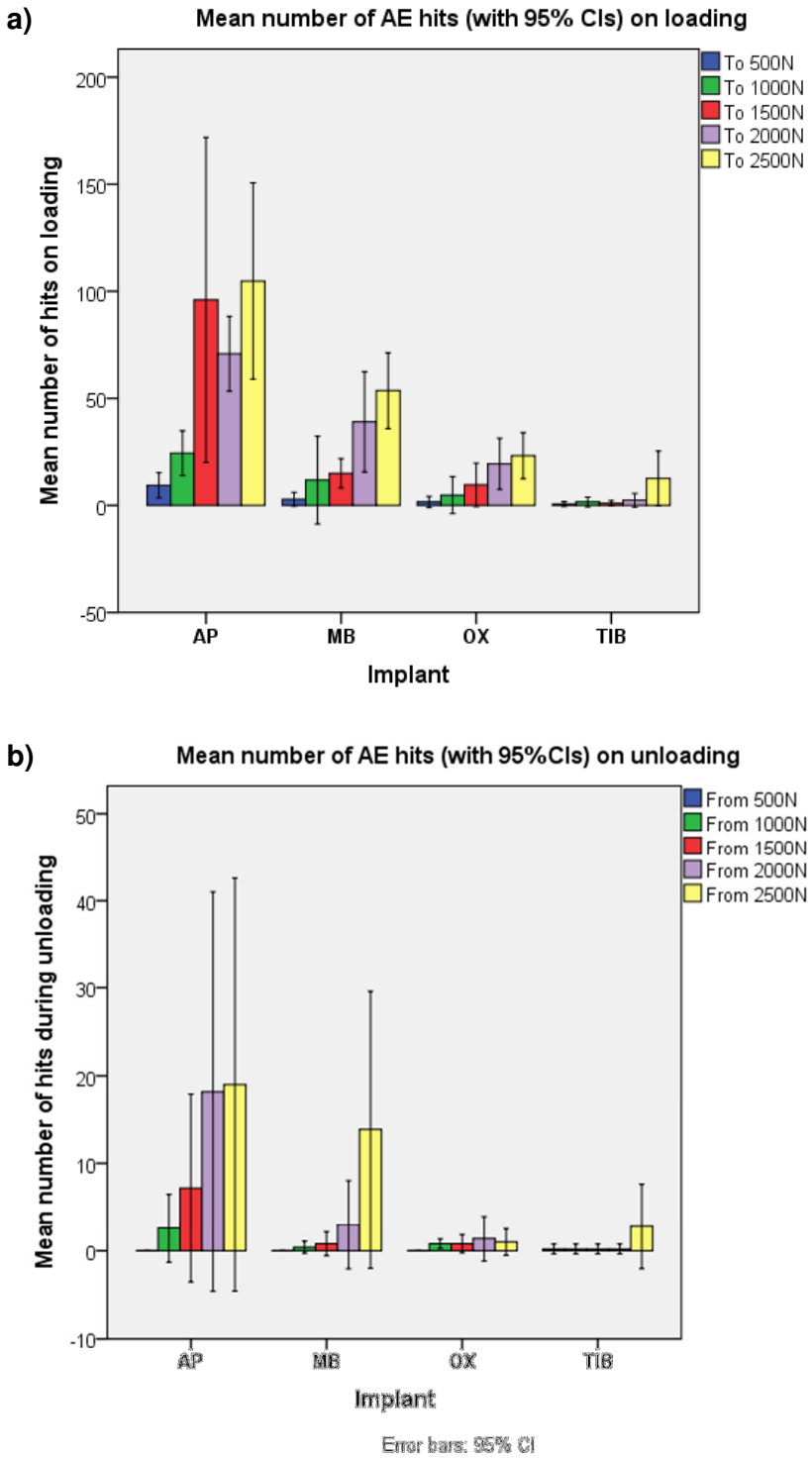

Figure 2.13 AE activity on a) loading to and b) unloading from different loads in each implant type.

2.5 Finite Element Model Creation and Validation

2.5.1 Aims and Objectives

1. To develop a finite element model (FEM) of the proximal tibia implanted with cemented medial UKRs of two different designs:
    a. A fixed bearing UKR implant with an all-polyethylene tibial component
    b. A fixed bearing UKR implant with a metal backed tibial component
2. To validate this model using digital image correlation and acoustic emission data from previous mechanical testing (Appendix 3).

2.5.2 Parts

2.5.2.1 UKRs

Sigma Partial medial UKR implants (DePuy, Johnson & Johnson Professional Inc, Raynham, Massachusetts, USA) were selected for this element of the study. This UKR implant is available with both all-polyethylene (AP) and metal backed (MB) tibial components of virtually identical geometries. The Sigma Partial UKR has 6 femoral and 6 tibial size options with AP thickness of 8-11mm and MB plus PE insert thicknesses of 7-11mm. Implants were sized using the Sigma Partial trials on a left medium composite Sawbone tibia. A size 3 femur, size 3 metal backed tibia, size 3 8mm tibial insert and a size 3 8mm all-polyethylene tibia were acquired.

The Sigma Partial UKR femur is a biconvex, polyradial cobalt-chrome-molybdenum (Co-Cr-Mo) metal alloy implant designed for up to 155° of flexion. The metal backed tibial components are also made of Co-Cr-Mo with Young's' Modulus E=210GPa (Completo, et al.,

2010). The polyethylene components consist of UHMWPE, *E*=0.69GPa (Callister and Rethwisch, 2011) and are non-conforming with the femur. Computer CAD models of these implants were created using Autodesk Inventor 2012 CAD software (Autodesk Inc, San Rafael, CA, USA) based on measurements taken using a Duratool DC150 digital calliper sensitive to 1/100mm. These were saved as STP files and imported into ABAQUS CAE Version 6.12 (Simulia, Dassault Systemes, France) for subsequent analysis. There are 2 subtle differences in the geometries of AP and MB implants (Figure 2.14.): the keel width is greater in the AP implant (AP 5mm, MB 2.55mm); and the undersurface offset for cement is greater in the AP implant (AP 1mm, MB 0.5mm).

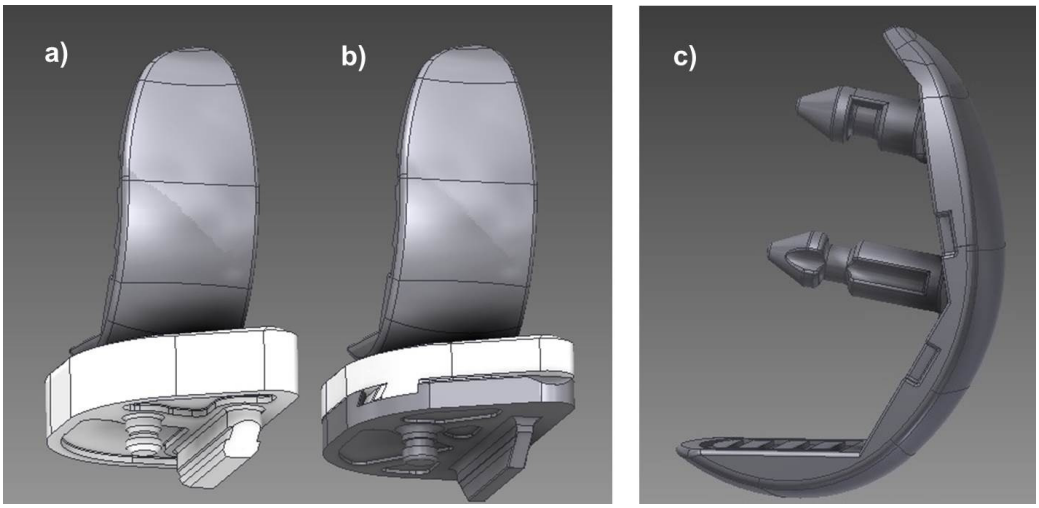

Figure 2.14 Drawn CAD models of the Sigma Partial UKR with a) all-polyethylene tibial component b) metal backed tibial component and c) polyradial femoral component.

2.5.2.2 Tibia

A three dimensional CAD model of a 4th generation left, medium, composite tibia (Sawbone, Pacific Research Laboratories, Vashon, Washington, USA) made available in the public domain was obtained (Biomed town). The CAD model was imported into ABAQUS CAE as separate cortical and cancellous parts. Datum planes were created to define the anatomical axes of the tibia in coronal and sagittal planes. The medial tibial plateau was cut around a datum plane set perpendicular to the anatomical axis of the tibia in the coronal

plane and at 6° of tibial slope in the sagittal plane to produce a posterior tibial slope of 6°. The resection depth was made at 6mm to accommodate an 8mm implant which would restore the articular surface to the correct level allowing for 2mm of cartilage. The vertical limb of the cut was set at a distance of 29.5mm from the medial cortex to create sufficient room for the medial tibial implant plus a 1.5mm cement mantle (Figure 2.15). The tibia was cut distally at 90° to the mechanical axis at 200mm below the articular surface to reduce the computational effort of modelling the entire tibia.

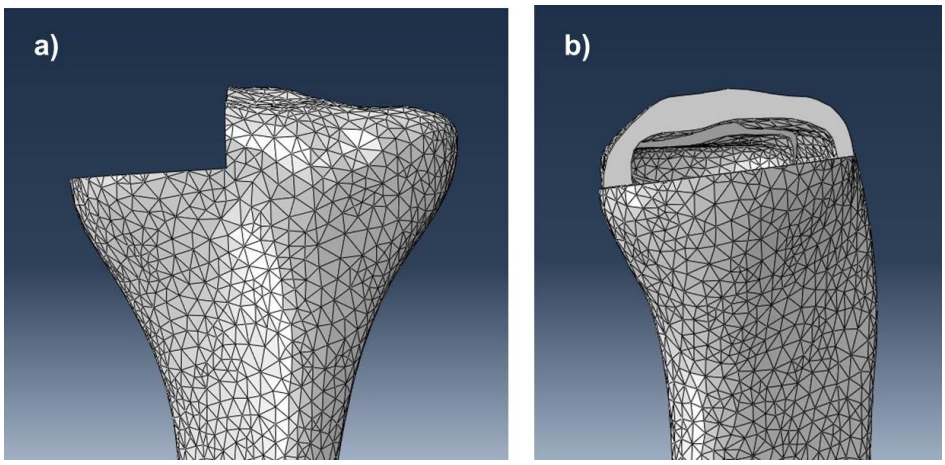

Figure 2.15 Cortical tibia with cut made for UKR tibial implant.

2.5.2.3 Cement

Within ABAQUS, two cement mantle CAD geometries were created: one to correspond to the all-polyethylene tibial component, and one to the metal backed tibial component. Both were designed to have a minimum 1.5mm mantle. The undersurface, with projections for both keel and pegs, was used to cut into the already prepared proximal tibial cancellous bone surface thus creating perfectly matching surfaces (Figure 2.16). The starting thickness of the AP cement mantle was 2.5mm to give a minimum visible mantle of 1.5mm after implantation allowing for the increased undersurface offset of this implant. The cement mantle for the metal cobalt-chrome (Co-Cr) tray had a starting thickness of 2mm giving a 1.5mm minimum mantle with the reduced undersurface offset in this implant. The top

surface of the cement mantle was shaped to the all-polyethylene and metal backed tibial components by using the cut function (Figure 2.17). The cancellous bone in the AP model occupied a volume of 86,329mm^3 and in the MB model 86,806mm^3.

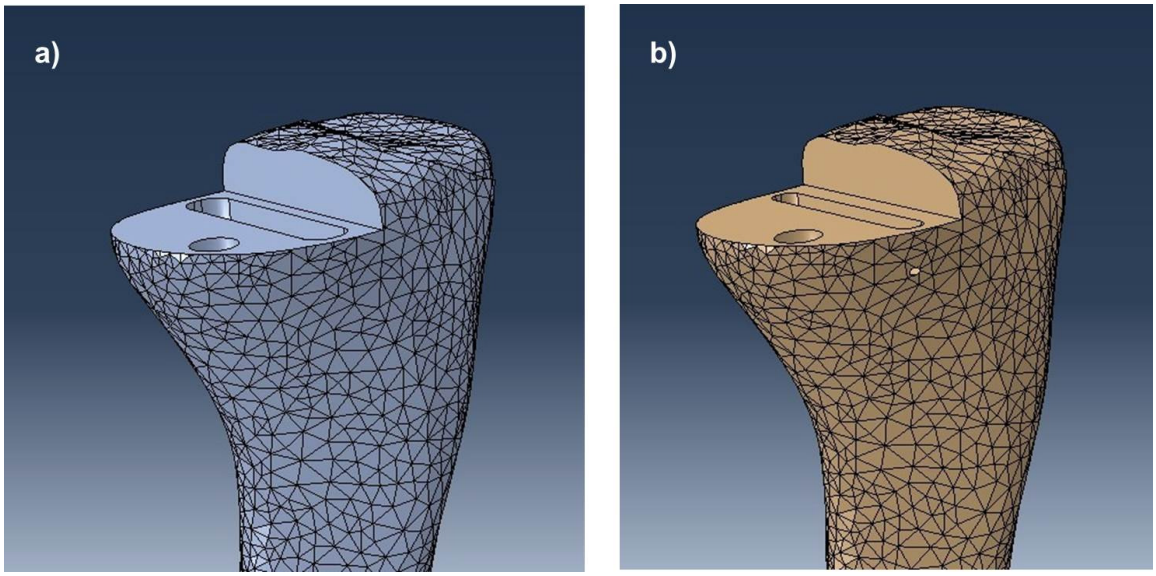

Figure 2.16 Cancellous tibial parts with cut surfaces for implantation of a) all-polyethylene tibia and b) metal backed tibia.

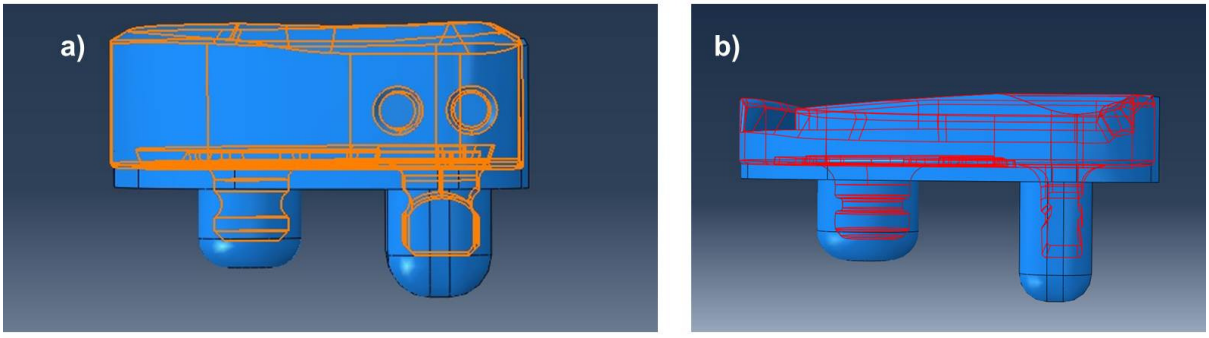

Figure 2.17 Creating the cement mantles for each tibial component.

2.5.3 Material Properties

All materials were assumed to be isotropic, homogenous, and linearly elastic. Cortical and cancellous bone are actually heterogeneous anisotropic materials (Donaldson, et al., 2011; Jenkins, et al., 2013) but the assumption of isotropy is frequently made (Conlisk, et al., 2015) to simplify the model and maintain transparency in the solution. The Young's moduli and Poisson's ratios assigned to each material in the FEM are detailed in Table 2.2.

Table 2.2 Material properties assigned to FEM parts (Callister and Rethwisch, 2011; Completo, et al., 2010)

Part	Elastic Modulus (GPa)	Poisson's ratio
Cortical bone	16.7	0.3
Cancellous bone	0.155	0.3
PMMA Cement	2.4	0.3
Polyethylene	0.69	0.46
Co-Cr tibial tray	210	0.3

2.5.4 Mesh

Each part was seeded with nodes with an internodal distance of 2mm and a linear tetrahedral mesh was generated (Figures 2.18 and 2.19, Table 2.3).

Table 2.3 Finite element model: elements.

Part	Elements	Type
Cortical bone	105,375	Linear tetrahedral
All-polyethylene tibia model		
AP tibial component	23,950	Linear tetrahedral
AP Cement mantle	19,691	Linear tetrahedral
AP Cancellous bone	93,880	Linear tetrahedral
Metal backed tibia model		
MB tibial tray	16,594	Linear tetrahedral
PE insert	22,313	Linear tetrahedral
MB cement mantle	6,371	Linear tetrahedral
MB cancellous bone	96,340	Linear tetrahedral

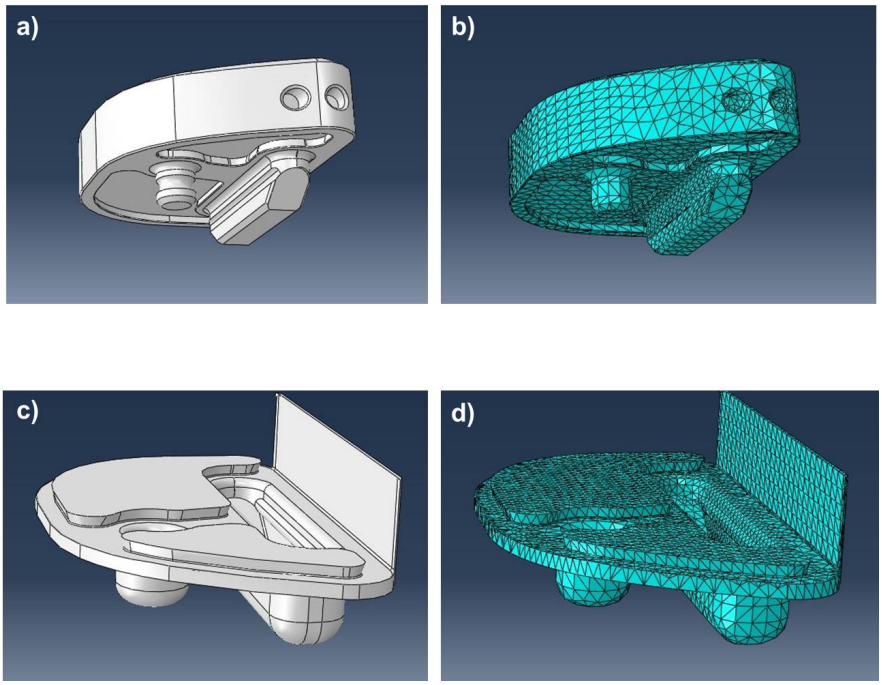

Figure 2.18 All-polyethylene tibial component a) part b) mesh c) corresponding cement part d) cement mesh.

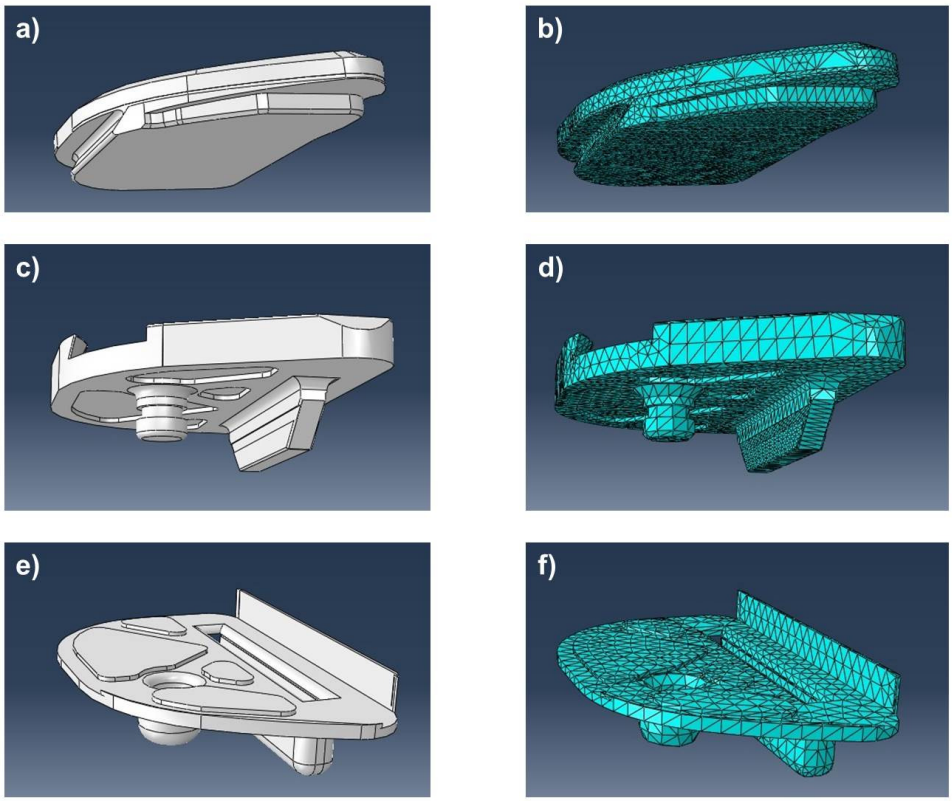

Figure 2.19 Metal backed tibial component a) PE insert part b) PE insert mesh c) metal baseplate part d) metal baseplate mesh e) corresponding cement part f) cement mesh

2.5.5 Assembly and Boundary Conditions

The parts were moved and assembled using coordinate translations and positional constraints. Table 2.4 details the part interfaces and constraints. Cement was rigidly bonded to bone, as was the tibial insert to the metal tibial baseplate. A coefficient of friction of 0.25 was used between implant (polyethylene tibia and metal baseplate) and PMMA cement (Completo, et al., 2010). Boundary conditions included an encastre constraint (i.e. fully restrained) distally at the cut end of the tibia (Figure 2.20). A translational constraint was added proximally at a node representing the ACL footprint (Figure 2.21a) to constrain medial/lateral and anterior/posterior translations to prevent non-physiological construct bending (Figure 2.21b).

Table 2.4 FEM part interactions.

Master surface	Slave Surface	Constraint
Cortical bone	Cancellous bone	Tie
PMMA cement	Cancellous bone	Tie
PMMA cement	Cortical bone	Tie
PMMA cement	Polyethylene tibial	Tie
PMMA cement	Co-Cr tibial tray	Tie
Polyethylene insert	Co-Cr tibial tray	Tie

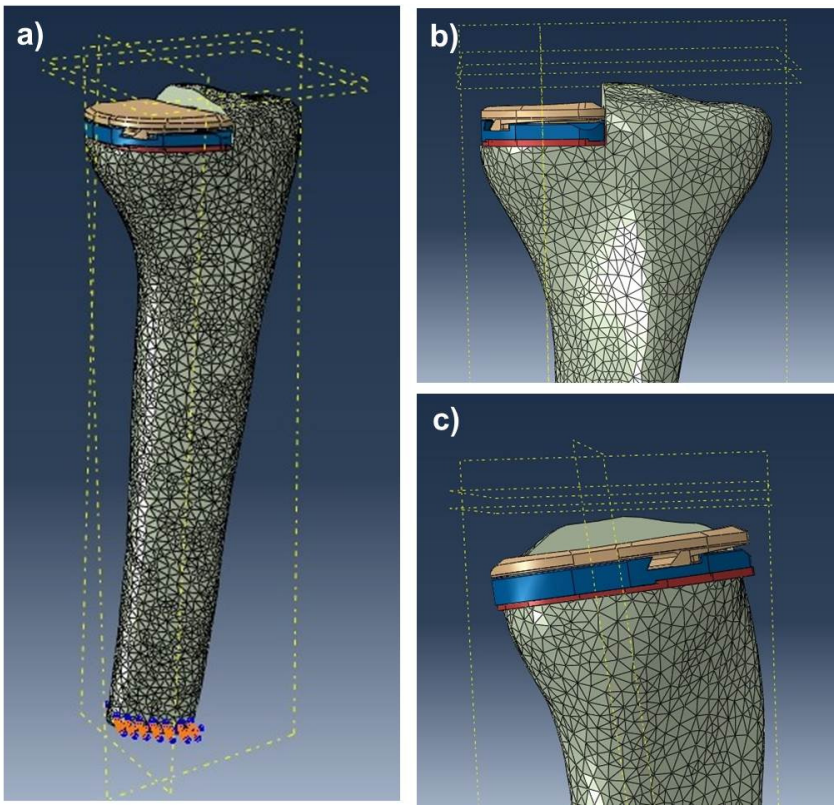

Figure 2.20 FEM with metal backed tibia. Datum planes of anatomical axes and to aid construction are shown. Distal constraint is also shown.

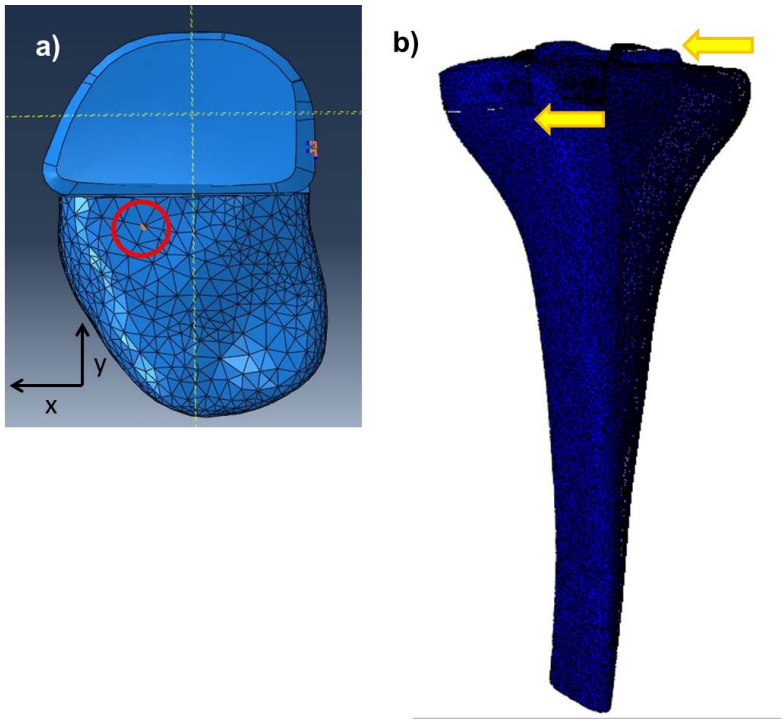

Figure 2.21 FE model proximal constraint at a) a node representing the ACL footprint to prevent b) non-physiological bending on the application of a medial only load (deformation magnified x47).

Two FEMs were thus created:

1. A composite tibia implanted with a cemented 8mm all-polyethylene tibial component.

2. A composite tibia implanted with a cemented 8mm metal backed tibial component with a polyethylene insert (Figure 2.20).

2.5.6 Loading

To simplify the model, load was applied directly to the polyethylene articular surface and not through a femoral component. To mimic the experimental model set-up (Appendix 3) for validation purposes the medial plateau only was loaded (models for a more physiological loading are discussed in the following section). The central node on the superior surface of the polyethylene implant or insert was identified using datum planes, partitioning and a surface node set (Figure 2.22). A coupling constraint was used to apply a distributed load with uniform weighting at this central node with a radius of influence of 6mm (Figure 2.23). That is, a distributed load was applied over a 113.1mm^2 circular area with its epicentre at the centre of the polyethylene bearing. This closely reflected the contact area found for these implants experimentally of 116mm^2 (Appendix 3). It also reflects the location of the point of contact of femur on tibia found in kinematic studies of fixed bearing UKRs: the midline in anteroposterior and medial-lateral directions (Argenson, et al., 2002; Li, et al., 2006). A 2500N load was applied parallel to the mechanical axis of the tibia to represent loading in knee extension. Data was recorded at each 500N increment.

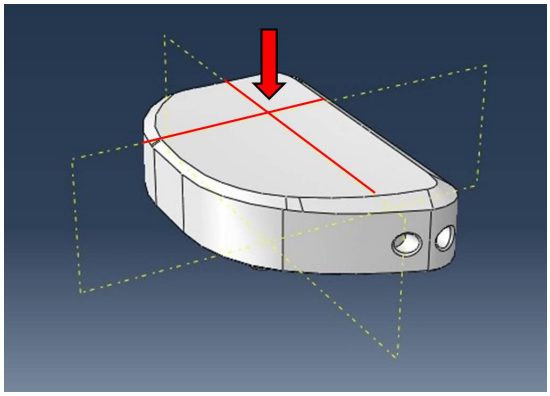

Figure 2.22 Using datum planes to identify the central node.

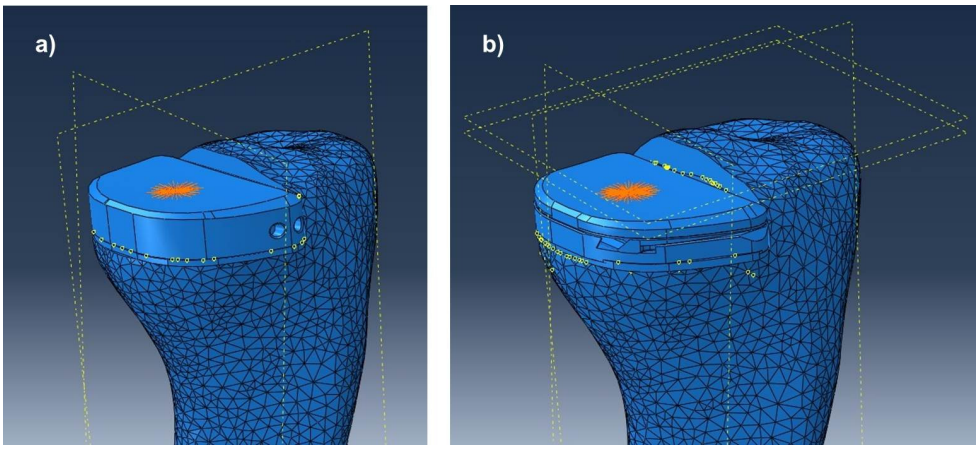

Figure 2.23 Applying the load via a 6mm radius coupling constraint.

2.5.7 Data collection

Contours of minimum principal strain (compressive strain) were obtained for each model at each load increment. Numerical data was collected at each 500N medial load increment up to 2500N for each element in the model for minimum principal strain and maximum principal strain. This numerical data was exported to Excel (Microsoft 2010) for onward analysis. The volume of cancellous bone elements experiencing compressive strain less than -1500, -3000 and -7000 με or tensile strain exceeding 1500, 3000 and 7000με were calculated for each model at each 500N loading increment.

2.6 Model Validation

2.6.1 Aims and Objectives

1. To develop a finite element model (FEM) of the proximal tibia implanted with cemented medial UKRs of two different designs:
    a. A fixed bearing UKR implant with an all-polyethylene tibial component
    b. A fixed bearing UKR implant with a metal backed tibial component

2. To validate this model using digital image correlation and acoustic emission data from previous mechanical testing (Appendix 3).

2.6.2 Validation Method

Each FEM containing 8mm tibial components was validated against experimental mechanical testing data from both digital image correlation (DIC) and acoustic emission (AE) (Appendix 3). The FEMs described above were designed to replicate experimental conditions (Figure 2.24) with identical loading (of the medial plateau only) and boundary conditions including full restraint of the tibia 20cm distal to the plateau and a proximal constraint to prevent medial-lateral and anterior-posterior translation as described above (Figure 2.24a).

The mean vertical surface strain as measured along an anteromedial line using DIC in 5 specimens of each implant was compared to the vertical normal strain in cortical bone at nodes along a corresponding line in the FE model at 2500N loads for each implant. The mean cumulative AE hits of amplitude >40dB on loading and unloading 5 specimens of each implant with their associated absolute energy at each 500N increment were correlated with the FE data for cancellous bone peak strain, and the volume of cancellous bone elements

with principal compressive strain below -1500, -3000 and -7000με and the volume of cancellous bone elements with principal tensile strain above 1500, 3000 and 7000με for each model at each load.

2.6.3 Validation Statistics

Correlation between parametric variables was assessed using Pearson's correlation coefficient. Linear regression analysis was used to further explore significant correlations in continuous data with linear relationships. Autocorrelation was tested for using the Durbin-Watson statistic (0 = positive autocorrelation, 4 = negative autocorrelation, 2 = no autocorrelation) and residuals were determined to be normally distributed prior to linear regression analysis.

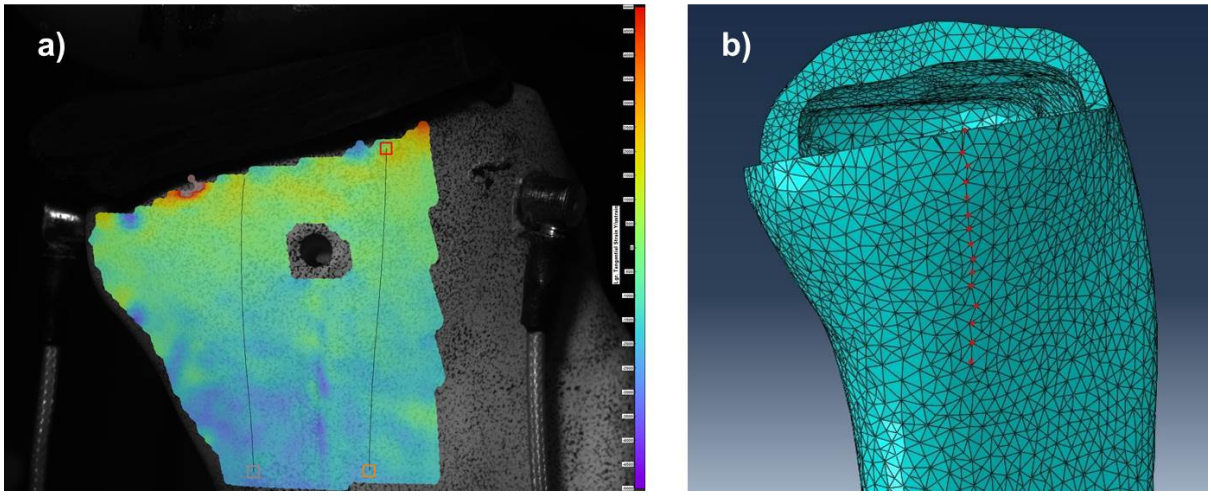

Figure 2.24 a) DIC vertical strain map with an anteromedial line along which strain data was compared with b) an anteromedial line of FEM cortical bone nodes (red).

2.6.4 Model Validation: Cancellous Bone Compressive Strain

Contours of minimum principal strain show considerably more cancellous bone to be overstrained (<-7000με) under the AP tibial component compared to the MB tibial component (Figures 2.25 and 2.26). Loading only the medial plateau resulted in a considerable volume of understrained (>-50με) cortical and cancellous bone in both models, but more so in the MB model (Figure 2.25 and 2.26). Numerically a greater volume of cancellous bone was strained below -1500, -3000 and -7000με in the AP than the MB model at every load increment (Table 2.5, Figure 2.27). At 2500N load the volume of cancellous bone elements with compressive strain <-7000με was found to be 13.5 times greater for the AP implant in comparison to the MB implant; an exponential increase from 1.65 times when comparing volumes below -3000με. Though the volume of cancellous bone elements with compressive strain <-3000με appeared to converge for both implants at higher loads (Figure 2.27a), the volume of elements with strain <-7000με remained 11 to 14 times higher in the AP implant than in the MB (Figure 2.27b). This indicates that while compressive strain increases uniformly with the MB implant, the increment for the AP implant is more localised.

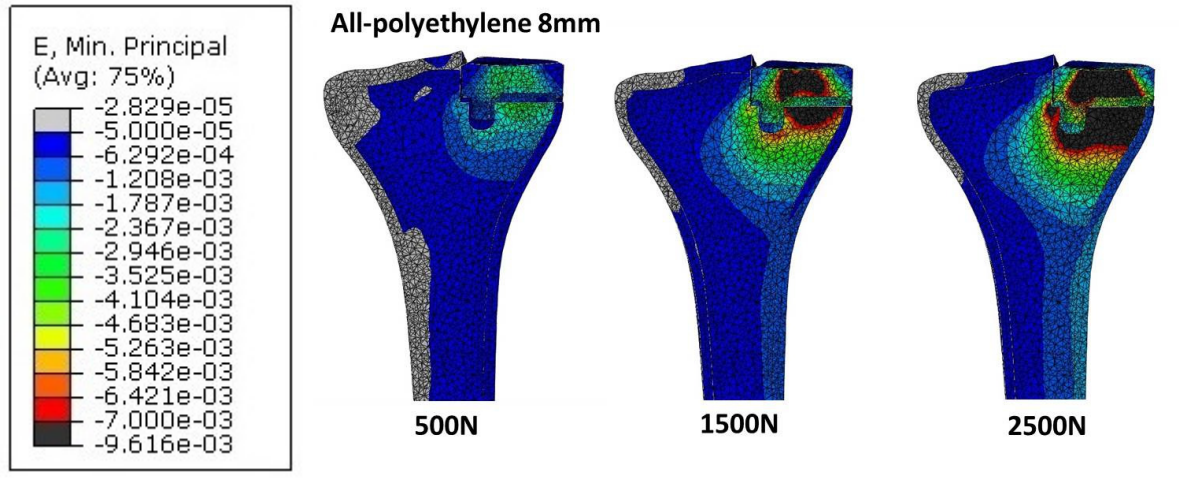

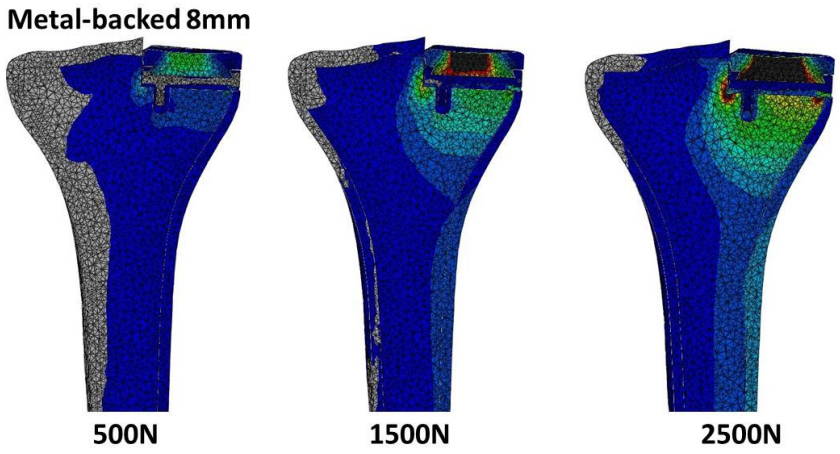

Figure 2.25 Mid-coronal plane contours of the entire model for each implant with medial load only. Strain >-50με appears pale grey, strain <-7000με appears black.

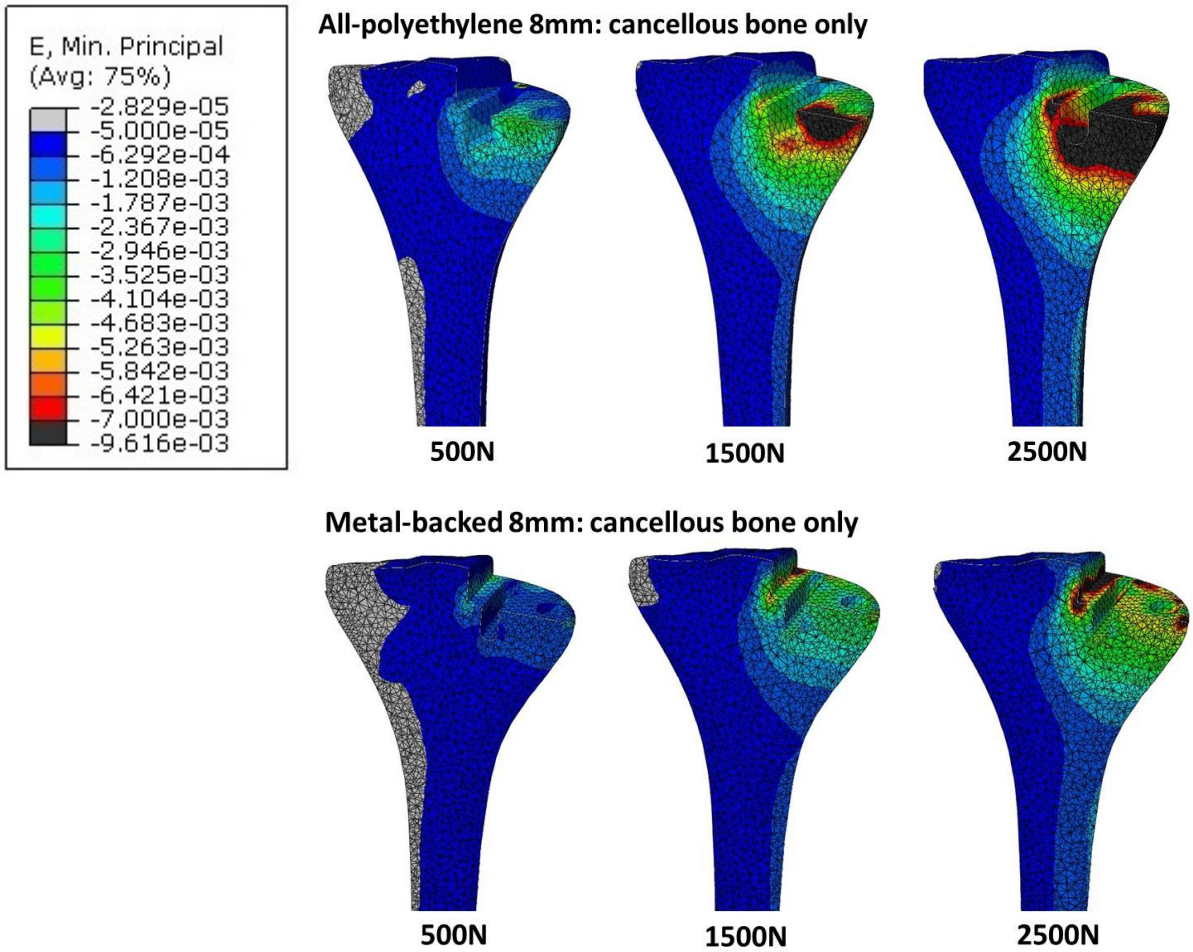

Figure 2.26 Mid-coronal plane oblique contours of the cancellous bone only for each implant with medial load only. Strain >-50με appears pale grey, strain <-7000με appears black.

Table 2.5 The volume of elements with compressive strain below defined microstrain limits at each 500N increment of a 2500N medially applied load for both all-polyethylene (AP) and metal backed (MB) 8mm implants.

Model	Load (N)	Total Volume of Elements (mm^3) with compressive strain (με):			Percentage Volume of Elements (%) with compressive strain (με):		
		<-1500	<-3000	<-7000	<-1500	<-3000	<-7000
8mm AP Tibia	500	3922	312	5	4.54	0.36	0.01
	1000	9824	3887	9	11.38	4.50	0.11
	1500	12942	7718	974	14.99	8.94	1.13
	2000	15387	9840	2620	17.82	11.39	3.03
	2500	17400	11500	4580	20.15	13.31	5.3
8mm MB Tibia	500	324	17	0	0.37	0.02	0.00
	1000	4120	324	6	4.75	0.37	0.01
	1500	8850	1390	72	10.20	1.60	0.08
	2000	11600	4150	177	13.32	4.78	0.2
	2500	13536	6940	339	15.59	8.00	0.46

a)

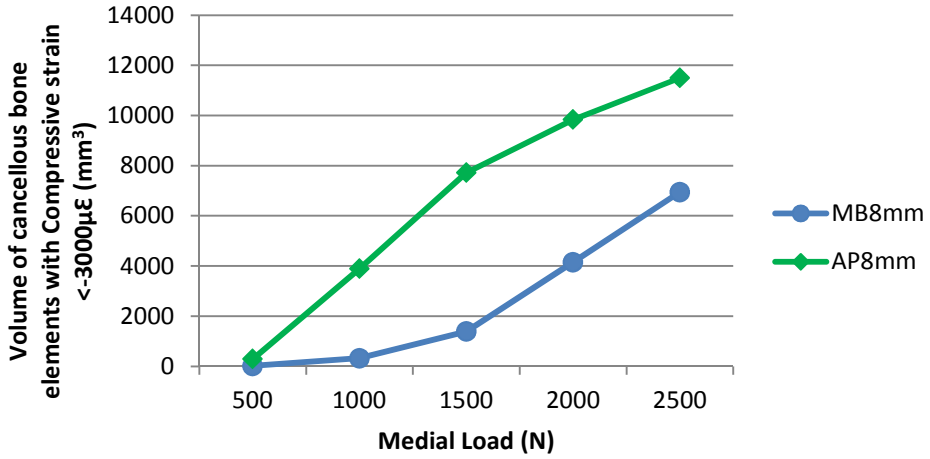

b)

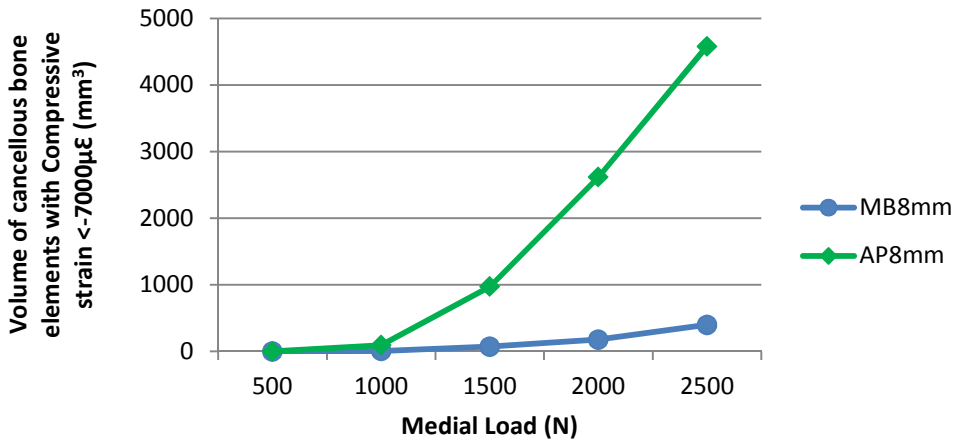

Figure 2.27 Compressive strain (minimum principal strain) when load is applied to the medial plateau only in both AP and MB 8mm implants: a) volume of cancellous bone elements with compressive strain <-3000με and b) <-7000με.

2.6.5 Model Validation: Cancellous Bone Tensile Strain

The cancellous bone volume with strain >3000με in the AP implant was up to 3.6 times that of the MB implant, and diverging (Figure 2.28a). It is important to note that the loading is compressive and thus a far greater volume of bone is under compression than tension (compare Figures 2.27 and 2.28) and a significant proportion of tensile strains are likely to be due to Poisson's effect. As a consequence the volume of elements with tensile strains >7000με was very small (Figure 2.28b). In this case the MB implant had a greater volume of elements strained above 7000με at every load examined. This likely reflects loading of the medial plateau only with resultant bending forces affecting the lateral side of the bone model thus producing higher tensile strains than expected in the MB implant where more load is transmitted directly to the cancellous bone, and not dissipated by bending of the implant itself.

a)

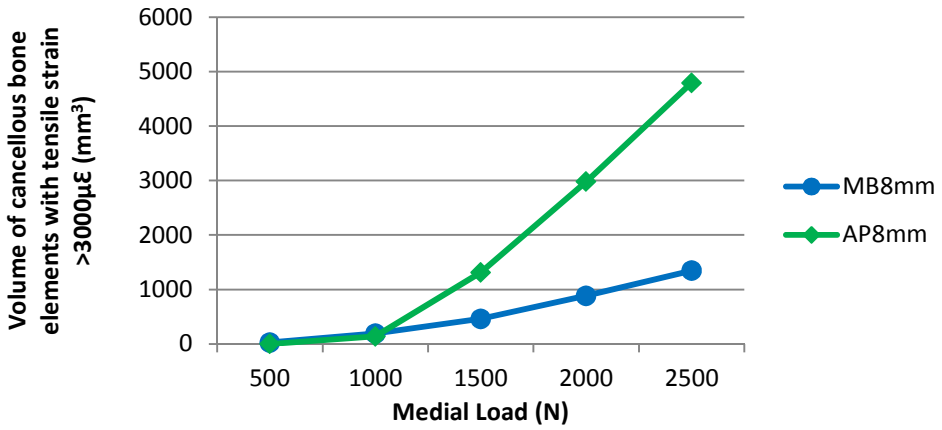

b)

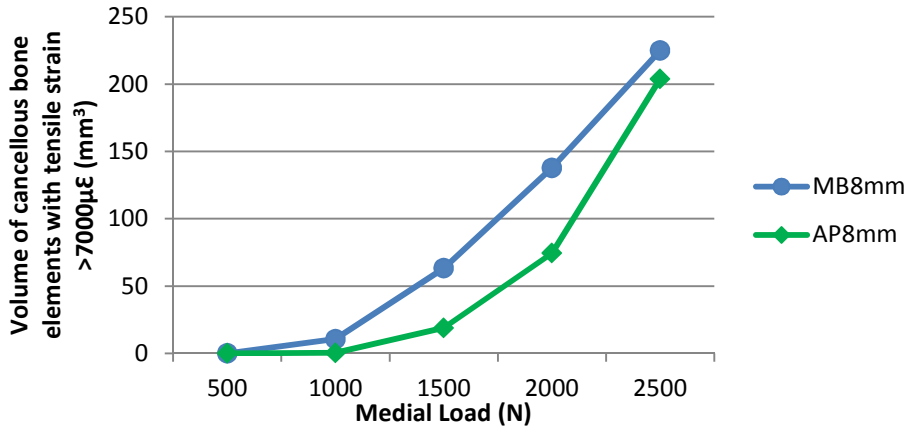

Figure 2.28 Tensile strain (maximum principal strain) when load is applied to the medial plateau only in both AP and MB 8mm implants: a) volume of cancellous bone elements with tensile strain >3000με and c) >7000με.

2.6.6 Model Validation: Digital Image Correlation Experimental Data

Figures 2.29 and 2.30 compare the cortical bone vertical surface strain along an anteromedial line (Figure 2.24) as measured by DIC in the experimental model (Appendix 3), with the vertical component of minimal principal strain experienced by a set of cortical bone nodes along the same line in the FEM for each implant.

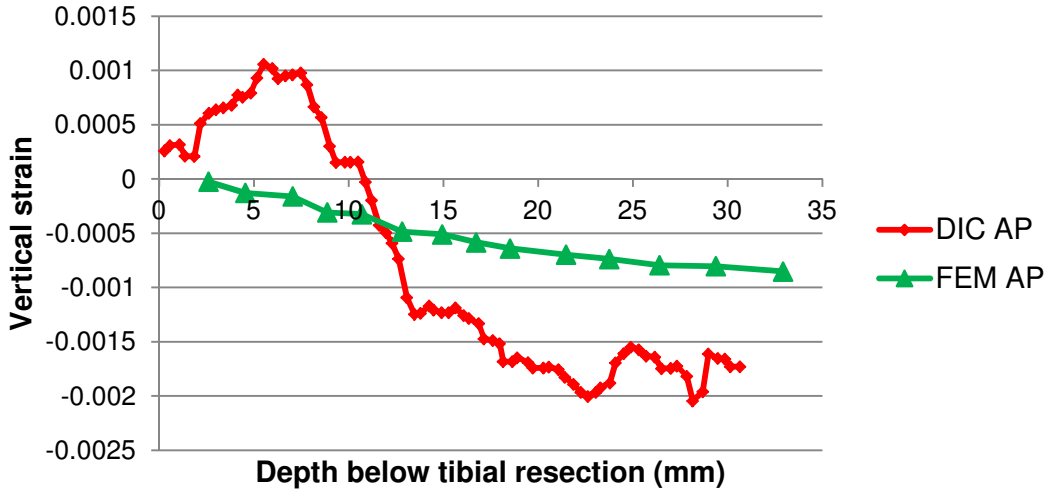

Figure 2.29 Cortical bone vertical strain along an anteromedial line for the AP 8mm implant. (Experimental DIC data Vs. predicted FEM data).

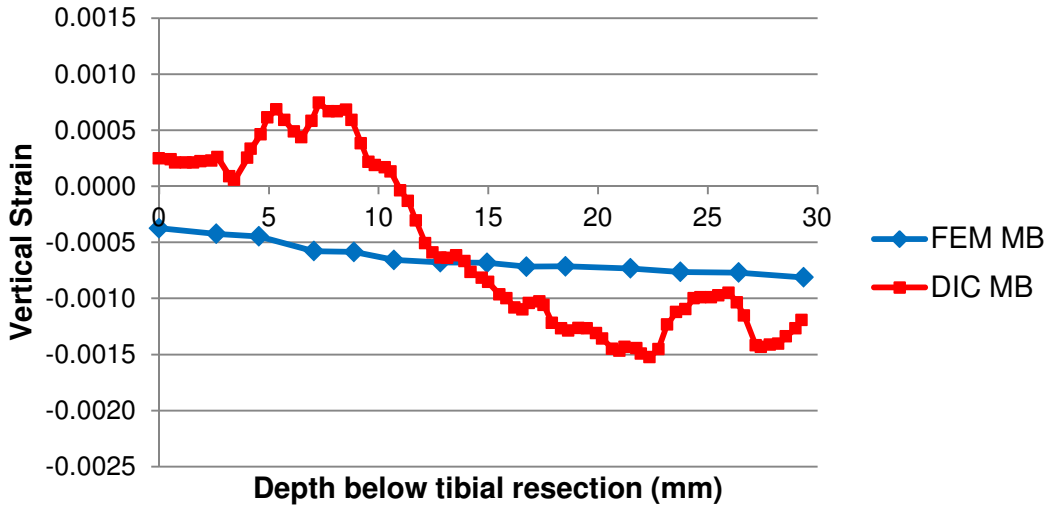

Figure 2.30 Cortical bone strain along an anteromedial line for the MB 8mm implant (Experimental DIC data Vs. predicted FEM data).

For the AP implant, vertical strain correlated significantly between experimental DIC data and predicted FEM data (Pearson's correlation 0.956, p=0.01). There was no significant difference in the mean cortical strain between DIC (-0.00079) and FEM data (-0.00050) (p=0.226, paired T-tests) for the AP implant. For the MB implant, vertical strain again correlated significantly between experimental DIC data and predicted FEM data (Pearson's correlation 0.885, p=0.01). There was no significant difference in the mean cortical strain between DIC (-0.00057) and FEM data (-0.00064) (p=0.692, paired T-tests) for the MB implant.

2.6.7 Model Validation: Acoustic Emission Experimental Data

The volume of cancellous bone elements with compressive strain less than -1500, -3000 and -7000με and tensile strain above 1500, 3000 and 7000με, were correlated with the acoustic emission results (mean cumulative hit number >40dB and cumulative absolute energy) for each model at each load. Acoustic emission (AE) hits (on loading, unloading, and total hits) displayed better correlation with FE parameters than did AE absolute energy for both implants. Correlations between AE hits and FE data for both implants are shown in Table 2.6.

Table 2.6 Pearson's correlation of acoustic emission and finite element parameters. (*=p<0.01).

FE Parameter	AE Hits		
	Loading	Unloading	Total hits
Compressive Strain:			
Vol of elements <-3000με	0.947*	0.942*	0.970*
Vol of elements <-7000 με	0.802	0.854*	0.831*
Tensile Strain:			
Vol of elements >3000με	0.848*	0.914*	0.881*
Vol of elements >7000 με	0.540	0.699	0.581

Overall, compressive strain variables correlated with AE data more closely than tensile strain. The greatest correlation was identified between the volume of cancellous bone elements with compressive strain <-3000με and the number of AE hits on loading and when combined with hits on unloading.

Scatter graphs (Figures 2.31 and 2.32) show the nature of the relationships between AE hits on loading and FEM data. Hits on unloading were not included as an unloading scenario was not simulated in the FEM. Numerical analysis showed that linear, cubic or quadratic curves fitted the data well when data for both implants was combined (Table 2.7). This was not the case for variables where the AP and MB implant results differed the most: the volume of cancellous bone elements with tensile strain >7000με or compressive strain <-7000με and tensile strain >3000με. For these variables, each implant was better considered individually (Figures 2.31e and 2.32e).

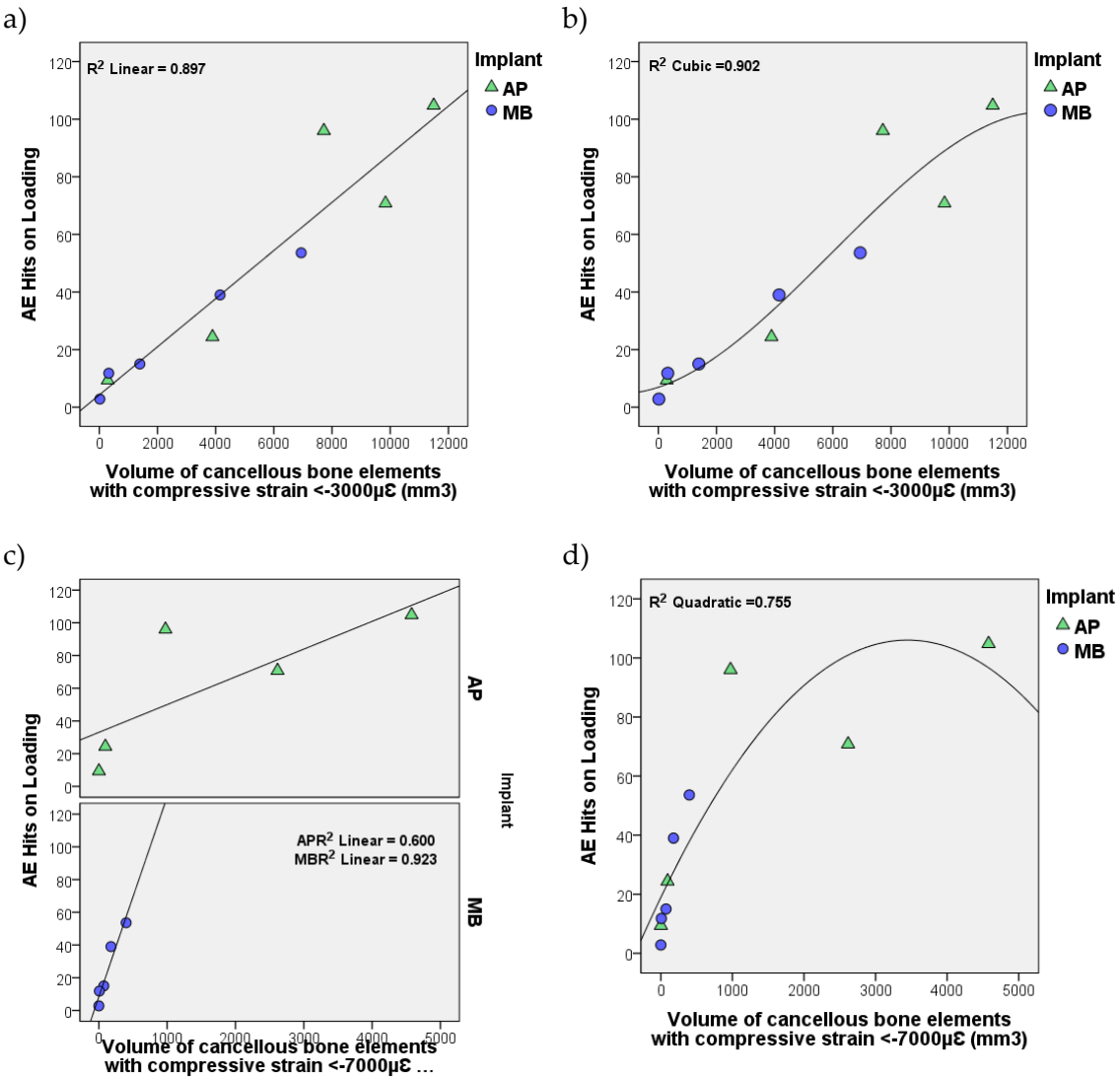

Figure 2.31 Scatter graphs for both implants showing the number of AE hits on loading compared to compressive strain FE data with both linear a) and c) and non-linear , b) and d) best-fit curves.

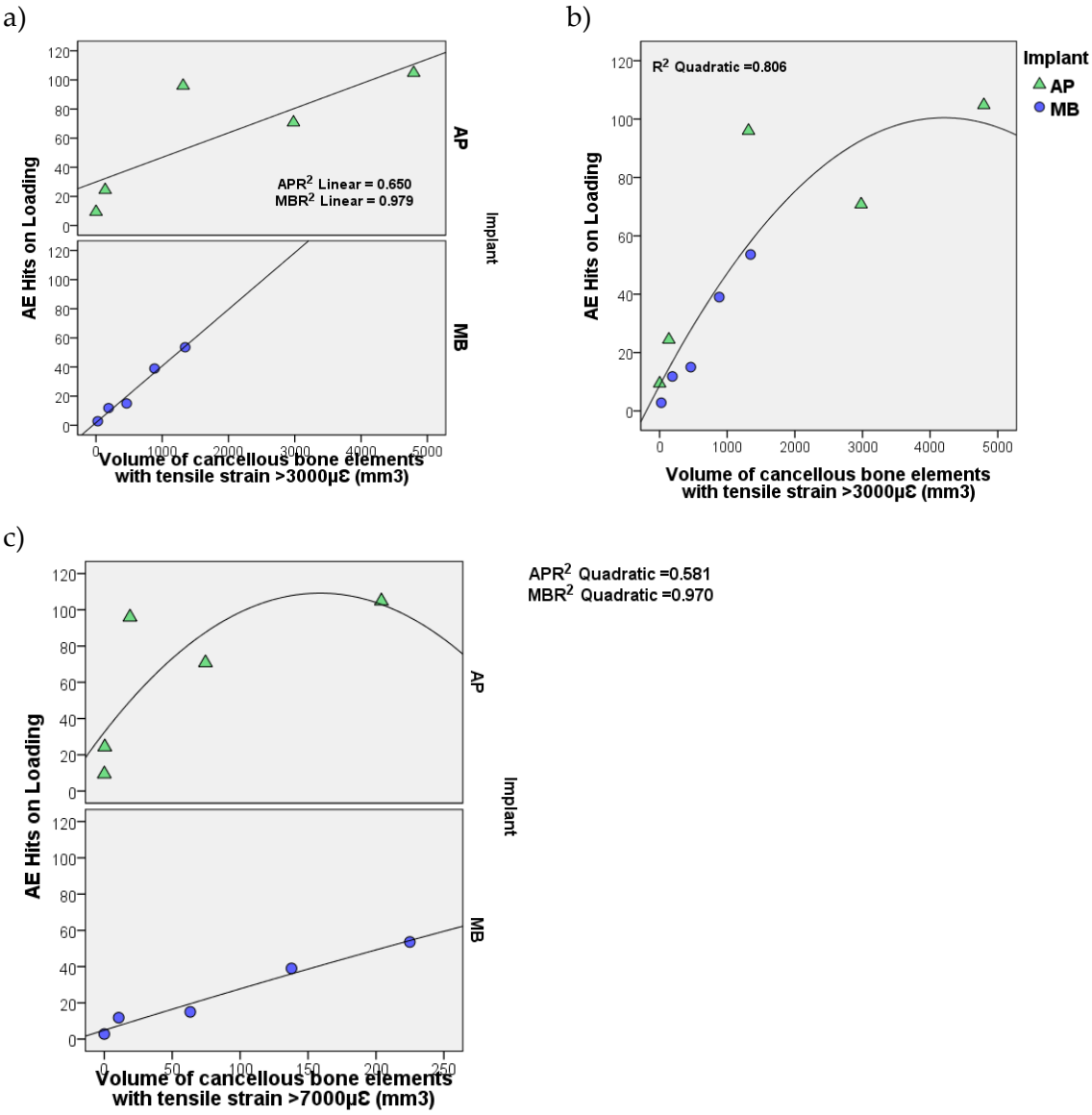

Figure 2.32 Scatter graphs for both implants showing the number of AE hits on loading compared to tensile strain FE data with both linear a) and c) and non-linear b) and c) best-fit curves.

Table 2.7 AE hits on loading Vs FE data: Measuring linearity. * ANOVA

AE hits on loading Vs:		**R**	**R^2**	**p-value***
Compressive Strain				
Volume of elements <-3000με	Linear	0.947	0.897	<0.001
	Cubic	*0.950*	*0.902*	*0.002*
Volume of elements <-7000με	Linear	0.802	0.643	<0.001
	Quadratic	*0.869*	*0.755*	*0.007*
Tensile Strain				
Volume of elements >3000με	Linear	0.848	0.720	0.002
	Quadratic	*0.898*	*0.806*	*0.003*
Volume of elements >7000με	Linear	0.540	0.291	0.107
	Quadratic	*0.522*	*0.304*	*0.281*

Linear regression analysis was performed to further investigate the relationship between AE hits on loading and FE compressive and tensile strain parameters (volume of elements strained >3000με or <-3000με) (Table 2.8). Regression equations pertaining to all implant data, fitted the data significantly well as indicated by ANOVA of $p<0.005$. That is, the dependant outcome variable (AE hits on loading) was significantly predicted by the regression model using the independent FEM variables of volume of elements with strain >3000 με or <-3000 με.

For the MB implant data alone, regression equations fitted significantly well for all FE variables investigated (ANOVA $p<0.01$). For the AP implant data alone, regression equations fitted significantly well (ANOVA $p<0.05$) for volume of elements with compressive strain <-3000με. The equation for the volume of elements with tensile strain >3000 με did not predict AE hits significantly well (ANOVA $p=0.099$). This is to be expected in a model loaded in compression.

Table 2.8 Linear regression analyses of AE hits (dependent variable) against FEM parameters (*x*: independent/predictive variables).

AE hits Vs:	R	R^2	SE of Estimate	DW	Linear Regression *y=a+bx*		SE of b	T score (p-value)	95% CI	
					a	*b*				
Volume elements <-3000με compressive										
AP	0.917	0.840	19.6	3.49	4.12	0.009	0.002	3.98 (0.028)	0.002	to 0.015
MB	0.989	0.978	3.6	2.87	6.24	0.007	0.001	11.6 (0.001)	0.005	to 0.009
All	***0.947***	***0.847***	***12.6***	***3.3***	***4.27***	***0.008***	***0.001***	***8.37 (<0.001)***	***0.006 0.011***	***to***
Volume elements >3000με tensile										
AP	0.806	0.650	29.1	2.25	29.98	0.017	0.007	2.36 (0.099)	-0.006	to 0.04
MB	0.989	0.979	3.56	3.45	1.83	0.039	0.003	11.7 (0.001)	0.028	to 0.049
All	***0.848***	***0.720***	***20.8***	***1.8***	***18.2***	***0.02***	***0.004***	***4.5 (0.002)***	***0.01 0.031***	***to***

The linear regression analysis was based on discrete AE hit data and FEM predicted strains. The best correlations were apparent between AE and FEM for the MB implant where correlation coefficients were highest throughout (R=0.966 to 0.989) with the lowest standard error of the estimate (SE=3.56 to 6.3 AE hits) and the lowest percentage error of *b* (7.7 to 15.5%) indicating strong linear relationships. The corresponding T-tests with $p<0.008$ confirmed these correlations to be significant. When data for both implants are combined, the best correlation existed between AE hits and FE predicted volume of elements with compressive strain <-3000με where a high correlation coefficient (R=0.947) and a low standard error of estimates (SE=12.6 AE hits) were obtained with the lowest percentage error of *b* (12.5%) with correlation significant at the $p<0.001$ level (T-test). The volume with tensile strain >3000με also displayed high R values with statistically significant correlations on T-testing. Therefore, the AE measured microdamage and the FE predicted strains were related to each other with a confidence of greater than 95%.

2.7 Finite Element Analyses

2.7.1 Aims and Objectives

To improve the experimentally validated finite element models to reflect more physiological conditions by loading both plateaus.

To use the new loading environment to investigate the effect of metal backing and varying implant polyethylene thickness using:

a. All-polyethylene tibial components with 6-10mm thickness
b. Metal backed tibial components with 6-10mm thickness

2.7.2 Altering the Loading Environment

In addition to the medial plateau load, a load was applied to the lateral plateau to better mimic physiological conditions. Though the point of loading is known to translate considerably in an anterior-posterior direction throughout a range of motion (Iwaki 2000), this was modelled as a static point (Figure 2.33). A datum plane was created at the midsagittal plane of the lateral plateau. The shallowest point along this plane was selected as the centre point of load application. Again the load was applied via a coupling constraint with radius 6mm to give a distributed load across this area (Figure 2.33a). The meniscus and articular cartilage were not modelled on the lateral side. Load is normally divided unequally across the knee joint, with 60% passing through the medial tibial plateau, and 40% through the lateral plateau in stance (Conlisk, et al., 2015; Haddad and Bentley, 2000; Marti, et al., 2001). The values of the medial loads were unchanged and corresponding lateral loads were applied as per Table 2.9. These loads were considered representative of the loads encountered by the knee during the activities of daily living for a 70kg person with a 60% medial and 40% lateral division of load.

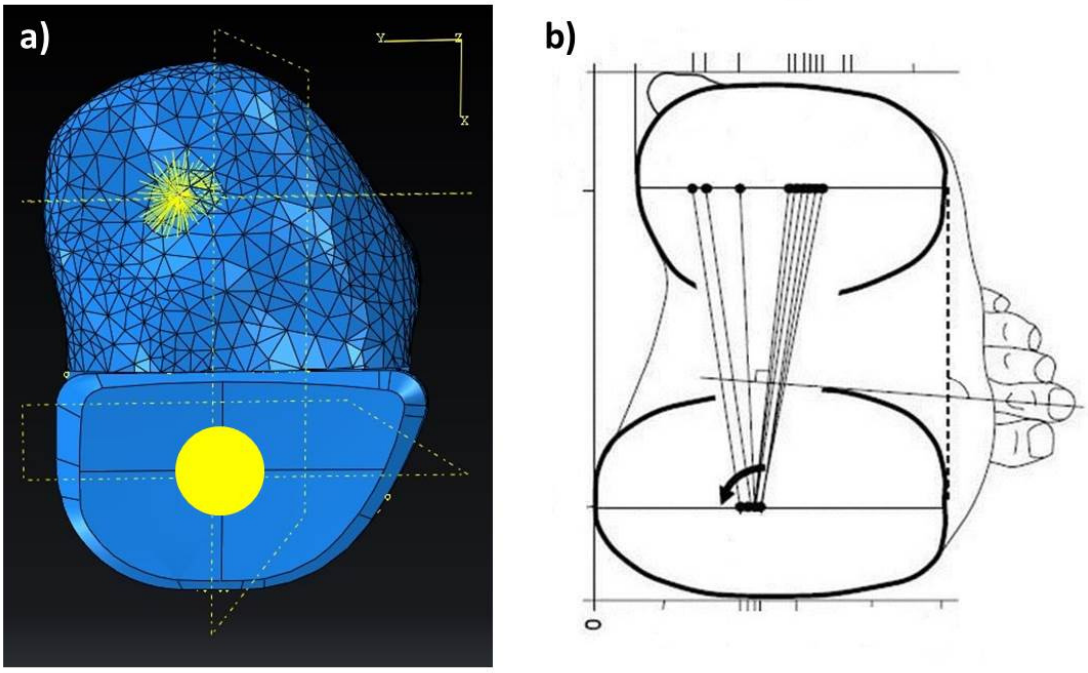

Figure 2.33 Axial views of the tibial plateaus showing a) the areas of load application to both plateaus in the FEM b) the points of contact of the femoral condyles with the plateau throughout a range of motion as determined by kinematic studies (Iwaki 2000).

Table 2.9 Loading of both plateaus in a 60:40 medial: lateral division with multiples of body weight for a 70kg person. Examples physical activities corresponding to these loads are also given (Andriacchi, et al., 1980; Kuster, et al., 1997; Kutzner, et al., 2010; Morrison, 1970).

Medial Load (N)	Lateral Load (N)	Total Load (N)	Multiples of BW	Corresponding Activity
500	334	834	1.2	Cycling
1000	668	1668	2.4	Level walking
1500	1002	2502	3.6	Stair climbing, chair rising
2000	1336	3336	4.8	Uphill walking
2500	1670	4170	6	Stair descent, downhill walking

2.7.3 Altering Implant Thickness

2.7.3.1 Creating new parts - AP Tibia

The 8mm AP tibia CAD file was manipulated in Autodesk Inventor 2012 (Autodesk Inc, San Rafael, CA, USA) to create AP tibias of thickness 6 and 10mm by adding or removing 1mm slices of its transverse/axial plane geometry. At its thinnest point, the 8mm AP tibia implant measures 7.26mm from bearing surface to recessed undersurface, or 8.44mm to the unrecessed inferior surface. A workplane was created 6mm offset superiorly from the recessed inferior surface. This plane was used to divide the 8mm AP tibia into two new parts: a base and a surface. This plane was also used to create a 1mm slice of the AP tibia. The base, surface and 1mm slice instances were re-assembled and merged to form a new 10mm AP tibial component part. To create the 6 AP tibial components the same workplane was used, but instead of adding volume by inserting 1mm of projected geometry, 1mm was removed twice as an extruded cut. The new base and surface were merged as before. New parts (Figure 2.34) were saved as STP files and were imported into ABAQUS CAE for subsequent analysis.

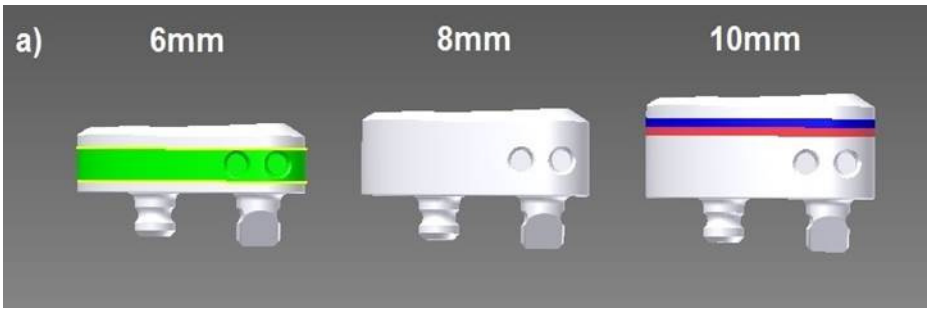

Figure 2.34 AP tibias of different thickness created from the original 8mm implant. The red and blue sections represent 1mm thickness additions. The yellow line on the 6mm AP tibia represents the levels at which 1mm has been subtracted.

2.7.3.2 Creating New Parts - MB Tibia

A similar method was used to create tibial inserts of different thicknesses for the MB tibial component. The 8mm MB tibial insert CAD file was manipulated in Autodesk Inventor 2012 to create tibial inserts that would give MB tibias of thickness 6 and 10mm by adding or removing geometry. At its thinnest point, the 8mm MB tibia insert measures 6.435mm from the bearing surface to its flat inferior face. A workplane was created 5mm offset superiorly from the inferior face and new parts (base, surface, 1mm slices, and base minus 2mm) were created as previously. The geometry of the clip-in mechanism of the insert was maintained. The new parts so created were again merged to produce individual tibial inserts to give 6-10mm MB tibias when assembled with tibial base plates as shown in figure 2.35 below. These were saved as STP files and imported into ABAQUS for subsequent analysis.

Figure 2.35 MB tibias of different thickness created from the original 8mm implant. The red and blue sections represent 1mm thickness additions. 2mm has been removed from the superior surface of the green part to create the 6mm implant.

2.7.3.3 Mesh, Assembly and Loading

As for the original 8mm parts, new 6mm and 10mm parts were seeded with an internodal distance of 2mm and a linear tetrahedral mesh was generated. Instances of these altered polyethylene parts were imported into the previously created assemblies and

exchanged for the 8mm parts. The same material properties, interactions, constraints and boundary conditions were employed as in the validated FEM. Load was applied to both plateaus as described above. Data was collected for the same variables at the same load increments as described previously.

3 Clinical Outcomes

3.1 Aims and Objectives

The aims of this study were to examine differences in patient reported outcome measures (PROMs) and survivorship for patients treated with medial UKR of two designs:

a. A mobile bearing metal backed implant (Oxford)
b. A fixed bearing all-polyethylene implant (Preservation).

The primary outcome measure was the Oxford Knee Score. Secondary outcome measures included survivorship, patient satisfaction and measures of pain.

3.1.1 Research Question

1. Do UKRs with all-polyethylene tibial components display poorer patient reported outcome measures and elevated ongoing postoperative pain compared to those with metal backed tibial components?

3.2 Chapter Summary

"Unexplained" pain in medial unicompartmental knee replacements (UKRs) accounts for ~25% of UKR revisions and may result from elevated proximal tibial strain with repetitive microfracture and remodelling. The effect of tibial component material, all-polyethylene or metal backed, on this pain is uncertain. The aim of this study was to perform a retrospective cohort study with >5 year follow up to compare patient reported outcome and survivorship of medial UKRs of two designs: a metal backed mobile bearing implant (Oxford) and an all-polyethylene fixed bearing implant (Preservation). From 1999-2007, 289 Oxford and 111 Preservation were performed. 26 Oxford and 11 Preservation were revised leaving 158 Oxford (mean age 66, 43% female) and 75 Preservation (mean age 68, 57% female) UKRs eligible for PROMs follow up at 1 and >5 years using: SF-12 physical (PCS) and mental component scores, Oxford Knee Scores (OKS), visual analogue pain scores (VAS) and satisfaction scores. Long term follow up (>5 years) occurred at a mean of 100 months. Both PCS and OKS improved significantly by 1 year in both implants ($p<0.001$) with no further improvement to >5 years. There were no significant differences between implants in OKS improvement at 1 year (Oxford 15.6, Preservation 13.4, $p=0.208$), long term VAS pain (20.2 and 22.2, $p=0.525$) or location of ongoing pain. In both implants a BMI >35 ($p=0.001$) and age >75 ($p=0.039$) were associated with significant deterioration in OKS from 1 to >5years. All cause survival for each implant was: Oxford 92% (95%CI 89-96), Preservation 90% (84-96) at 5 years and Oxford 90% (86-94), Preservation 80%(61-99) at 10 years. Preservation UKRs were revised significantly earlier (38 Vs 62 months, $p=0.02$) and were more likely to be revised for unexplained pain ($p=0.005$). Oxford UKRs were more likely to require augmented implants or increased constraint at revision. Despite different modes of failure, no significant differences were apparent between implants in terms of long term outcome or pain.

3.3 Introduction

Joint registries consistently show higher rates of revision for unicompartmental knee replacements (UKRs) compared to total knee replacements (TKRs) (Australian, 2012; NJR, 2012; Swedish, 2011). Unexplained pain is the second most common reason for UKR revision after aseptic loosening (Baker, et al., 2012; Baker, et al., 2012). This undoubtedly contributes to the poorer survival of UKR compared to TKR where far fewer revisions are performed for pain. It has been suggested that elevated proximal tibial strain with repetitive microfracture and remodelling may be a cause of this pain (Simpson, et al., 2009). Tibial bone models have shown significantly greater microdamage under UKRs with all-polyethylene tibial components compared to metal-backed components (Appendix 3). In TKR, metal backing of tibial components distributes tibial stresses more evenly than in all-polyethylene implants, but is associated with stress shielding (Bartel, et al., 1982). The clinical significance of this is unclear with equivalent long term results in both metal-backed and all-polyethylene TKRs (Bettinson, et al., 2009). Both overloading and under-loading (stress/strain shielding) of bone can alter bone mineral density (BMD). Stress shielding and low BMD may cause reduced cancellous support to implants resulting in microfracture, pain and subsidence. Alternatively, proximal tibial microdamage and adaptive remodelling from overload may cause pain and a relative increase in BMD, or sclerosis, under the implant.

3.4 Results

3.4.1 UKR Patient Identification

Three hundred and sixteen Phase III Oxford and 111 Preservation UKRs were performed since 1999. Of these, 289 Oxfords were performed from 1999-2007 and 111 Preservations were performed from 2003-2007 with a minimum follow-up of 5 years. Fifty two patients from the Oxford group (with 57 UKRs) and 11 from the Preservation group had died of unrelated causes with their UKR in situ. Twenty six (11.2%) Oxford UKRs and 11 (11.1%) Preservation UKRs had been revised.

The Oxford group had a mean age of 66.6 (46-84), BMI of 28.9 (20-42) and weight of 81.6kg (52 – 125). The Preservation group had a mean age of 67.9 (48-87), BMI of 28.7 (20-42) and weight of 78.8kg (48-110). There were no statistically significant differences between the baseline characteristics of each population (Table 3.1). Age (Figure 3.1), BMI and weight were normally distributed in both groups.

Table 3.1 Unrevised UKR patient preoperative characteristics by implant. No significant differences in demographics between Oxford and Preservation groups were apparent.

	Oxford (n=171)	Preservation (n=75)	P value	95% CI
Female Sex	94 [53.7]	44 [57.1]	0.101$^{\tau}$	
Age	66.9 (7.79)	68.4 (9.16)	0.189*	-3.67 to 0.73
Weight (kg)	80.9 (14.2)	78.4 (15.22)	0.231*	-1.63 to 6.71
BMI	28.8 (4.22)	28.6 (4.74)	0.678*	-0.977 to 1.53
OA	177 [99.4]	76 [97.4]	0.870$^{\tau}$	
Left Sided	91 [51.1]	47 [60.3]	0.26$^{\tau}$	

Mean (SD) or number [%] $^{\tau}$ Chi squared test *Two-tailed student T-test

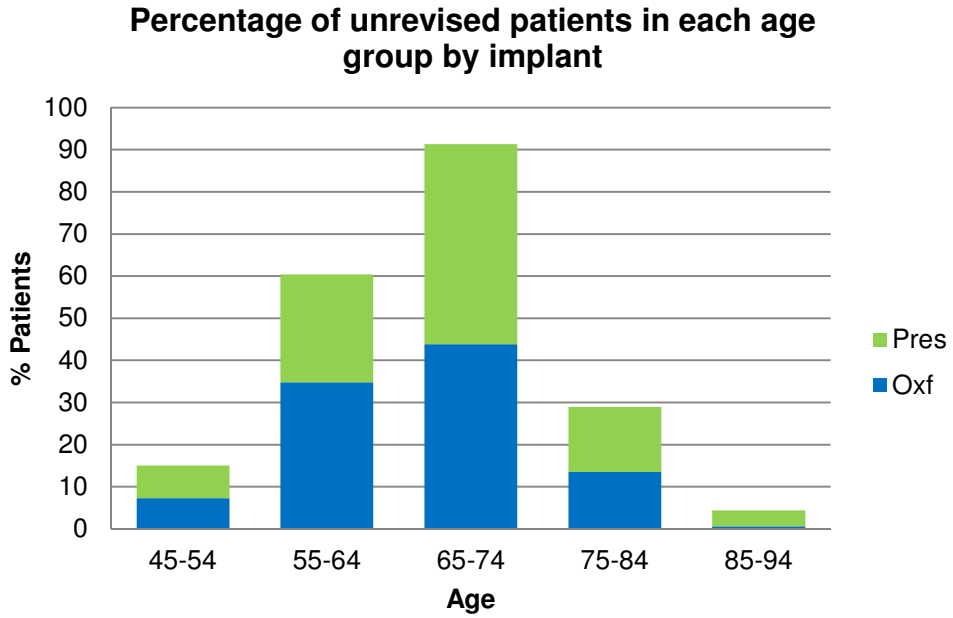

Figure 3.1 Patient age by UKR implant.

3.4.2 PROMs Study

3.4.2.1 Patients

Preoperative and 1year outcome measures were available on 158/171 Oxfords and 75/75 Preservations (Figure 3.2). Long term (>5year) questionnaires were returned by 133/171 intact Oxford UKR patients (77.7%), and by 71/75 with an intact Preservation UKR (94.7%). There was a significantly higher proportion of females in the non-responders group, but there were no significant differences in other demographics between responders and non-responders (Table 3.2). Two of the Oxford non-responders were known to have developed dementia and were unable to complete the questionnaire.

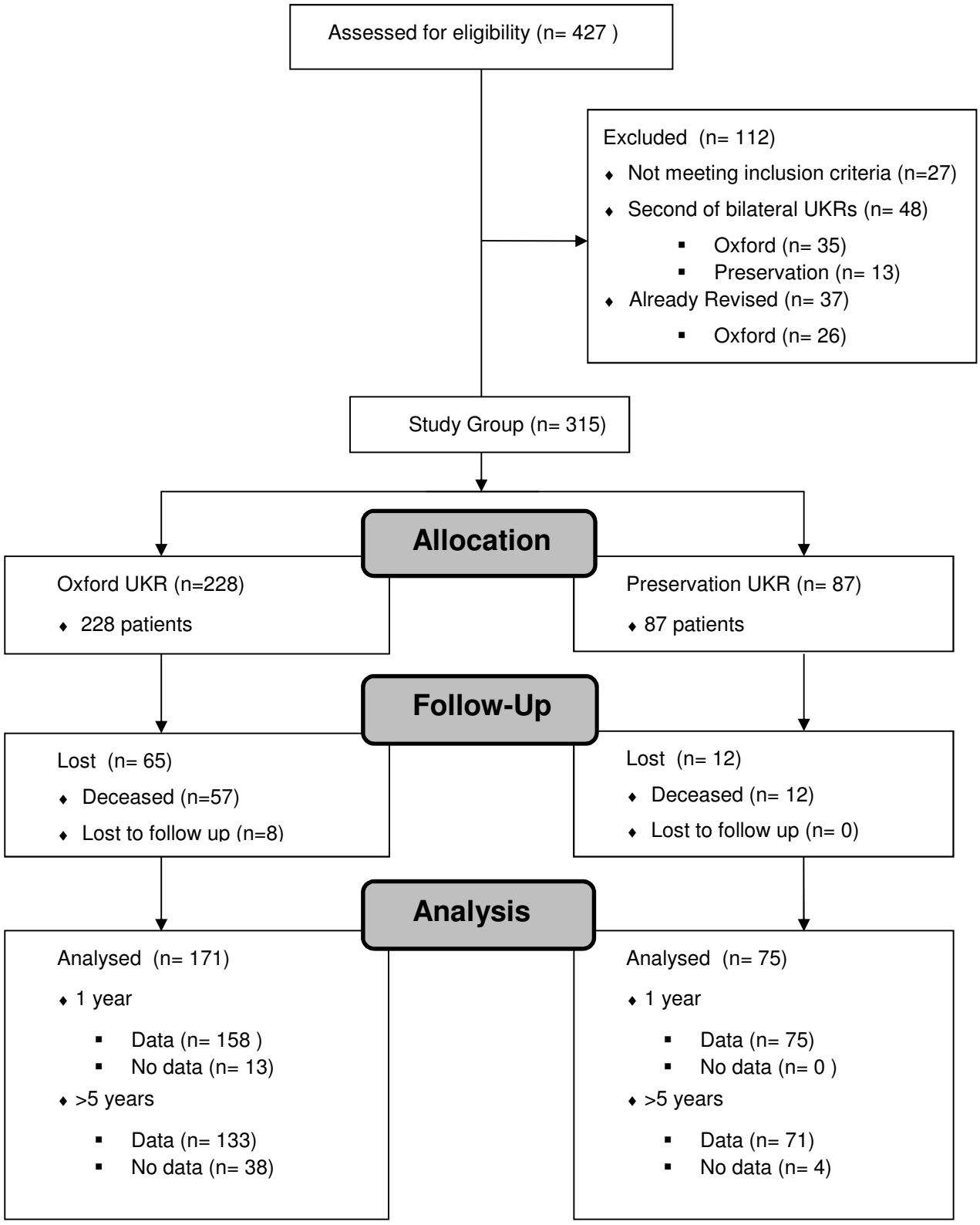

Figure 3.2 PROMs study cohort.

Table 3.2. Demographics of PROMs responders and non-responders.

	Responders (n=204)	Non-responders (n=42)	P value	95% CI
Female Sex	96 [47]	28 [67]	0.021 ᵀ	
Age	67.3 (8.3)	67.0 (8.1)	0.848*	-3.0 to 2.5
Weight (kg)	81.1 (14.8)	76.7 (12.9)	0.128*	-9.9 to 1.3
BMI	28.9 (4.6)	28.5 (3.4)	0.641*	-2.1 to 1.3

Mean (SD), number [%], ᵀ Chi squared test, *Two-tailed student T-test

Amongst responders, the Preservation group contained a higher proportion of women and this difference was significance (Table 3.3). There were no other significant differences in the baseline characteristics of the UKR groups.

Table 3.3 Preoperative patient characteristics in the PROMs study by implant.

	Oxford (n=158)	Preservation (n=75)	P value	95% CI
Female Sex	68 [43.0]	43 [57.3]	0.052 ᵀ	
Age	66.8 (7.83)	68.3 (8.96)	0.214*	-3.69 to 0.829
Weight (kg)	81.2 (14.26)	78.7 (15.13)	0.251*	-1.78 to 6.78
BMI	28.8 (4.2)	28.7 (4.76)	0.789*	-1.12 to 1.47
OKS	39.5 (7.69)	39.8 (5.92)	0.787∞	-2.73 to 2.06
SF-12				
PCS	30.3 (6.39)	31.23 (7.11)	0.400*	-3.12 to 1.25
MCS	50.5 (11.78)	50.8 (11.51)	0.957∞	-4.07 to 3.65
Comorbidities				
Depression	15 [9.5]	6 [8.0]	0.698 ᵀ	
Back Pain	63 [39.9]	27 [36.0]	0.570 ᵀ	
Pain other Joints	81[51.3]	34 [45.3]	0.344 ᵀ	
Total comorbidities	2 {3}	1{3}	0.927∞	

Mean (SD), number [%], or median {IQR},

ᵀ Chi squared test, *Two-tailed student T-test, ∞ Mann-Whitney U-test

The mean length of follow-up for the >5year questionnaire was 100 months across all UKRs (42-158). In the Oxford group, >5yr follow-up was at a mean of 109 months (SD 26, range 55 -158), and 82 months in the Preservations (SD 13, range 55-104). This difference was significant ($p<0.001$, 95%CI 20.6 to 33.2, unpaired T-test). Implantation of Preservation UKRs began 4 years after that of the Phase III Oxford UKR.

3.4.2.2 General Health Questionnaire SF-12

There were significant improvements in PCS at 1 year in both implants ($p<0.001$) with no further significant change by >5 years (Oxford $p=0.203$, Preservation $p=0.793$, Wilcoxon sign rank) (Figure 3.3).

As shown in figure 3.4 there was no significant change in MCS between preoperative and 1 year scores in either group (Oxford $p=0.666$, Preservation $p=0.958$ Wilcoxon sign rank). Overall there was a reduction in MCS between 1 and >5 years (Figure 3.4). This was significant in the Oxford ($p=0.03$) but not the Preservation group ($p=0.207$, Wilcoxon sign rank). No significant differences existed in PCS or MCS change at 1 or >5 years between UKR implants (Table 3.4). The length of >5year follow up displayed a significant negative correlation with absolute PCS at >5years (Pearson correlation -0.223, $p=0.002$ two-tailed) and with change in PCS (PC -0.183, $P=0.036$). That is, PCS reduced in a linear fashion as time since surgery, and thus age, increased (Figure 3.5). This reduction was proportional to length of follow up with greater length correlated with larger change (Figure 3.6). No such correlation existed in the MCS (Pearson's correlation 0.069, $p=0.69$ two-tailed) or change in MCS.

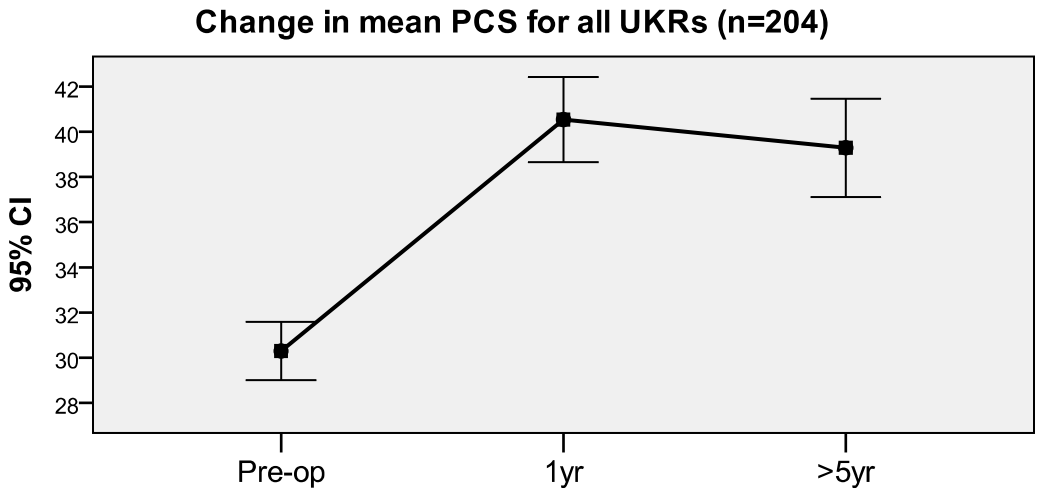

Figure 3.3 Physical component score trend over >5 years in all UKRs

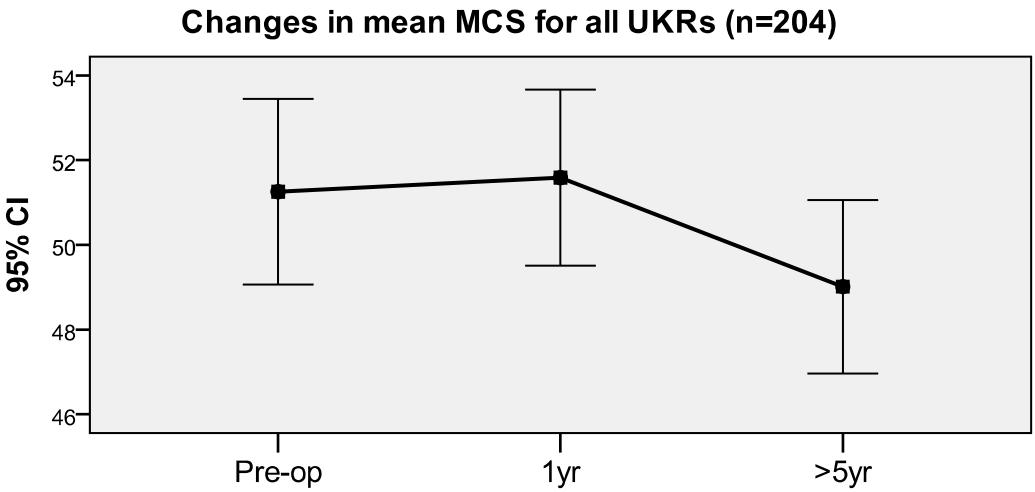

Figure 3.4 Mental component score trend over >5 years in all UKRs

Table 3.4 Changes in postoperative PROMs by implant (Imp=improvement)

	Oxford (n=158)	Preservation (n=75)	P value	95% CI
OKS				
Imp to 1 yr.	15.6 (9.90)	13.4 (8.17)	0.208*	-1.22 to 5.56
Imp to 5 yrs.	14.1 (10.29)	14.73 (8.82)	0.727*	-4.27 to 2.99
PCS				
Imp to 1 yr.	11.0 (10.66)	9.6 (10.89)	0.486*	-2.65 to 5.54
Imp to 5 yrs.	8.6 (11.61)	9.6 (11.01)	0.652*	-5.08 to 3.20
MCS				
Imp to 1 yr.	1.1 (11.41)	0.13 (9.06)	0.644*	-3.16 to 5.08
Imp to 5 yrs.	-2.08 (12.27)	-1.45 (12.04)	0.777*	-5.07 to 3.79
Pain VAS 5 yr.	20.2 (25.69)	22.2 (26.99)	0.525∞	-10.41 to 6.47

Mean (SD), number [%], * Two sample T-test, ∞ Mann-Whitney U-test

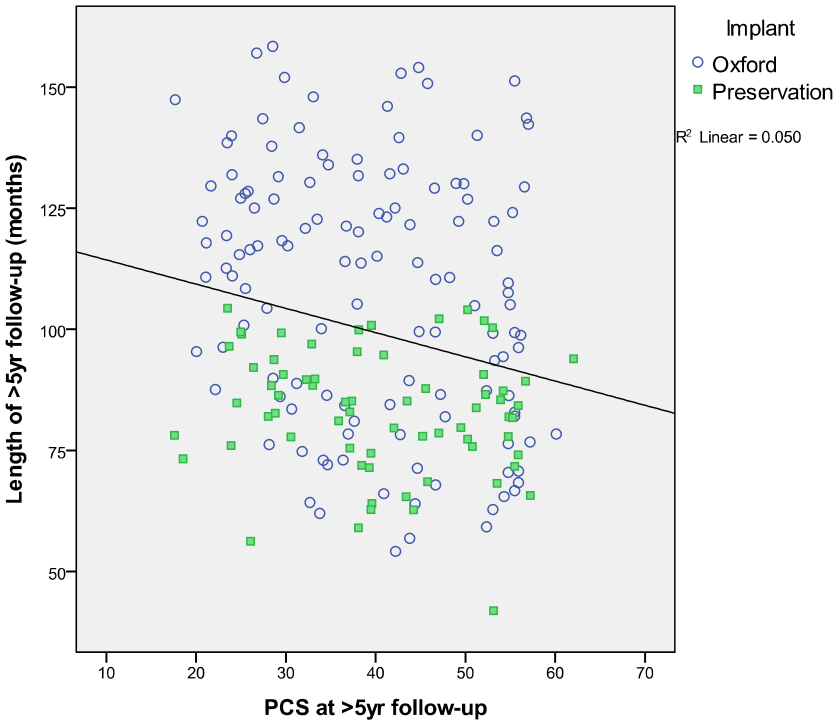

Figure 3.5 Scatter graph of length of follow-up and >5 year PCS. Across all UKRs this negative correlation was significant (Pearson's correlation -0.223, p=0.002).

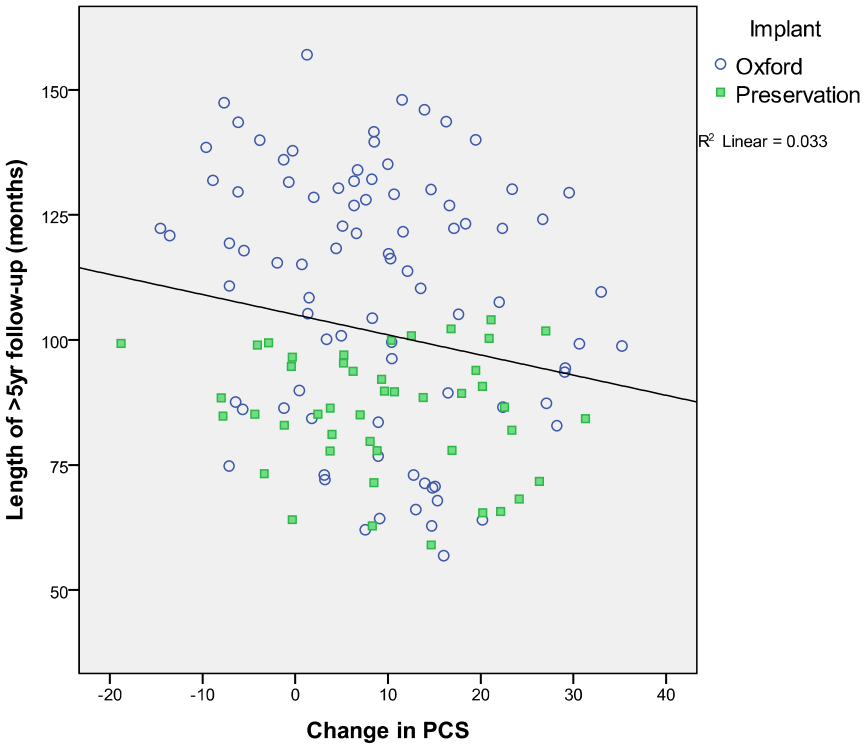

Figure 3.6 Scatter graph of length of follow-up and change in PCS. Across all UKRs, this negative correlation was borderline significant (Pearson's correlation -0.183, p=0.036).

3.4.2.3 Oxford Knee Score

Oxford knee score improved significantly in both UKR implants (Table 3.4, Figure 3.7). Repeated measures ANOVA showed significant improvements in OKS in both the Oxford ($p<0.001$) and Preservation implants ($p<0.001$) (Figure 3.8). No difference was found in OKS from 1 to 5 years in the Oxford ($p=0.280$, paired T-test) or the Preservation group ($p=0.404$). There were no significant differences in improvement in OKS between implants at 1 or 5 years (Table 3.4). A mild deterioration in OKS at >5years occurred with longer follow-up (Figure 3.9), but there was no significant correlation between change in OKS and length of follow-up (Figure 3.10).

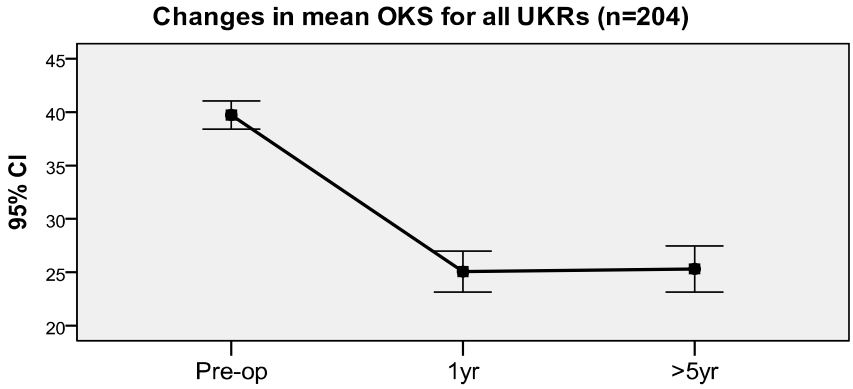

Figure 3.7 OKS trend over >5 years for all UKRs.

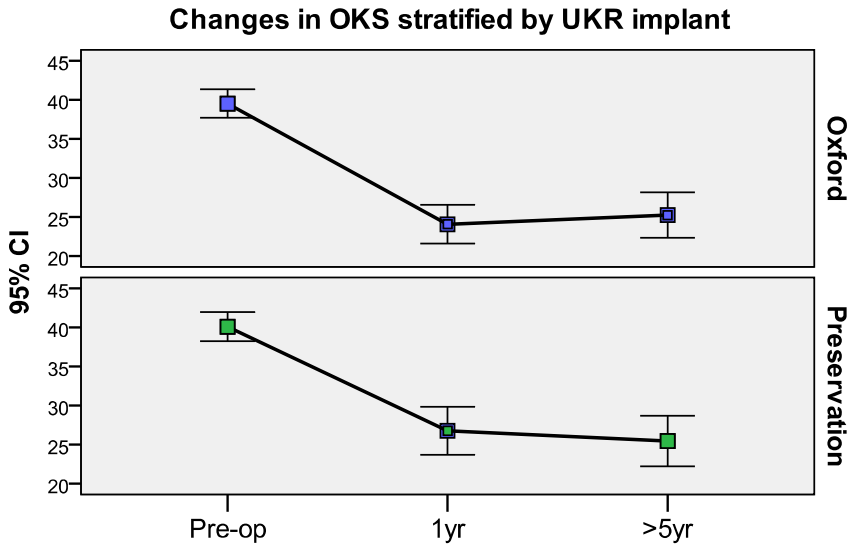

Figure 3.8 OKS trend over >5 years by implant.

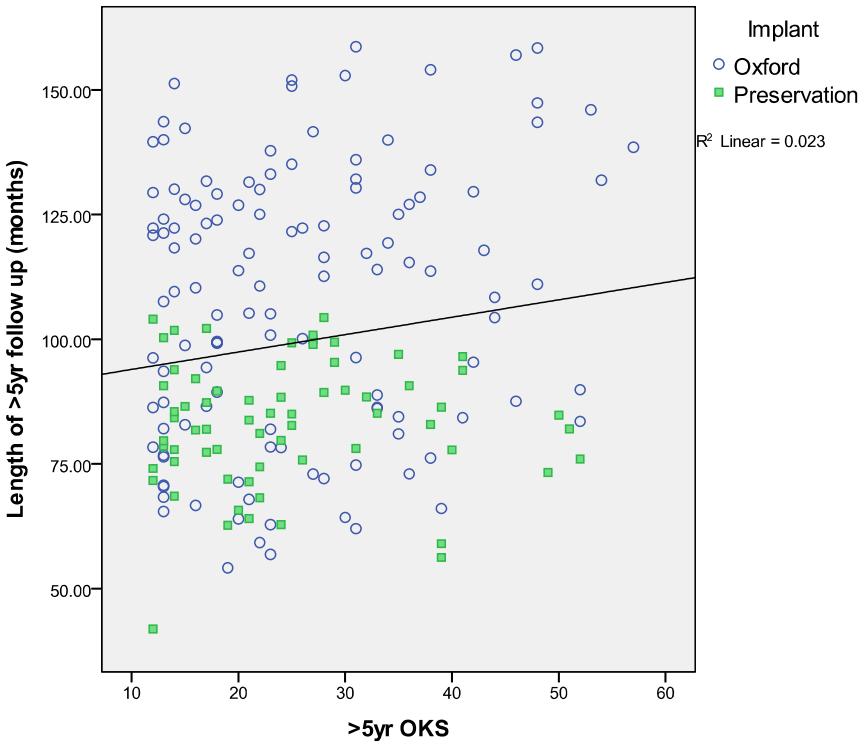

Figure 3.9 Scatter graph of length of follow-up and >5 year OKS

(Pearson's correlation -0.152, p=0.036).

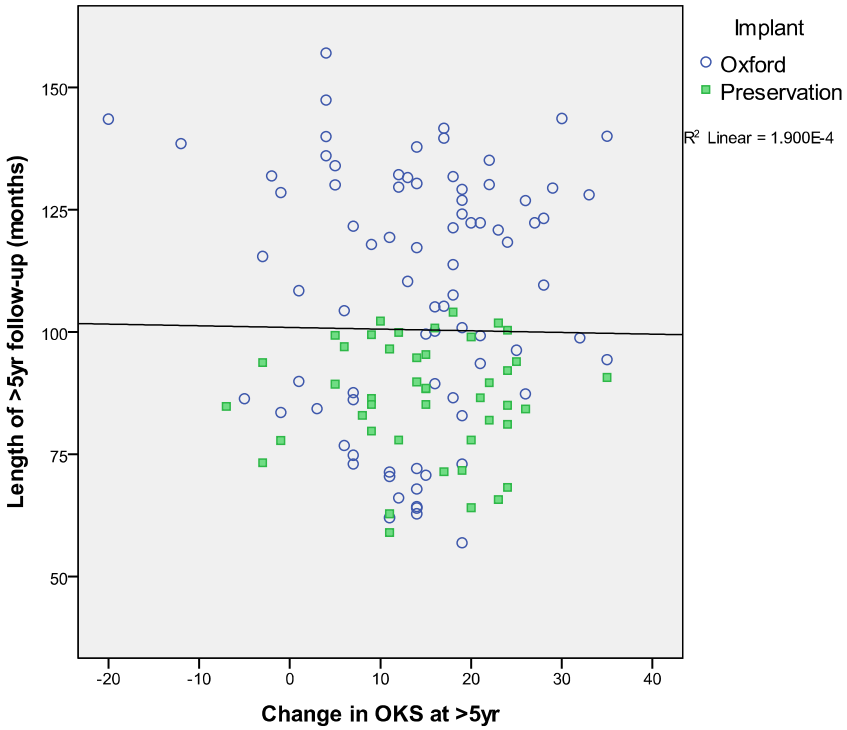

Figure 3.10 Scatter graph of length of follow-up and change in >5 year OKS

(Pearson's correlation -0.014, p=0.879).

Age, BMI and weight did not correlate with improvement in OKS at 1 year in either implant. At >5 years, significant correlations existed between OKS and BMI in both implants (Table 3.5). When stratified into the World Health Organisation BMI grades (underweight <18.5, normal 18.5-24.9, overweight 25-29.9, obese 30-34.9, morbidly obese >35) a BMI of >35 is associated with worsening OKS from 1 to >5 years of a mean 8.7 points (Figure 3.11. This is not seen in those with a BMI of <35 who show a mean improvement of 0.4. This difference is significant (p=0.001, 95%CI -14.3 to -3.8, unpaired T-test). Age showed a weak correlation with >5 year OKS in the Oxford implant only (Table 3.5). When stratified into age groups (Figure 3.12), the over 75s displayed a significant decline in OKS from 1 to >5 years compared to the under 75s (p=0.039, 95%CI -10/6 to -0.3, unpaired T-test). Unsurprisingly the OKS correlated strongly with the VAS for pain, PCS and MCS in both groups (Table 3.5).

Table 3.5 Correlations with >5year OKS

	Pearson's Correlation with >5 yr OKS	
Variable	**Oxford**	**Preservation**
5yr PCS	-0.721**	-0.729**
5yr VAS	0.646**	0.575**
5yr MCS	-0.544**	-0.442**
BMI	0.325*	0.307*
Age	-0.198*	-0.167
Weight	0.101	0.181

** Significant at 0.01 level, *Significant at 0.05 level

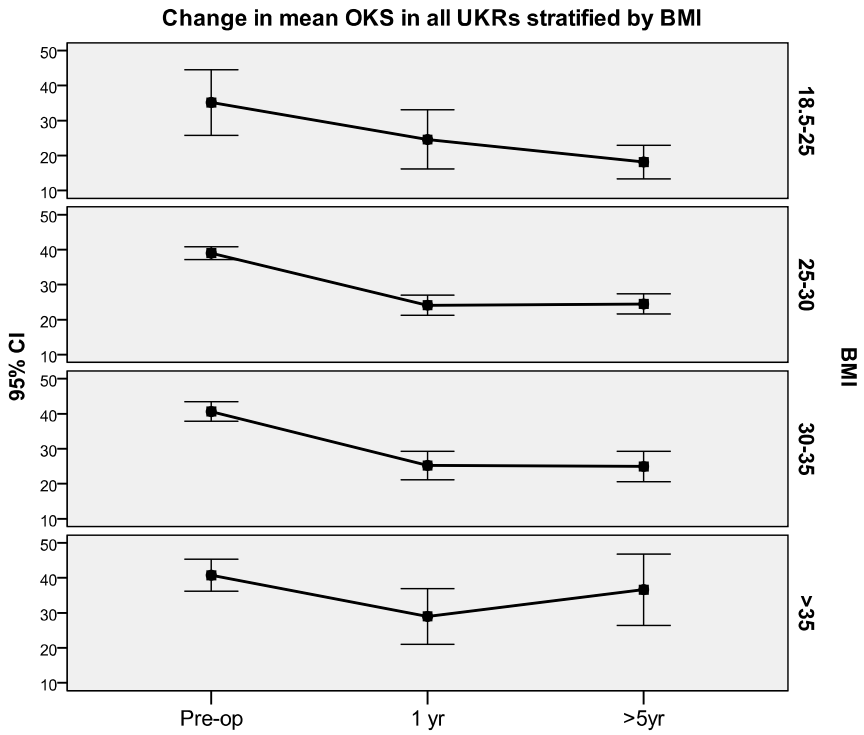

BMI	18.5-25	25-30	30-35	>35	Total
Frequency	27	100	49	22	198
%	13.6	50.5	24.7	11.1	100

Figure 3.11 Changes in OKS by BMI grades for all UKRs. The decline in OKS from 1 to 5 yrs in those with a BMI of >35 compared to those with BMI<35 is significant (p=0.001).

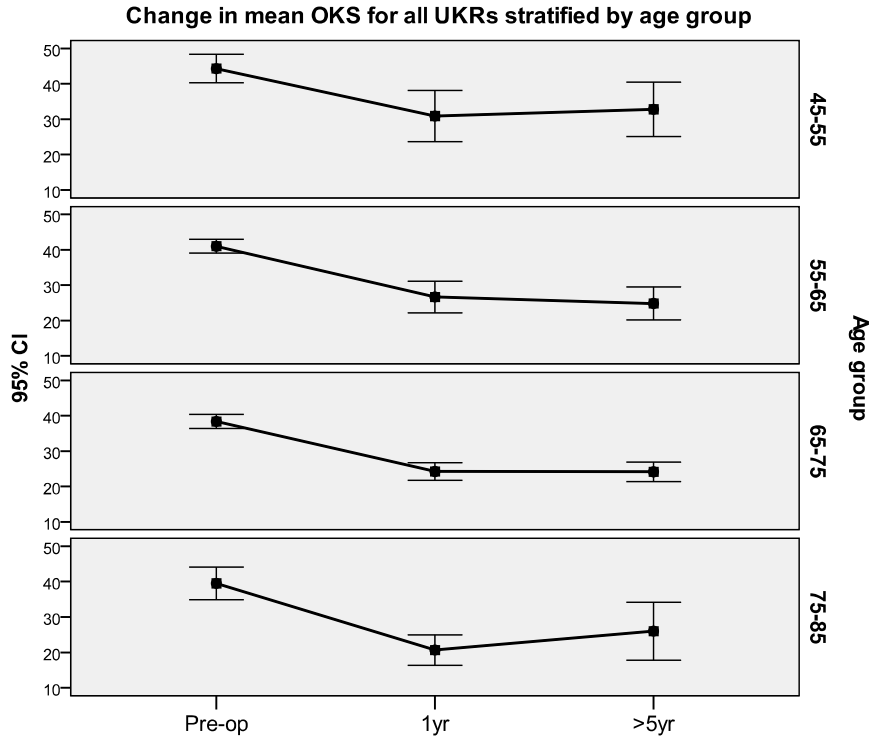

Age	45-54	55-64	65-74	75-85	>85	Total
Frequency	18	74	106	34	2	234
%	7.7	31.6	45.3	14.5	0.9	100

Figure 3.12 Changes in OKS by age groups for all UKRs. The decline in OKS from 1 to 5 yrs in those with >75 years compared to those <75 is significant (p=0.039).

Depression (Figure 3.13) and total number of comorbidities were not associated with either preoperative OKS, or improvements therein, at 1 and 5 years in either group. The presence of back pain was significantly associated with a worse preoperative OKS (p=0.021, two sample t-test), but was no longer significant postoperatively (1 year p=0.744, 5 years p=0.159).

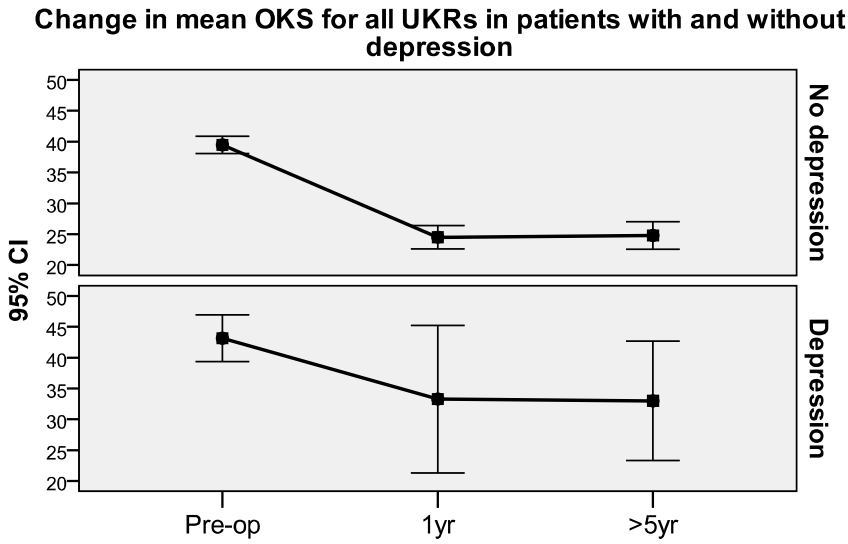

Figure 3.13 Trends in OKS for UKR patients with and without depression.

3.4.2.4 Patient Satisfaction

Overall, 99/122 (81.1%) of patients with an Oxford UKR and 54/69 (78.3%) with a Preservation UKR were satisfied with their knee at 5 years (Figure 3.14). Satisfaction was significantly associated with improvement in OKS in the Oxford group (p<0.001, two sample T-test) but not in the Preservation group. Satisfaction with pain relief was high in both groups: Oxford 88.7%(110/124): Preservation 87.6% (57/65). There were no significant differences in satisfaction parameters between implants (figure 3.14).

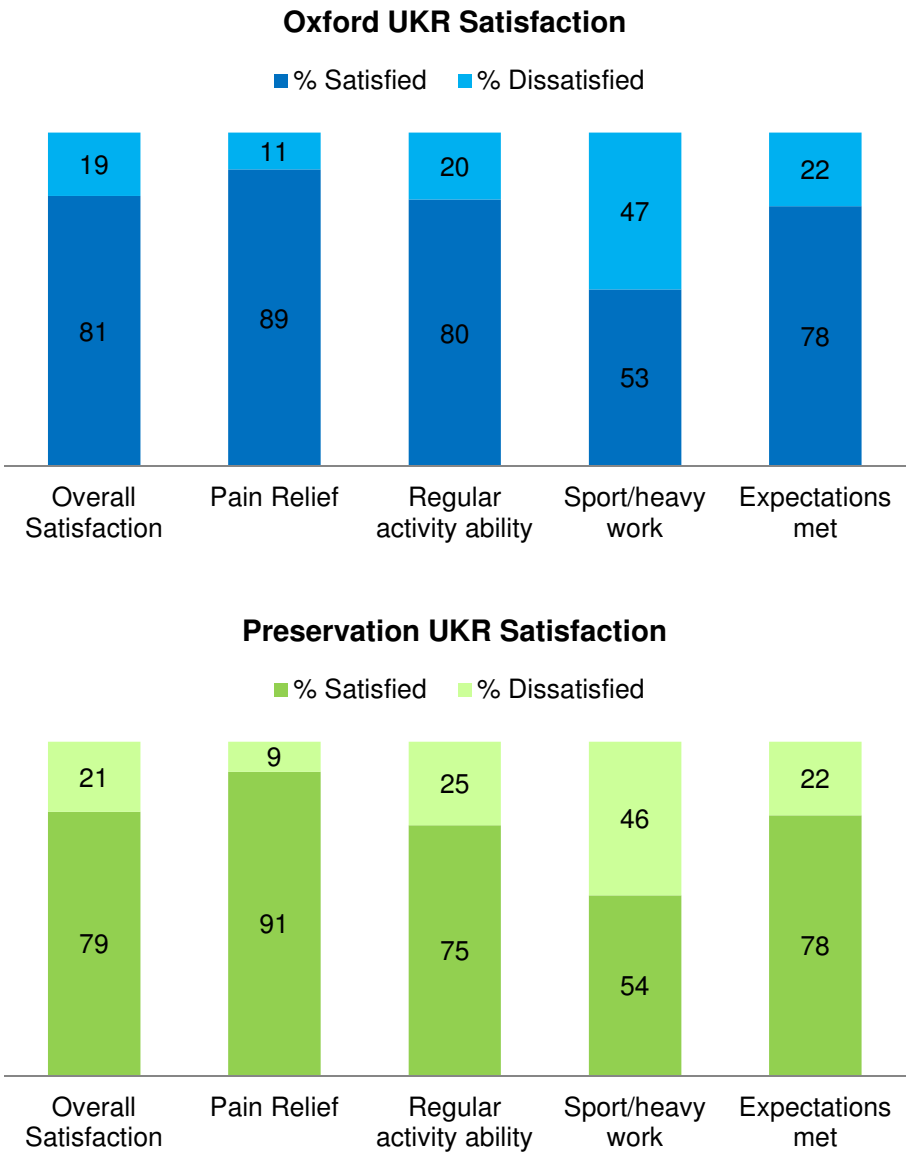

Figure 3.14 Patient satisfaction at >5 years by UKR implant.

Patient satisfaction at 5 years was significantly associated with preoperative MCS and depression in both groups (Table 3.6). Age, sex, BMI, weight, preoperative OKS and PCS were not significantly associated with long-term satisfaction.

Table 3.6 Preoperative predictors of satisfaction at >5years.

	Oxford (n=158)			Preservation (n=75)		
	Satisfied	**Dissatisfied**	**P value**	**Satisfied**	**Dissatisfied**	**P value**
Female	47/96 [49]	8/23 [35]	0.221 $^{\tau}$	32/54 [59]	8/15 [53]	0.681 $^{\tau}$
Age	67.5 (7.4)	65.0 (8.6)	0.167*	68.1 (8.8)	66.7 (10.5)	0.609*
BMI	28.7 (4.3)	30.6 (4.4)	0.084*	28.2 (4.4)	29.8 (6.4)	0.285*
Wt (kg)	82.5 (13.7)	82.5 (17.4)	0.990*	79.0 (15.3)	78.5 (16.7)	0.927*
PROMs						
OKS	39.3 (8.1)	39.2 (7.7)	0.986*	39.6 (5.3)	36.7 (6.4)	0.237*
PCS	30.5 (6.8)	28.4 (4.55)	0.211*	30.5 (7.3)	35.5 (5.5)	0.119*
MCS	52.9 (10.6)	44.8 (13.5)	0.007*	53.4 (10.4)	43.3 (7.6)	0.031*
Co-morbidities						
Depression	3/99 [3]	8/23 [35]	<0.001 $^{\tau}$	2/54 [4]	4/14 [29]	0.003 $^{\tau}$
Back Pain	36/99 [36]	13/23 [56]	0.076 $^{\tau}$	16/54 [30]	8/14 [57]	0.055 $^{\tau}$
POJ	46/99 [46]	16/23 [70]	0.046 $^{\tau}$	24/54 [44]	8/14 [57]	0.396 $^{\tau}$
Total	1 {1}	1{0.75}	0.150 $^{\tau}$	1	3 {3}	0.019 $^{\tau}$

Mean (SD), number [%] , median {IQR}. $^{\tau}$ Chi squared test, * two sample T-test,

Postoperatively, >5 year PCS, MCS, VAS pain score, OKS and improvement in OKS were all significantly associated with patient satisfaction at >5 years in the Oxford group (Table 3.7). Only VAS pain score was significantly associated with satisfaction in the Preservation group.

Table 3.7 Associations with satisfaction at >5years.

	Oxford (n=158)			Preservation (n=75)		
	Satisfied	**Dissatisfied**	**P value**	**Satisfied**	**Dissatisfied**	**P value**
OKS						
5yr	22.14 (8.67)	42.04 (9.44	<0.001*	24.7 (10.8)	23.3 (12.6)	0.736*
Imp to 5 yrs	17.1(8.5)	3.3 (8.97)	<0.001*	14.0 (9.5)	16.5 (10.3)	0.575*
SF-12						
PCS	42.0 (11.2)	30.5 (7.6)	<0.001*	39.5 (11.4)	46.6 (9.4)	0.102*
MCS	51.7 (9.6)	41.4 (13.8)	<0.001*	51.1 (10.0)	44.5 (9.4)	0.093*
Pain VAS	14.9 (21.1)	48.0 (32.7)	<0.001 $^{\infty}$	14.6 (20.5)	47.7 (33.3)	0.010 $^{\infty}$

Mean (SD), number [%]. * Two sample T-test, $^{\infty}$ Mann-Whitney U-test

3.4.2.5 Pain

Pain, as reported on a VAS at 5 years, was no different between implants (Table 3.7). There was no significant correlation between 5yr VAS and BMI or weight in either group (Table 3.8). Five year OKS, PCS and MCS and VAS correlated well in both groups. A mild correlation existed between pain and younger age in the Oxford group only.

Table 3.8 Correlations with pain VAS at >5 years by implant.

	Pearson's Correlation with 5 yr VAS	
Variable	**Oxford**	**Preservation**
5yr OKS	0.646**	0.575**
5yr PCS	-0.441**	-0.313*
5yr MCS	-0.296**	-0.300*
Age	-0.220*	0.029
BMI	0.145	0.198
Weight	0.027	0.159

** Significant at 0.01 level, *Significant at 0.05 level

The location of pain did not differ significantly between UKR implants (Figure 3.15). Though there is a trend towards more medial pain in the Preservation group, this was not significant (p=0.127, Chi squared).

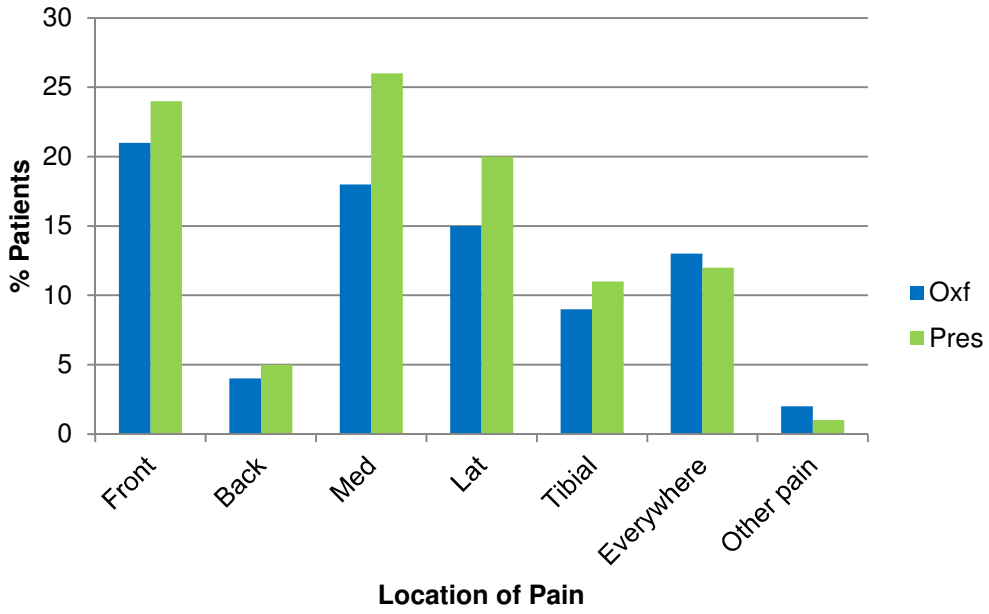

Figure 3.15 The location of pain at 5 years by implant.

In the Oxford group there was a significant association between medial knee pain and age (p=0.02, 95% CI 0.47 to 5.3, two sample T-test), but no association with BMI (p=0.393) or weight (p=0.944). In the Preservation, there was a non-significant trend to medial pain with increased weight (p=0.073, 95% CI -16.6 to 0.75) but no significant relationship with BMI (p=0.221) or age (p=0.615). The presence of medial pain was significantly associated with satisfaction in the Oxford group (p<0.001 Chi squared) but not the Preservation group (p=0.187 Chi squared).

3.4.2.6 Expectations

Of patients with an Oxford UKR, 98/121 (81%) reported that their UKR met their expectations at 5 years. This was 49/64 (77%) in the Preservation UKR group. This difference was not significant (p=0.566, Chi squared test). One hundred and fifty four patients completed full expectation questionnaires. Figure 3.16 shows the percentage of patients whose expectations were fulfilled in each group. Though the Preservation group displays less fulfilment with daytime pain relief (73% compared with 90.5%) this was not significant (p=0.247 Chi squared). There was no difference in overall expectation fulfilment scores between implants (Oxford 22.7, Preservation 21.1, p=0.508, Mann Whitney U test).

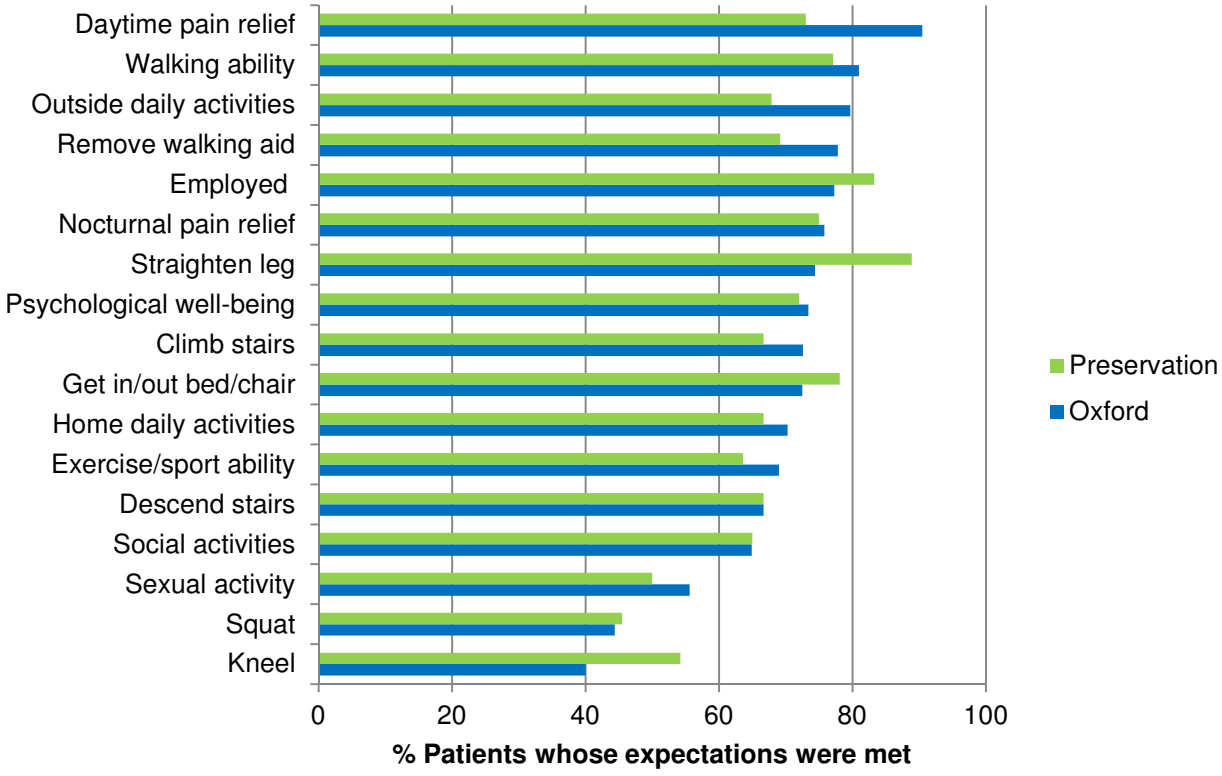

Figure 3.16 Expectation fulfilment at 5 years by UKR implant.

3.4.3 Implant Survivorship

All 289 Phase III Oxford and 111 Preservation UKRs performed between 1999 and 2007 were included (Figures 3.17). Forty patients within the Oxford group and 13 patients in the Preservation group had undergone bilateral procedures. Fifty seven patients from the Oxford group and 12 from the Preservation group had died of unrelated causes with their UKR in situ. Twenty six Oxford UKRs (11.2%) and 11 Preservation UKRs (11.1%) had been revised at the time of writing. Three of the Oxford UKR patients who had undergone revision had subsequently died of unrelated causes. Eight patients (3.25%), all with Oxford UKRs, were lost to follow-up and could not be traced. Tables 3.9 and 3.10 detail the revisions in each UKR group including mode of failure and revision implants required. Table 3.11 details other reoperations.

Table 3.9 Preservation UKR revisions. Survival in months, mode of failure confirmed at revision and the revision components required are included.

Sex	Age	Survival	Mode of failure	Revision Components	
				Constraint	**Augment**
M	66	2	Tibial subsidence	TKR	Med tibia
F	71	26	Femoral loosening	TS	Stems
F	78	26	Lateral OA	TKR	None
F	55	27	Pain	TKR	None
M	61	29	Pain	TKR	None
M	61	31	Periprosthetic fracture	TKR	Med tibia
M	65	36	Pain	TKR	None
F	60	42	Pain	TKR	None
M	65	42	Pain	TKR	None
F	70	55	Lateral OA	TKR	None
F	61	101	Lateral OA	TKR	None

TKR- cruciate retaining TKR. TS – total stabilised TKR prosthesis.
Med tibia– medial tibial block augment with stem, Stem – tibial stem only,
Stems – both femoral and tibial stems.

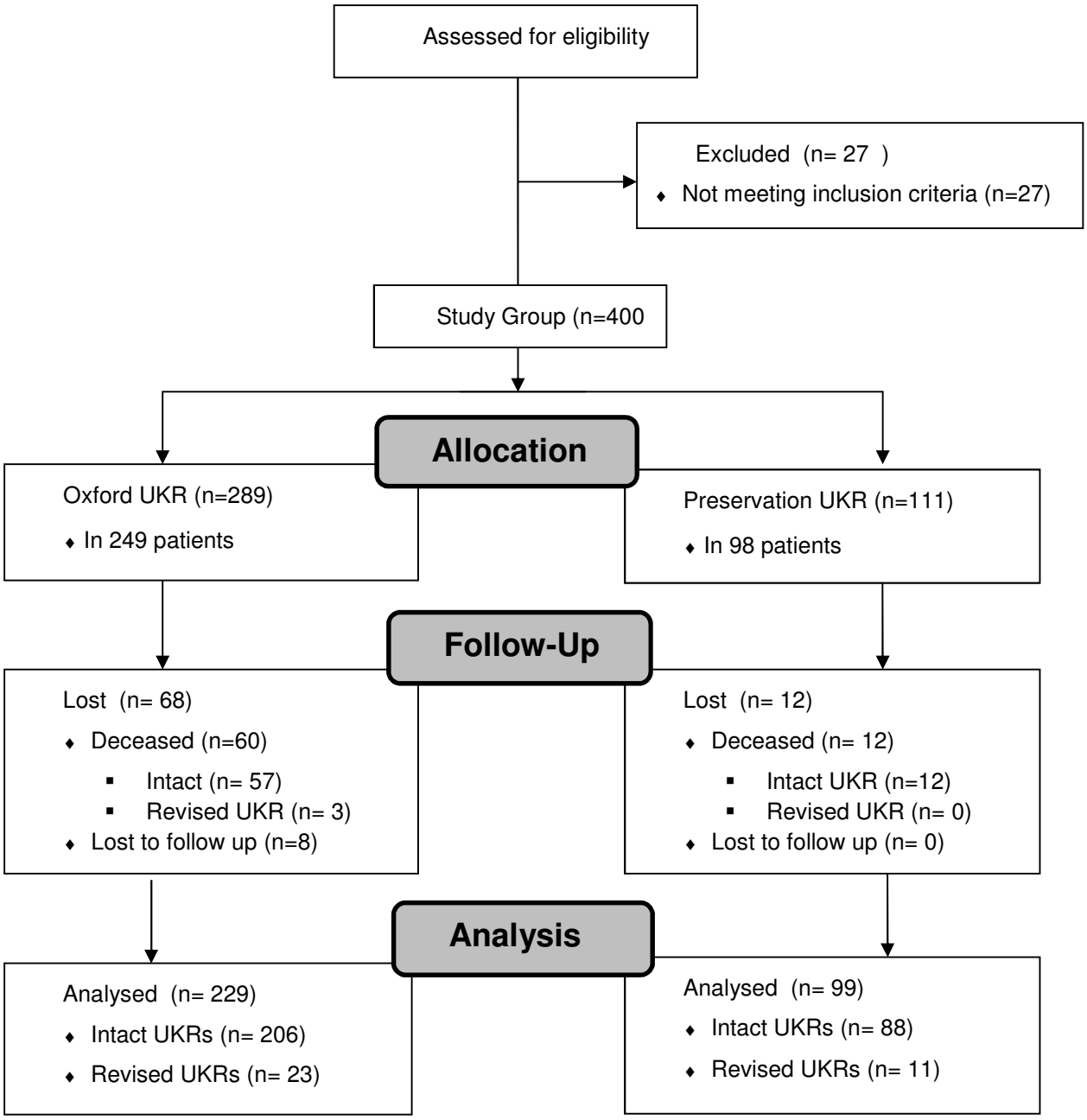

Figure 3.17 The UKR survivorship cohort.

Table 3.10 Oxford UKR revisions. Survival in months, mode of failure confirmed at revision and the revision components required are included. Cases underlined in bold required further revision. Cases in italics are deceased.

Sex	Age	Survival	Mode of failure	Revision Components	
				Constraint	**Augments**
F	68	2	Tibial loosening	TKR	Med tibia
M	*76*	*10*	*Periprosthetic fracture*	*TKR*	*None*
M	74	15	Bearing dislocation	TKR	None
F	56	17	Tibial subsidence and loosening	TKR	Med tibia
F	72	18	Pain	TKR	None
M	**59**	**19**	**Femoral loosening**	**TKR**	**None**
F	72	20	Tibial subsidence and loosening	TKR	Med tibia
F	*75*	*23*	*Tibial subsidence and loosening*	*TKR*	*Stem*
F	**65**	**27**	**Tibial subsidence and loosening**	**TKR**	**Med & lat**
M	60	31	Tibial subsidence and loosening	TKR	Stem
F	81	40	Lateral OA	TKR	Stem
M	**51**	**41**	**Septic loosening**	**TKR**	**Stem**
M	*69*	*45*	*Pain*	*TKR*	*Med tibia*
F	56	54	Tibial subsidence and loosening	TS	Stems
F	77	57	Lateral OA	TKR	Stem
M	79	74	Lateral OA	TKR	None
F	83	75	Lateral OA	Hinge	Stems
M	59	88	Tibial and femoral loosening	TKR	None
M	48	100	Lateral OA	TKR	None
M	60	106	Tibial subsidence and loosening	TKR	Med tibia
F	57	111	Lateral OA	TKR	None
F	55	117	Lateral OA	TKR	Med tibia
F	69	120	Lateral OA	TKR	None
M	53	126	Lateral OA	TKR	Stem
M	64	137	Lateral OA	TKR	None
M	59	140	Lateral OA	TKR	None

Table 3.11 Reoperations (excluding revisions) for both UKR implants.

Sex	Age	Months to reoperation	Re-operation	Indication
Oxford				
M	70	0.5	Debridement and bearing exchange	Infection
M	58	5	MUA	Stiffness
M	51	10	Arthroscopy – r/o LB	Locking
F	62	106	Arthroscopy – ACL attrition rupture	Instability
Preservation				
F	72	2.5	MUA	Stiffness
M	68	19	Arthroscopy – r/o cement LB	Locking
F	48	59	Arthroscopy – r/o LB	Locking

r/o – removal of, LB – loose body, MUA – manipulation under anaesthetic, ACL – anterior cruciate ligament

There were 3 cases of re-revision in the Oxford group. The first was a 51 year old male who underwent arthroscopic removal of a loose body at 10 months post Oxford UKR and developed a sensitive *Staph aureus* infection as a complication of this procedure. He underwent arthroscopic washout and subsequent open debridement and polyethylene exchange 2 weeks following the arthroscopy and was treated with appropriate antibiotics. He went on to develop septic loosening of femoral and tibial components and underwent single stage revision at 41 months post index UKR. He was revised to a TKR implant with impaction grafting of a contained (Anderson Orthopaedic Research Institute grade T1) medial tibial defect with a stemmed tibial component. This subsequently failed for mechanical reasons with an atraumatic periprosthetic proximal tibial fracture requiring re-revision to a total stabilised implant with complex proximal tibial reconstruction (mesh and impaction grafting) and both tibial and femoral augments and stems. The second patient requiring re-revision was a 65 year old lady initially revised at 27 months for tibial subsidence and loosening. She was revised to a TKR with medial and lateral tibial augments and a tibial stem. Thirty one months following this (58 months post index UKR) she sustained a traumatic periprosthetic fracture necessitating re-revision to a hinged prosthesis.

Lastly, a 59 year old man underwent revision to a TKR without augments at 19 months post Oxford UKR for femoral loosening. Four years following this (68 months post index UKR) the TKR required revision to a total stabilized implant with medial tibial augment and tibial and femoral stems for tibial loosening.

Kaplan-Meier survival analysis demonstrated no significant differences in survival between the two UKR implants for all causes of failure (p=0.303, Log Rank), though 10 year survival was markedly higher in the Oxford group at 90% (95% CI 86 to 94.3%) compared to the Preservation at 80% (95% CI 60.7 to 99.1%) (Figure 3.18, Table 3.12). Examining failures for mechanical reasons, by excluding septic loosening and lateral OA development, again there was no difference in implant survival over the study period (p=0.408, Log Rank). Similarly no differences were apparent for failure by tibial collapse or loosening (p=0.653). There was, however, significant differences in failure due to unexplained pain between the implants with a higher failure rate in the Preservation all-polyethylene cohort (p=0.005, Log Rank) (Figure 3.19).

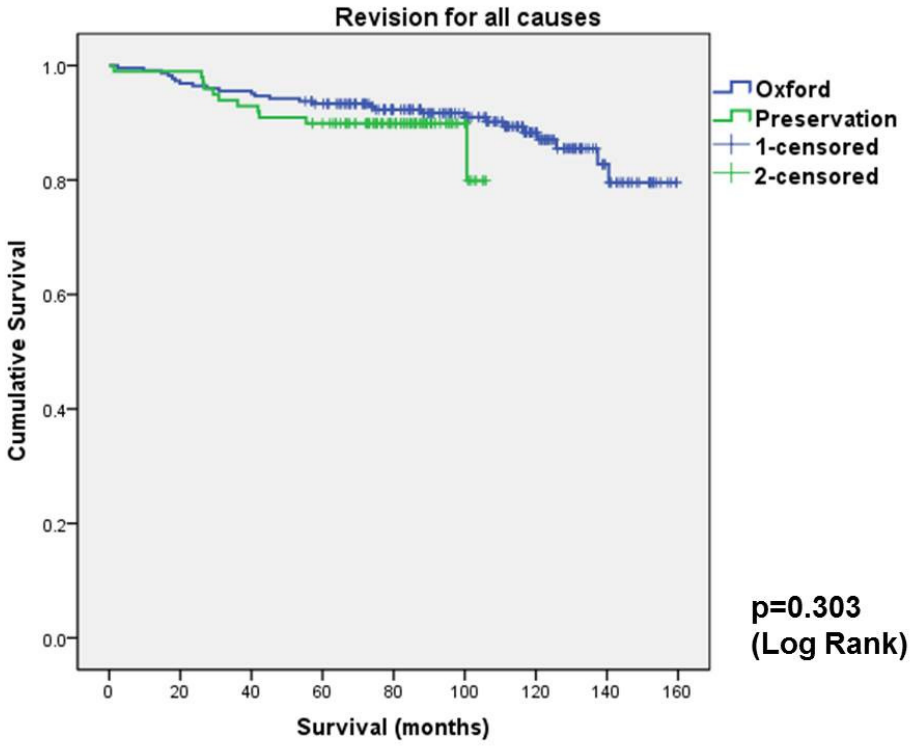

Figure 3.18 Kaplan Meier survival curve for both UKR implants (all cause failures).

Table 3.12 Kaplan-Meier UKR implant survival up to 15 years with 95% confidence intervals for all cause failures.

Survival	Oxford Mean (95%CI)	Preservation Mean (95% CI)	p-value
5yr	92.3 (89.0 to 95.6)	89.9 (84.0 to 95.8)	0.303
10yr	90.2 (86.0 to 94.3)	79.9 (60.7 to 99.1)	
15yr	85.5 (79.4 to 91.6)	-	

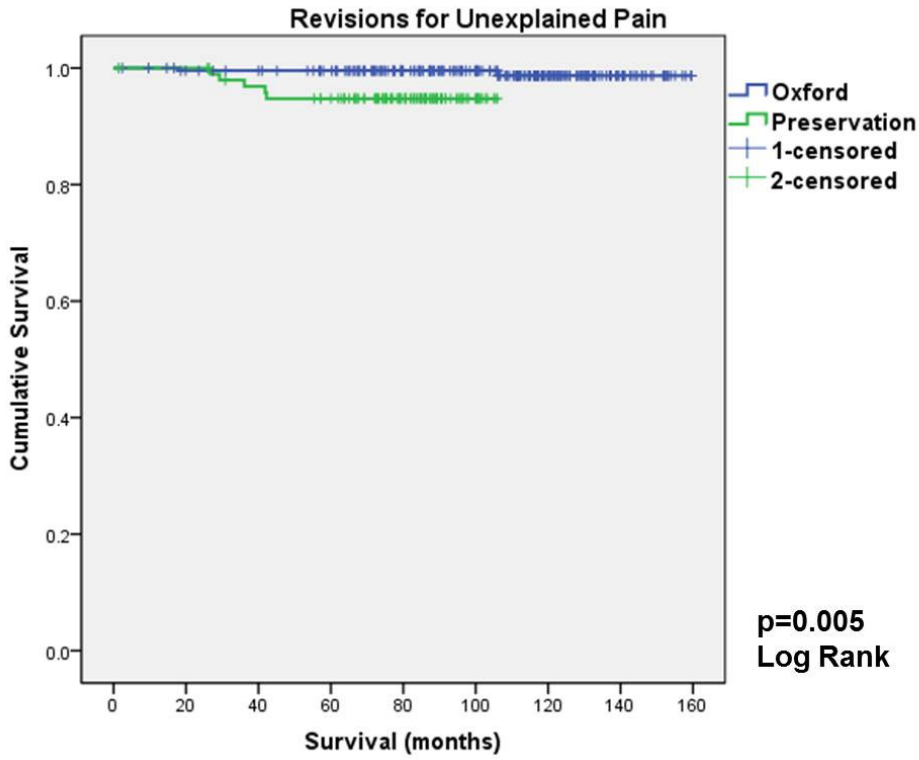

Figure 3.19 Kaplan-Meier survival curve for revisions due to unexplained pain, both UKR implants.

There were no significant differences in preoperative variables (age, sex, BMI, weight, OKS, SF12) between those patients who went on to revision, and those whose implant survived for either UKR implant (Tables 3.13 and 3.14).

Table 3.13 Preoperative characteristics of intact and revised Oxford UKRs. Deceased patients excluded.

Oxford UKR	Intact (n=206)	Revised (n=26)	P value	95% CI
Female Sex	101 [49]	13 [50]	0.775 ᵀ	
Age	66.5 (8.0)	64.3 (10)	0.218*	-1.3 to 5.8
BMI	29.0 (4.25)	28.1 (4.0)	0.376*	-1.1 to 2.9
Weight (kg)	81.0 (13.9)	80.4 (15.8)	0.611*	-6.0 to 7.2
OKS	39.5 (7.7)	41.9 (6.0)	0.337*	-7.4 to 2.5
PCS	30.3 (6.4)	26.3 (6.2)	0.059*	-0.16 to 8.2
MCS	52.3 {17.9}	54 {21.4}	0.949∞	

Mean (SD), number [%] , median {IQR},

ᵀ Chi squared test, * two sample T-test, ∞Mann-Whitney U test

Table 3.14 Preoperative characteristics of intact and revised Preservation UKRs. Deceased patients excluded.

Preservation UKR	Intact (n=88)	Revised (n=11)	P value	95% CI
Female Sex	50 [57]	6 [55]	0.886 ᵀ	
Age	68.0 (8.8)	65.4 (6.3)	0.345*	-2.9 to 8.1
BMI	28.9 (4.7)	29.6 (3.5)	0.639*	-3.6 to 2.2
Weight (kg)	79.5 (15.2)	79.4 (12.5)	0.986*	-9.4 to 9.6
OKS	39.8 (5.9)	42.3 (8.1)	0.486*	-9.7 to 4.7
PCS	31.2 (7.1)	40.1 (7.9)	0.091*	-19.1 to 1.5
MCS	54.0 {16.2}	35.7 {26}	0.184∞	

Mean (SD), number [%]

ᵀ Chi squared test, * two sample T-test, ∞Mann-Whitney U test

Preservation UKRs were revised significantly earlier (mean 38 months) than Oxford UKRs (mean 62 months, p=0.023, T-test) (Table 3.15). There were no significant differences in age, sex, BMI, weight or pre-revision PROMs between Oxford and Preservation groups. However, the improvement in OKS following revision of UKR was greater in the Oxford group (19.9 points compared to 8.3) and this approached significance (p=0.061, unpaired T-test). The modes of failure were different for the implants (Figures 3.20 and 3.21). The development of lateral compartment OA was the most prevalent mode of failure in the Oxford group, with revision for unexplained pain predominating in the Preservation group. 6/13 (46%) of Preservation revisions were for pain compared to 2/26 (7.6%) of Oxford revisions. This difference was significant (p=0.007, Chi square), consistent with the Kaplan-Meier analysis above (Figure 3.19). Implant type and mode of failure displayed association that approached significance (Cramer's V association 0.622, Chi square 0.069).

Table 3.15 Comparison of Oxford and Preservation UKR revisions.

Variable	Revised Oxford UKR (n=26)	Revised Preservation UKR (n=11)	P value	95% CI
Implant Survival	62.0 (45.2)	37.9 (24.8)	0.023*	4.3 to 53.4
Female sex	13 [50]	6 [55]	0.897 $^{\tau}$	
Age	64.3 (10.0)	65.4 (6.3)	0.687*	-6.9 to 4.6
BMI	28.1 (4.0)	29.6 (3.5)	0.316*	-4.4 to 1.5
Wt (kg)	80.4 (15.6)	79.4 (12.5)	0.860*	-10.3 to 12.3
Pre-Revision				
PCS	25.9 {11}	40.6	0.539$^{\infty}$	
MCS	54 {21}	35.7	0.785$^{\infty}$	
OKS	40.5 {10}	40.5	0.607$^{\infty}$	
Post-Revision				
Imp OKS	19.9 (11.4)	8.3 (10.9)	0.061*	-0.59 to 23.7

Mean (SD), number [%], or median {IQR}

$^{\tau}$ Chi squared test, *Two-tailed student T-test, $^{\infty}$ Mann-Whitney U-test

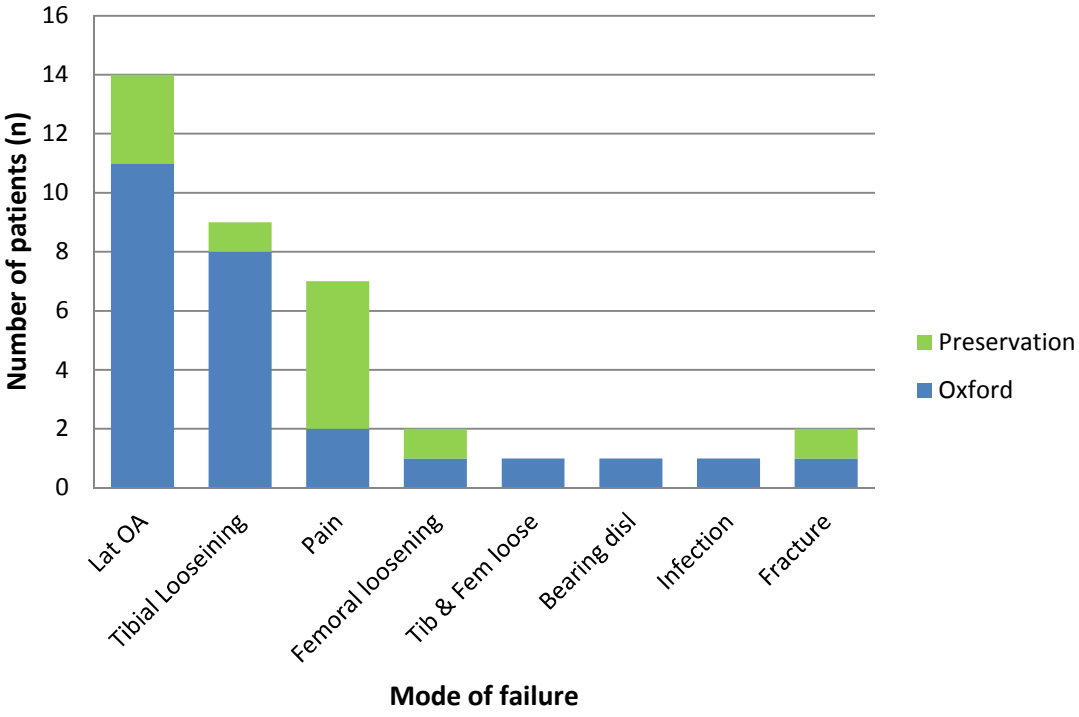

Figure 3.20 Modes of failure of UKR by implant.

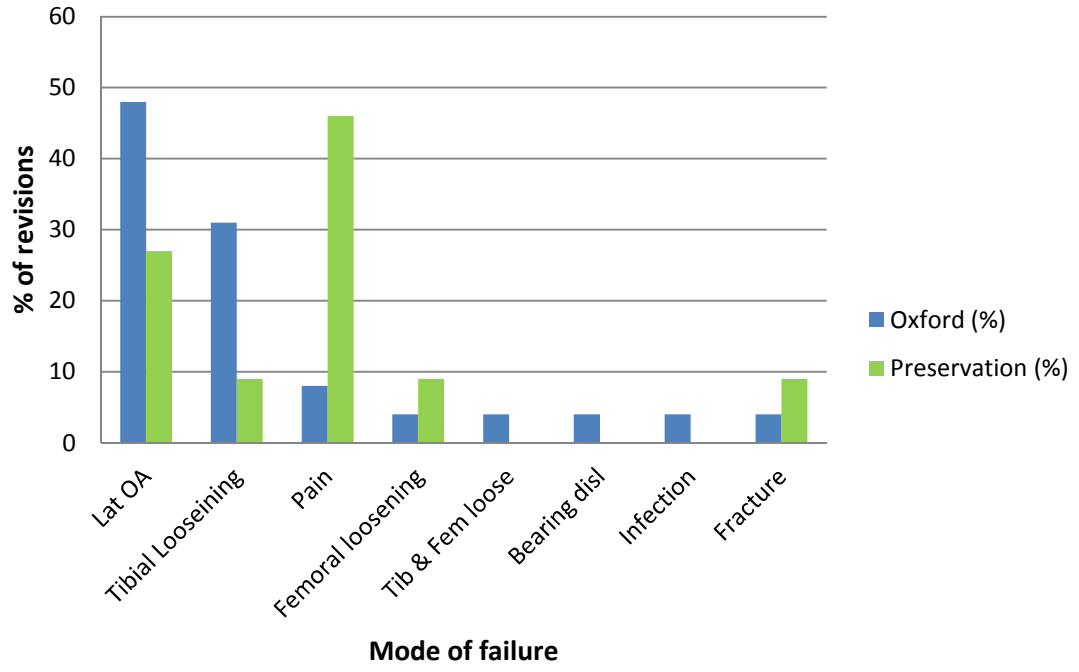

Figure 3.21 Modes of failure of UKR by implant (percentage of revisions).

The revision implants necessary to recreate a balanced, stable knee joint differed between UKR designs (Figure 3.22). Revision of Oxford UKRs necessitated the use of augments or increased constraint more frequently than did revision of the Preservation UKRs. A non-augmented standard primary TKR implant was used in 8/11 (73%) of Preservation revisions compared to 10/26 (38%) of Oxford revisions. This difference approached significance (p=0.057, Chi squared). Those UKRs revised to a non-augmented primary TKR (that did not require re-revision) were revised at a mean of 89 months (SD46.4). Those revised to augmented or constrained implants ultimately, underwent first revision at a mean of 52 months (SD39.6). It would normally be expected that later revisions would be associated with more bone loss and greater deformity secondary to lateral compartment OA and would thus be more likely to require augmentation or constraint.

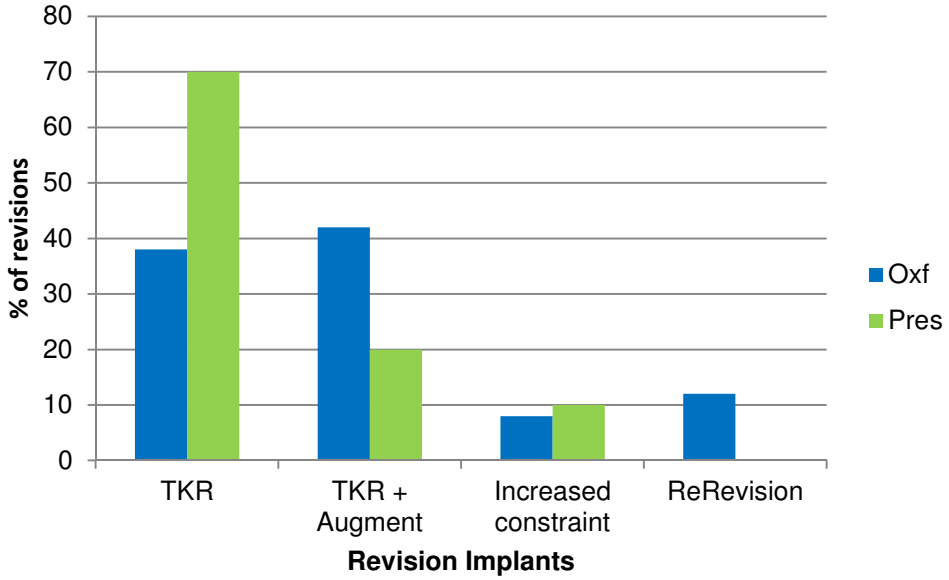

Figure 3.22 Revision components required at first revision by UKR implant.

3.4.3.1 UKR Revisions for Pain

The 8 UKR patients revised for pain consisted of 5 men and 3 women. There was no significant difference in age or absolute weight between those revised for pain and those not. Those revised for pain had a significantly greater BMI than the entire study population (p=0.024, 95%CI 0.7 to 6.6), those unrevised (p=0.027, 95%CI 0.6 to 6.4) and revisions for all other causes (p=0.011, 95%CI 1.2 to 7.3 unpaired T-tests) (Figure 3.23). There was significantly less improvement in the OKS post-revision in those revised for unexplained pain across implants (4.25, SD 11.1) when compared to all other modes of failure (19.4, SD 10.6) (p=0.026 unpaired T-test, 95% CI -28.2 to -2.1). This undoubtedly contributes to the worse improvement in OKS following Preservation revision.

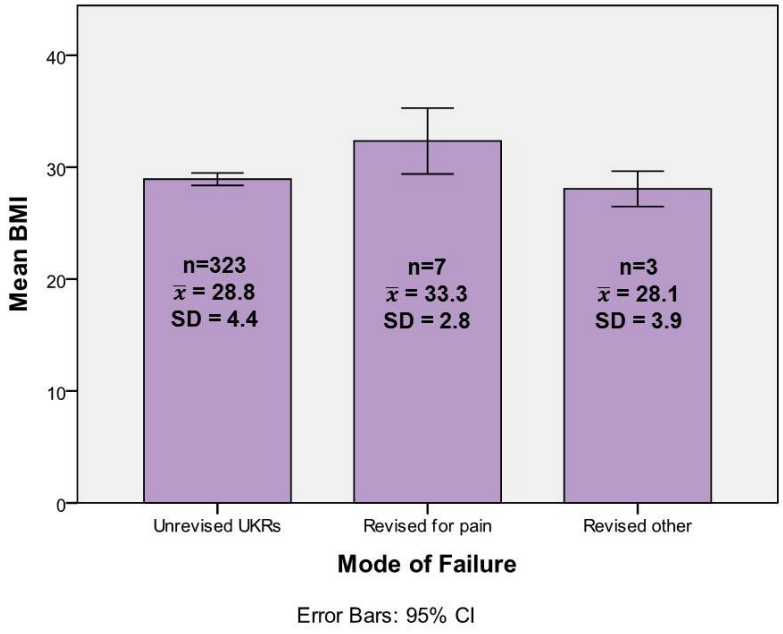

Figure 3.23 Mean BMI in revised and unrevised implants (all UKRs). BMI was significantly greater in those revised for pain compared to those unrevised (p=0.027, 95%CI 0.6 to 6.4) and those revised for other reasons (p=0.011, 95%CI 1.2 to 7.3 unpaired T-tests).

Within the Preservation cohort, those revised for pain had significantly greater BMIs and were younger than those unrevised (Figures 3.24 and 3.25). There were no differences in sex distribution or absolute weight.

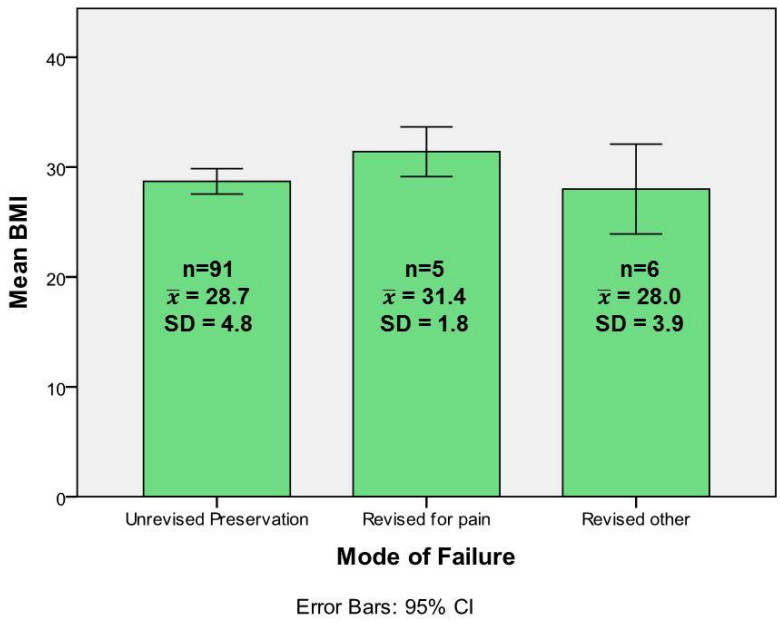

Figure 3.24 Mean BMI in revised and unrevised Preservation UKRs. Those revised for pain had significantly greater BMIs compared to those unrevised (p=0.024, 95%CI 0.44 to 5.0). There was no significant difference when compared to those revised for other reasons (p=0.097, 95%CI -0.79 to 7.6, unpaired T-tests).

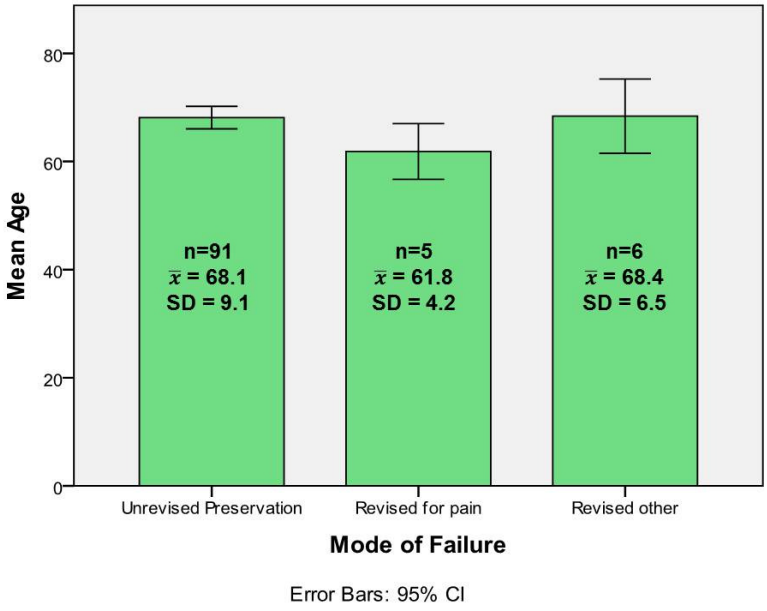

Figure 3.25 Mean age in revised and unrevised Preservation UKRs. Those revised for pain were significantly younger compared to those unrevised (p=0.022, 95%CI -11.3 to -1.2). There was no significant difference when compared to those revised for other reasons (p=0.077, 95%CI -14.0 to 0.88, unpaired T-tests).

3.5 Chapter Discussion

Though outcome did not differ wildly between UKR designs, subtle differences were present in terms of both survival and patient reported outcomes. Though all cause failure did not differ significantly between implants on Kaplan Meier analysis, ten year survival was significantly higher for the Oxford (90%) than the Preservation UKR (80%) and modes of failure differed significantly. The predominant mode of failure in the Oxford UKR was development of lateral compartment OA necessitating revision at mean 100 months. Unexplained pain predominated in the Preservation group with revisions for this cause at a mean of 35 months. Compared to revisions for other modes of failure, and intact UKRs, patients revised for pain had significantly greater BMIs and younger ages. Though the proportion of revisions for pain was significantly greater in the Preservation group, the overall proportion of painful UKRs (patients dissatisfied with pain relief, figure 3.14) was the same across implants. This difference in revision number may represent a different approach to painful Preservation UKRs and painful Oxford UKRs due to a concern regarding lack of implant stiffness in the all-polyethylene Preservation tibias. The larger proportion of revisions for unexplained pain in the Preservation group undoubtedly contributed to the significantly earlier time to revision in this implant (38 versus 62 months).

Adaptive remodelling in the proximal tibia following TKR is known to continue up to 2 years postoperatively and can be detected by persistently elevated uptake on bone scans. It has been previously suggested that as adaptive remodelling stabilises at approximately 2 years, painful UKRs should settle then too (Simpson, et al., 2009). This is not supported by our results where most revisions for pain (6/7) were performed considerably later than 24 months and 18-26% of patients reported ongoing medial pain at >5 years. This is consistent with data from the National Joint Registry where revisions for unexplained pain occur steadily up to 7 years (Baker, et al., 2012; Baker, et al., 2012). Revisions for pain had poorer post-operative outcomes than revisions for other reasons and this supports the findings of others (Kerens, et al., 2013). This fact undoubtedly contributed to the poorer improvement in OKS following Preservation UKR revision compared to Oxford UKR revision.

Interestingly, there were no differences between UKR implants in the percentage of revisions performed for tibial component failures (collapse or loosening). When the Phase III cemented Oxford UKR was first introduced, radiolucent lines were noted around the tibial component in a number of patients. Though these radiolucent lines were subsequently found to be non-progressive and non-pathological by a number of authors (Gray, et al., 2010; Gulati, et al., 2009; Kendrick, et al., 2012), a number of Oxford UKRs had been revised prior to this recognition, particularly those that had been implanted earlier. Seven of fifteen (47%) early Oxford UKR failures at <5 years in this cohort were due to tibial loosening. If these were excluded, the gap between implants in terms of early failures and tibial sided failure would broaden considerably in favour of the Oxford UKR.

In addition to different modes of failure between UKR implants, different revision implants were required. Stems and augments were required more often than not for reconstruction following the metal backed Oxford UKR. The requirement for bone defect management when revising UKRs means that a revision UKR and a standard primary TKR differ considerably in terms of technical difficulty, augment use, constraint and ultimately outcome and survival (Chou, et al., 2012; Pearse, et al., 2010).

The response rate to the >5year follow up questionnaire was good with 204/246 (83%) eligible patients responding. This exceeds the level reported by the National PROMs Programme of England where 65–80 % data capture is reported (Hospital-Episode-Statistics.). Importantly there were no differences between responders and non-responders in terms of preoperative characteristics. The length of >5 year follow up was significantly greater in the Oxford UKR group, reflecting the time period over which this implant used, and this is important in the interpretation of data from this time point for this implant, particularly when comparing long term results of the Oxford UKR with that of TKRs.

Oxford Knee Score improved significantly postoperatively in both UKR implants. There were no differences in *changes* in OKS postoperatively between intact Oxford and Preservation implants. However, patients who had undergone revision, often for pain and by 5 years in the Preservation group, were excluded from this PROMs analysis. For both UKR implants, OKS improvement occurred within the first year, with no significant changes thereafter to >5 years. This is the same pattern as is seen in TKRs (Scott, et al., 2014). Unlike reports for TKRs, the PCS reduced from 1 to >5 years in UKRs, but this likely reflects the significantly longer follow up (mean 100 months) than 5 years in this study.

Across both UKR implants BMI had no effect on one year OKS or improvement therein. However, longer term follow up at >5 years showed a significant decline in OKS in those with a BMI of >35 which was not apparent in those with BMI<35. Cavaignac et al (Cavaignac, et al., 2013) reported no difference in revision risk or patient reported outcomes in 212 UKR patients with BMIs above and below 30 at up to 7 years. This risk of poorer long term UKR outcome with BMI >35 has not previously been reported.

In those with intact UKRs at >5 years, satisfaction was no different between UKR implants (78% Preservation and 81% Oxford). This is comparable with TKR satisfaction reported at one year (Scott, et al., 2010). Patient satisfaction in TKR is known to be multifactorial, but multivariate analysis and complex modelling has shown that patient expectations, clinical outcome (mainly pain relief), and experience of healthcare delivery influence patient satisfaction the most (Hamilton, et al., 2013). Interestingly satisfaction with pain relief here was higher than overall satisfaction for both implants at 88% and 89% respectively. Satisfaction with the ability to do heavy work and sport was however significantly lower (54% and 52%). The slightly lower than anticipated overall satisfaction may reflect a failure to meet expectations of high demand activities rather than a dissatisfaction with pain relief. It must also be borne in mind that this is >5 year, and not one year, satisfaction.

Questions pertaining to pain gave somewhat conflicting results when comparing implants. Visual analogue pain scales and satisfaction with pain relief at >5years displayed no differences between implants. However, fulfilment of pain relief at >5years was significantly lower in the Preservation UKR (73%) compared to the Oxford (91%) with a trend to more medial pain in the intact Preservation UKRs.

The limitations of this study include the retrospective and non-randomised nature of the study, the unequal patient cohort sizes, and the different lengths of follow up. A post-hoc power analysis using the method of Lehr (Petrie, 2006) with 80% power at the two-tailed 5% level, has shown that to detect a clinically significant 3 point difference in the improvement in OKS at one year, each cohort would require 144 patients. As the Preservation cohort eligible for the PROMs element of the study was 75, this may well have led to a type 2 error and failure to detect real differences in the outcomes of these UKR designs.

Medial UKRs incorporating an all-polyethylene tibial component have a higher rate of early failure than a metal backed mobile bearing UKR, predominantly due to revisions prior to 5 years for unexplained pain. Revisions for unexplained pain display significantly less improvement in OKS following revision, than revisions for all other causes. Modes of failure and the reconstruction implants requirements differ significantly between UKR implant types. Metal backed UKRs result in larger bone loss requiring stems and augments more frequently than all-polyethylene tibial components. In those UKRs not revised, patient reported outcome measures are similar for both UKR implants, but morbidly obese patients (BMI>35) may experience an early decline with poorer long term outcomes.

4 Radiological Analysis

4.1 Aims and Objectives

The aims of this study were:

1. To develop a quantitative method of measuring tibial BMD from plain radiographs
2. To use this method to examine changes in tibial BMD in patients treated with medial UKR of two designs:
    a. a mobile bearing metal backed implant (MB)
    b. a fixed bearing all-polyethylene implant (AP).

Secondary aims included correlating these changes with patient reported outcome measures and pain, from Chapter 3.

4.1.1 Research Questions

1. Can a reproducible quantitative proxy for BMD be developed using plain knee radiographs?
2. Does this BMD proxy measurement (GSRb) change under metal backed implants and all-polyethylene implants?
3. Are significant increases in proximal tibial GSRb associated with persistent pain?

4.2 Chapter Summary

Proximal tibial strain in medial unicompartmental knee replacement (UKR) may cause pain and alter bone mineral density (BMD). The aims of this retrospective study were to quantify changes in proximal tibial BMD in medial UKRs and to correlate this with outcome. Two UKR designs were studied: metal backed mobile bearing (Oxford) and all-polyethylene fixed bearing (Preservation). Anteroposterior knee radiographs of 173 Oxford and 72 Preservation UKRs were analysed using digital radiograph densitometry at 0, 1, 2 and 5 years. The mean greyscale of 4 proximal tibial regions was measured over time and converted to a ratio of the most medial region to the remaining proximal tibia (Grey Scale Ratio b (GSRb): where >1 represents relative medial sclerosis). This ratio was correlated with age, sex, BMI, pain and Oxford Knee Score (OKS). Women, younger patients and those with BMI>30 had higher preoperative GSRb. Overall GSRb reduced significantly to 1 year and stabilised in both implants. In patients whose GSRb increased by >10% at 1 year (40/255), there was significantly less improvement in OKS compared to patients whose GSRb reduced by >10% at both one (8.2 Vs 15.8, p=0.002) and five years (9.6 Vs 15.8, p=0.022). Patients with persistently painful UKRs (17/255) were significantly younger and heavier than those without and showed no reduction in GSRb at one year compared to a 20% reduction in those without pain (p=0.05). GSRb can either increase or decrease under medial UKRs. Painful UKRs are associated with young age, elevated BMI and relative medial sclerosis (elevated GSRb) which may reflect ongoing strain and adaptive remodelling.

4.3 Introduction

Both overloading and under-loading (stress shielding) of bone can alter bone mineral density (BMD). Qualitative assessment of the presence or otherwise of sclerosis on radiographs is performed routinely by surgeons in their assessment of bone disease and arthropathies to aid diagnosis and inform further management or investigations. These subjective measures display marked variability between observations and observers. The advent of digital imaging has further changed the way in which we view and report radiographs. Assessment of bone quality or sclerosis is influenced by the resolution and size of the screen on which the image is viewed, the ambient lighting, image magnification or manipulation of the image using digital software such as the PACS system where greyscale can be manipulated along with many other variables.

Bone mineral density is routinely measured using dual x-ray absorptiometry (DEXA), but can also be measured using quantitative CT scanning, radiogrammetry and quantitative digital radiography. Digital radiological densitometry is a quantitative digital radiography technique, whereby changes in BMD are derived from calibrated anteroposterior radiographs of the knee, and has been validated against DEXA (Hernandez-Vaquero, et al., 2005). It has been used to assess changes in tibial BMD in TKR (Small, et al., 2013). Stress shielding and low BMD may cause reduced cancellous support to implants resulting in microfracture, pain and subsidence. Alternatively, proximal tibial microdamage and adaptive remodelling from overload may cause pain and a relative increase in BMD (sclerosis) under the implant.

4.4 Results

4.4.1 Developing the BMD Quantitative Measure

4.4.1.1 Patients

One hundred and ninety four Oxford UKRs (171 in situ, 23 revised) and 86 Preservation UKRs (75 in situ, 11 revised) were eligible for the image analysis study. Of these, radiographs were available for image analysis on 247 cases (165 Oxford UKRs and 82 Preservations) (Figure 4.1). In total 945 of radiographs were analysed up to 5 years (Figure 4.2).

Table 4.1 Timing of radiographs (months).

	Pre-op	1 year	2 years	5 years
Oxford	-1.28 (6)	12.4 (2.8)	26.7 (9.9)	63.8 (16.7)
Preservation	-0.79 (6)	12.3 (2.1)	26.2 (9.6)	61.0 (12.8)

Median (IQR)

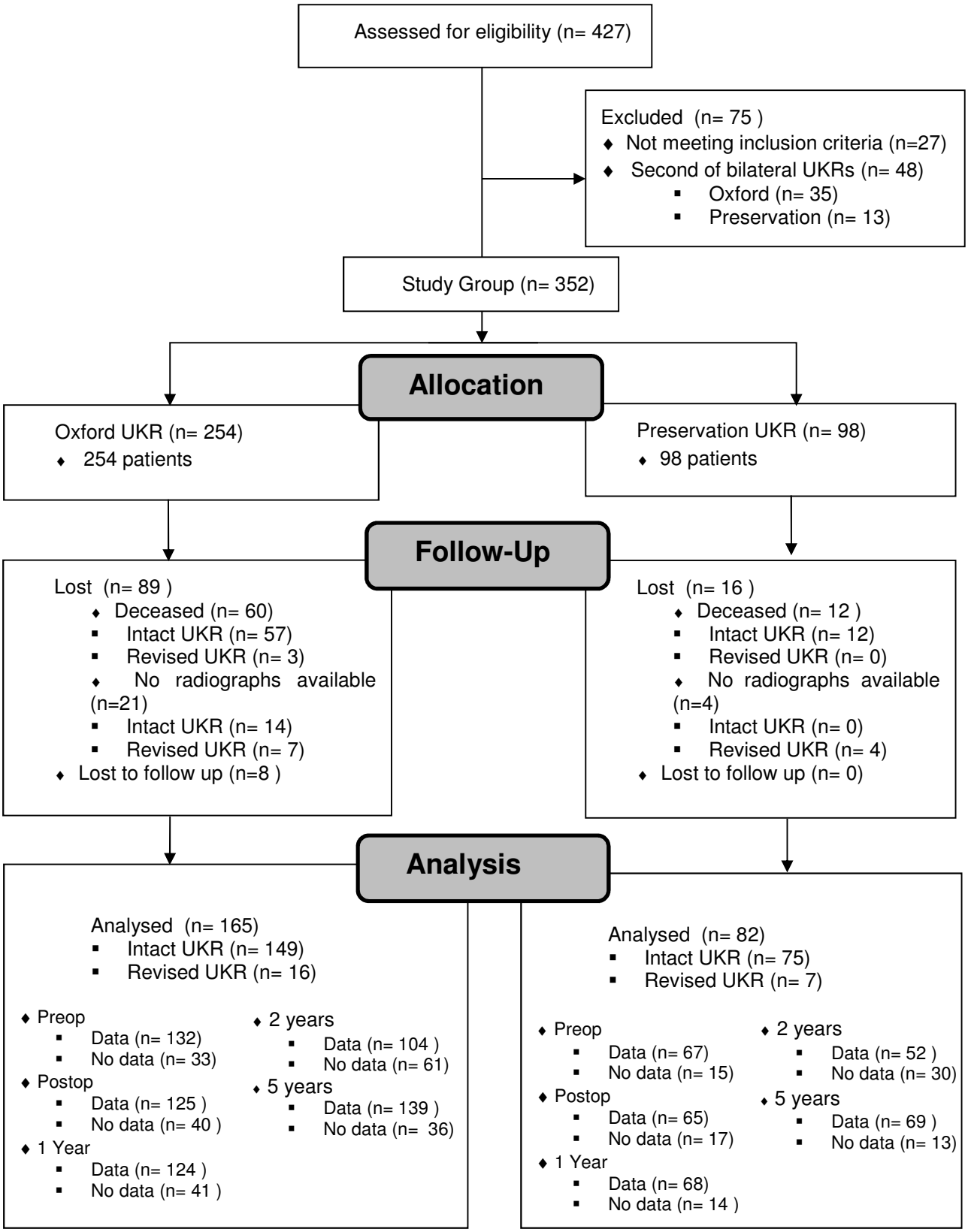

Figure 4.1 The UKR image analysis cohort.

All preoperative radiographs were on traditional hard copy x-ray film. Thereafter the proportions of each radiographic modality are shown in figure 4.2. There were no significant differences in the GSR (a or b) measured on film or digital radiographs at any time point (1 year p=0.743, 2 year p=0.520 , 5 year p=0.487, unpaired T-tests).

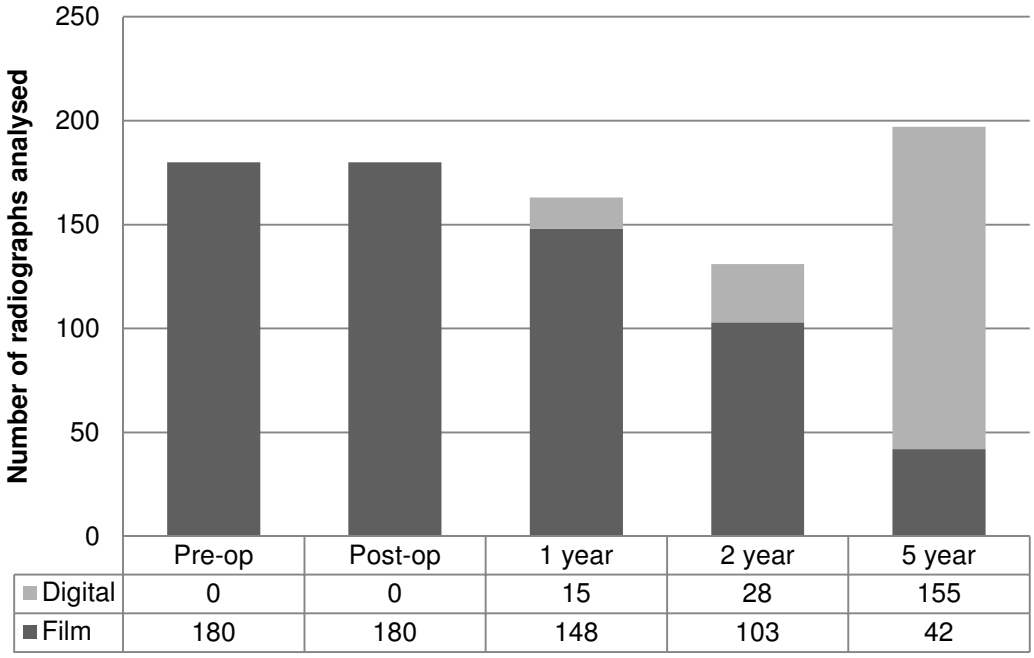

Figure 4.2 Modality of analysed radiographs.

4.4.1.2 Qualitative BMD Measures

One hundred and ninety one preoperative radiographs (127 Oxford and 64 Preservation) and 185 one year radiographs were qualitatively assessed. Table 4.2 details the inter and intra-observer agreement of qualitative sclerosis assessment. Intra-observer agreement for the presence of sclerosis was poor (κ=0.134) for preoperative radiographs and very good (κ=0.893) for 1 year radiographs. Inter-observer agreement preoperatively was moderate (κ=0.588) and good (κ=0.763) at 1 year. Intra-observer agreement between magnified and

unmagnified images was poor (κ=0.121) on pre-operative images, and good (κ=0.625) on 1 year radiographs.

Table 4.2 Intra and inter-observer agreement of qualitative sclerosis.

	Pre-operative Radiographs		1 Year Radiographs	
	κ	P value	κ	P value
Intra-observer				
Obs1 Time 1 Vs Obs1 Time 2	0.134	0.65	0.893	0.0001
Intra-observer with magnification				
Magnified Obs1 Vs Obs1 Time 1	0.121	0.032	0.625	0.0001
Magnified Obs1 Vs Obs1 Time 2	0.316	0.0001	0.531	0.0001
Inter-observer				
Obs1 Time 1 Vs Obs2	0.588	0.0001	0.763	0.0001
Obs1 Time 2 Vs Obs2	0.075	0.301	0.742	0.0001

Obs=observer

4.4.1.3 Quantitative BMD Measurement

The areas of the regions of interest (A1-4) analysed are shown in Figure 4.3. There were no significant differences in the relative area of each region of interest (A1-4) between implants at any time point. The A4 lateral condyle area consistently constituted a smaller percentage of the area analysed than the corresponding medial region A1. This was due to exclusion of composite shadowing from the fibular head.

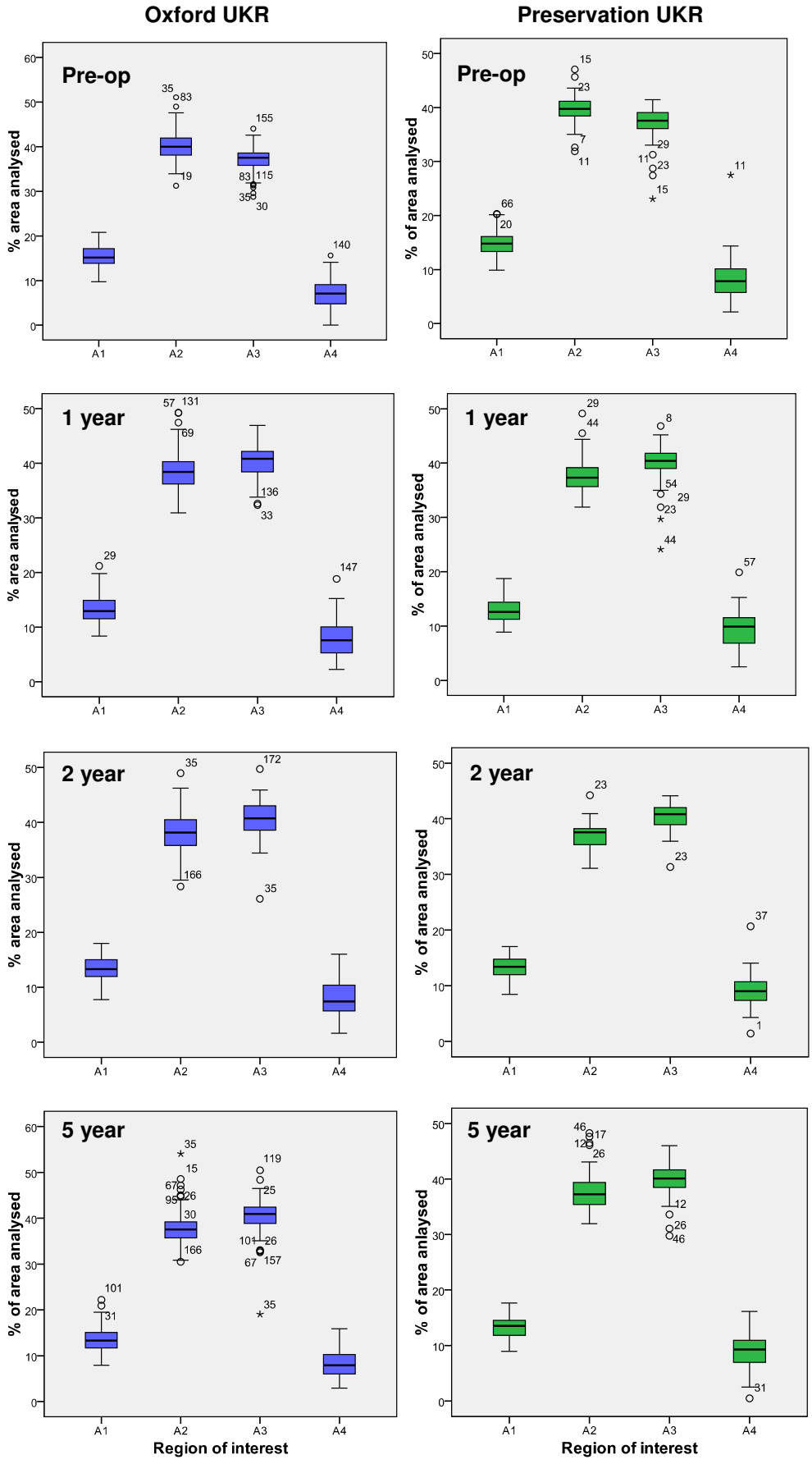

Figure 4.3 ROI areas at each time point by implant.

The distribution of grey-scale within each region A1-4 typically followed a normal distribution as shown by Figure 4.4. The mean grey-scale was therefore considered an appropriate quantitative measure. Whilst the spread of greyscale (standard deviation) remains similar between radiographs taken at different times with different penetrations, absolute means differ considerably in all regions emphasising the need for a comparative ratio for each radiograph rather than a comparison of the means themselves.

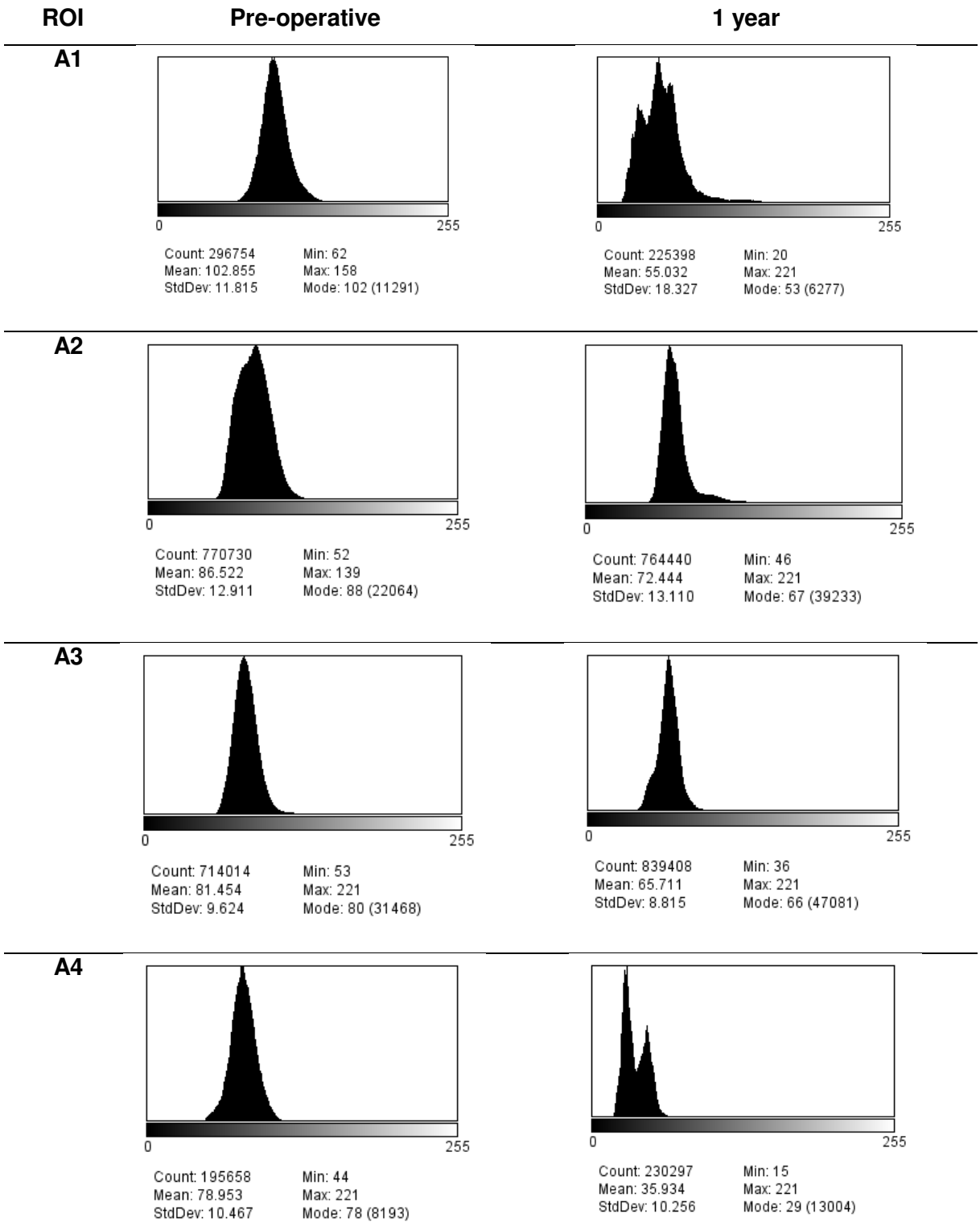

Figure 4.4 Histograms of each ROI preop and at 1 year in an example Preservation UKR patient. Count=pixel number and therefore area.

The quantitative measures of sclerosis assessed were:

1. GSRa = the medial (A1&A2) to lateral (A3&A4) GSR adjusted for relative areas
2. GSRb = the GSR of region A1 compared to A2-4 adjusted for area
3. GSR1:4 = the GSR of the peripheral ROIs A1 to A4;

Table 4.3 shows the correlation of quantitative measures with the subjective assessment of sclerosis on magnified preoperative and 1 year radiographs. All quantitative measures displayed significant differences between those patients subjectively determined to have sclerosis and those who did not.

Table 4.3 The quantitative proxy measures of BMD with and without qualitative sclerosis.

Quantitative sclerosis measure	Qualitative Sclerosis (n=71)	No sclerosis (n=109)	P value	95% CI
Pre-operative				
GSRa	1.17 (0.14)	0.92 (0.15)	<0.001*	0.20 to 0.29
GSRb	1.17 (0.21)	0.82 (0.23)	<0.001	0.29 to 0.42
GSR1:4	1.56 (0.74)	1.04 (0.47)	<0.001*	0.33 to 0.69
1 year				
GSRa	1.16 (0.22)	0.93 (0.18)	<0.001	0.16 to 0.30
GSRb	1.09 (0.29)	0.68 (0.23)	<0.001*	0.32 to 0.5
GSR1:4	1.62 (0.94)	1.03 (0.53)	<0.001*	0.36 to 0.83

Mean(SD), * Students T-test, unpaired

The area measured as A4 was often small due to exclusion of the fibular head (Figure 4.3), and so the GSR1:4 was considered less reflective of true sclerosis than the other measures of medial to lateral greyscale, GSRa and GSRb. Additionally, GSR1:4 displayed greater variance than GSRa and b with a broader confidence interval. The ratios of medial to

lateral condyle (GSRa) and of A1:A2-4 (GSRb) were therefore selected as measures of sclerosis for onward analysis. These measures were normally distributed throughout the population on preoperative radiographs (Figure 4.5). This parametric distribution was maintained at each time point for each UKR implant. Both GSRa and GSRb differed significantly in patients with and without qualitative sclerosis at every timepoint (Figures 4.6 and 4.7). The trend in GSRa and GSRb over time is shown in Figure 4.8. The greatest change occurs from preoperative to 1 year radiographs for both GSR parameters, though is more dramatic in GSRb. The GSRb measure better represents differences in the region immediately beneath the implant compared to the remainder of the proximal tibia.

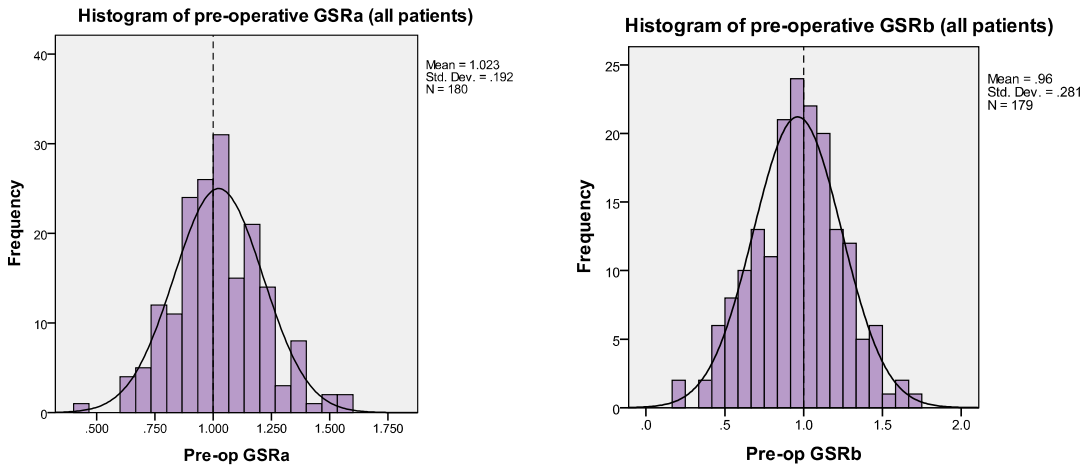

Figure 4.5 Histograms of GSRa and GSRb for all UKRs

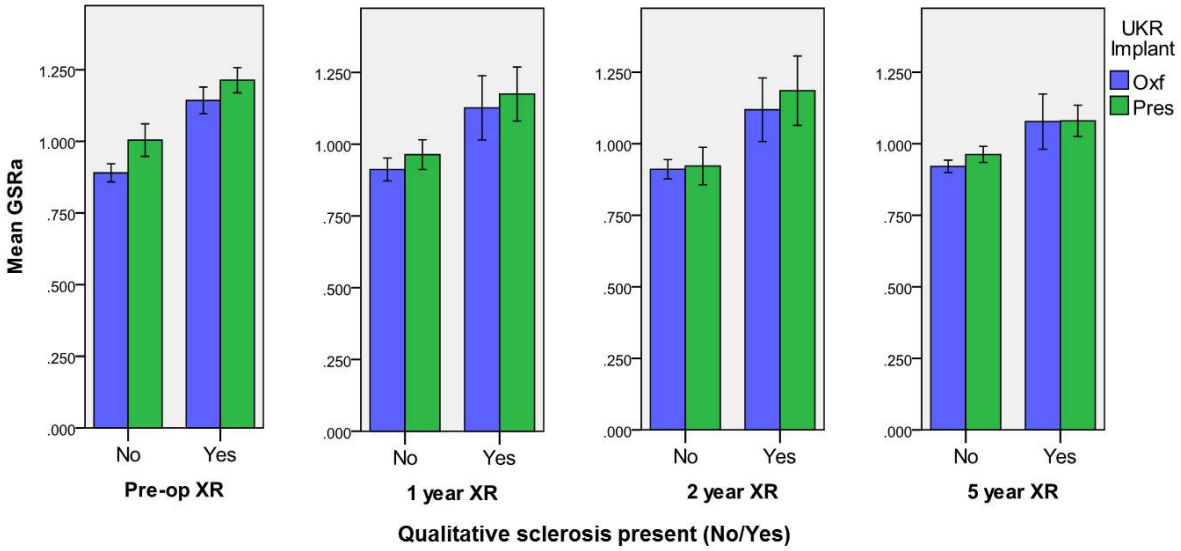

Figure 4.6 GSRa in patients with and without qualitative sclerosis by implant and time (with 95% CIs). The difference in the mean GSRa in those with and without qualitative sclerosis was significant at every time-point ($p<0.001$, unpaired T-test).

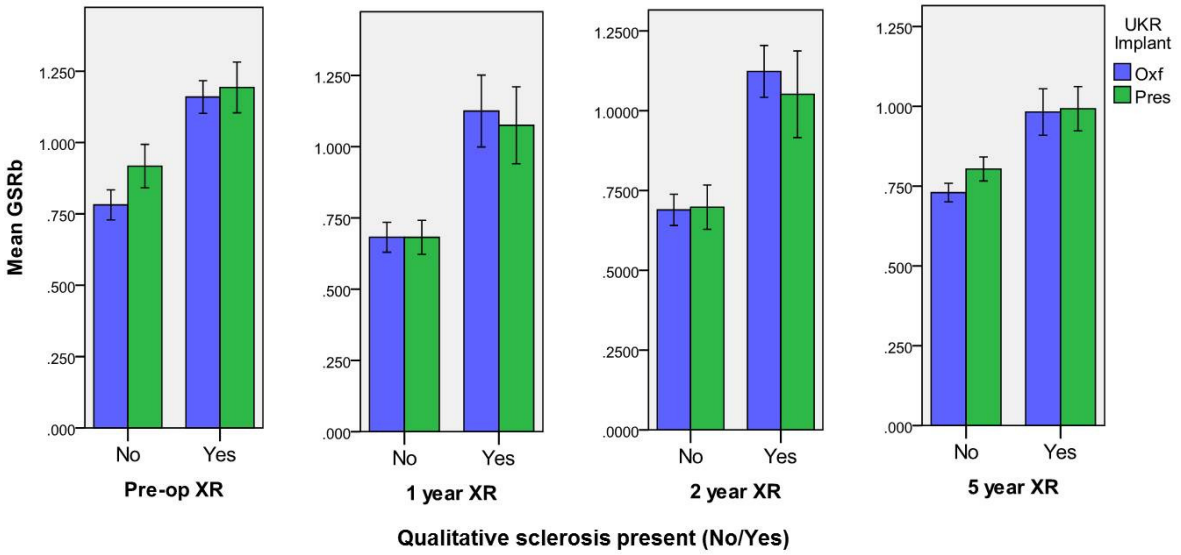

Figure 4.7 GSRb in patients with and without qualitative sclerosis by implant and time (with 95% CIs). The difference in the mean GSRb in those with and without qualitative sclerosis was significant at every time-point ($p<0.001$, unpaired T-test).

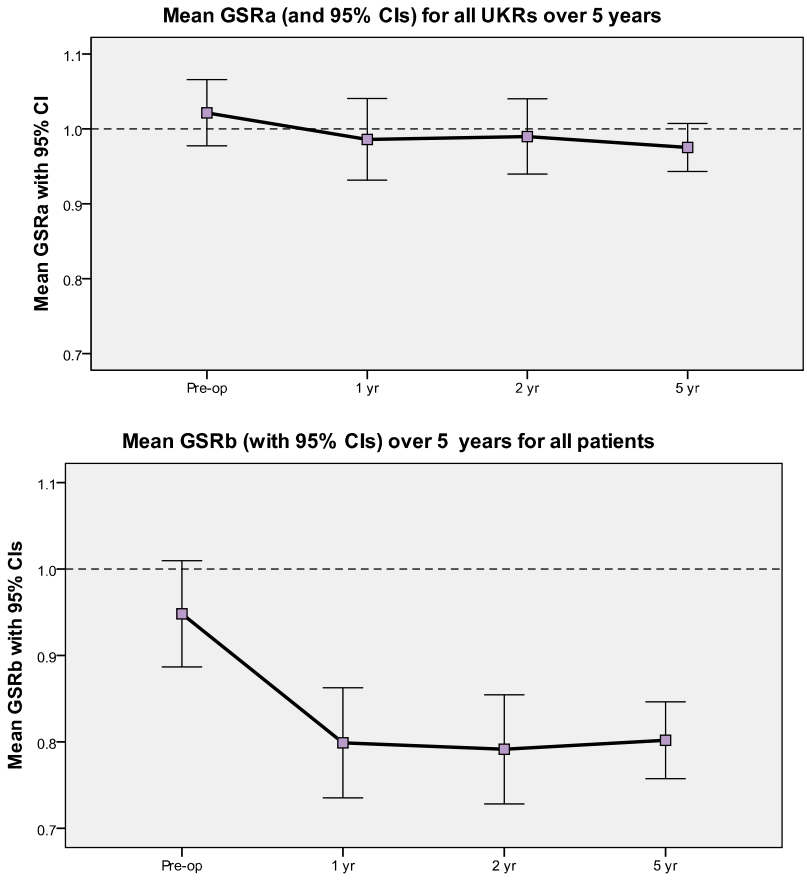

Figure 4.8 Trend in GSRa and GSRb over time for all UKRs.

4.4.2 Applying Image Analysis to the Clinical Cohort

4.4.2.1 Power Calculation for the Greyscale Ratio

The Lehr method (Petrie, 2006) for 80% power at the two-tailed 5% level (H_o rejected if $p<0.05$) was used to perform a power analysis:

$$n = \frac{16}{(d/s)^2}$$

Where: n = number of observations in each group

d = important difference in means

s = standard deviation of the observations in each group (assuming equal variance)

Table 4.4 Power analysis

Outcome Measure	Minimum sample size (n)	Standard Deviation	Difference detected as significant (d %)
GSRa			
GSRa 1yr	67	0.213	10.4
Change at 1yr	67	0.213	10.4
GSRb			
GSRb 1 year	67	0.298	14.5
Change at 1yr	67	0.309	15.1

With the sample sizes available for this study, differences of 10-15% in the mean GSR measures between Oxford and Preservation UKRs will be detected as significant.

4.4.2.2 Patients

There were no significant differences in the baseline characteristics (sex, age, BMI, weight, and OKS) of patients who were included in the radiographic analysis, and those who were excluded due to radiographs not being available for analysis (Table 4.5).

Table 4.5 Characteristics of patients included and excluded for radiographic analysis.

Variable	Included (n=255)	Excluded (n=25)	P value	95% CI
Female Sex	128 [50.2]	7 [28.0]	0.128 $^{\tau}$	
Age	67.1 (8.3)	69.6 (7.5)	0.192*	-6.3 to 1.3
BMI	28.8 (4.4)	29.1 (3.6)	0.854*	-3.4 to 2.8
Wt (kg)	80.5 (14.7)	78.0 (12.4)	0.642*	-8.6 to 12.9
OKS	39.4 (7.3)	41.3 (6.2)	0.347*	-5.7 to 2.0

Mean (SD), number [%] $^{\tau}$ Chi squared test, *Two-tailed student T-test

There was a significantly higher proportion of females in the Preservation cohort than the Oxford cohort (p=0.044) (Table 4.6). The Oxford group had significantly greater proximal tibial varus deformity (p=0.023), but no difference in overall FTA. The Preservation group had significantly more pre-operative sclerosis as assessed by all sclerosis measures, qualitative and quantitative (Table 4.6).

Table 4.6 Baseline characteristics of radiographic analysis cohort by UKR implant.

Variable	Oxford (n=173)	Preservation (n=82)	P value	95% CI
Demographics				
Female Sex	79 [45.6]	49 [59.8]	0.044 τ	
Age	66.4 (7.8)	68.3 (9.1)	0.127*	-4.2 to 0.53
BMI	28.8 (4.3)	28.7 (4.8)	0.886*	-1.24 to 1.4
Wt	81.4 (14.5)	78.7 (15.1)	0.218*	-1.6 to 7.2
OKS	39.2 (7.8)	39.9 (6.0)	0.614*	-3.2 to 1.9
Alignment (degrees)				
FTA	181.7 (2.9)	181.6 (2.6)	0.952*	-0.83 to 0.88
TPA	85.0 {3.6}	85.6 {2.5}	0.023§	
PTS	3.5 {11}	3.5 {4}	0.458§	
XR Analysis				
Time of preop XR (months)	1.18 {6}	0.79 {6}	0.938§	
GSRa	0.98 (0.19)	1.10 (0.18)	<0.001*	-0.18 to -0.07
GSRb	0.91 (0.28)	1.05 (0.26)	0.002*	-0.22 to -0.05

Mean (SD), number [%], median {IQR}

τ Chi squared test, *Two-tailed student T-test, § Kruskal Wallis test

4.4.2.3 Alignment

Table 4.7 details the immediate postoperative alignment of each implant. Significantly more proximal tibia, as measured by D4, is resected to implant the metal backed mobile bearing Oxford implant (<0.001, unpaired T-test) when compared to the fixed bearing all-polyethylene Preservation. Greater overhang was present in the Oxford group with mean underhang in the Preservation (<0.001). The Oxford UKR was implanted with a tendency to 0-2mm of overhang, whereas the tendency in the Preservation was for 0-2mm of underhang (Figure 4.9). Though there was no difference in resultant FTA or change therein from preoperative level, the Preservation tibia was implanted statistically significantly more varised and with greater PTS than the Oxford. The corresponding Preservation femoral component was more extended and less valgised in the coronal plane than the Oxford. The extent of these differences is of doubtful clinical significance.

Table 4.7 Postoperative UKR alignment by implant.

	Oxford (n=173)	Preservation (n=82)	P value	95% CI
Overhang (mm)	0.3 (1.7)	-0.9 (1.4)	<0.001*	0.75 to 1.6
Resection depth (D4 %)	21.8 (3.6)	17.9 (2.6)	<0.001*	3.15 to 4.74
Coronal balance (degrees)				
FTA	177.3 (2.6)	178.2 (3.1)	0.06*	-1.59 to 0.04
Change in FTA	4.5 {4.1}	3.75 {3.2}	0.111§	
Tibia (degrees)				
MPTA	87.1 {4.0}	86.4 {3.7}	0.186§	
Change in MPTA	2.2 {5.2}	0.7 {3.6}	0.011§	
PTS	86 {5.5}	88 {3}	<0.001§	
Change in PTS	-1 {5}	2 {4}	<0.001§	
Femur (degrees)				
LDFA	82.1 (5.2)	85.5 (5.1)	<0.001*	-4.7 to -2.0
Femoral flexion	2.65 (6.5)	-1.5 (7.1)	<0.001*	2.2 to 6.2

Mean (SD), number [%], median {IQR} *Two-tailed student T-test, §Kruskal Wallis test

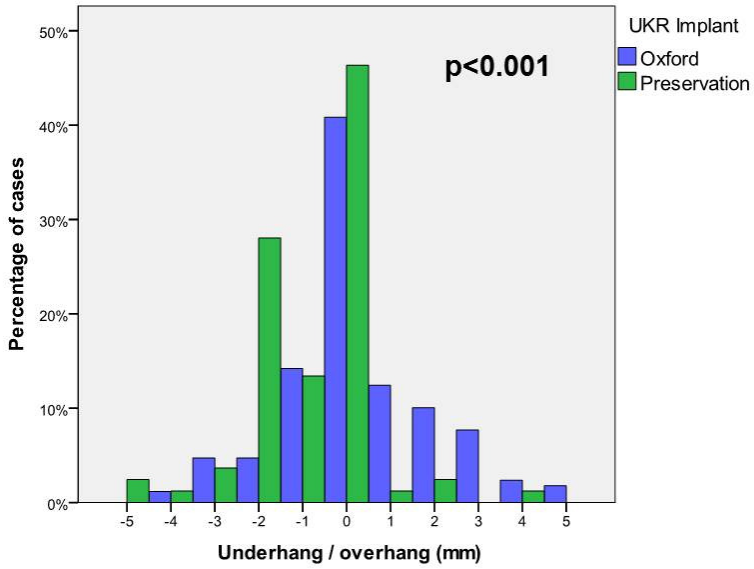

Figure 4.9 Distribution of overhang and underhang by UKR implant.

4.4.2.4 Greyscale Ratio Associations

4.4.2.4.1 Implant

The Preservation group had significantly higher GSRs prior to surgery than the Oxford group. Both GSRa and GSRb changed in both implants over the five year follow up (Figure 4.10). Repeated measures ANOVA showed significant changes in GSRb over the 5 year period in the Preservation UKR ($p<0.001$) and the Oxford UKR ($p=0.014$). Further analysis using Wilcoxon signed rank test for related samples confirmed that these significant changes in GSRb occurred in the first postoperative year in both the Preservation ($p<0.001$) and the Oxford implant ($p<0.001$), with no further significant change thereafter. Such trends were not evident in the GSRa measurement (Figure 4.10a) where repeated measures ANOVA showed no significant changes in the distribution of GSRa between radiographs in either group (Oxford $p=0.464$, Preservation 0.154).

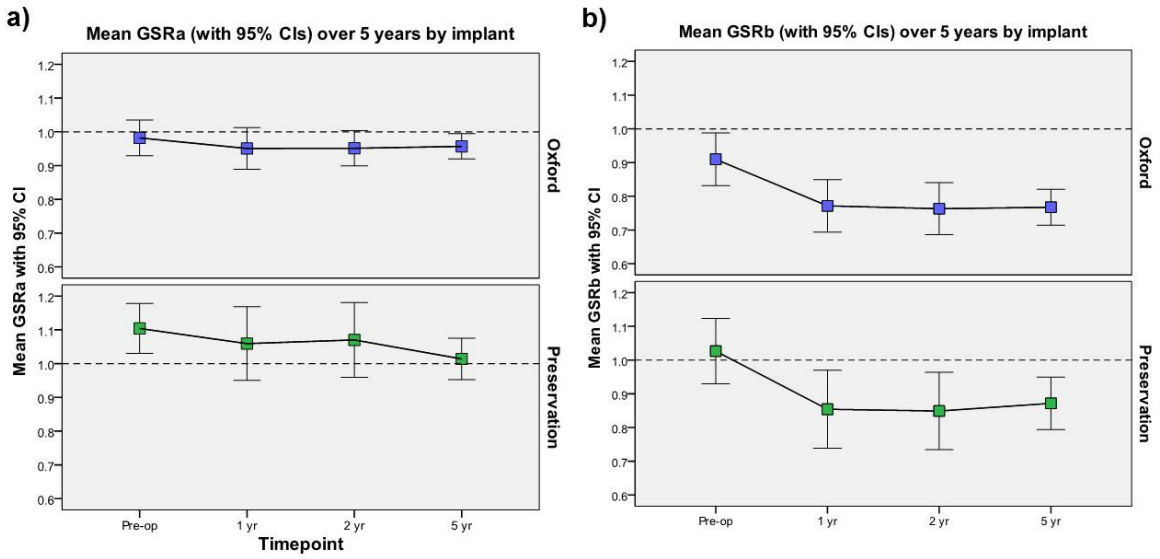

Figure 4.10 Trends in a) GSRa and b) GSRb over time by UKR implant.

4.4.2.4.2 Gender

High GSRa and GSRb were significantly associated with female sex in both groups at every time point (Figure 4.11). In the Oxford group, the mean preoperative GSRa in women was 1.06 compared to 0.91 in men ($p<0.001$, 95% CI -0.21 to -0.08, unpaired T-test). This difference was also present for GSRb where women had mean preoperative level of 0.99 compared to 0.85 in men ($p=0.005$, 95%CI -0.25 to -0.05), a difference which remained significant at 1 year. There was no significant difference in the change in GSRa ($p=0.704$, unpaired T-test) or GSRb ($p=0.602$) over the first year between men and women with Oxford UKRs. In the Preservation group, women had a significantly higher mean preoperative GSRa of 1.16 compared to men 1.01 ($p<0.001$, 95%CI -0.24 to -0.07, unpaired T-test) and GSRb of 1.13 compared to men 0.93 ($p=0.001$, 95% CI -0.33 to -0.08, unpaired T-test). Once again these differences remained at 1 year with no significant differences in the change in GSRa or GSRb over the year between the sexes.

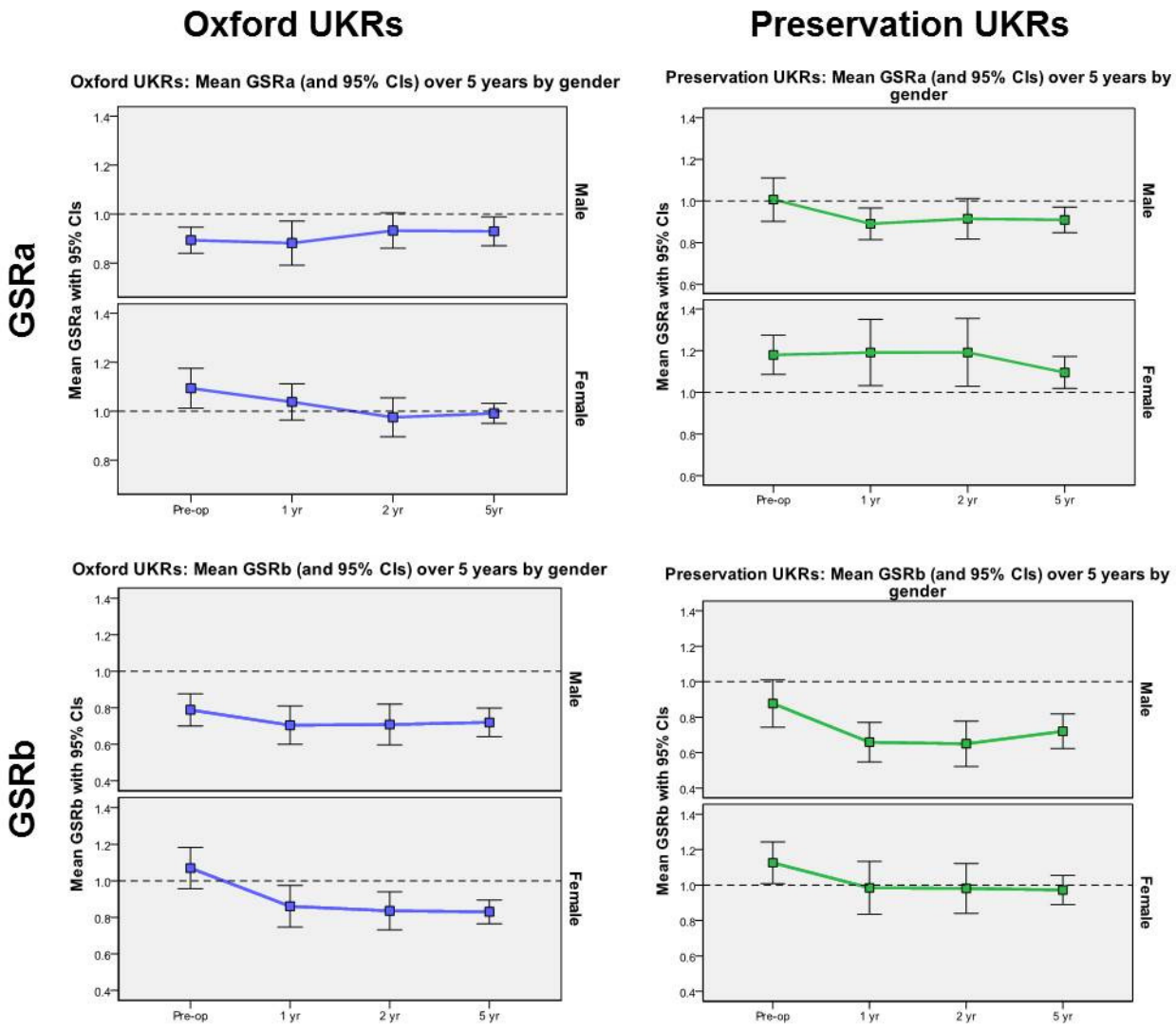

Figure 4.11 GSRa and GSRb by sex and UKR implant

4.4.2.4.3 BMI

Patients with a BMI >30 had significantly higher preoperative GSRb (1.03, SD 0.28) than those with BMI <30 (0.93, SD0.27, p=0.025, 95%CI -0.2 to -0.01 unpaired T-test). There were no significant differences in change in GSRa or GSRb for patients with BMIs of above or below 30 in the Oxford group (Figure 4.12).In the Preservation group, preoperative GSRb was significantly greater in those with a BMI of >30, 1.13, compared to those with a BMI<30, 0.96 (p=0.012, 95%CI -0.29 to -0.04). This difference was no longer significant at 1 year and was not present for GSRa at any timepoint.

Preoperative GSRa did not correlate significantly with age, BMI, weight or OKS in either group. Preoperative GSRb had a negative correlation with age for the entire UKR population but displayed no correlation with absolute BMI, weight or pre-operative OKS.

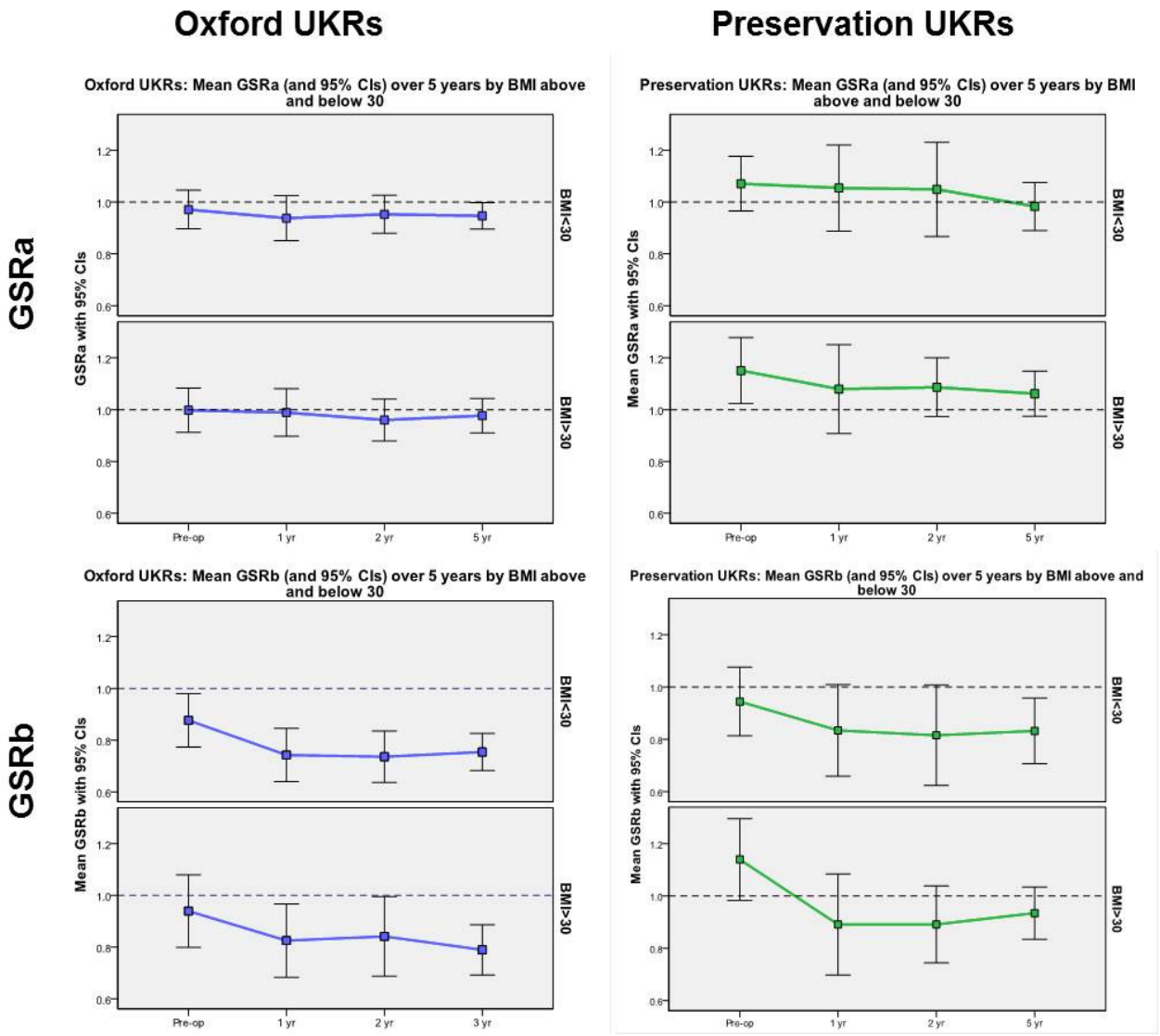

Figure 4.12 GSRa and GSRb by BMI and UKR implant

In both UKR implants, there was a significant negative correlation between preoperative GSRb and change in GSRb by 1 year (Pearson's correlation Preservation -0.292, $p<0.05$; Oxford -0.607, $p<0.01$). No significant correlation was apparent between change in GSRb at 1 year and age, BMI, weight or tibial resection depth in either implant. No significant differences in GSRb change existed between the sexes. The effect of implant overhang on subsequent sclerosis development was investigated using one way ANOVA. This showed a significant effect of Preservation implant overhang on change in GSRb by 1 year ($p=0.015$) whereby overhang of the all-polyethylene implant appeared related to sclerosis progression (Figure 4.13). No such relationship was found for the Oxford UKR ($p=0.165$).

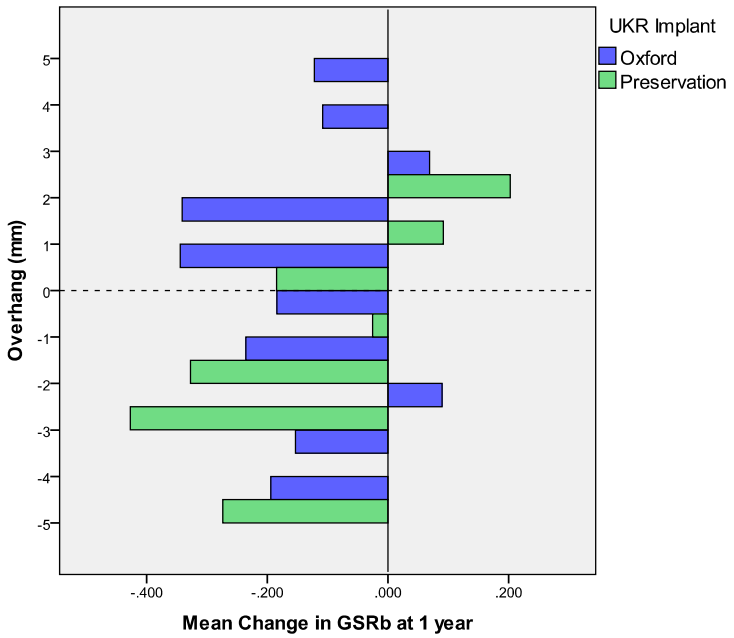

Figure 4.13 UKR implant overhang and GSRb change.

Forty UKR patients displayed a >10% increase in GSRb over 1 year with a mean increase of 0.21 (SD0.17). This group included 12 (30%) Preservations and 28 (70%) Oxford UKRs, a distribution representative of the study population. One hundred and twelve patients became less sclerotic over the first postoperative year with a >10% decrease in GSRb, mean decrease of 0.337 (SD 0.20).

4.4.3 Correlating Clinical Outcomes with Radiological Analysis

Improvement in OKS at 1 and 5 years differed significantly between UKR patients whose GSRb increased by >10% (increasing sclerosis) at 1 year, and those whose GSRb had decreased by >10% (Table 4.8). This relationship was not linear (Figure 4.14).

Table 4.8 Change in GSRb and OKS over time by UKR implant.

	↑GSRb over 1 year	↓GSRb over 1 year	P value	95% CI
All UKRs	(n=40)	(n=112)		
OKS Imp at 1yr	8.2 (9.99)	15.8 (8.3)	0.002*	-12.4 to -2.8
OKS Imp at 5 yrs	9.6 (11.4)	15.8 (9.1)	0.022*	-11.4 to -0.9
Oxford	(n=28)	(n=64)		
OKS Imp at 1yr	9.0 (11.6)	16.6 (6.5	0.023*	-14.2 to -1.1
OKS Imp at 5 yrs	10.2 (11.3)	15.6 (9.9)	0.129*	-12.5 to 1.7
Preservation	(n=12)	(n=49)		
OKS Imp at 1yr	6.4 (4.6)	14.9 (8.2)	0.033*	-16.2 to -0.7
OKS Imp at 5 yrs	8.2 (11.8)	8.4 (16.0)	0.086*	-16/7 to 1.2

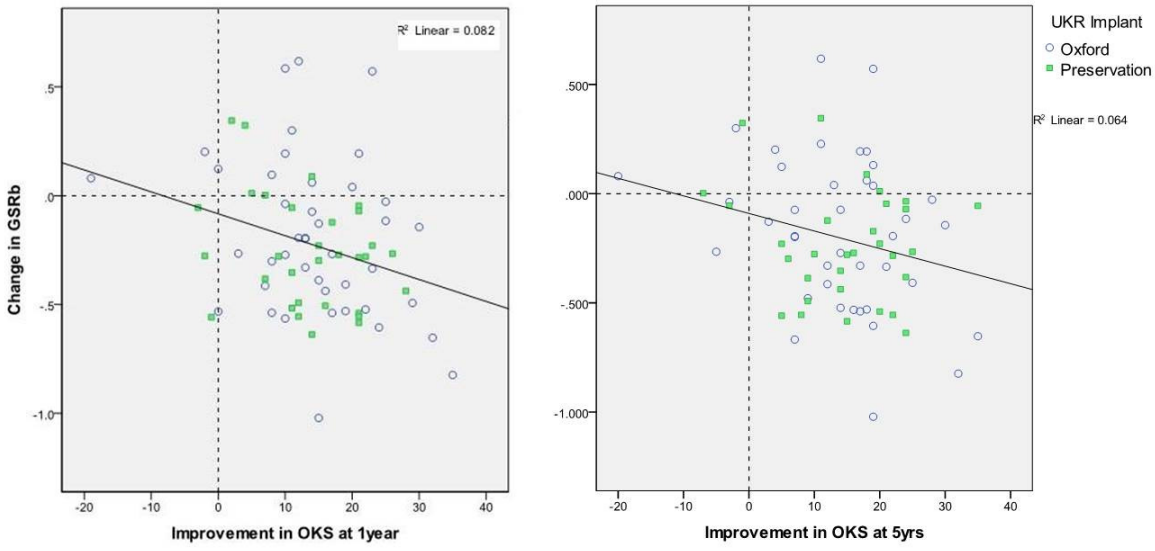

Figure 4.14 Change in GSRb and improvement in OKS by UKR implant

In patients who went on to revision of their UKR the preoperative GSRa was significantly lower, i.e. less sclerotic, preoperatively in the revised compared to the intact Preservation implants (p=0.028, unpaired T-test). In the Oxford cohort, there was no significant difference. Differences in other preoperative characteristics between revised and unrevised patients have been presented in Chapter 3.

4.4.3.1 Pain and GSR

Of those UKRs revised for pain 71% had Preservation implants and all revisions for pain were performed prior to 5 years. Following Preservation UKR, those revised for pain displayed a mean increase in GSRa compared to a reduction in those unrevised. This difference approached but did not reach significance (p=0.059, unpaired T-test). However, change in GSRb at 1 year did differ significantly between those revised for pain with a mean increase in GSRb of 10% compared to those not revised for pain whose GSRb reduced by 20% (p=0.017, 95%CI 0.06 to 0.6) (Figure 4.15b).

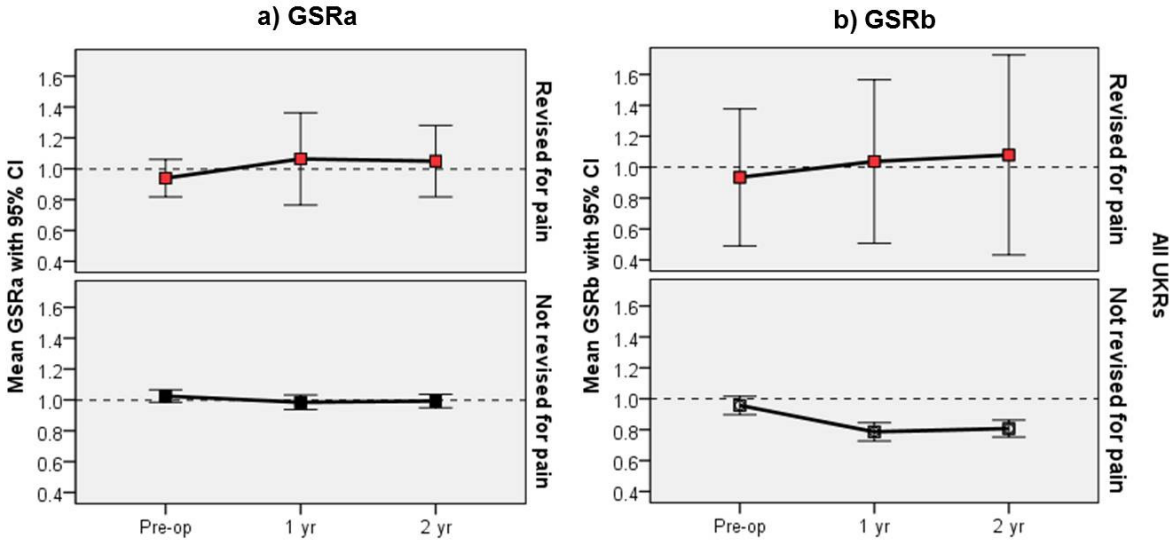

Figure 4.15 GSRa and GSRb in UKRs revised for pain and those not revised for pain.

If UKR patients revised for pain (n=8, 2 Oxford and 6 Preservations) are combined with patients who were "poorly" satisfied with the pain relief from their UKR, but who weren't offered revision (n=10, 6 Oxford and 4 Preservation), this population is significantly younger and heavier than those with intact UKRs or whose UKR was revised for other reasons (Table 4.9). Age and BMI remained significantly different between painful and not painful UKRs when corrected for implant (Figures 4.16 and 4.17). Preoperative OKS and GSR measures were not predictive of postoperative complaints of pain. Both measures of sclerosis, GSRa and GSRb, increased over time in painful UKRs of both designs (Figure 4.18). This change was more pronounced in GSRb than GSRa.

Table 4.9 Preoperative variables in ultimately painful and not painful UKRs.

Variable	Painful UKR (n=17)	Not painful UKR (n=237)	P value	95% CI
Female Sex	8 [47]	120 [51]	0.961 $^{\tau}$	
Age	60.4 (7.6)	67.4 (8.2)	0.001*	-11.2 to -2.8
BMI	32.7 (5.1)	28.5 (4.2)	<0.001*	1.9 to 6.5
Wt	88.1 (17.6)	79.8 (14.4)	0.034*	0.6 to 16.1
Preop OKS	44.1 (7.5)	39.2 (7.1)	0.061*	-0.2 to 10.0
Preop GSR a	1.07 (0.23)	1.02 (0.19)	0.435*	-0.07 to 0.16
Preop GSR b	1.04 (0.30)	0.96 (0.28)	0.334*	-0.09 to 0.26

Mean (SD), number [%], $^{\tau}$ Chi squared test, * two sample T-test

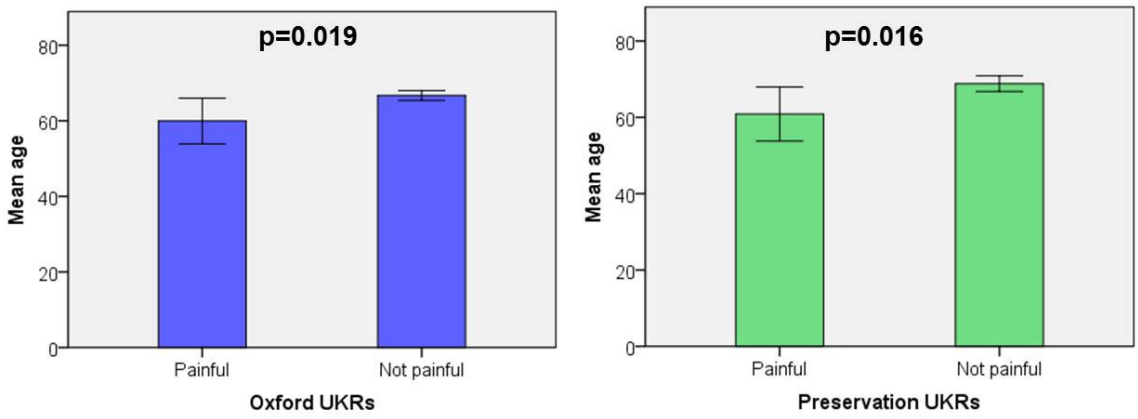

Figure 4.16 Mean age in painful and not painful UKRs by implant (95% CI error bars, Unpaired T-tests)

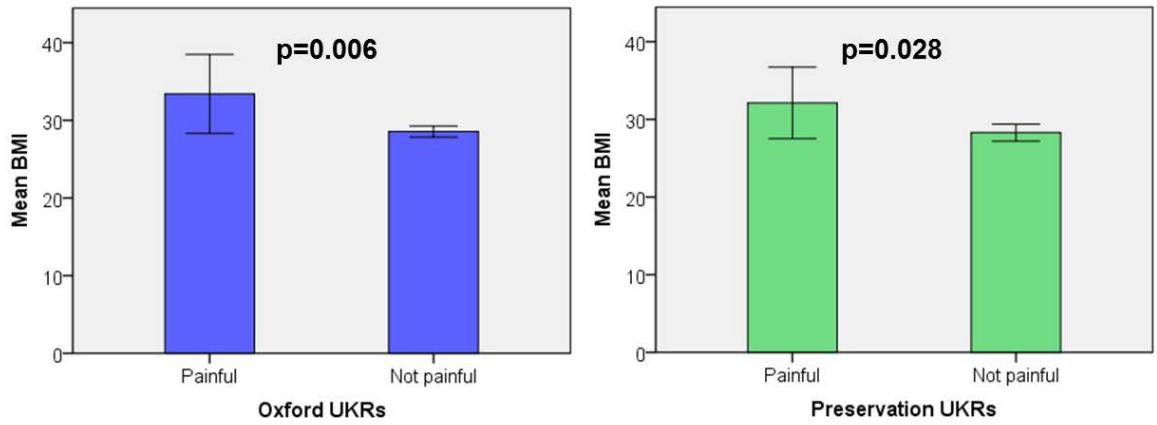

Figure 4.17 Mean BMI in painful and not painful UKRs by implant (95% CI error bars, Unpaired T-tests)

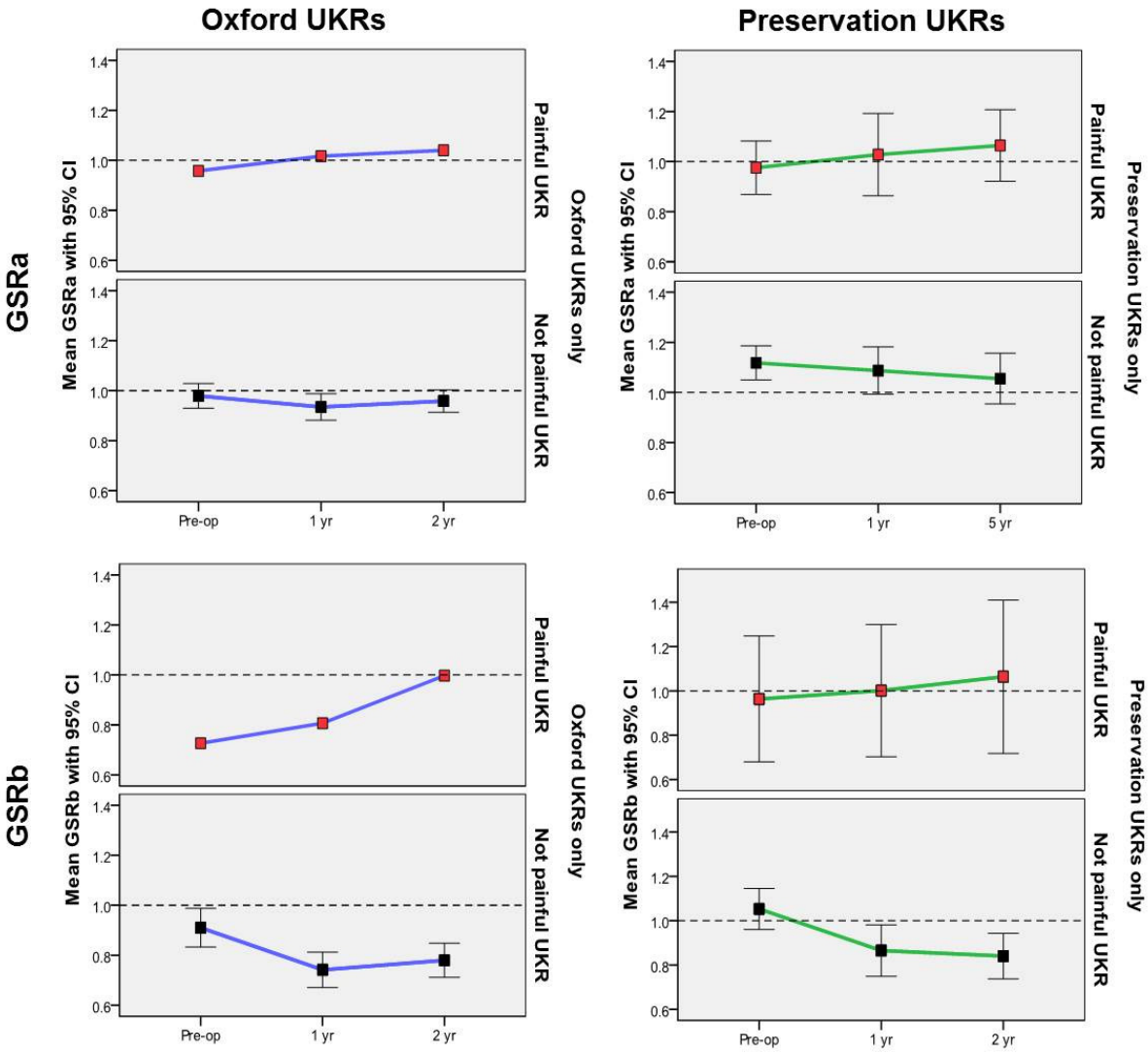

Figure 4.18 Trends in GSRa and GSRb in painful and not painful UKRs by implant.

4.4.3.2 Alignment and GSR

In the Oxford group, there were no significant differences between revised and unrevised implants in terms of tibial or femoral component alignment (Table 4.10, Figure 4.19 and 4.20), or tibial resection depth. The same was true in the Preservation group.

Table 4.10 Radiographic analysis parameters for revised and unrevised UKRs by implant.

	Intact UKR	Revised UKR	P value	95% CI
Oxford	**(n=206)**	**(n=16)**		
GSRa	0.98 (0.18)	0.98 (0.23)	0.997*	-0.13 to 0.13
GSRb	0.92 (0.28)	0.87 (0.32)	0.632*	-0.15 to 0.24
FTA(°)	181.6 (2.95)	181.8 (2.91)	0.869*	-2.1 to 1.76
Preservation	**(n=88)**	**(n=7)**		
GSRa	1.11 (0.18)	0.98 (0.10)	0.028*	0.017 to 0.2
GSRb	1.06 (0.26)	0.98 (0.26)	0.497*	-0.15 to 0.3
FTA (°)	181.8 (2.6)	180.1 (2.8)	0.124*	-0.49 to 3.9

Mean (SD), number [%] , * Unpaired T-test

Though there was no difference in resultant femorotibial angle (FTA), the AP tibia was implanted significantly more varised and with greater PTS than the MB (Table 4.7). The mean tibial component coronal alignment for all UKAs was 86.7° (range 78-93).

There was no correlation between GSRb and tibial component coronal alignment (-0.073) or resultant FTA (0.106, Pearson's correlation). There was no significant difference in GSRb between patients with varus tibial components and those without using both 87° (1.0 Vs 0.96, p=0.263 student T-tests) and 85° (0.98 Vs. 0.99, p=0.865, student T-tests) definitions. There was no difference in the tibial coronal alignment in those with painful UKAs (+/- revision) (mean 86.6°) and those without (86.2°, p=0.684 student T-tests). Similarly there was no difference in sagittal alignment between those dissatisfied with painful UKAs (+/- revision)

(mean 87.6°) and those without (86.7°, p=0.237 Mann Whitney U test). The overall limb alignment, measured by the FTA, did not differ significantly in those with painful UKAs and those without (177.4 Vs 177.5, p=0.882, student T-test). There were no significant differences in the mean coronal plane tibial component alignment (or range thereof) in patients whose GSRb increased by >10%, decreased by >10% or whose changed <10% following UKR (Table 4.11). There was similarly no significant differences in the overall coronal plane limb alignment (FTA) between these patient groups (Table 4.11).

Table 4.11 Tibial component implant alignment in patients whose GSB changed, or did not change, significantly by one year.

GSRb Change to 1 year		MPTA (◦)		FTA (◦)	
		Range	Mean (SD)	Range	Mean (SD)
↑GSRb >10%	(n=40)	79.3-93.4	177.9(3.5)	170.0-184.5	86.3(3.2)
Change <10%	(n=103)	78.0-91.2	177.5(2.3)	172.6-183.5	86.3(2.8)
↓GSRb >10%	(n=112)	79.3-91.2	177.4(3.0)	168.6-184.7	86.2(3.0)
	P value		0.624*		0.638*

*ANOVA

4.4.3.3 BMI, Alignment and GSR

Coronal plane tibial component alignment did not differ significantly in patients with a BMI greater than 35 (mean MPTA 86.4(4.3), range 82.4 to 88.7) compared to those with BMI less than 35 (86.1(3.1), range 77.7 to 93.4, p=0.681 unpaired T-test, -1.76 to 1.16 95%CI). Nor did coronal plane lower limb alignment (FTA): BMI>35 178.0(2.6); BMI <35 177.6(2.8), (p=0.586 unpaired T-test, -1.6 to 0.9 95%CI). There was no significant difference in the mean BMI of patients with and without varus aligned tibial components using both 87◦ (p=0.815 unpaired T-test, -1.18 to 1.5) and 85◦ (p=0.651 unpaired T-test, -1.1 to 1.8) definitions. Nor was there an association with BMI above or below 35 and varus tibial component alignment: 87◦ (p=0.291), 85◦ (p=0.359, Chi squared).

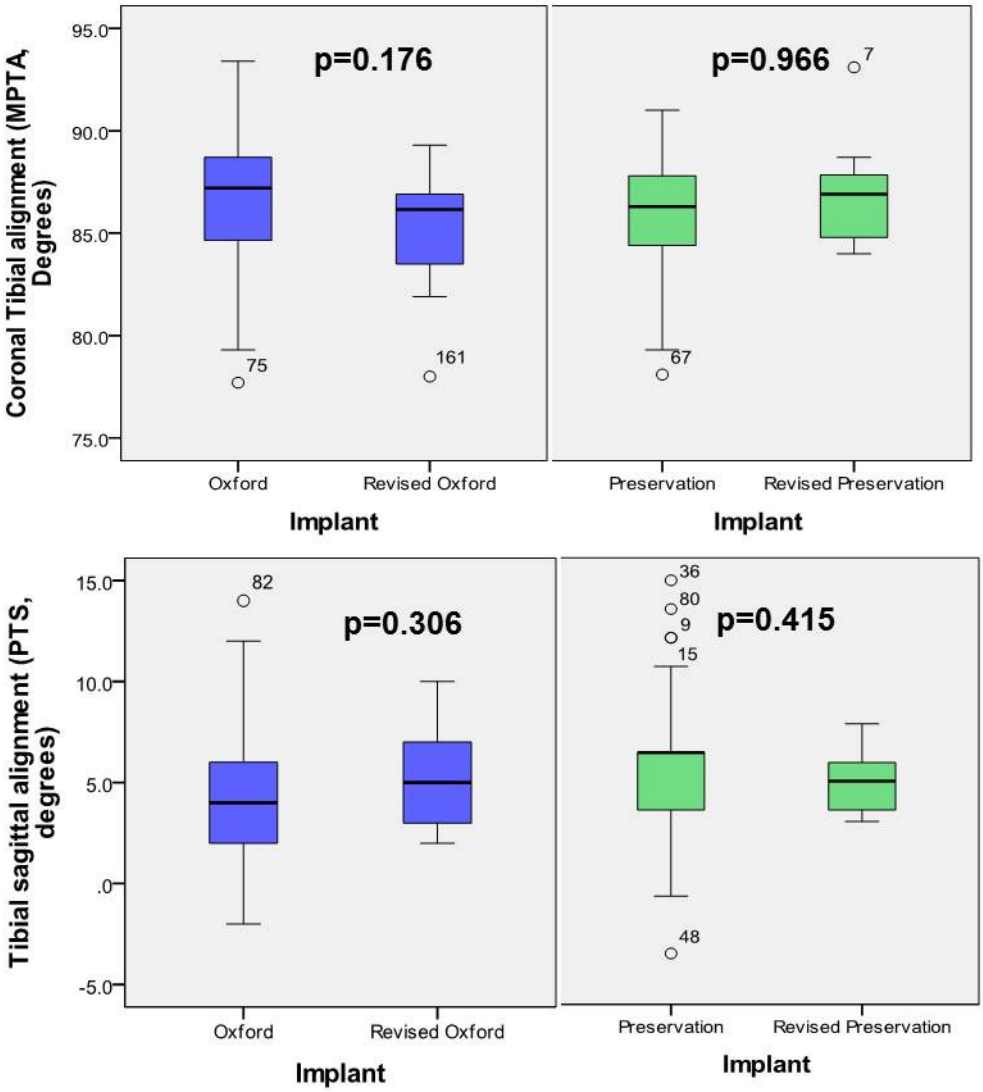

Figure 4.19 Tibial component alignment in revised and unrevised UKRs by implant (Mann Whitney U tests).

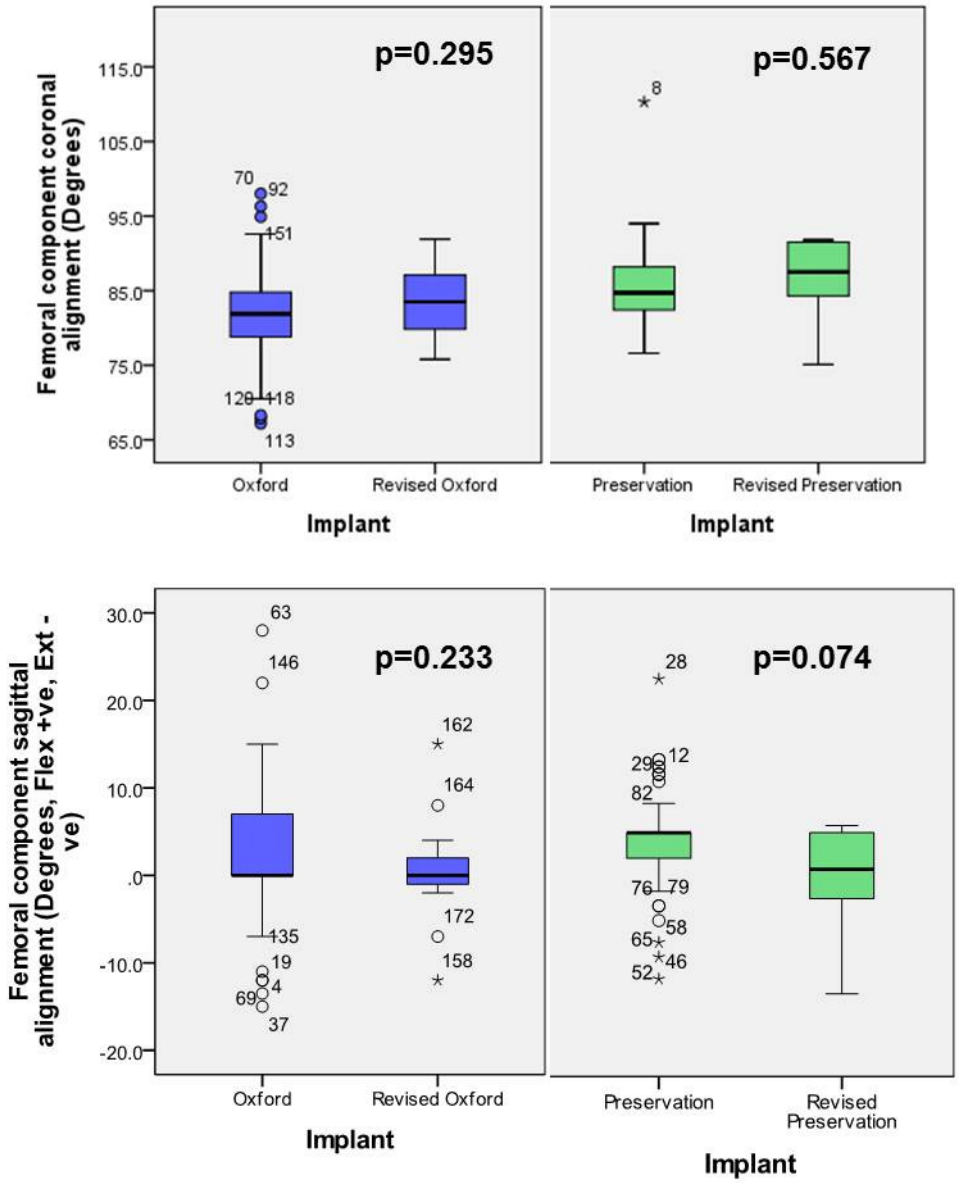

Figure 4.20 Femoral component alignment in revised and unrevised UKRs by implant (Unpaired T-tests).

4.5 Chapter Discussion

The greyscale ratios developed here as quantitative measures of BMD, appeared to reflect changes in BMD with significant differences in both measures (GSRa and b) in patients with and without qualitative sclerosis. Such quantitative measures should eliminate the observer bias inherent in qualitative measures when not blinded to the implant, i.e. on postoperative radiographs.

The greatest changes in GSR were found immediately beneath the UKR tibial components at the most medial quadrant measured, reflected by the GSRb being the most reactive measure. This is consistent with the findings of previous DEXA studies of medial UKRs whereby significant BMD changes occur in the medial plateau only (Soininvaara, et al., 2013). Overall, there was a mean decrease in GSRb (medial sclerosis) after UKR. A similar mean reduction in medial BMD has also been reported in TKR (Small, et al., 2013). In isolated medial compartment osteoarthritis, the medial tibial condyle is progressively overloaded and has a significantly higher BMD than the lateral condyle as a consequence (Li and Nilsson, 2000). Restoring medial compartment height and femorotibial angle with a UKR should relatively offload the medial condyle with a subsequent reduction in sclerosis and GSRb. This change occurred during the first postoperative year, stabilising thereafter. This concurs with the hypothesis of Simpson et al (Simpson, et al., 2009) and with the DEXA findings of others (Richmond, et al., 2013; Soininvaara, et al., 2013). To my knowledge this is the first study to correlate these changes with outcome, especially pain.

Three previous studies have examined BMD in UKRs. Hooper et al (Hooper, et al., 2013) measured BMD using DEXA in 79 patients with uncemented Oxford mobile bearing UKRs comparing operated and non-operated knees at 2 years. They found a mean decrease in BMD in all regions of the tibia in the operated knee. This was greatest medially immediately under the implant in a ROI corresponding to A1 here. They did not examine changes over time, and comparisons were with the non-operated, not the preoperative knee. Soininvaara et al (Soininvaara, et al., 2013) performed DEXA scanning on 21 metal-backed fixed bearing

UKRs up to 7 years postoperatively. In contrast, they found a significant mean increase in medial tibial condyle BMD of 9% up to 1 year. The lateral condyle underwent a non-significant reduction in BMD. They did not correlate BMD with clinical outcome and the ROIs used did not exclude cement, cortical condensations or composite shadowing from the fibular head. Richmond et al (Richmond, et al., 2013) used quantitative CT to asses tibial BMD in 26 metal backed and 24 all-polyethylene UKRs reporting a mean reduction in BMD medially under the tibial component of <5% in both UKRs, but significantly greater in the AP implant. Though studies are few, there is little consistency in findings regarding BMD in UKR. It appears that BMD increases in some patients and decreases in others. The bigger sample size in our study has facilitated a more detailed examination of this than has been possible previously. We found no differences in *changes* in GSRb or OKS postoperatively between implants.

Painful UKRs were associated with an elevated postoperative GSRb (medial sclerosis) compared to non-painful UKRs where GSRb decreased. Pain was associated with younger age and elevated weight and BMI. Oxford scores were significantly worse in patients whose GSRb increased by 10% at one year compared to those whose decreased or remained unchanged. Further subgroup analysis failed to show an association of an increase or decrease in GSRb of >10% and tibial component alignment, lower limb alignment or BMI. Patients with elevated BMIs did not display tibial component malalignment, as can happen when adiposity makes surgery technically more difficult.

The association between younger age and revision for pain has been reported before (Kerens, et al., 2013) with no apparent differences in incidence between fixed and mobile bearing UKRs (Baker, et al., 2012). The association between medial sclerosis and pain has not been previously reported and suggests that younger, heavier patients may experience prolonged adaptive remodelling in the proximal tibia consequent from persistent overload even in MB implants.

Interestingly, women had the greatest GSRb preoperatively. Previous studies of BMD in TKR have shown men to have a higher lateral condyle BMD than women (Small, et al., 2013). This difference would falsely reduce the GSRb in men in the absence of a poor medial BMD. Alternatively, elevated GSRb may reflect a greater sclerotic nature of arthritis in women. The greater proportion of women in the Preservation group undoubtedly contributed to the higher starting GSRb in this group. Patient selection for UKR may have biased this result by excluding women with known osteoporosis or osteopenic appearing bone on plain radiograph from undergoing UKR. This approach would appear to be supported by the finding that preoperative GSRa was significantly lower (less sclerotic, more osteopenic) in those UKRs ultimately revised for pain compared to those not revised for pain across both implants.

Patients with elevated BMIs (>30) displayed more preoperative medial sclerosis (greater GSRb) than those with lower BMIs. BMI and BMD have been previously shown to positively correlate in the proximal tibia (Small, et al., 2013). Older patients displayed less preoperative sclerosis (lower GSRb) than younger patients. These results would appear to suggest that GSRb is reflecting medial loading in terms of both weight and activity.

The limitations of this study include the fact that one implant (Oxford) was mobile bearing and the other (Preservation) fixed bearing. Though the tibial component was not the only variable to differ between implants, registry data has shown no difference in unexplained pain incidence between mobile and fixed bearing implants in the medial compartment (Baker, et al., 2012). Digital radiological densitometry is an inferred rather than a true measure of BMD, though as a technique has been validated against DEXA scanning (Hernandez-Vaquero, et al., 2005). We have tried to strengthen this methodology by representing our findings as a ratio of medial to lateral ROIs rather than as absolute values. This methodology can be used retrospectively and enables a greater sample size to be assessed. It also does not require any additional radiation, a disadvantage of quantitative CT.

Despite a mean reduction in GSRb, a proxy measure of medial tibial BMD, following medial UKRs, some patients display a localised increase in medial tibial density, or sclerosis. This is associated with elevated BMI and when it occurs is associated with persistent pain. This relative medial sclerosis may reflect ongoing microdamage and adaptive remodelling in overloaded and overstrained bone.

5 Finite Element Analysis

5.1 Aims and Objectives

1. To improve the experimentally validated finite element models to reflect more physiological conditions by loading both plateaus.

2. To use the new loading environment to investigate the effect of metal backing and varying implant polyethylene thickness using:
    a. All-polyethylene tibial components with 6-10mm thickness
    b. Metal backed tibial components with inserts of 6-10mm thickness

5.1.1 Research Questions

1. Do medial UKRs with all-polyethylene tibial components display greater proximal tibial cancellous bone strain than metal backed implants?
2. Does implant thickness have a greater effect on proximal tibial strain in all-polyethylene than metal backed medial UKR tibial components?

5.2 Chapter Summary

Unicompartmental knee replacements (UKRs) offer an attractive option when treating isolated medial compartment knee osteoarthritis. Concerns have been raised that elevated proximal tibial bone strain under these implants may result in ongoing pain. Finite element models (FEMs) can be very useful tools for investigating stresses and strains in the presence of orthopaedic implants (Pankaj, 2013). To enhance confidence in the results produced by FEMs, they are often validated against *in vitro* experiments. Validated FEMs facilitate the investigation of many more scenarios than are possible with *in vitro* or *in vivo* experiments (Pankaj, 2013).

The aim of this chapter was to investigate the effect of metal backing and polyethylene thickness on cancellous bone strain using experimentally validated finite element models under realistic loading conditions. Computer aided design (CAD) models of cemented fixed bearing medial UKRs with all-polyethylene and metal backed tibial components were created and implanted into a composite tibia consisting of cortical and cancellous bone parts. Analysis was performed using ABAQUS 6.12 (Dassault Systèmes, Waltham, Massachusetts) software. Models were validated using experimental digital image correlation (DIC) and acoustic emission (AE) data. Cortical bone vertical normal strain measured experimentally by DIC correlated significantly with cortical bone vertical strain predicted by the FEM for both implants (Pearson's correlation: AP 0.956, p=0.01, MB 0.885, p=0.01). Linear regression analysis indicated the best correlation between measured AE hits and predicted volume of cancellous bone elements with principal compressive strain <-3000με: correlation coefficients ($R= 0.947$, $R^2= 0.847$), standard error of the estimate (12.6 AE hits) and percentage error (12.5%) significant at $p<0.001$. Correlations were highest for the MB implant where AE hit number was lowest.

In the validated FEM, polyethylene thickness was varied from 6-10mm in 2mm increments. Both tibial plateaus were loaded up to 4170N (medial load 2500N) with a 60:40 (medial: lateral) split. Peak cancellous bone compressive and tensile strains were calculated in addition to the volume of cancellous bone strained below -3000 and -7000με limits. AP implants displayed greater cancellous bone strains than MB implants for all strain

parameters at all loads. Compressive strain was concentrated at the lateral edge of the MB implant. In the AP implant concentrations were present at the keel, anteromedially at the peg and centrally in the region of load application with a greater depth and volume of elements significantly overstrained <-7000με compared to the MB implant at all loads. Altering polyethylene insert thickness had no effect on cancellous bone strain in the MB implant. AP implants had 2.2 (10mm) to 3.2 (6mm) times the volume of cancellous bone compressively strained <-7000με than the MB implant. Exponential increases in the volume of bone with tensile strain >7000 occurred in the 6mm AP implant at total loads >2502N implying imminent bone failure. Increasing the thickness of all-polyethylene implants to 10mm does not overcome the differences in cancellous bone strain between AP and MB tibial components and is accompanied by the cost of greater bone resection.

5.3 Introduction

Whilst finite element analyses of UKRs exist in the literature (Tables 5.1 and 5.2), they are few in number and most frequently analyse the cemented mobile bearing Oxford UKR (Gray, et al., 2008; Gray, et al., 2007; Hopkins, et al., 2010; Kwon, et al., 2014; Pegg, et al., 2013; Simpson, et al., 2008; Simpson, et al., 2011; Simpson, et al., 2009; Tuncer, et al., 2013) with all but three (Hopkins, et al., 2010; Kwon, et al., 2014; Tuncer, et al., 2013) originating from the Oxford UKR design centre. Those investigating fixed bearing UKRs have typically examined polyethylene bearing stresses and strains rather than those of the bone into which they are implanted (Kwon, et al., 2014; Simpson, et al., 2008). One previous study (Sawatari, et al., 2005) reports cancellous bone strain in a metal backed fixed bearing device, investigating the effect of implant alignment upon this. Though a UKR with a fixed bearing all-polyethylene tibial component has been modelled before (Simpson, et al., 2008), bone strains were not reported and implant thickness was not varied. Elevated proximal tibial bone strain has been reported by FEM in the Oxford UKR previously (Simpson, et al., 2009), but the effect of metal backing and polyethylene thickness on proximal tibial strain, has not been investigated. Where bone stresses and strains have been examined, Von Mises stress and strain have been the outcome measure investigated. Yielding and failure of bone is based on strain rather than stress (Nalla, et al., 2005) and strain based criterion have been found to be numerically more efficient than stress based criterion in addition to being more accurate (Pankaj and Donaldson, 2013). Of the strain criteria used, strain based-plasticity, i.e. maximum and minimum principal strain, is more accurate than Von Mises strain (Pankaj and Donaldson, 2013).

Table 5.1 UKR finite element model validation studies.

Author	Year	Bone Model	Implant	Experimental Method	FE Parameter
Tuncer	2013	Cadaveric tibiae	Oxford (cemented & uncemented)	Strain gauge	Cortical bone strain
Gray	2008	Cadaveric tibia	Oxford	Strain gauge	Cortical bone strain
Gray	2007	Composite tibia	Oxford	Strain gauge	Cortical bone strain

Table 5.2 Finite Element Analyses of UKRs in the literature with investigated variables.

Author	Year	Bone Model	UKR Implant	Outcome measure	Variables
Kwon	2014	Patient tibia	Oxford MB fixed bearing (both cemented)	Contact stress	Gait cycle
Pegg	2013	Patient tibia	Oxford	Von Mises bone strain	Muscle forces Loading position Gait pattern
Simpson	2011	Patient tibia	Oxford (cemented & uncemented)	Von Mises bone strain	Cement Medial tie
Hopkins	2010	Patient tibia	Oxford (medial and lateral)	Contact stress	Gait cycle
Simpson	2009	Patient tibia	Oxford	Von Mises bone Strain	Over/underhang Malalignment
Simpson	2008	Cadaveric tibia	Congruent mobile bearing (Oxford) Non-congruent MB Non-congruent AP	PE Contact stress & Von Mises stress	UKR implant type PE thickness (MB implants only)
Sawatari	2005	Patient tibia	MB fixed bearing	Cancellous bone stress	Malalignment.

(Oxford = cemented medial, mobile bearing, metal backed UKR unless stated,

MB = metal backed, AP=all-polyethylene).

Finite element models can be very useful tools when designing and developing new orthopaedic implants, when investigating the stresses and strains created by these implants, and when deciding the patients for whom these implants are best suited. However, FE models are simplifications of the *in vivo* environment and include a number of assumptions in order to make them computable. To ensure that the output they produce is reliable, FE models are generally validated against experimental data, though both (FEM and experiment) are approximations of the complex *in vivo* scenario.

Traditionally strain gauge experiments have been used to validate FEMs in orthopaedics. The disadvantage of using this technique is that strain gauges measure strain only at the point of the structure to which they are attached. Though multiple strain gauges can be used to increase the number of strain data points obtained, digital image correlation (DIC) provides a better "full-field" measure of strain. DIC has been used previously to validate FE models of the proximal femur (Dickinson, et al., 2011; Grassi, et al., 2013), hemipelvis (Ghosh, et al., 2012), ankle (Terrier, et al., 2014) and human soft-tissue (Moerman, et al., 2009). To our knowledge DIC has not been previously used for FE model validation of the proximal tibia.

Acoustic emission is an engineering technique for measuring construct failure. It is based upon detecting autogenerated sound waves produced by material as it experiences stresses and strains (Hirasawa, et al., 2002; Leung, et al., 2009; Mavrogordato, et al., 2011). When an object is exposed to load, it undergoes first elastic and then post-elastic deformation whereby the material is permanently altered and does not recover to its original form on unloading. Post-elastic deformation may be due to plasticity or damage. Plasticity and damage involve atomic planes sliding past each other or microcracks propagating through a material. These events release elastic waves of energy which travel through the material and can be detected on its surface by piezoelectric sensors transforming the acoustic waves into voltage. Strain and microdamage can therefore be detected and quantified in real time (Leung, et al., 2009; None-Listed, 2012; Roques, 2004). Most detectable AE activity occurs during plastic deformation when a material is loaded near to its yield point. Figure 5.1

shows an AE wave form and its associated features. Amplitude is proportional to crack propagation velocity. Brittle cracking and ductile plastic deformation display different AE waveforms. Brittle cracking is indicated by a shorter rise time and medium duration. Energy versus duration plots display the extent of damage within a specimen (Leung, et al., 2009). Long durations and high energies indicate more damage.

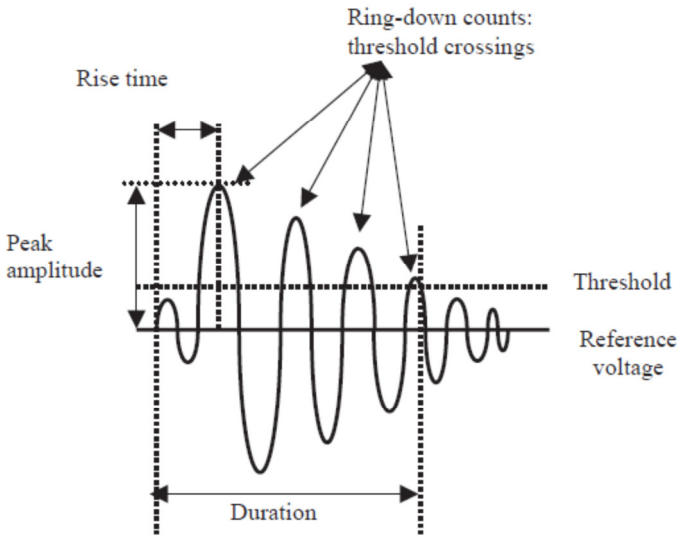

Figure 5.1 An acoustic signal wave form and its parameters (Roques, 2004).

Acoustic emission has been used in conjunction with micro-CT (μCT) in some studies to verify the extent of structural microdamage occurring in the presence of AE detected events (Leung, et al., 2009; Mavrogordato, et al., 2011). Leung et al (Leung, et al., 2009) correlated AE at the cement-bone interface with μCT concluding that early failure was detected, located and characterized using AE with "hits" of >60dB associated with damage on μCT (Leung, et al., 2009). Acoustic emission may even be preferable to μCT as some microcracks close up on unloading and may be missed on μCT in an unloaded condition or where metal artefacts obscure microcracks.

The AE technique is used in a number of mechanical and structural engineering applications for early detection of crack formation and propagation: in pressure vessels and pipelines, in reinforced concrete structures, in substances being welded, and in the

aerospace industry (Eaton, et al., 2011; Hirasawa, et al., 2002; Holford, et al., 2009). AE is also used by seismologists for earthquake detection and location (Qi, et al., 2000). In the field of orthopaedic research it has been used to investigate cortical and cancellous bone properties (Nicholls and Berg, 1981; Wells and Rawlings, 1985); fracture healing and callus formation (Hirasawa, et al., 2002); fatigue crack location and propagation in cement (Qi, et al., 2000; Roques, 2004); bone-cement interface integrity (Leung, et al., 2009); wear in metal-on-metal hip prostheses (Rowland, et al., 2004) and loosening of hip prosthesis (Mavrogordato, et al., 2011). Though AE is a highly appropriate way to evaluate microdamage, and thus strain, in bone models, it has not been used previously to validate a finite element model.

5.4 Results

In finite element modelling the convention is to denote compressive stresses and strains as negative and tensile stresses and strains as positive. Element volumes with compressive (minimum principal) strains below a certain threshold and tensile (maximum principal) strains above a certain threshold were evaluated for each model. Results were correlated with experimental results using both digital image correlation and acoustic emission (Appendix 3). The full validation is reported in the Methods chapter 2.6.

5.4.1 Loading Both Plateaus

Loading both plateaus gave a more physiologic distribution of strain within the proximal tibia than when only the medial plateau was loaded (Figures 5.2 and 5.3). This was the case for both implants. The strain shielding of the lateral cortical and cancellous bone, present in the medially only loaded model, was resolved by loading both plateaus (Figures 5.2 and 5.3, Tables 5.3 and 5.4). The cortical strain concentration medially at the metaphyseal

flare also diminshed with the addition of a lateral load. This likely represents resolution of a bending moment in this region resultant of unilateral loading. Unsurprisingly, increasing the total load by adding a lateral load, increased the proportion of cancellous bone elements experiencing strain <-3000με particularly at total loads >2502N (medial loads >1500N) (Tables 5.3 and 5.4).

Loading both plateuas produced similar effects for both implants. The volume of cancellous bone elements with compressive strain <-3000με converged faster between implants as greater total loads were applied (Figure 5.4a). Greater divergence between AP and MB implants, was apparent in the volume of cancellous bone elements with compressive strain <-7000με (Figure 5.4b) and tensile strain >3000 με (Figure 5.5a). This is to be expected: differences in the volume of elements experiencing <-3000με between implants disappear when load is increased whereas reducing the threshold to <-7000με becomes more discriminating. The effect of loading both plateaus on the volume of elements with tensile strain >7000με is less obvious (Figure 5.5b), but appears to increase exponentially in the AP implant at high loads reaching twice that of the MB implant at total loads of 4170N (medial load 2500N).

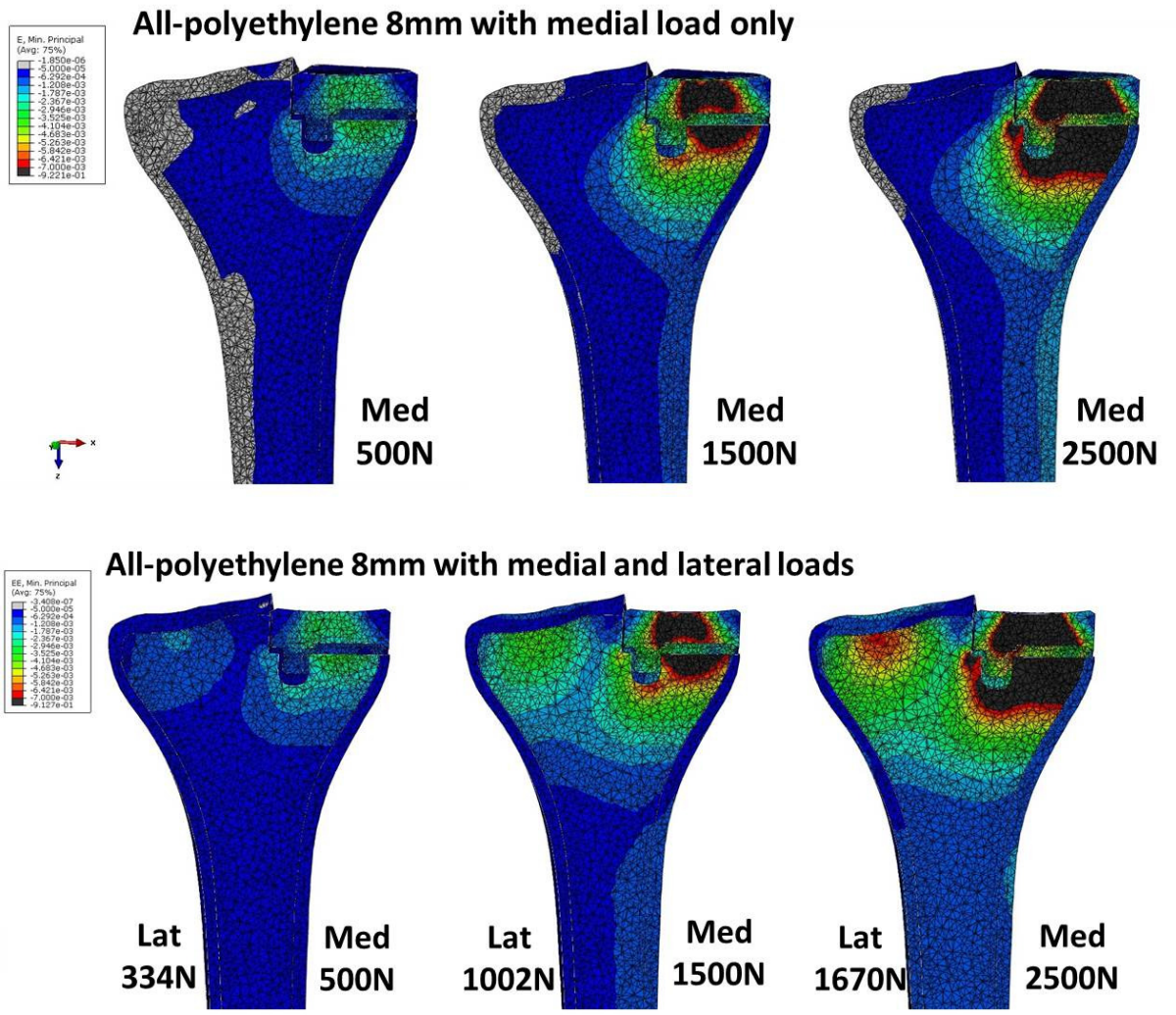

Figure 5.2 Mid-coronal plane contours of the entire model with the AP 8mm implant with loading of medial only and both plateaus. Strain >-50με appears pale grey, strain <-7000με appears black.

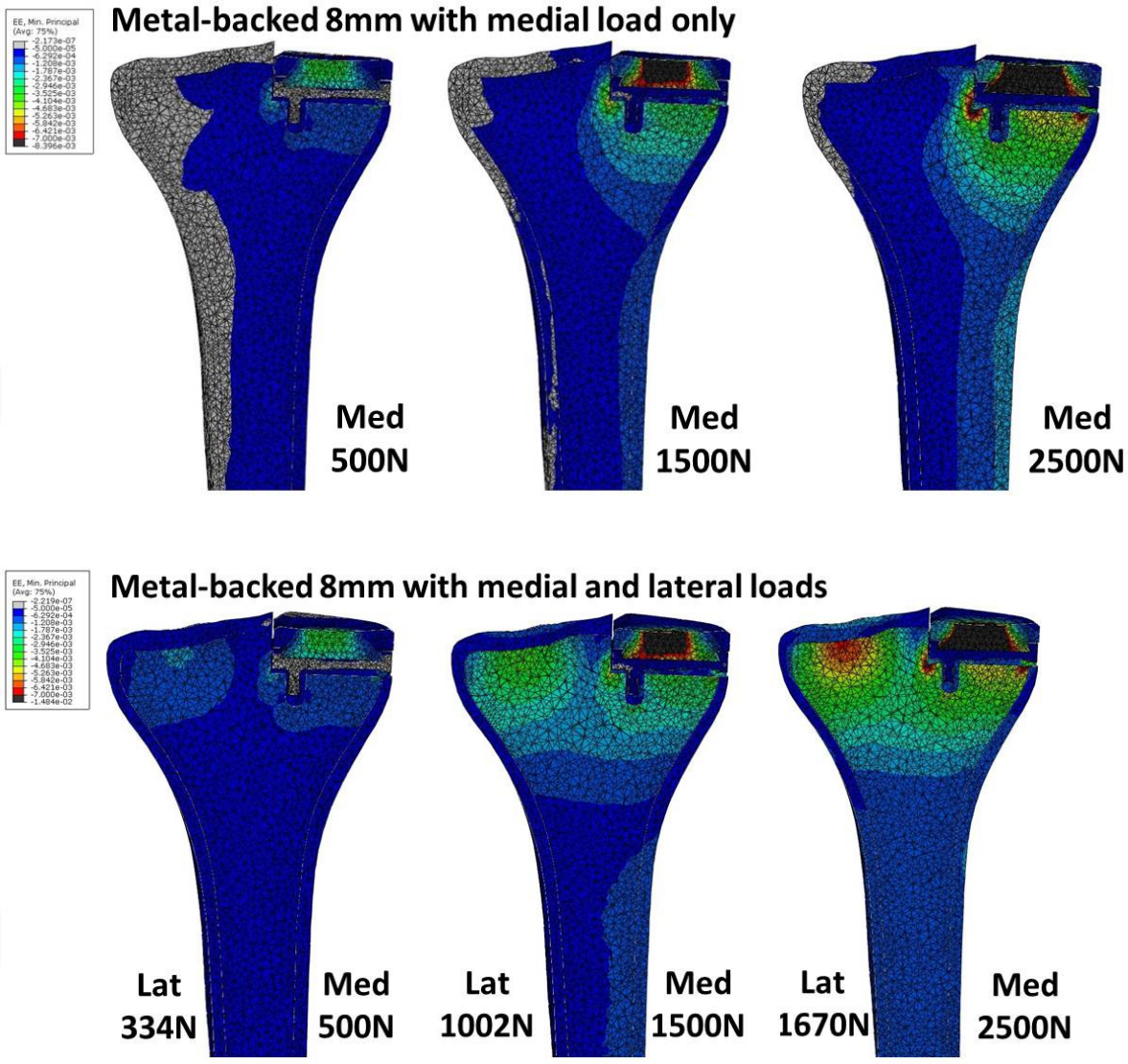

Figure 5.3 Mid-coronal plane contours of the entire model with the MB 8mm implant with loading of medial only and both plateaus. Strain >-50με appears pale grey, strain <-7000με appears black.

Table 5.3 Compressive (minimum principal) strain in each implant at each load when load is applied to medial plateau only and to both plateaus.

		Medial load only				Both plateaus loaded			
Model	**Medial Load (N)**	**Volume of Elements (mm^3) with compressive (Minimum principal) microstrain (με):**				**Volume of Elements (mm^3) with compressive (Minimum principal) microstrain (με):**			
		>-50	**<-1500**	**<-3000**	**<-7000**	**>-50**	**-<-1500**	**<-3000**	**<-7000**
8mm AP Tibia	**500**	9201.06	3874.17	289.38	0.89	46.67	5167.04	347.90	1.89
	1000	1256.61	9824.84	3887.80	94.06	3.29	16126.26	5191.64	120.18
	1500	322.06	12942.83	7718.74	973.68	1.38	24754.46	11238.51	1229.83
	2000	125.80	15387.34	9836.37	2615.57	0.65	32399.58	16148.95	3448.61
	2500	77.10	17394.35	11492.90	4578.53	0.65	39819.10	20517.26	6142.12
8mm MB Tibia	**500**	14566.8	324.25	17.18	0.07	352.06	1788.03	31.32	0
	1000	3360.90	4120.28	324.16	6.52	42.72	14304.77	1802.37	8.34
	1500	1266.54	8853.16	1390.97	72.25	16.74	24341.94	6856.05	262.05
	2000	487.44	11565.08	4150.67	177.02	6.03	30070.76	14384.7	1019.92
	2500	125.66	13536.62	6940.30	398.93	3.43	34024.84	20133.16	2244.38

Table 5.4. Tensile (maximum principal) strain in each implant at each load when load is applied to medial plateau only and both plateaus.

		Medial load only			Both plateaus loaded		
Model	**Medial Load (N)**	**Volume of Elements (mm^3) with tensile (Maximum principal) microstrain (με):**			**Volume of Elements (mm^3) with tensile (Maximum principal) microstrain (με):**		
		>1500	**>3000**	**>7000**	**>1500**	**>3000**	**>7000**
8mm AP Tibia	**500**	137.80	0.94	0.00	217.09	13.52	0.00
	1000	2965.75	137.94	0.36	3553.39	218.37	0.22
	1500	6556.63	1314.93	18.90	9248.53	1586.91	41.54
	2000	9648.66	2980.15	74.48	18032.93	3565.13	109.04
	2500	12058.24	4794.13	203.97	25246.01	6170.45	298.11
8mm MB Tibia	**500**	189.59	25.81	0.00	128.03	14.92	0
	1000	880.20	189.59	10.60	803.16	127.98	8.64
	1500	1848.22	461.89	63.29	5588.88	381.98	40.46
	2000	3124.21	883.23	137.83	10563.25	804.23	83.66
	2500	4713.30	1345.02	224.92	15643.91	2794.24	158.3

a)

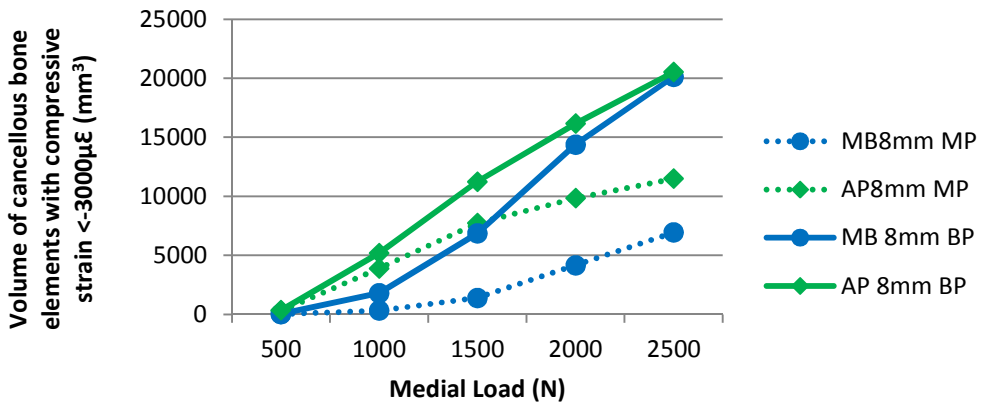

b)

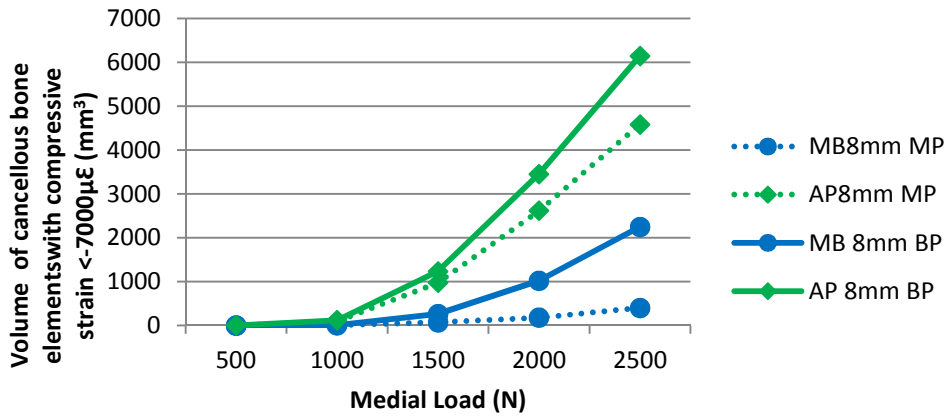

Figure 5.4 The effect of loading the medial plateau only (MP) and both plateaus (BP) on cancellous bone element compressive strain in both 8mm implants: a) Total strain, b) Volume of cancellous bone elements with strain >3000με, and c) Volume of cancellous bone elements with strain >7000με.

a)

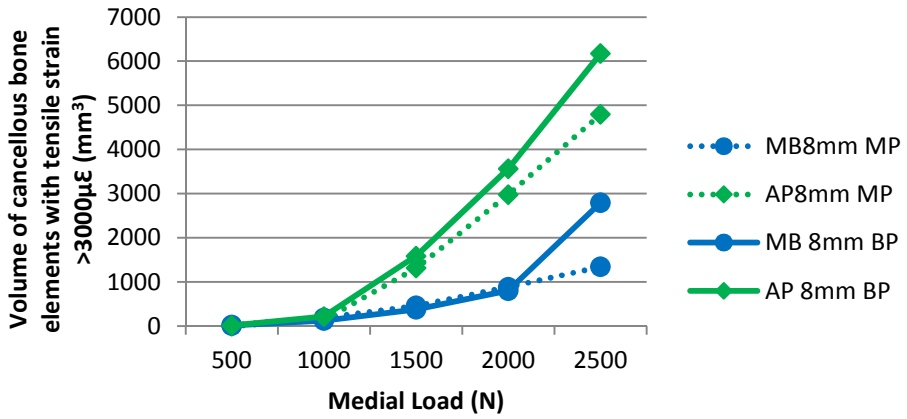

b)

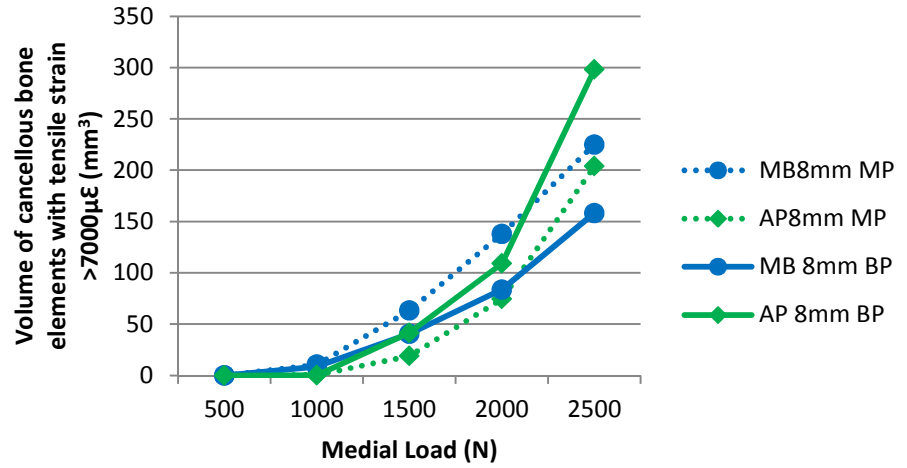

Figure 5.5 The effect of loading the medial plateau only (MP) and both plateaus (BP) on cancellous bone element tensile strain in both 8mm implants: a) Volume of cancellous bone elements with strain >3000με, and b) Volume of cancellous bone elements with strain >7000με.

5.4.2 Comparing All-Polyethylene and Metal-Backed Implants

At low loads (884N, ~body weight), differences were apparent between implants in the volume of cancellous bone experiencing very low minimum principal strain (>-50με). Seven times more cancellous bone elements were shielded from compressive strain (>-50με) in the MB implant compared to the AP implant at this lowest load (Figure 5.6). As would be expected, when the compressive load is increased, the volume of understrained elements falls rapidly and thus no difference is appreciable between implants.

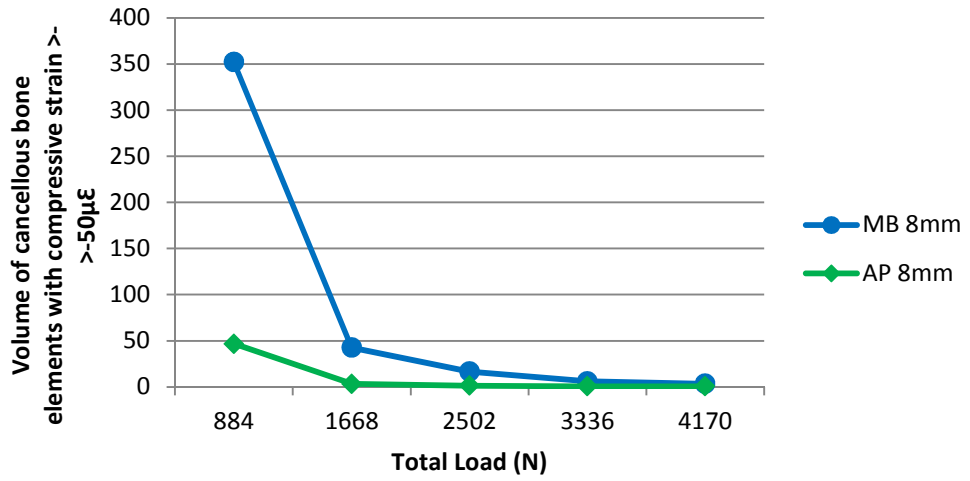

Figure 5.6 Cancellous bone compressive strain shielding (volume of elements with >-50με).

At the largest loads applied, significantly greater volume of cancellous bone exhibits compressive strain <-7000με in the AP compared to the MB implant (Figure 5.7). This is concentrated posteriorly, possibly consequent of the posterior tibial slope. Whereas strain is concentrated most obviously around the posteromedial rim of the tibial cancellous bone in the AP implants, the maximal concentration in th MB implant appears laterally at the apex where horizontal and vertical cuts for the implant converge.

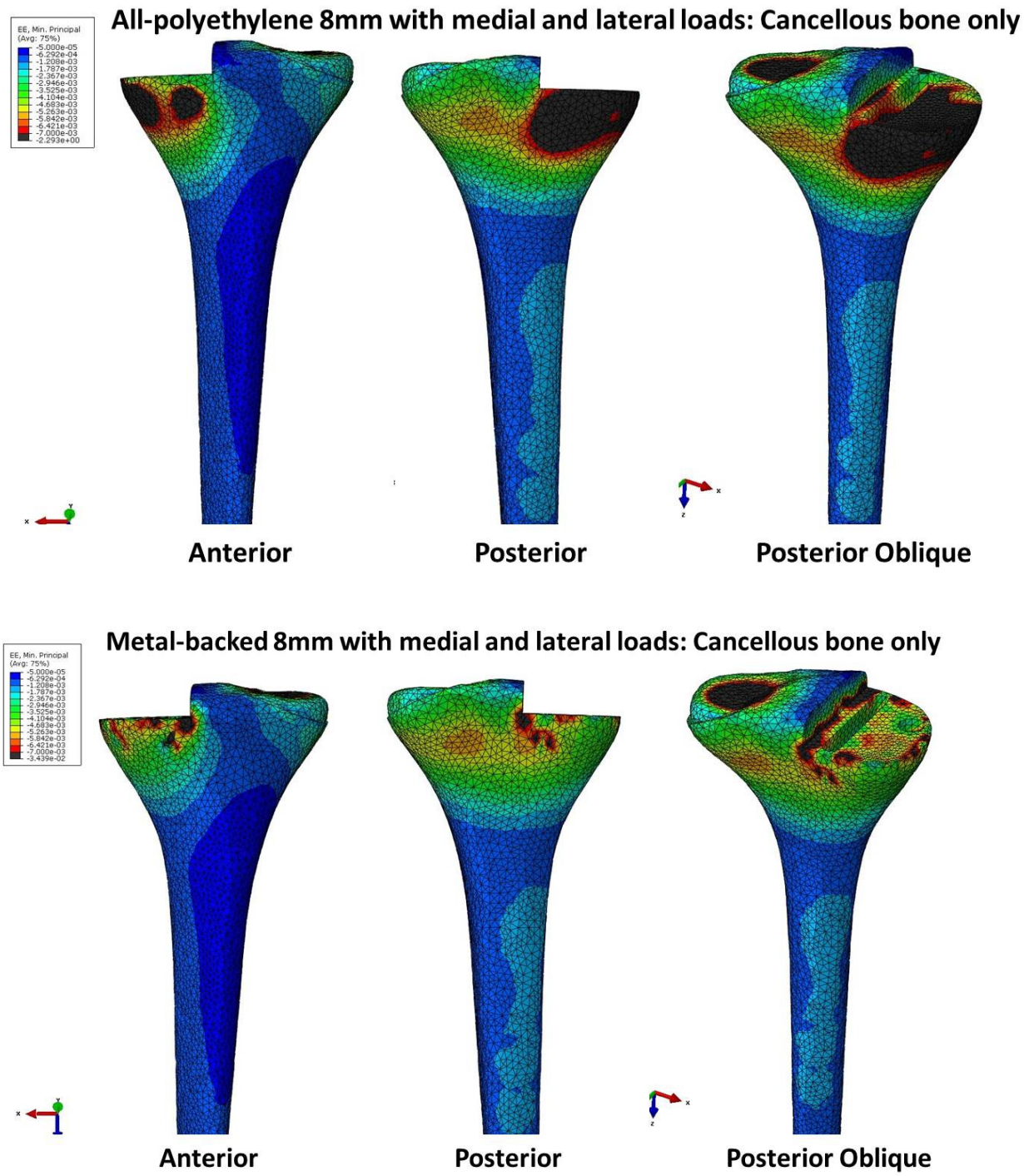

Figure 5.7 Contours of cancellous bone outer surface for each implant from different aspects with a total load of 4170N. Strain >-50με appears pale grey, strain <-7000με appears black.

To examine the distribution of compressive strain in more detail, Figure 5.8 shows coronal sections of the cancellous bone. While compressive strain is concentrated to the level of the cut surface of the tibia at the corner of the implant for the MB tibial component, it extends much deeper into the cancellous bone under the AP implant. This is the case even at lower loads (2502N, 3-3.5x body weight) which would be encountered during normal stair climbing.

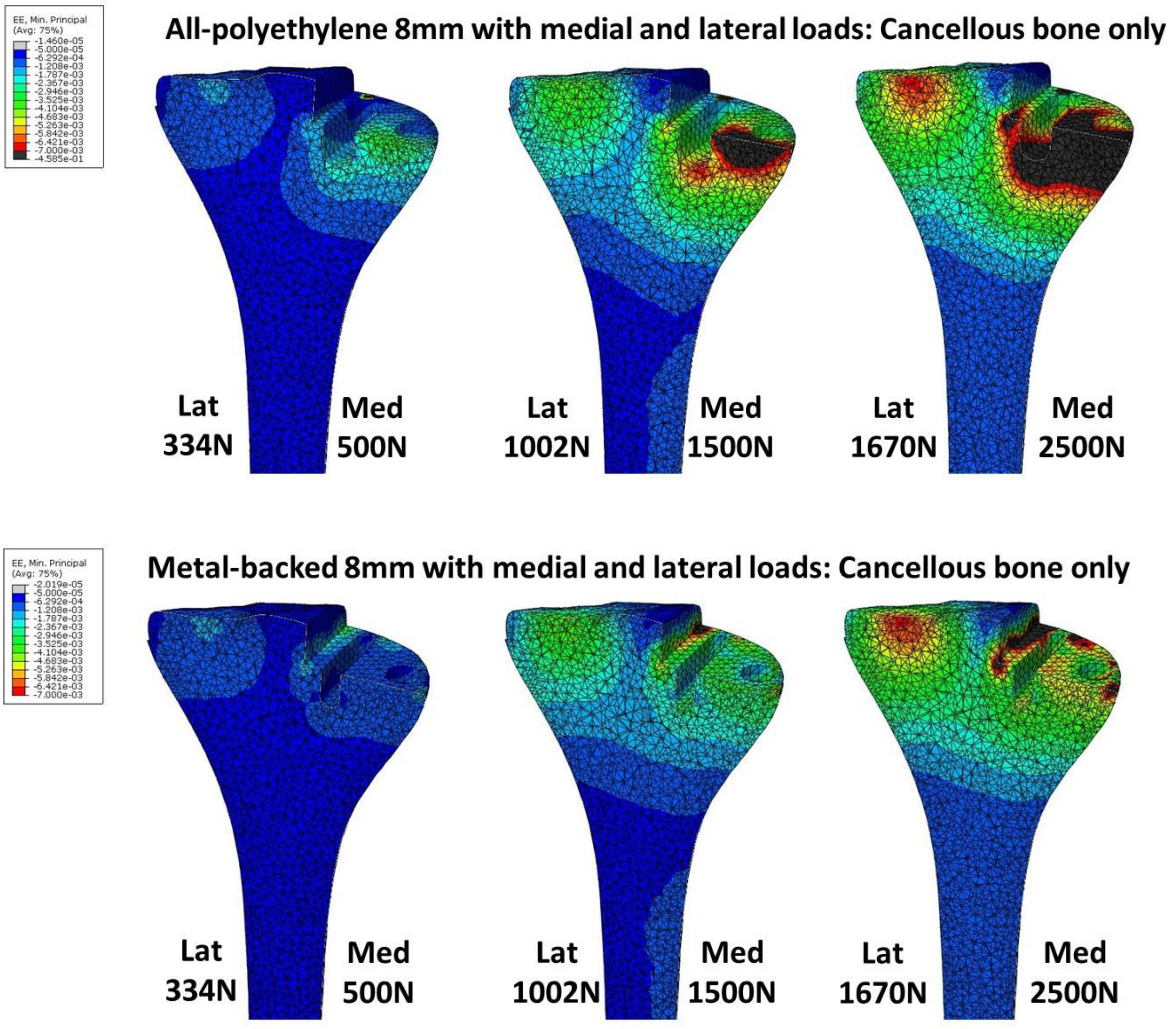

Figure 5.8 Mid-coronal oblique contours of the upper surface of cancellous bone for each implant. Strain >-50με appears pale grey, strain <-7000με appears black.

Contours of the cut surface of the cancellous tibia (axial view) again emphasize the difference in the volume of bone overstrained compressively <-7000με between AP and MB implants (Figure 5.9). This figure also shows that strain is being transmitted to the bone by the AP peg and keel in a manner not displayed by the MB implant.

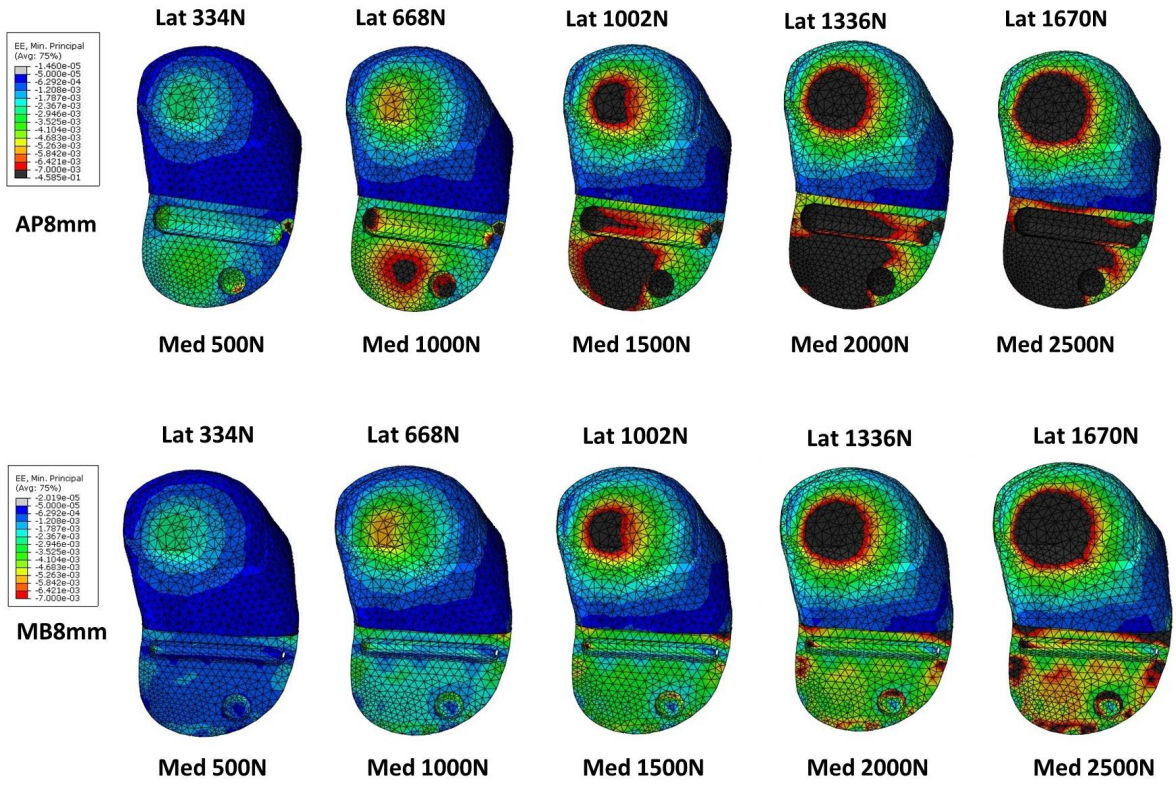

Figure 5.9 Contours at the upper surface of cancellous bone for each 8mm implant. Strain >-50με appears pale grey, strain <-7000με appears black.

As before (Chapter 5), a <-7000με compressive strain threshold is more discriminating for differences between implants at higher loads where the volume of elements with strain <-3000με plateaus in both implants (Figure 5.10). In the AP implant nearly 3 times the volume of cancellous bone is pathologically overstrained at high loads (4170N, 5-6 x body weight) compared to the MB implant (Figure 5.10b). Tensile strains are the result of Poisson's effect when the load is applied in compression. Tensile strains display the same S shaped curve as compressive strains. Therefore, differences between implants in the volume of cancellous bone with tensile strain >3000 με are maximal at lower loads (1668N) than that which occurs when the threshold is increase to >7000με (4170N) (Figure 5.11).

a)

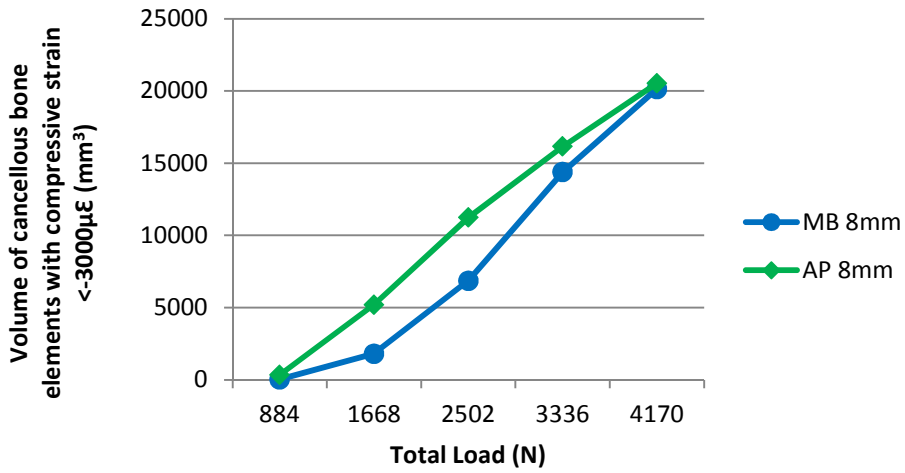

b)

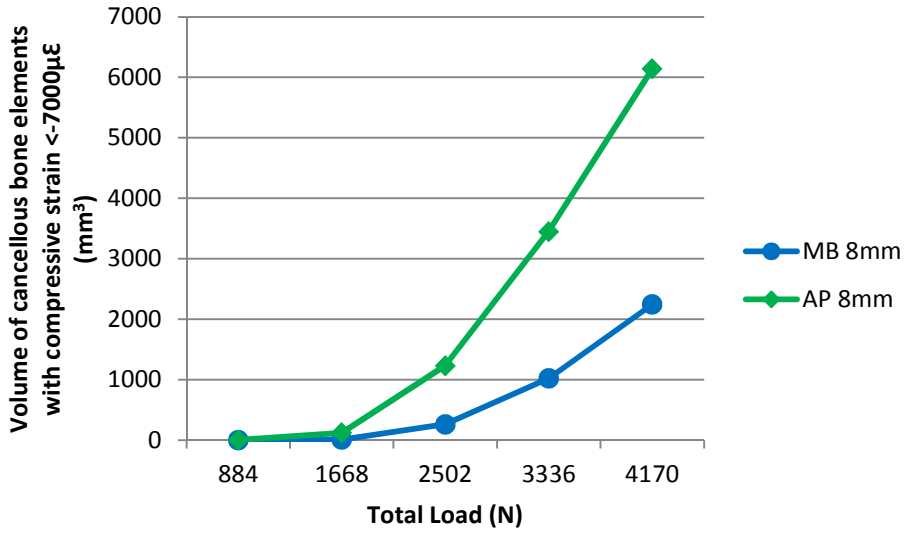

Figure 5.10 Volume of cancellous bone elements with compressive strain (minimum principal strain) a) <-3000με and b) <-7000με for both MB and AP 8mm implants.

a)

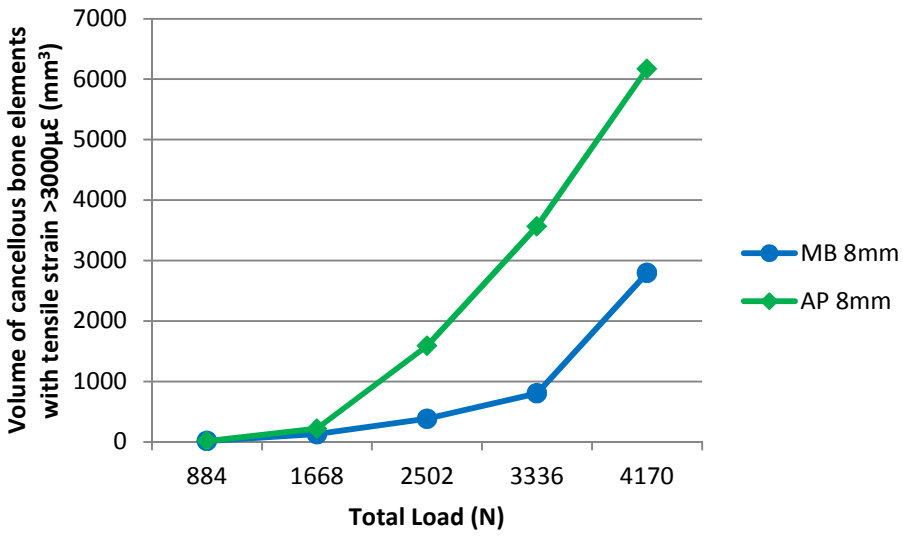

b)

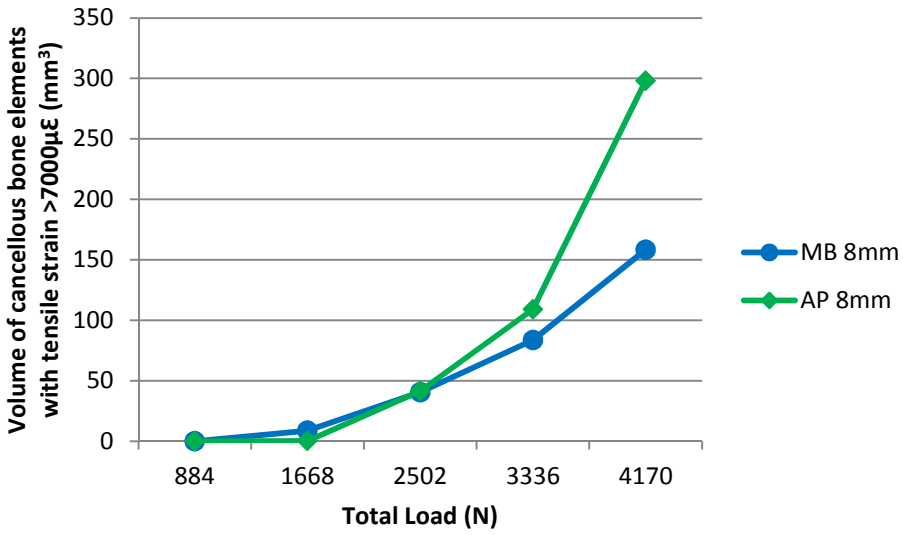

Figure 5.11 Volume of cancellous bone elements with tensile strain (maximum principal strain) a) >3000με and b) >7000με for both MB and AP 8mm implants.

Figure 5.12, showing the medial aspect of the proximal tibial cancellous bone, demonstrates the anteromedial strain concentration in association with the keel and peg of the AP implant. This strain concentration is present under the AP implant even at low loads (medial load 1000N, total load 1668N, 2 x body weight). Though at high loads strain overloading appears to be worst posteriorly in the AP implant, the anteromedial strain concentration occurs much earlier in loading. In both implants, the cancellous bone elements experiencing the *peak* strains (minimum principal and maximum principal) are located in this region: the anteromedial tibia at the implant keel (Figures 5.13 and 5.14). In the MB implant, strain concentrates in the region of the keel, but to a lesser degree than in the AP, with a relative shielding occurring in the region of the peg (Figure 5.12).

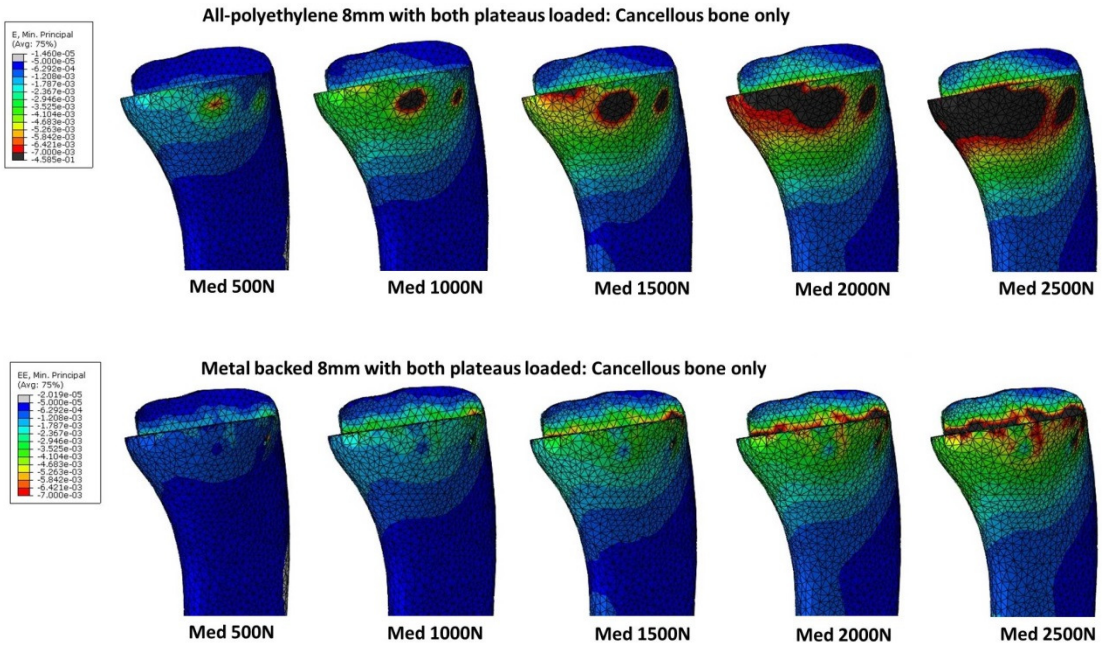

Figure 5.12 Medial aspect contour of the outer surface of cancellous bone for each 8mm implant. Strain >-50με appears pale grey, strain <-7000με appears black.

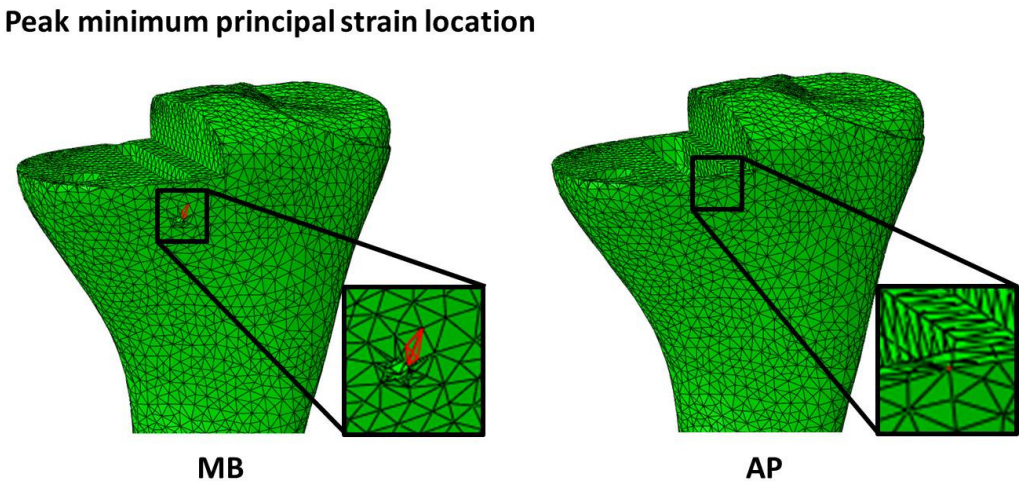

Figure 5.13 Location of the cancellous bone element experiencing the peak compressive strain on loading (both implants).

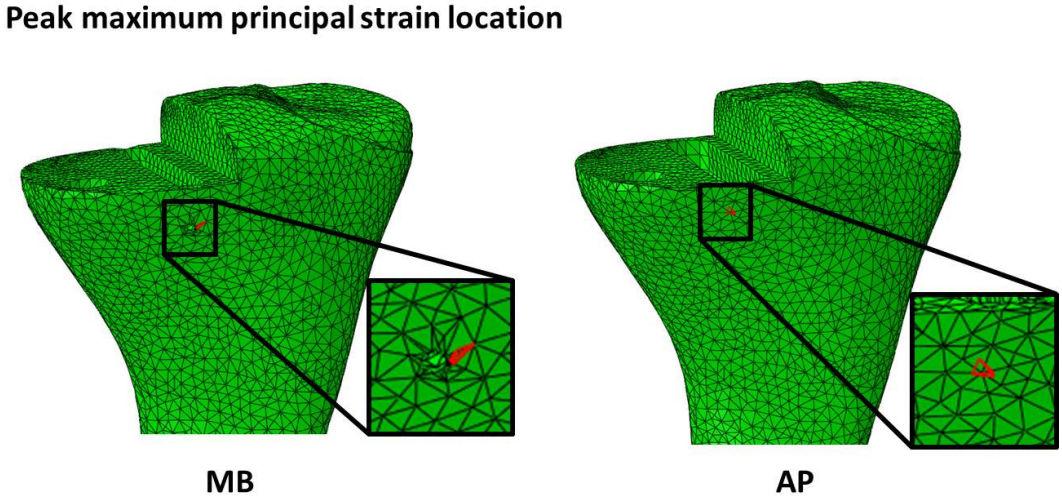

Figure 5.14 Location of the cancellous bone element experiencing the peak tensile strain on loading (both implants).

The deformation of each implant on loading differed between AP and MB implants. This is demonstrated by figures 5.15 and 5.16 below. The AP implants underwent more bending than the stiffer metal backed implant in both coronal and sagittal planes (Figure 5.15 and 5.16). Strain within the substance of the polyethylene was less in the AP implant where deformation was greatest. In the MB implant, with its stiff metal backing, the polyethylene

experienced higher strain within its substance, as strain energy was not dissipated by deformation.

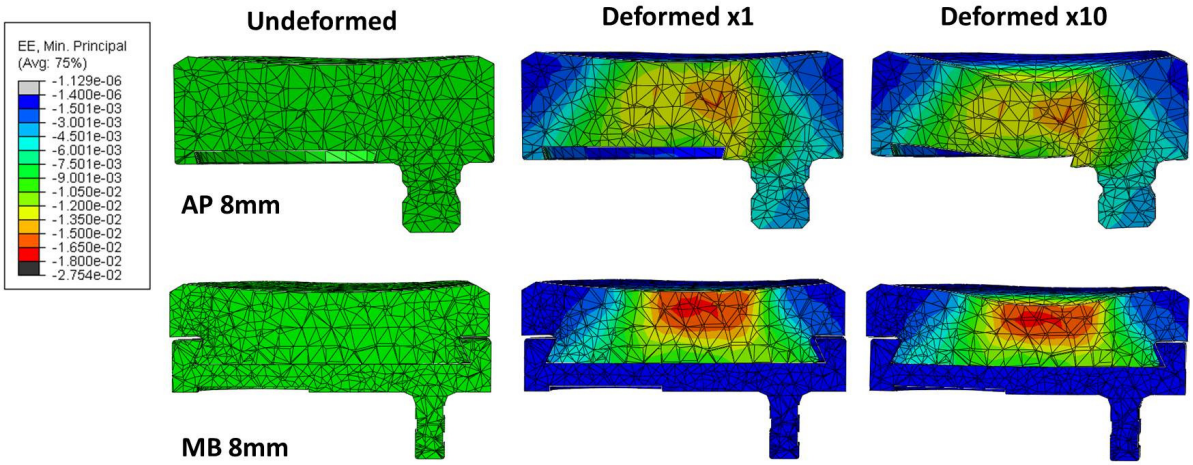

Figure 5.15 Coronal plane contours showing implant deformation (middle column) with a 2500N medial load. The deformation has been magnified x10 (right hand column) to illustrate the pattern of bending more clearly.

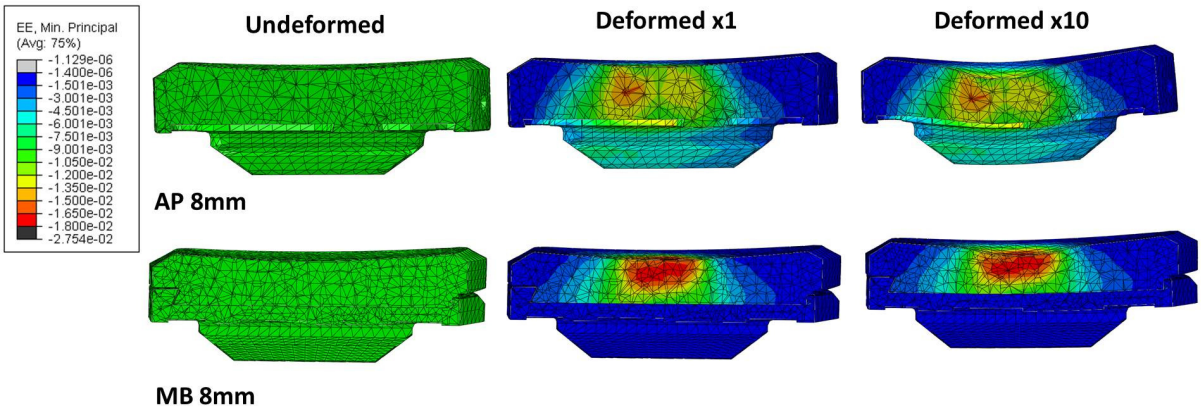

Figure 5.16 Sagittal plane contours showing implant deformation (middle column) with a 2500N medial load. The deformation has been magnified x10 (right hand column) to illustrate the pattern of bending more clearly.

5.4.3 Altering Implant Thickness

Peak compressive and peak tensile strains were significantly higher in the AP implants at all loads (Table 5.5). As this is a linear analysis, peak strains increased linearly with load for all thicknesses of both implants. The elements experiencing the peak minimum principal (compressive) and maximum principal (tensile) strains were located in the same cancellous bone region for both implants – anteromedially in association with the implant keel (Figures 5.13 and 5.14). In the MB implants there was little difference between peak strain values for both tensile and compressive strain. Peak tensile strains were much higher than peak compressive strains in the AP implants and this difference increased with increasing load, reaching 2 to 3 times at loads >2502N. This may reflect bending of the implant in this region. Altering the thickness of the AP implant had little effect on peak tensile strains, but peak compressive strain was 1.4 times greater in the 6mm compared to the 10mm AP implant.

The volume of cancellous bone exposed to compressive strain of <-3000με differed between AP and MB implants at lower loads with approximately twice the volume strained above this in the AP implant at 1668N and 2502N loads (2.5-4 times body weight) (Table 5.6, Figure 5.17a). At higher loads (4170N, 5-6 times body weight), the volume of elements experiencing compressive strain <-7000με is again greater in the AP implants (Figure 5.17b). This results in 2.2 (10mm) to 3.2 (6mm) times the volume of cancellous bone compressively overstrained <-7000με in the AP compared to the MB implant at a 4170N load. Altering the polyethylene thickness of the MB implant makes little, if any, difference to the volume of bone with compressive strain <-3000 or <-7000 με (Table 5.6, Figure 5.17a and b), or tensile (Table 5.7, Figure 5.18) strain above 3000με or 7000με. Altering the thickness of the AP implant makes significant differences, especially at loads >2502N where reducing implant thickness from 10 to 6mm increases the cancellous bone volume with compressive strain <-7000με by 1.5 to 3 times (Table 5.6, Figure 5.17b). Altering implant thickness had no effect on the volume of cancellous bone strain with compressive strain >-50με in either implant (Figure 5.17c).

Table 5.5 Peak strains (compressive and tensile) for both AP and MB implants of 6-10mm thicknesses at loading increments.

PE Thickness	Load	Peak Strain	
		Compressive (Minimum Principal)	Tensile (Maximum Principal)
Metal Backed			
6mm	**884**	-0.0073	0.0072
	1668	-0.0145	0.0143
	2502	-0.0218	0.0215
	3336	-0.0289	0.0287
	4170	-0.0361	0.0359
8mm	**884**	-0.0070	0.0069
	1668	-0.0139	0.0138
	2502	-0.0207	0.0207
	3336	-0.0276	0.0277
	4170	-0.0344	0.0346
10mm	**884**	-0.0069	0.0070
	1668	-0.0138	0.0140
	2502	-0.0207	0.0211
	3336	-0.0275	0.0281
	4170	-0.0343	0.0351
All-Polyethylene			
6mm	**884**	-0.0142	0.0314
	1668	-0.0283	0.0628
	2502	-0.0425	0.0942
	3336	-0.0566	0.1255
	4170	-0.0708	0.1569
8mm	**884**	-0.0118	0.0319
	1668	-0.0236	0.0639
	2502	-0.0354	0.0958
	3336	-0.0472	0.1277
	4170	-0.0590	0.1596
10mm	**884**	-0.0102	0.0320
	1668	-0.0204	0.0639
	2502	-0.0306	0.0959
	3336	-0.0408	0.1279
	4170	-0.0510	0.1598

Table 5.6 Compressive strain parameters for both AP and MB implants of 6-10mm thicknesses at 500N increments.

PE Thickness	Total Load (N)	Volume of Elements (mm^3) with compressive microstrain (minimum principal strain):			
Metal Backed		**>-50**	**-<-1500**	**<-3000**	**<-7000**
6mm	**884**	313.04	1827.37	32.29	0.07
	1668	42.56	14827.36	1845.27	10.44
	2502	16.52	24715.38	7227.33	275.01
	3336	6.03	30407.19	14924.57	1049.01
	4170	3.43	34317.07	20562.68	2305.41
8mm	**884**	352.06	1788.03	31.32	0.00
	1668	42.72	14304.77	1802.37	8.34
	2502	16.74	24341.94	6856.05	262.05
	3336	6.03	30070.76	14384.70	1019.92
	4170	3.43	34024.84	20133.16	2244.38
10mm	**884**	346.66	1819.11	32.52	0.00
	1668	43.02	14184.47	1835.93	9.51
	2502	15.29	24536.11	6757.26	274.96
	3336	6.03	30255.21	14265.49	1039.10
	4170	3.43	34230.93	20290.19	2294.26
All-Polyethylene		**>-50**	**<-1500**	**<-3000**	**<-7000**
6mm	**884**	46.67	6562.31	857.59	4.16
	1668	3.29	16905.81	6590.14	446.53
	2502	1.38	25620.38	12066.09	2104.15
	3336	0.65	33362.09	16931.23	4715.91
	4170	0.65	40966.39	21285.81	7385.94
8mm	**884**	46.67	5167.04	347.90	1.89
	1668	3.29	16126.26	5191.64	120.18
	2502	1.38	24754.46	11238.51	1229.83
	3336	0.65	32399.58	16148.95	3448.61
	4170	0.65	39819.10	20517.26	6142.12
10mm	**884**	46.44	4044.33	109.57	1.17
	1668	3.29	15393.73	4065.60	44.80
	2502	1.38	23899.60	10381.01	698.24
	3336	0.65	31510.15	15427.14	2432.06
	4170	0.65	38886.41	19793.15	4963.40

a)

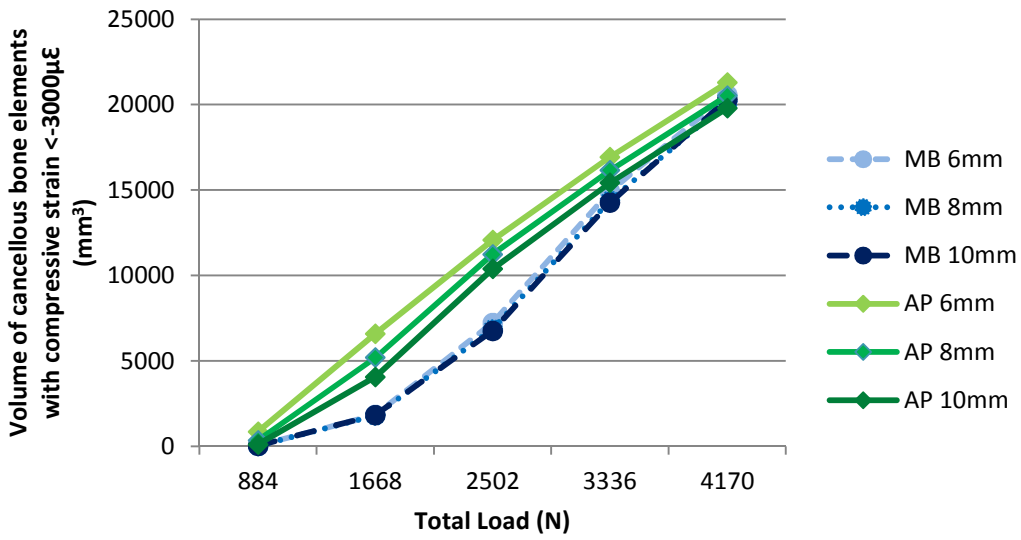

b)

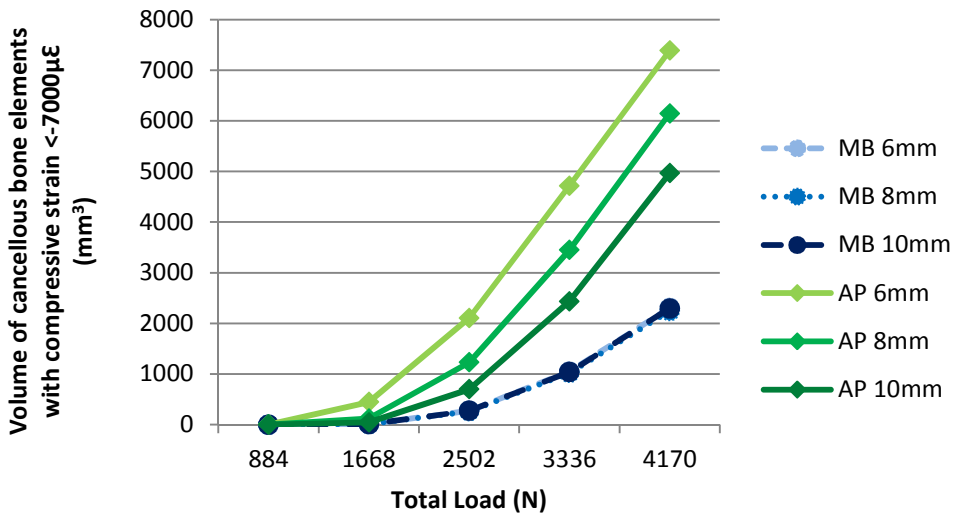

c)

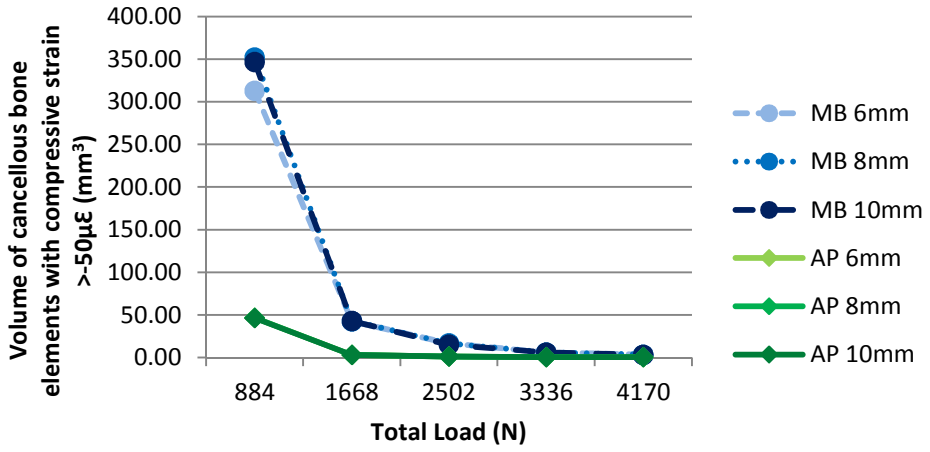

Figure 5.17 Volume of cancellous bone elements with compressive (minimum principal) strain a) <-3000με b) <-7000με and c) >-50με for both MB and AP implants of 6-10mm thickness.

Though peak tensile strains exceed peak compressive strains in the AP implant (Table 5.5), the volume of cancellous bone elements with tensile strain >3000με or >7000με is significantly less for tensile compared to compressive strain for both implants. This is to be expected as the model is loaded in compression with tensile strains predominantly consequent of the Poisson effect.

The volume of cancellous bone exposed to tensile strain of >3000με differed significantly between AP and MB implants at loads of 2502N and above (Figure 5.18). Altering the thickness of the MB implant polyethylene made no difference to the volume of cancellous bone overstrained above both 3000με and 7000με at any load (Table 5.7, Figure 5.18). Reducing the AP thickness from 10 to 6mm increased the volume of cancellous bone with tensile strain >3000με by 1.5 to 3.24 times at loads of 2502N and higher (Table 5.7, Figure 5.18a). Comparing 6mm AP and MB implants found 5.7 times the volume of cancellous bone with tensile strain >3000με at 2502N and 2.4 times at 4170N. For the 10 mm implants the corresponding values are 2.2 times at 2502N and 1.8 times at 4170N.

The volume of cancellous bone exposed to tensile strain of >7000με again differed significantly between AP and MB implants, but at loads of 4170N. At this maximum load, the volume of cancellous bone overstrained above 7000με increases exponentially in the 6mm AP implant, and this may reflect impending catastrophic failure (Figure 5.18b).

Table 5.7 Tensile strain parameters for both AP and MB implants of 6-10mm thicknesses at 500N increments.

PE Thickness	Total Load (N)	Volume of Elements (mm^3) with tensile microstrain (maximum principal strain):		
Metal Backed		**>1500**	**>3000**	**>7000**
6mm	**884**	140.77	16.52	0.02
	1668	853.47	140.77	9.69
	2502	5748.18	411.76	43.11
	3336	10822.93	856.12	88.95
	4170	15957.36	2940.40	174.24
8mm	**884**	128.03	14.92	0.00
	1668	803.16	127.98	8.64
	2502	5588.88	381.98	40.46
	3336	10563.25	804.23	83.66
	4170	15643.91	2794.24	158.30
10mm	**884**	137.99	16.43	0.02
	1668	830.86	137.99	9.62
	2502	5704.36	401.98	42.62
	3336	10663.27	835.94	88.36
	4170	15646.46	2908.76	174.54
All-Polyethylene		**>1500**	**>3000**	**>7000**
6mm	**884**	481.96	14.60	0.00
	1668	4527.35	487.67	0.48
	2502	10304.26	2352.38	44.81
	3336	18803.61	4543.18	146.83
	4170	25844.91	7136.16	742.40
8mm	**884**	217.09	13.52	0.00
	1668	3553.39	218.37	0.22
	2502	9248.53	1586.91	41.54
	3336	18032.93	3565.13	109.04
	4170	25246.01	6170.45	298.11
10mm	**884**	180.29	13.50	0.00
	1668	2782.01	180.43	0.06
	2502	8389.91	895.87	37.15
	3336	17247.52	2794.86	88.04
	4170	24549.04	5273.60	237.98

a)

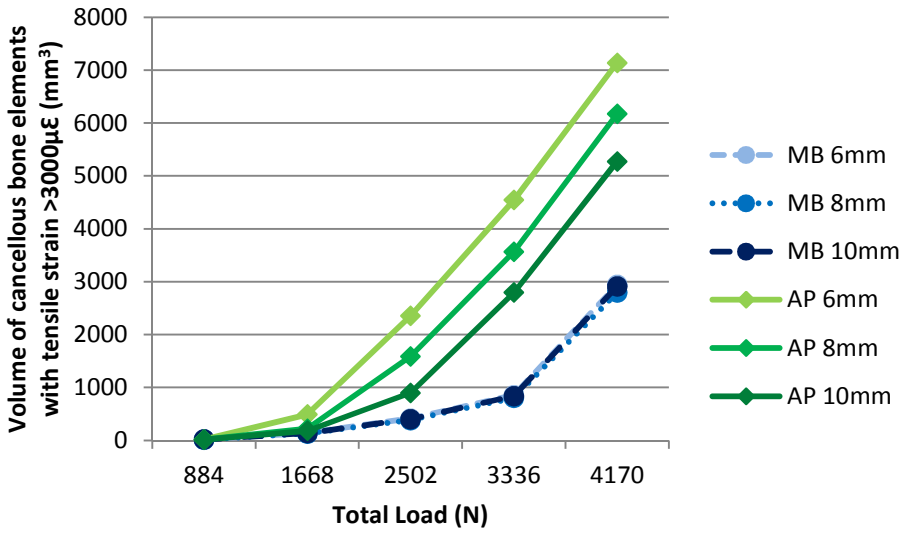

b)

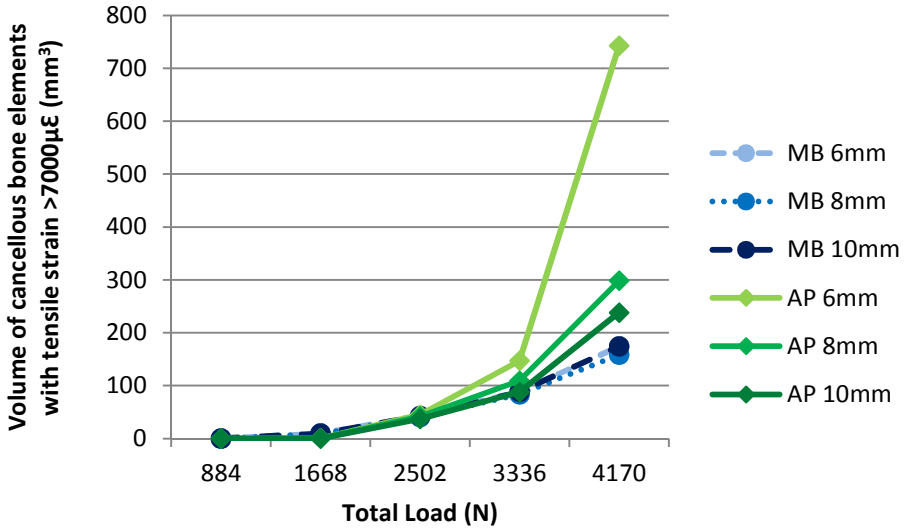

Figure 5.18 Volume of cancellous bone elements with tensile strain (maximum principal strain) a) >3000με and b) >7000με for both MB and AP implants of 6-10mm thickness.

Figures 5.19 and 5.20, show axial view compressive contours for the different thicknesses of both AP and MB implants. The differences between AP and MB implants have been reported in the previous section. In the AP implants reducing the polyethylene thickness significantly increases the volume of cancellous bone pathologically overstrained (<-7000με) with strain concentrations in the regions of the peg and keel which are larger and occur at lower loads in the AP implant than the MB. In the MB implants, altering polyethylene thickness had little effect on the distribution of strain concentrations which remain

associated with the anterior part of the keel and the lateral corner of the implant where horizontal and vertical bone cuts meet in all implant thicknesses.

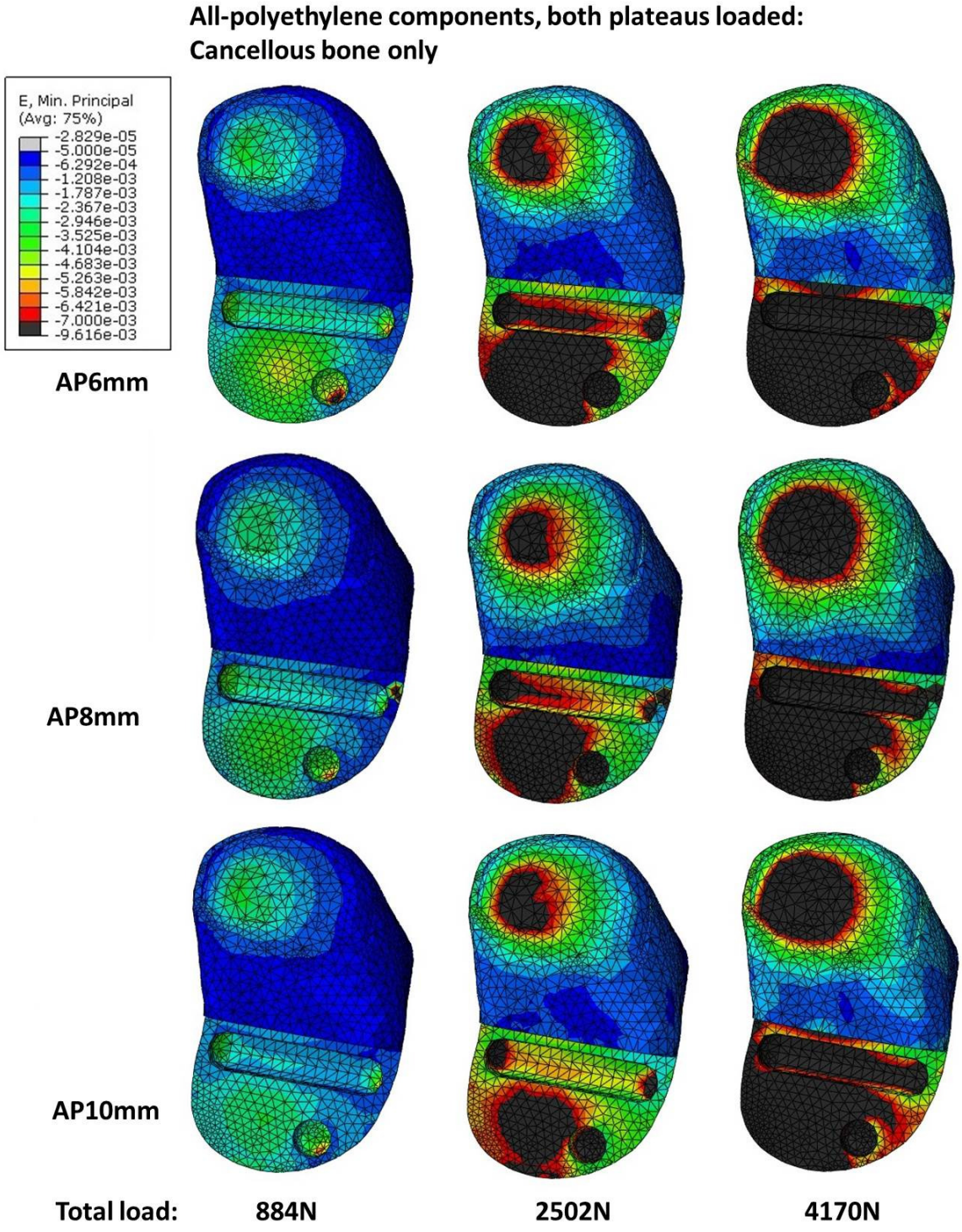

Figure 5.19 Axial compressive (minimum principal) contours of the upper surface of cancellous bone for all-polyethylene implants of different thickness. Strain >-50με appears pale grey, strain <-7000με appears black.

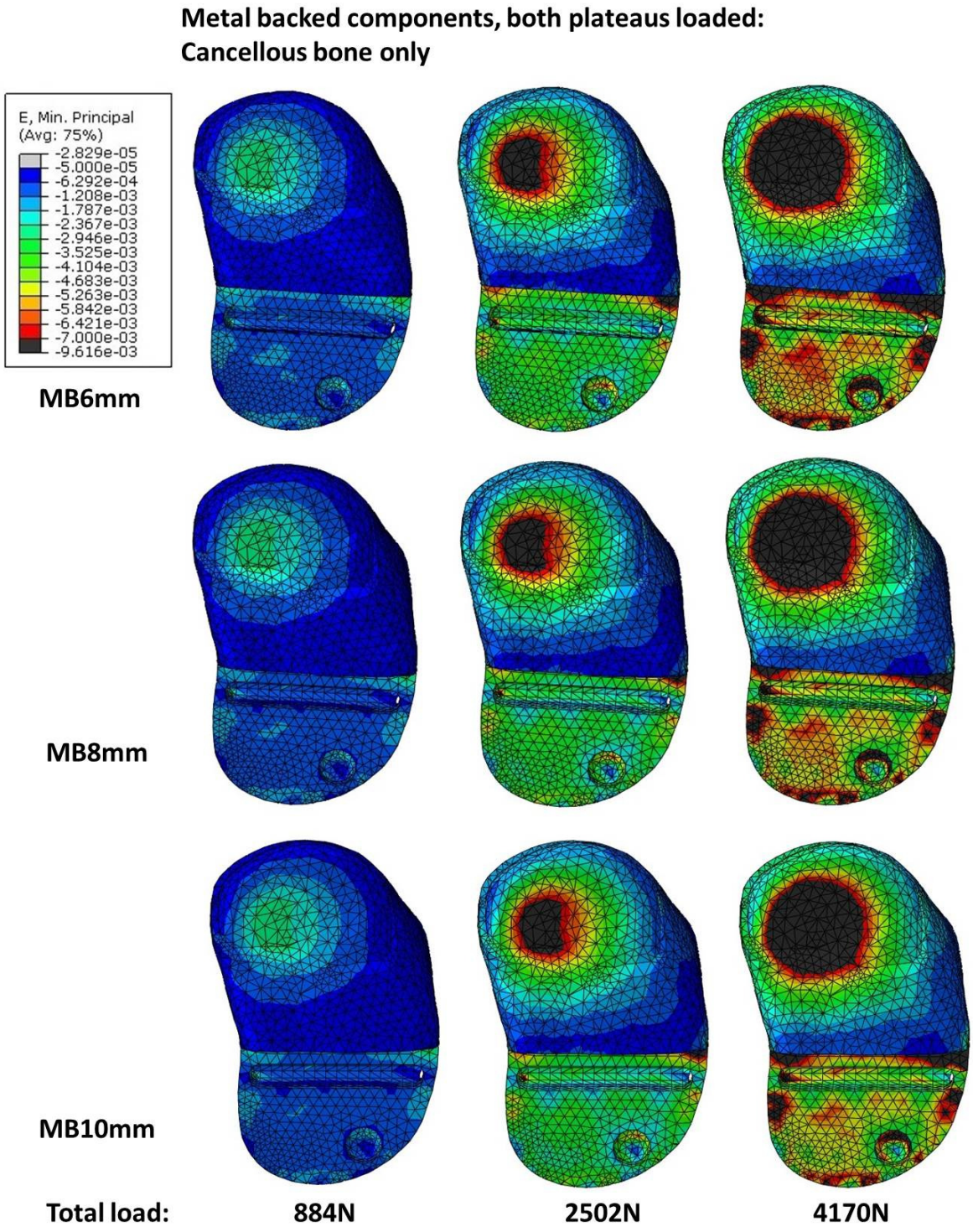

Figure 5.20 Compressive (minimum principal) contours of the upper surface of cancellous bone for metal backed implants of different thickness. Strain >-50με appears pale grey, strain <-7000με appears black.

5.5 Discussion

The results of the finite element models created to replicate previous mechanical testing conditions closely reflect the experimental results previously reported (Appendix 3). Mechanical testing showed that AP implants displayed significantly more microdamage, measured by cumulative AE hits, than MB implants at all loads (1.8 to 6 times). This was most pronounced at loads >1000N. Additionally, AE hits in the AP implants were associated with high amplitudes and high absolute energies even at low loads whereas MB implants produced high energy hits only at high loads. The FEMs created here displayed a greater volume of cancellous bone compressively strained below -1500, -3000 and -7000με in the AP model compared to the MB model at every load. Eleven to 14 times the volume of cancellous bone was compressively strained below -7000με in the AP compared to the MB implant at medial loads up to 2500N (total load 4170N). The volume of cancellous bone elements with tensile strain exceeding 7000με was not greater in the AP implant. This is to be expected where loading is compressive and tensile strain occurs due to Poisson's effect.

Validation of the FE model was possible using acoustic emission, and to a lesser extent DIC. Digital image correlation provides the ability to measure full-field surface strain as opposed to strain over a finite area of attachment in strain gauges. In an inhomogeneous, anisotropic composite material with complex geometry such as bone, full-field measurement has obvious advantages. However, DIC is not a perfect technique, and limitations include increased error when applied to curved surfaces or complex geometry where some areas are not well visualised by both cameras (Ghosh, et al., 2012). Difficulties selecting the start point for analysis if a poor speckle pattern has been applied is another potential difficulty. In the experimental model used here for comparison, the two cameras were placed adjacent to one another and orthogonal to the mechanical axis of the tibia to capture two slightly different views of the medial proximal tibia. In this region the proximal tibia is curved in multiple planes. This curvature is the largest at 20-30mm distal to the plateau surface. This anatomical feature may lead to less accurate DIC strain readings in this region. As FEM strain outputs are independent of visualisation, this may help to explain the divergence of

strain values in this region in particular. Despite this, correlation between DIC and FE strain data along the anteromedial line measured showed good correlation: 0.956 in the AP and 0.885 in the MB implant. This is consistent with that accepted for validation of other models using DIC in the literature (Grassi, et al., 2013).

The experimental and FEMs also differed slightly in their proximal constraint. In the experimental model, medial-lateral translation was possible proximally until the vertical cut edge of the tibia impinged on the femoral component. After this impingement, medial-lateral movement was restrained, as was transverse plane rotation. An anterior constraint also resulted from the posterior slope of the implanted tibial component. Posterior translation was minimal. The FE model was totally constrained proximally against medial-lateral and anterior-posterior translations by a point in the ACL footprint region. This proximal constraint limited bending of the construct.

A linear elastic FEM model was used in this study. Though bone is known to be viscoelastic and display non-linear behaviour, linear modelling can be used where appropriate. In this study, loading conditions were designed to replicate physiological loading and models were not loaded to failure. When loading bone within its elastic limits, a linear FEM has advantages over a non-linear model in terms of rationalising computer power without losing accuracy. The use of a linear FEM was supported by our experimental data. In acoustic emission testing two important phenomena occur and provide information as to the nature of any deformation: Kaiser and Felicity effects. The Kaiser effect describes the phenomenon whereby if a specimen is loaded, unloaded, and reloaded within its elastic limit, no acoustic activity is emitted on reloading until the previous maximum load is reached (Leung, et al., 2009). The Felicity effect, describes AE activity that occurs before the previous maximum applied load is reached, indicating that the material has undergone permanent damage (Mavrogordato, et al., 2011). The Felicity effect was displayed by only one specimen during mechanical testing, indicating that significant damage or plastic deformation had not occurred at the loads applied. Both of these phenomena must be borne in mind when using AE data to validate an FE model. The absence of these effects in the

experimental data support the use of a linear, as opposed to non-linear, finite element model.

The volume of elements in an FEM which can experience strains above or below threshold limits (e.g. 1500, 3000, 7000με) is finite. As the volume of elements experiencing high strain (e.g. <-3000 με) increases (e.g. at high loads), the volume of elements available to experience high strains reduces. Therefore, as greater volumes of elements experience high strain, fewer elements are available to experience high strain when the load is increased. This produces an S shaped (sigmoid) curve (Figure 5.21) with a plateau region where further increases in load cannot increase the volume of elements experiencing high strain as there are no elements left with low strain. This is very similar to what occurs in acoustic emission: when microfracture has occurred with the emission of a hit, that region cannot emit further hits, therefore as more AE hits are detected, fewer future AE hits *can be* detected. This again produces an S shaped curve with a "toe-in" region where strain has not exceeded the threshold for fracture, and a "plateau" region where so much of the material volume has already failed that further increases in strain cannot cause further fracture. The consequence of these S shaped curves is that cubic or quadratic curves best fit the data, especially where greater microdamage is recorded in the AP implant. This also explains the data obtained from the FEM for both implants. At lower strain thresholds (e.g. volume of elements with minimum strain <-3000με, figure 2.27a) the graphs for AP and MB implants begin to converge as plateaus are approached. When the threshold is increased (e.g. to <-7000με, figure 2.27b) the data shift left to the linear region of the curve and differences between implants are more apparent. As MB implants remain in the linear region of the curve for the parameters measured, linear curves fit the MB data well and subsequent linear regression analyses are more accurate for this implant with better predictive regression equations. This is reflected by the greater predictive value, and thus greater statistical significance on both ANOVA and T-testing, of the MB regression equations compared to those for the AP implants, and compared to equations for all implants where AP implant inclusion causes a tendency to less linearity.

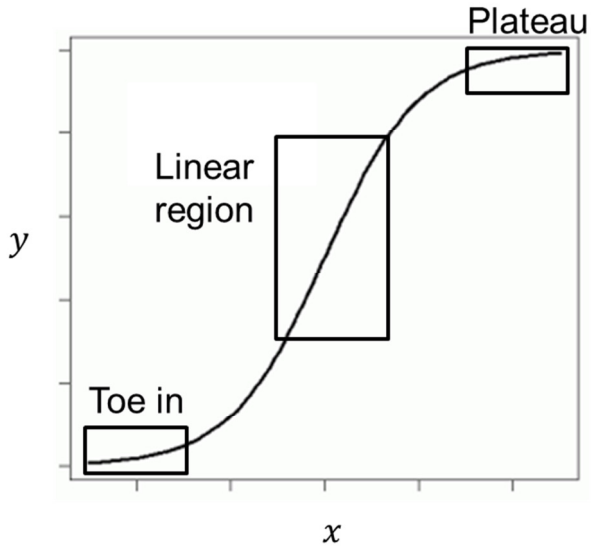

Figure 5.21 A sigmoid curve

This also explains the differing relationships between implants in terms of the volume of cancellous bone elements with tensile and compressive strain <-7000με. A strong linear relationship exists for this variable in the MB implant, but a quadratic one is found in the AP implants (Figures 2.31c and d and 2.32c). Again, the number of AE hits remains low across all loads in the MB implant and therefore the resultant curve remains in the "toe-in" or linear part of an S-shaped curve. However, the AP implant, with a significantly greater number of AE hits than the MB implant at all loads, reaches the plateau region of the curve and is therefore best modelled with a quadratic rather than linear curve. The higher R^2 values in the MB equations also reflect the greater amount of dependent variable (AE hit) variation explained by the FE model for these implants compared to the AP implants.

Higher R^2 values, lower standard error of the estimate, lower percentage standard error in b and Durbin-Watson statistics closer to 2 occurred where fewer AE hits were detected, i.e. in the MB implant. This suggests that AE can be used to validate a non-linear FE model over a range of loading values, but that this validation is most accurate in the linear region of the curve (Figure 5.21) where AE activity is low, for example at low loads. Under these conditions the experimental model is not significantly damaged, AE hit frequency has not yet begun to plateau and the Felicity effect has not yet become apparent.

Digital image correlation has previously been used to validate FE models of intact and implanted hemipelves (Ghosh, et al., 2012), cadaveric tibias with implanted total ankle replacements (Terrier, et al., 2014), composite femora (Dickinson, et al., 2011; Grassi, et al., 2013) and human soft tissue (Moerman, et al., 2009). In these studies R values of 0.81 to 0.94 were reported and accepted as evidence of correlation significant enough to validate the corresponding FE model. Finite element models of UKRs are scarce in the literature, with 8 three dimensional studies reported. Validation is reported for even fewer and involves cortical strain correlation in all. Gray et al (Gray, et al., 2007) used 17 strain gauges to validate a composite tibia model implanted with the Oxford UKR reporting an R^2 value of 0.962 with a percentage error of 5%. Gray et al (Gray, et al., 2008) report on cadaveric tibiae implanted with mobile bearing Oxford UKRs validated using 17 strain gauge rosettes in different loading conditions. They report R^2 values of 0.98 for intact tibias and 0.97 for those implanted with UKRs with corresponding percentage errors of 6 and 8.8%. Similarly, Tuncer et al (Tuncer, et al., 2013) used strain gauge experiments to validate their cadaveric tibia models implanted with cemented and uncemented mobile bearing Oxford UKRs with R^2 values of 0.85 and 0.62 respectively. Kwon et al (Kwon, et al., 2014) compared polyethylene contact stresses in both the Oxford mobile bearing UKR and a metal backed fixed bearing UKR using an FE model reported to have previously validated against strain gauge data with Pearson's correlation >0.75. The correlation values found in this study between observed AE data and predicted FE data compare very favourably to these previous studies with Pearson's correlation values of up to 0.947 with R^2 0.847 and percentage error 12.5% for FE volume of elements with compressive strain <-3000με. This also represents the first time that anything other than cortical bone strain has been used to validate an FE model.

Acoustic emission data can be used to validate a finite element model of implanted composite bone. Other experimental techniques for validation, including strain gauges and DIC, can be applied to a material surface only. As such, this restricts their use to cortical bone stress/strain validation only. The acoustic emission technique can be used for correlation of whole model or cancellous bone strain. As the material with the lowest Young's' modulus within the model, and thus the expected region of greatest damage, cancellous bone typically shows more variation in strain than cortical bone. Demonstrating

good correlation of this data with that predicted by a finite element model is therefore a more accurate validation technique.

Loading both plateaus created a more physiologic pattern of strain in the FEM by reducing the volume of the model shielded from strain and reducing tibial bending moments. The loading of both plateaus increased the total load to which the model was subjected, but the total loads used remained representative of those encountered by patients in normal life. The increase in strain expected by increasing the total load applied was proportional to the load increase and did not alter or obscure the effect of implant material (AP or MB) on cancellous bone strain.

Cancellous bone strain differed significantly between AP and MB UKR implants. All-polyethylene implants displayed greater volumes of pathologically overstrained cancellous bone than MB implants, both in compression (<-7000με) and tension (>7000με), and much higher peak tensile strains. Structure stiffness is a function of both geometry and material properties. There were very few differences in implant geometry between the AP and MB implants, but large differences in their Young's moduli: polyethylene E=0.69GPa compared with cobalt-chrome E=210. This causes greater bending of the AP implant on loading compared to the MB implant (Figure 5.15 and 5.16), and localised strain elevations in the regions of this bending (Figure 5.19 and 5.20). The metal backed implant underwent much less bending and thus distributed load more uniformly to the cancellous bone of the proximal tibia.

At low loads there was less strain shielding in the AP than the MB implant. In TKR, the flat surface of the proximal tibia is under compression, but localised stress shielding does occur in association with tibial undersurface projections, such as stems and posts. The degree of this stress shielding is influenced by implant material with greater bone shielding occurring with stiffer implants when the difference in Young's modulus between implant and bone is greatest (Au, et al., 2007; Completo, et al., 2008; Scott and Biant, 2012). Greater strain is therefore expected under the projections of a polyethylene implant (E=0.69GPa)

than a cobalt-chrome tray (*E*=210). This is apparent here where strain contours (Figure 5.17 and 5.18) show strain concentrations in the AP implant at both the keel and the peg, with a relative shielding in these regions in the MB implant.

Altering the polyethylene thickness (i.e. the geometry) had marked consequences on proximal tibial strain in the AP but not the MB implant. Reducing AP implant thickness reduces implant stiffness further facilitating greater bending on loading with a subsequent increase in the volume of cancellous bone exposed to pathological levels of tensile and compressive strains and the peak compressive strain. The 6mm AP implant displayed an exponential increase in cancellous bone volume strained in tension above 7000με at loads of greater than 4000N appearing to indicate imminent failure. Strain values for all parameters were significantly higher in the AP than the MB implants, even when AP thickness was increased to 10mm.

In TKR, tibial component polyethylene thickness, of either insert or all-polyethylene component, is known to affect the proximal tibial strain underneath the implant (Bartel, et al., 1986; Bartel, et al., 1982) in addition to the wear characteristics of the polyethylene. Similar studies examining optimum polyethylene thickness in UKRs have only been reported for metal backed implants (Simpson, et al., 2008) and have examined polyethylene stress and failure rather than that of the surrounding bone. When examining implant thickness as a variable, it is important to recognise that the implant thickness stated by the manufacturer is not the minimum thickness of the implant/insert. The difference between these two numbers depends upon the radius of curvature of the polyethylene component which varies between manufacturers and polyethylene design (conforming or non-conforming). Table 6.8 details the minimum polyethylene thickness for each implant included in this study.

Table 5.8 Quoted polyethylene thickness and minimal polyethylene thickness for AP and MB implants.

Implant	Quoted Thickness (mm)	Minimum Thickness (mm)
All-polyethylene	6	5.26
	8	7.26
	10	9.26
Metal backed insert	6	4.435
	8	6.435
	10	8.435

Whilst there was little difference in proximal tibial cancellous bone strain (compressive and tensile) and in the volume of elements pathologically overstrained, between the different thicknesses of MB implant, the wear characteristics of an implant with less than 6mm of standard polyethylene (a 6 or 7mm insert) could be questionable (Bartel, et al., 1986). Simpson et al (Simpson, et al., 2008) compared contact and Von Mises stresses in different thicknesses of polyethylene in fully congruent mobile bearing with non-congruent fixed bearing UKRs using FEM. They reported peak stresses within the polyethylene of the metal backed fixed bearing UKR to exceed the fatigue failure limit for polyethylene for all thicknesses up to 8.5mm, with a 25% increase in peak Von Mises stress when polyethylene thickness was reduced from 8 to 3mm. This is the only FEM of which I am aware to investigate the effect of polyethylene thickness in UKR. It does include a single all-polyethylene model, but does not vary the polyethylene thickness in this model, and reports on stress within the polyethylene, not in the surrounding bone.

The all-polyethylene Sigma Partial tibial component is not available in thicknesses less than 8mm (minimum thickness 7.26mm). However, all-polyethylene components from other manufacturers are. The predecessor of the Sigma Partial UKR, the Preservation, was available with AP implants of 7.5mm. As already discussed, the minimum PE thickness of a 7.5mm implant is considerably less than this. Though no data has been published previously on the effect of altering PE thickness in UKR AP tibial components, it is interesting that when redesigning the Preservation UKR as the Sigma Partial, one of the design differences

was to increase the minimum PE thickness of the AP implant. The metal backed Sigma Partial is available with a minimum 7mm insert (5.435mm minimum thickness). The maximum thickness available for both AP and MB implants is 11mm.

The regions of strain concentration and pathologically overstrained bone also differed between implants. In the AP implant compressive strain was concentrated at both the peg and the keel, in addition to the region directly under the applied load, resulting in an anteromedial strain concentration not seen to the same degree in the MB implant. Simpson et al (Simpson, et al., 2009) have previously reported a 40% increase in von Mises strain in the anteromedial tibia in their Oxford UKR FEM when compared to an intact tibia. This was maximal at 13.6mm below the resection and has been hypothesised as a possible cause of unexplained anteromedial pain in UKRS. Though not as large in the MB as the AP implant, a similar anteromedial concentration is apparent here, and appears to be located just anterior to the implant keel. The larger concentration apparent in the AP implant, with a larger volume of pathologically overstrained bone, may lead to increased pain in this region in AP UKRs. The posteromedial concentration that occurs in the AP implant at high loads appears to reflect the pattern found previously in FEM studies of intact tibias (Completo, et al., 2009). This pattern of compressive strain differed significantly from that found in the MB implant where relative shielding was apparent at the peg, with strain concentration along the lateral corner of the implant where horizontal and vertical bone cuts meet. The strain concentration at the corner region of the MB UKR implant has been reported before in an FE model of the Oxford metal backed mobile bearing implant (Simpson, et al., 2011; Simpson, et al., 2009). It has not previously been reported in a fixed bearing UKR. This is the region where the implant has no cortical support and may therefore be experiencing more bending than in cortically supported regions. Pathological overstraining of the bone in this region of metal backed implants, as opposed to pathological strain shielding, may be responsible for the radiolucent lines sometimes seen in metal backed medial UKRs (Simpson, et al., 2011). Non-pathological radiolucencies immediately under the cemented metal backed Oxford UKR tibial base plate at the cement-bone interface are common. Complete radiolucencies are reported in 30% of cases and incomplete radiolucencies in an additional 32% (Gulati, et al., 2009). Despite >3 significant design changes (Phase I, II, and III), localised radiographic

radiolucencies with well demarcated sclerotic edges, have persisted in association with the Oxford UKR implant, and are also reported in the new uncemented version (Hooper, et al., 2012). Longitudinal studies have shown these radiolucencies to be stable, histological study has shown them to be inactive fibrous tissue or fibrocartilage (Kendrick, et al., 2012), and long-term survivorship, reported as 95% (90.8 to 99.0% 955 CI) at 10 years independently (Svärd and Price, 2001) and 96% (92.5 to 99.5 95% CI) at 10 years by the design centre (Pandit, et al., 2010), appears unaffected by them. They have not been associated with pain or any detrimental effect on outcome (Gulati, et al., 2009). FE modelling of these features (Gray, et al., 2010) has suggested that stiffening of the bone by remodelling at the region of strain concentration is responsible for the formation of the adjacent sclerotic line.

Limitations of this study include the use of a composite tibia, and not a scanned patient or cadaveric tibia. This has the advantage of the results being applicable to the "average" tibia and not just to one individual, but the disadvantage of not reflecting the graduated trabecular structure of proximal tibial cancellous bone. Anisotropic, heterogeneous bone with non-linear behaviour was modelled as homogenous and a linearly elastic analysis was performed. However, this is a common method and should not discredit the differences found between MB and AP implants. The knee was modelled in extension with load applied in the line of the mechanical axis of the tibia. The gait cycle was not modelled. As kinematic studies have shown the point of contact to change little throughout a range of motion in fixed bearing UKRs, and as medial compartment OA is primarily disease of extension, this was considered acceptable. The soft tissues of the intact lateral compartment (articular cartilage and meniscus) were not modelled and this will undoubtedly have affected lateral proximal tibial strain.

This validated FE study has shown that AP implants are associated with greater proximal tibial cancellous bone strain, both compressive and tensile, when compared to metal backed implants of the same geometry. These differences are typically increased at higher loads, but also exist at lower loads representative of physiologic knee loading during activities of daily living. Altering the thickness of the polyethylene insert in metal backed

implants has little effect on proximal tibial strain, but thin polyethylene in MB tibial components may have undesirable wear characteristics. In all-polyethylene UKR tibial implants, altering implant thickness has marked effects on proximal tibial strain with thinner implants associated with greater strains. Increasing the thickness of all-polyethylene implants to 10mm does not overcome this difference and comes at the cost of greater bone resection.

6 Discussion

These studies confirm proximal tibial strain to be elevated under a UKR incorporating an all-polyethylene tibial component compared to a metal backed one. Proximal tibial strain is further affected by component thickness in all-polyethylene tibial components.

6.1 Implant Factors

The Oxford UKR is associated with a consistent survivorship across joint registries. Survival of this metal backed mobile-bearing UKR is reported to be as high as 96% at ten years (95%CI 92.5 to 99.5) in 1000 patients operated on at the design centre (Pandit, et al., 2010). However, even in this series 6/17 revisions were for unexplained pain making it the second commonest mode of failure in this mobile bearing device. In contrast, there are a number of reports in the literature of poor results with all-polyethylene tibial components from different manufacturers. The Norwegian Arthroplasty Register (Norwegian, 2010) reports a significantly higher rate of revision at 5 years in 2 all-polyethylene designs when compared to 3 metal backed mobile bearing devices. Saenze et al. (Saenz, et al., 2010) report a failure rate of 11% (16/144) at a mean of 36 months with tibial component loosening or subsidence in 12/16 failures. Mariani et al. (Mariani, et al., 2007) report a 38% revision rate (15/39) at 12 months with femoral component loosening in all 15 failures. Hamilton et al (Hamilton, et al., 2006) reported 9/221 (4%) revisions at 1-26 months, 4 of which were performed for tibial loosening, including 3 with collapse. No comment has been made of proximal tibial pain or evidence of elevated strain and remodelling, such as sclerosis, preceding any tibial collapse. These implants came with a minimum polyethylene (PE) thickness of 7.5mm. However, other UKR designs with all-polyethylene components, such as the St Georg Sled (Waldemar Link, Hamburg, Germany), report good long term survival in the literature, 90-92% at 10-15years (Newman, et al., 2009; Steele, et al., 2006) with no revisions for on-going pain and no early failures. The minimum polyethylene thickness of

the St Georg Sled is 9mm. Adaptive remodelling in the proximal tibia beneath all-polyethylene UKR components has been reported before (Gillies, et al., 2007), with evidence of stress shielding in the presence of a keel, and increased bone mineral density without. though implants thicknesses in this study were not reported. All-polyethylene components of 6mm thickness have previously been shown to be significantly associated with clinical failure (Heck, et al., 1993), increased wear and osteolysis (Hernigou, et al., 2008). Osteolysis, or tibial collapse, may be secondary to pathological cancellous bone overload, affecting implants with thinner polyethylene more so than thicker implants with more reliable reported survivorships. Load transfer is undoubtedly dependent upon implant stiffness, and thus thickness, in all-polyethylene components. It appears that even implants of 10mm thickness perform inferiorly in terms of proximal tibial strain when compared to metal backed implants. Increasing the depth of tibial resection to create space for thicker implants is associated with reduced cancellous bone strength (Hvid, 1988) and increased strain (Simpson, et al., 2009), thus tibial component thickness must be balanced with the need for larger resection and may preclude the use of all-polyethylene components.

Less stiff all-polyethylene components bend more on loading than metal backed implants (Figure 6.1). In metal backed implants bending is greatest where cortical rim support is absent and also appears greater when the thickness of metal backing is less. This is suggested both by mechanical testing (Appendix 3) and by the distribution of pathological (<-7000με) overstraining on FEM. The clinical risk of this bending phenomenon is tibial component subsidence secondary to pathological overstraining.

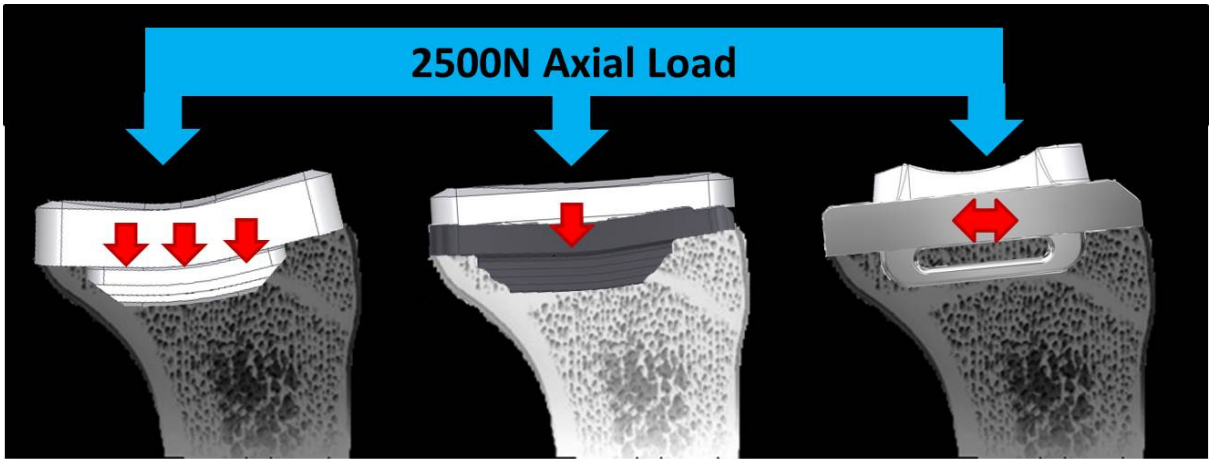

Figure 6.1 Diagrammatic representation of UKR tibial component bending on loading. Bending is theoretically greater at the implant lateral edge with no cortical support and in all-polyethylene components compared to metal backed. Bending also decreases with thicker metal backing and is thus less in the Oxford (2.5mm Co-Cr) than the Sigma Partial (1.5mm Co-Cr).

Limitations of this study include the different metal backed UKR implants used in the FE and clinical elements of the study. The all-polyethylene component used in the clinical arm (the Preservation), though produced by the same manufacturer, was redesigned prior to undertaking the finite element analysis (as the Sigma Partial). It was not possible to obtain a metal backed version of the Preservation to develop a CAD model from and so it was decided to proceed with the more modern Sigma Partial fixed bearing UKR for the FE study to investigate the effect of metal backing and implant thickness. The design differences present in the Sigma Partial implant include the addition of a peg to the tibial components; a wider keel in the AP implant; a difference in geometry between AP and MB implants (thicker keel in the AP implant with increased undersurface offset); different sizing algorithm; thinnest AP implant 8mm (previously 7.5mm); thinnest MB implant 7mm (previously 9.5mm); and the addition of an extra peg to the femoral component. In addition to different AP implants being used for the different elements of this study, different metal backed implants were used also: the Oxford mobile bearing for the clinical and the Sigma partial fixed bearing for the FEM. These implants have different thicknesses of metal backing (2.5mm in the Oxford and 1.54mm in the Sigma Partial), in addition to different

bearing concepts. The consequence of this is that the Oxford implant is stiffer. The FE study results are not therefore applicable to this implant.

Other implants from other manufacturers are available with thinner minimum PE thicknesses. Metal backed implants vary in the thickness of the construct available and in the thickness of the metal backing itself, so as to minimise the bone resection needed to insert adequate thickness of polyethylene without deleteriously affecting the wear characteristics of the PE and its resistance to delamination. This should be considered in UKR implant selection and in the decision to operate on patients with elevated BMI's who will be exposing the implant routinely to greater loads and bending.

6.2 Strain Magnification and Bone Remodelling

Elevated bone strain eventually leads to microdamage and fracture which stimulates remodelling if within an appropriate window. Both cortical and cancellous bone are anisotropic with heterogeneous microstructures and both have a considerable ability to accumulate microdamage prior to the initiation of cracks (Christen, et al., 2012; Jungmann, et al., 2011; Nicolella, et al., 2005). Resistance to microcracking in bone is primarily determined by bone age and the presence of metabolic disease (Schaffler, et al., 1995). In cortical bone a number of structural elements act as stress risers to concentrate stress and strain to levels above those of the global strain applied to the bone: Haversian canals, Volkmann's canals, osteocyte lacuna, canaliculi (Nicolella, et al., 2005). Whist lacunae have previously been thought to have a role in arresting fatigue crack propagation in cortical bone (Lanyon, 1993), the idea of microscopic features acting as stress risers for microdamage initiation has been borne out by the work of Reilly (Reilly, 2000). Their work showed that microcracks in cortical bone (bovine, equine and human) were found to frequently initiate at osteocyte lacunae. Christen et al (Christen, et al., 2012) again report on the somewhat contradictory mechanical role of osteocyte lacunae whereby they both reduce bone strength by concentrating stress and strain and facilitating crack formation, whilst also contributing to bone toughness by blunting crack tips.

In vivo measures of mid-diaphyseal tibial cortical strain during vigorous activities using strain gauges (Burr, et al., 1996) demonstrate minimum principal (compressive) strain of -1200με and maximum shear strain of 1900με. Many times this strain is required for the mechanical stimulation of osteoblasts causing increased production of osteopontin mRNA, prostaglandin (PGE_2) and nitric oxide (You, et al., 2000). When osteocytes are located in areas of stress and strain concentration, they are exposed to strains far greater than those measured at the bone surface. These levels of strain may be many magnitudes higher than surface strain and thus reach a level high enough to alter biological activity and initiate remodelling. Nicolella et al (Nicolella, et al., 2005) examined microstructural strain in bovine tibia samples loaded in tension with a global applied strain of 2,000με (0.2%). They found microstructural strain (measured using DIC) to frequently exceed macroscopic strain (measured using strain gauges) with subsurface lacunae reaching levels of 12,000-16,000με with peak strains of 30,000με (3%). The mean microstructural strain was 7,900με, four times that of the applied global strain with a strain concentration factor of 1.88. Such apparently supra-physiological levels of strain are associated with adaptive remodelling of cortical bone in murine tibias which in turn reduces peak strain, creating a more uniform surface strain distribution (Sztefek, et al., 2010). It is therefore essential to perform some form of internal strain measure, such as acoustic emission examination, or finite element predictions, of cancellous bone strain in addition to cortical bone measurements when examining bone strain and the effect of prostheses on this. Surface strain is not representative of internal strain and is likely to grossly underestimate it. All of the previous published FEMs of UKRs have been validated using cortical bone strains. To our knowledge, the FEM presented here is one of only 2 to report cancellous bone strains, the other being Sawatari et al (Sawatari, et al., 2005).

Christen et al (Christen, et al., 2012) used a form of volumetric DIC to examine cortical bone microstructure using murine femora loaded to failure. The contours so obtained were correlated with μCT to establish that in cortical bone, microcracks initiate around canals or lacunae within the cortical bone, and from there propagate to the endosteal or periosteal

surface. These cracks are consistently parallel to the direction of loading in compression, with the largest deformations due to shear (Christen, et al., 2012). They also report that compressive strain plays only a minor role in microcrack propagation, and does so by acting locally as shear strain. Tensile strain however, is always present at microcracks where it accumulates strongly. This suggests that tensile strain is more important than compressive strain in the formation and propagation of microdamage in bone. To our knowledge, tensile strains have not been investigated in UKR FEMs before. As AP and MB UKR implants displayed greater differences in tensile than compressive strain in this FE model, this again suggests the potential for greater microdamage under an AP than an MB implant, worsened in thin implants.

6.3 Loading

In vivo studies using TKRs with telemetric tibial trays in 5 subjects have shown a mean load of 253% BW (185-299%) in double support knee bend (Kutzner, et al., 2010). At 35^{o} of flexion during stair ascent, the load across the tibiofemoral joint reaches 316% BW (298-345%) (Kutzner, et al., 2010). Between 57% (Zhao, et al., 2007) and 75% (Yang, et al., 2010) of this load passes through the medial compartment depending upon the nature of the activity being undertaken. The mean body weight of patients receiving medial UKRs in our unit is 80kg. The loading of our model therefore incorporated a 60:40=medial: lateral load division with total loads (up to 2500N medial load, or 4170N total load) representative of the physiological loads encountered as part of daily activities.

6.4 Conclusion

This study indicates that proximal tibial cancellous bone strain is elevated in all-polyethylene compared to metal backed UKR tibial components. Implant thickness has marked effects on this strain for AP implants, but not for MB implants. In AP implants thinner polyethylene is associated with elevated compressive and tensile strains resulting in significant volumes of pathologically overstrained bone. Proximal tibial GSRb (a proxy measure of bone mineral density) changes following implantation of both all-polyethylene and metal backed tibial UKR components, but it does not do so uniformly. Patients in whom the GSRb increases are younger or have elevated BMIs, and are more likely to have ongoing pain. This may reflect elevated strain and ongoing adaptive remodelling. This phenomenon is not restricted to all-polyethylene implants and though revision for unexplained pain is more likely in the AP implants, patients with metal backed implants display similar levels of ongoing postoperative pain. In those patients with low preoperative GSRb, there is an increased incidence of early revision of UKR for pain and this may reflect failure of relatively osteopenic bone to sufficiently support UKR implants, especially all-polyethylene ones. Despite these findings, in patients who do not undergo revision of their UKR, there are no detectable differences in patient reported outcomes or all-cause survival between the UKR implants studied.

7 Future Work

The developed validated FE model can be used to investigate the effect of further patient and implant variables on proximal tibial strain:

7.1 Patient Factors

The effect of patient BMI could be explored by altering the loads applied to the construct in the FE model. The material properties and microstructure of cortical and cancellous bone in the model could be altered to simulate osteoporotic bone to investigate the effect of poor bone quality on proximal tibial strain and implant subsidence.

7.2 Implant Factors

The effect of tibial component alignment could be investigated with the model to explore varus component alignment in particular. The load could be applied at a different angle to investigate the effect of resultant FTA and overall lower limb alignment.

The effect of undersurface projections, pegs and keels, on proximal tibial strain and regions of strain shielding can be investigated by manipulating the 8mm implants to remove the peg and/or the keel from the implant (Figures 7.1 and 7.2).

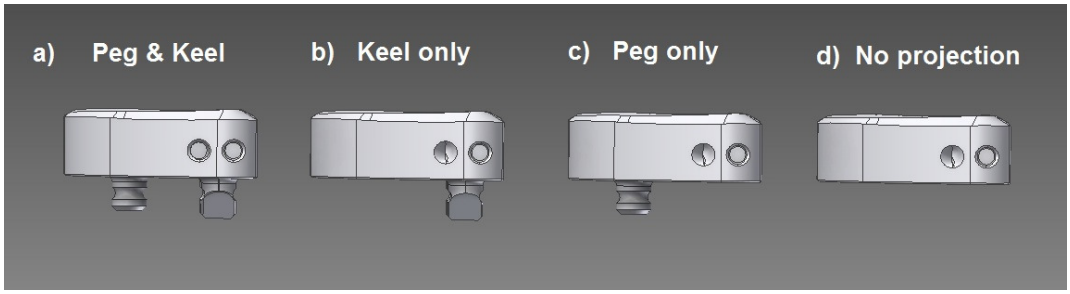

Figure 7.1 Altering the AP implant undersurface projections.

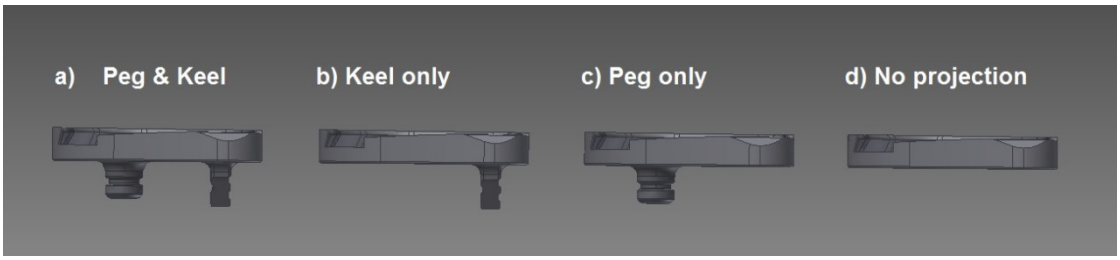

Figure 7.2 Altering the MB implant undersurface projections.

The effect of cortical rim support can be investigated using the 8mm AP and MB implants at 100% and 90% of their transverse plane size whilst maintaining undersurface projection depth and implant thickness. This 10% difference reflects the typical difference between sizes of implants and can be performed in Autodesk Inventor CAD software (Figures 7.3 and 7.4). The undersized (90%) implant with be implanted without cortical rim support, i.e. with under-hang, with subsequent proximal tibial strain compared to the 100% implant with cortical support and ideal rim fit. The effect of overhang can be similarly investigated using a 110% implant.

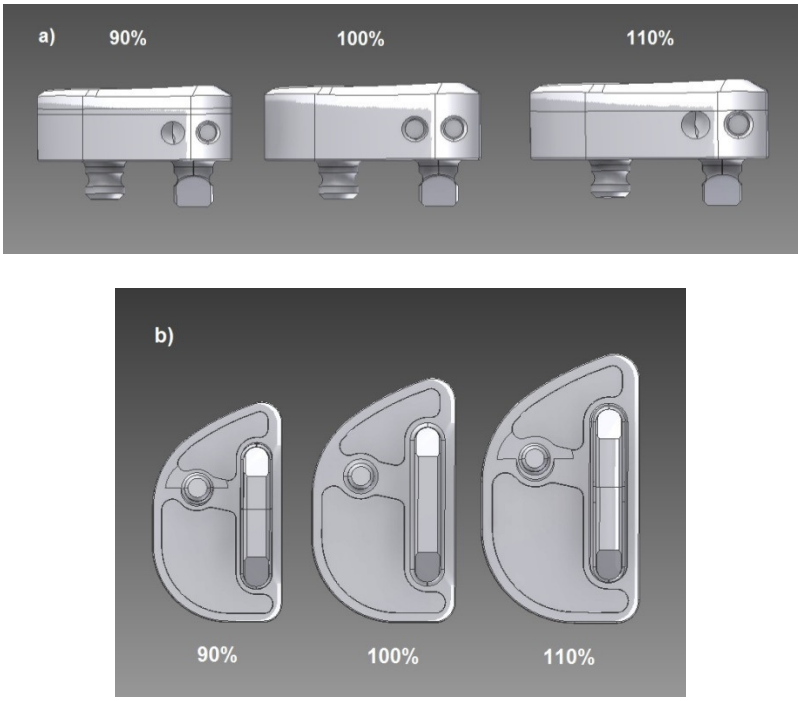

Figure 7.3 Rescaling the AP implant to investigate the effect of cortical rim support and overhang while maintaining implant height.

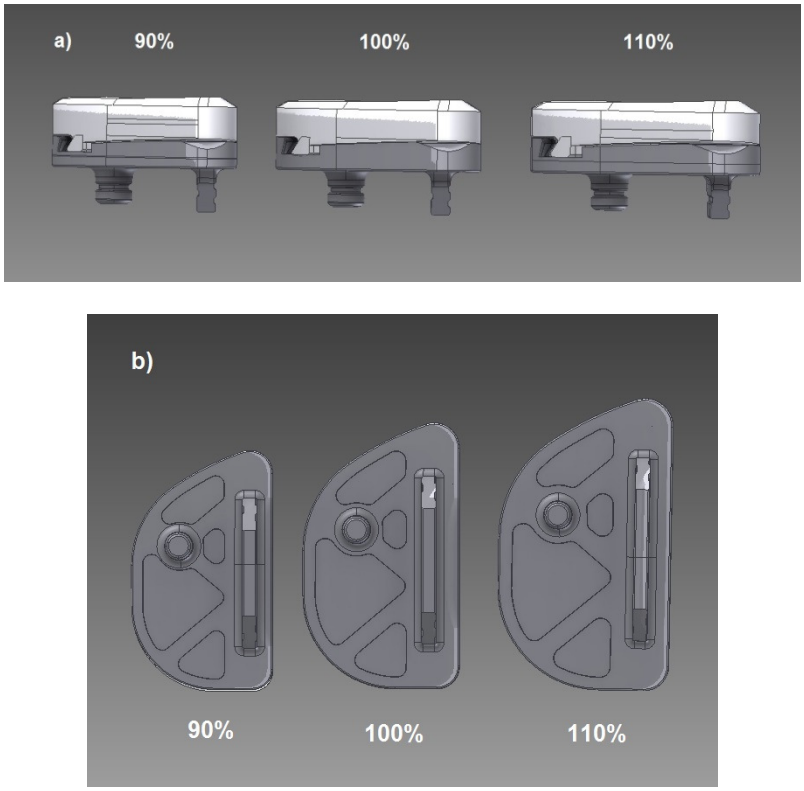

Figure 7.4 Rescaling the MB implant to investigate the effect of cortical rim support and overhang while maintaining implant height.

Bibliography

ImageJ. http://imagej.nih.gov/ij/downlod.html.

Abraham, R., *et al.* (2007) An anatomical study of tibial metaphyseal/diaphyseal mismatch during revision total knee arthroplasty, *The Journal of arthroplasty*, **22**, 241-244.

Anandacoomarasamy, A., *et al.* (2012) Weight loss in obese people has structure-modifying effects on medial but not on lateral knee articular cartilage, *Annals of Rheum Dis*, **71**, 26-32.

Andriacchi, T.P., *et al.* (1980) A study of lower-limb mechanics during stair-climbing, *The Journal of bone and joint surgery. American volume*, **62**, 749-757.

Argenson, J.A., *et al.* (2002) *In vivo* determination of knee kinematics for subjects implanted with unicompartmental arthroplasty, *The Journal of arthroplasty*, **17**, 1049-1054.

Au, A.G., *et al.* (2007) Contribution of loading conditions and material properties to stress shielding near the tibial component of total knee replacements, *Journal of biomechanics*, **40**, 1410-1416.

Au, A.G., *et al.* (2005) A parametric analysis of fixation post shape in tibial knee prostheses, *Medical engineering & physics*, **27**, 123-134.

Australian (2012) Australian Orthopaedic Association: National Joint Replacement Registry Hip and Knee Arthroplasty Annual Report 2012.

Azikuzi, S., *et al.* (2009) in vivo determination of kinematics for subjects having a zimmer unicompartmental high flex knee system, *The Journal of arthroplasty*, **24**, 963-971.

Baker, P.N., *et al.* (2012) Mid-term equivalent survival of medial and lateral unicondylar knee replacement: an analysis of data from a National Joint Registry, *The Journal of bone and joint surgery. British volume*, **94**, 1641-1648.

Baker, P.N., *et al.* (2012) Revision for unexplained pain following unicompartmental and total knee replacement, *The Journal of bone and joint surgery. American volume*, **94**, e126.

Baker, P.N., *et al.* (2007) The role of pain and function in determining patient satisfaction after total knee replacement. Data from the National Joint Registry for England and Wales, *The Journal of bone and joint surgery. British volume*, **89**, 893-900.

Bartel, D.L., Bicknell, V.L. and Wright, T.M. (1986) The effect of conformity, thickness, and material on stresses in ultra-high molecular weight components for total joint replacement, *The Journal of bone and joint surgery. American volume*, **68**, 1041-1051.

Bartel, D.L., *et al.* (1982) Performance of the tibial component in total knee replacement, *The Journal of bone and joint surgery. American volume*, **64**, 1026-1033.

Bettinson, K.A., *et al.* (2009) All-polyethylene compared with metal-backed tibial components in total knee arthroplasty at ten years. A prospective, randomized controlled trial, *The Journal of bone and joint surgery. American volume*, **91**, 1587-1594.

Bhattacharya, R., *et al.* (2012) Survivorship and patient satisfaction of a fixed bearing unicompartmental knee arthroplasty incorporating an all-polyethylene tibial component, *The Knee*, **19**, 348-351.

Bruni, D., *et al.* (2010) Minimally invasive unicompartmental knee replacement: retrospective clinical and radiographic evaluation of 83 patients, *Knee surgery, sports traumatology, arthroscopy : official journal of the ESSKA*, **18**, 710-717.

Burgess, S. (1999) Critical Characteristics and the Irreducible Knee Joint.

Burr, D.B., *et al.* (1996) In vivo measurement of human tibial strains during vigorous activity, *Bone*, **18**, 405-410.

Callister, W.D. and Rethwisch, D.G. (2011) *Materials Science and Engineering*. John Wiley and Sons, Inc., Asia.

Catani, F., *et al.* (2010) The Mark Coventry Award: Articular contact estimation in TKA using in vivo kinematics and finite element analysis, *Clinical orthopaedics and related research*, **468**, 19-28.

Cavaignac, E., *et al.* (2013) Obesity has no adverse effect on the outcome of unicompartmental knee replacement at a minimum follow-up of seven years, *The bone & joint journal*, **95-B**, 1064-1068.

Chang, T.W., *et al.* (2011) Biomechanical evaluation of proximal tibial behavior following unicondylar knee arthroplasty: modified resected surface with corresponding surgical technique, *Medical engineering & physics*, **33**, 1175-1182.

Chou, D.T., *et al.* (2012) Revision of failed unicompartmental knee replacement to total knee replacement, *The Knee*, **19**, 356-359.

Christen, D., *et al.* (2012) Deformable image registration and 3D strain mapping for the quantitative assessment of cortical bone microdamage, *Journal of the mechanical behavior of biomedical materials*, **8**, 184-193.

Christofolini, L. and Viceconti, M. (2000) Mechanical validation of whole bone composite tibia models, *Journal of biomechanics*, **33**, 279-288.

Churchill, D.L., *et al.* (1998) The transepicondylar axis approximates the optimal flexion axis of the knee, *Clinical orthopaedics and related research*, 111-118.

Completo, A., Fonseca, F. and Simoes, J.A. (2008) Strain shielding in proximal tibia of stemmed knee prosthesis: experimental study, *Journal of biomechanics*, **41**, 560-566.

Completo, A., *et al.* (2010) Biomechanical evaluation of proximal tibia behaviour with the use of femoral stems in revision TKA: an in vitro and finite element analysis, *Clinical biomechanics*, **25**, 159-165.

Completo, A., *et al.* (2009) Relationship of design features of stemmed tibial knee prosthesis with stress shielding and end-of-stem pain, *Materials & Design*, **30**, 1391-1397.

Conlisk, N., Howie, C.R. and Pankaj, P. (2015) The role of complex clinical scenarios in the failure of modular components following revision total knee arthroplasty: A finite element study, *Journal of orthopaedic research : official publication of the Orthopaedic Research Society*.

D'Lima, D.D., *et al.* (2011) The 2011 ABJS Nicolas Andry Award: 'Lab'-in-a-knee: in vivo knee forces, kinematics, and contact analysis, *Clinical orthopaedics and related research*, **469**, 2953-2970.

Dawson, J., *et al.* (2010) The routine use of patient reported outcome measures in healthcare settings, *Bmj*, **340**, c186.

Day, J.S., *et al.* (2001) A decreased subchondral trabecular bone tissue elastic modulus is associated with pre-arthritic cartilage damage., *Journal of orthopaedic research : official publication of the Orthopaedic Research Society*, **19**, 914-918.

Dickinson, A.S., *et al.* (2011) Experimental validation of a finite element model of the proximal femur using digital image correlation and a composite bone model, *Journal of biomechanical engineering*, **133**, 014504.

Dillon, C.F., *et al.* (2006) Prevalence of knee osteoarthritis in the United States: arthritis data from the Third National Health and Nutrition Examination Survey 1991-94., *J Rheumatol*, **33**, 2271-2279.

Ding, M., Danielson, C.C. and Hvid, I. (2001) Bone density does not reflect mechanical properties in early stage-arthritis, *Acta Orthop Scand*, **72**, 181-185.

Donaldson, F.E., *et al.* (2011) Relating age and micro-architecture with apparent-level elastic constants: a micro-finite element study of female cortical bone from the anterior femoral midshaft, *Proceedings of the Institution of Mechanical Engineers. Part H, Journal of engineering in medicine*, **225**, 585-596.

Dunbar, M.J., *et al.* (2001) Appropriate questionnaires for knee arthroplasty. Results of a survey of 3600 patients from the Swedish Knee Arthroplasty Register, *JBJS Br*, **83**, 339-344.

Eaton, M.J., *et al.* (2011) Principal Component Analysis of Acoustic Emission Signals From Landing Gear Components: An Aid to Fatigue Fracture Detection, *Strain*, **47**, e588-e594.

Eaton, M.J., Pullin, R. and Holford, K.M. (2012) Acoustic emission source location in composite materials using Delta T Mapping, *Composites Part A: Applied Science and Manufacturing*, **43**, 856-863.

Englund, M. and Lohmander, L.S. (2004) Risk factors for symptomatic knee osteoarthritis fifteen to twenty-two years after meniscectomy, *Arthritis and rheumatism*, **50**, 2811-2819.

Farr, J. (2005). Cartilage Restoration Centre of Indiana.

Frost, H.M. (1983) A determinant of bone architecture: the minimum effective strain., *Clinical orthopaedics and related research*, **175**, 286-292.

Frost, H.M. (1991) Some ABCs of skeletal pathophysiology. 5. Microdamage physiology., *Calcified tissue international*, **49**, 229-231.

Frost, H.M. (1997) Strain and other mechanical influences on bone strength and maintenance., *Curr OPin Orthop*, **8**, 60-70.

Furnes, O., *et al.* (2007) Failure mechanisms after unicompartmental and tricompartmental primary knee replacement with cement, *The Journal of bone and joint surgery. American volume*, **89**, 519-525.

Gardiner, A., *et al.* (2010) Osteotomies about the knee for tibiofemoral malalignment in the athletic patient, *The American journal of sports medicine*, **38**, 1038-1047.

Ghosh, R., *et al.* (2012) Experimental validation of finite element models of intact and implanted composite hemipelvises using digital image correlation, *Journal of biomechanical engineering*, **134**, 081003.

Gillies, R.M., *et al.* (2007) Adaptive bone remodelling of all polyethylene unicompartmental tibial bearings, *ANZ journal of surgery*, **77**, 69-72.

Grassi, L., *et al.* (2013) Experimental validation of finite element model for proximal composite femur using optical measurements, *Journal of the mechanical behavior of biomedical materials*, **21**, 86-94.

Gray, H.A., *et al.* (2008) Experimental validation of a finite element model of a human cadaveric tibia, *Journal of biomechanical engineering*, **130**, 031016.

Gray, H.A., Zavatsky, A.B. and Gill, H.S. (2010) The sclerotic line: why it appears under knee replacements (a study based on the Oxford knee), *Clinical biomechanics*, **25**, 242-247.

Gray, H.A., *et al.* (2007) Experimental validation of a finite element model of a composite tibia, *Proceedings of the Institution of Mechanical Engineers. Part H, Journal of engineering in medicine*, **221**, 315-324.

Gugenheim, J.J. and Brinker, M.R. (2003) Bone realignment with use of temporary external fixation for distal femoral valgus and varus deformities *The Journal of bone and joint surgery. American volume*, **85-A**, 1229-1237.

Gulati, A., *et al.* (2009) Localization of the full-thickness cartilage lesions in medial and lateral unicompartmental knee osteoarthritis, *Journal of orthopaedic research : official publication of the Orthopaedic Research Society*, **27**, 1339-1346.

Gulati, A., *et al.* (2009) The incidence of physiological radiolucency following Oxford unicompartmental knee replacement and its relationship to outcome, *The Journal of bone and joint surgery. British volume*, **91**, 896-902.

Haddad, F.S. and Bentley, G. (2000) Total knee arthroplasty after high tibial osteotomy: a medium-term review. , *The Journal of arthroplasty*, **15**, 597-603.

Hamilton, D.F., *et al.* (2013) What determines patient satisfaction with surgery? A prospective cohort study of 4709 patients following total joint replacement, *BMJ open*, **3**.

Hamilton, W.G., *et al.* (2006) Incidence and reasons for reoperation after minimally invasive unicompartmental knee arthroplasty, *The Journal of arthroplasty*, **21**, 98-107.

Harman, M.K., *et al.* (1998) Wear patterns on tibial plateaus from varus and valgus osteoarthritic knees, *Clinical orthopaedics and related research*, **352**, 149-158.

Heck, D.A., *et al.* (1993) Unicompartmental knee arthroplasty. A multicenter investigation with long-term follow-up evaluation, *Clinical orthopaedics and related research*, 154-159.

Hernandez-Vaquero, D., *et al.* (2005) Measurement of bone mineral density is possible with standard radiographs: a study involving total knee replacement, *Acta orthopaedica*, **76**, 791-795.

Hernigou, P., *et al.* (2008) retrieved unicompartmental implants with full PE tibial compaonent: the effects of knee alignment and polyethylene thickness on creep and wear, *Open Orthopaedics Journal*, **2**, 51-56.

Hill, P.F., *et al.* (2000) Tibiofemoral movement 2: the loaded and unloaded living knee studied by MRI, *The Journal of bone and joint surgery. British volume*, **82-B**, 1196-1198.

Hirasawa, Y., *et al.* (2002) Biomechanical monitoring of healing bone based on acoustic emission technology, *Clinical orthopaedics and related research*, **402**, 236-244.

Hoc, T., *et al.* (2006) Effect of microstructure on the mechanical properties of Haversian cortical bone, *Bone*, **38**, 466-474.

Holford, K.M., *et al.* (2009) Acoustic emission for monitoring aircraft structures, *Proceedings of the Institution of Mechanical Engineers, Part G: Journal of Aerospace Engineering*, **223**, 525-532.

Holliday, K.L., *et al.* (2011) Lifetime body mass index, other anthropometric measures of obesity and risk of knee or hip osteoarthritis in the GOAL case-control study., *Osteoarthritis & Cartilage*, **19**, 37-43.

Hollister, A.M., *et al.* (1993) The axes of rotation of the knee, *Clinical orthopaedics and related research*, 259-268.

Hooper, G.J., *et al.* (2013) The effect of the Oxford uncemented medial compartment arthroplasty on the bone mineral density and content of the proximal tibia, *The bone & joint journal*, **95-B**, 1480-1483.

Hooper, G.J., *et al.* (2012) The early radiological results of the uncemented Oxford medial compartment knee replacement, *The Journal of bone and joint surgery. British volume*, **94-B**, 334-338.

Hopkins, A.R., *et al.* (2010) Finite element analysis of unicompartmental knee arthroplasty, *Medical engineering & physics*, **32**, 14-21.

Hospital-Episode-Statistics. Finalised Patient Reported Outcome Measures (PROMs) in England: April 2009 – March 2010.

Howell, S.M., Howell, S.J. and Hull, M.L. (2010) Assessment of the radii of the medial and lateral femoral condyles in varus and valgus knees with osteoarthritis, *The Journal of bone and joint surgery. American volume*, **92**, 98-104.

Hsu, N.N. and Breckenridge, F.R. (1981) Characterization and Calibration of Acoustic Emission Sensors. , *Mater Eval*, **39**, 60-68.

Hurwitz, D.E., *et al.* (1998) Dynamic knee loads during gait predict proximal tibial bone distribution, *Journal of biomechanics*, **31**, 423-430.

Hvid, I. (1988) Trabecular bone strength at the knee, *Clinical orthopaedics and related research*, **227**, 210-221.

Insall, J., *et al.* (1976) Total condylar knee replacment: preliminary report, *Clinical orthopaedics and related research*, 149-154.

Insall, J., Tria, A.J. and Scott, W.N. (1979) The total condylar knee prosthesis: the first 5 years, *Clinical orthopaedics and related research*, 68-77.

Iwaki, H., Pinskerova, V. and Freeman, M.A.R. (2000) Tibiofemoral movement 1: the shapes and relative movements of the femur and tibia in the unloaded cadaver knee, *The Journal of bone and joint surgery. British volume*, **82-B**, 1189-1195.

Jenkins, P.J., *et al.* (2013) A micro-architectural evaluation of osteoporotic human femoral heads to guide implant placement in proximal femoral fractures, *Acta orthopaedica*, **84**, 453-459.

Jorgensen, U., *et al.* (1987) Long-term follow up of meniscectomy in athletes. A prospective longitudinal study, *The Journal of bone and joint surgery. British volume*, **69-B**, 80-83.

Jungmann, R., *et al.* (2011) Local strain and damage mapping in trabeculae during three-point bending tests., *Journal of the Mechanical Behaviour of Biomedical Materials*, **4**, 523-534.

Kapandli, I.A. (1970) *The Physiology of the Joints*. Churchill Livingstone, New York.

Kendrick, B.J., *et al.* (2012) Histology of the bone-cement interface in retrieved Oxford unicompartmental knee replacements, *The Knee*, **19**, 918-922.

Kendrick, B.J., *et al.* (2011) Polyethylene wear of mobile-bearing unicompartmental knee replacement at 20 years, *The Journal of bone and joint surgery. British volume*, **93**, 470-475.

Kerens, B., *et al.* (2013) Revision from unicompartmental to total knee replacement: the clinical outcome depends on reason for revision, *The bone & joint journal*, **95-B**, 1204-1208.

Khan, F.A., *et al.* (2008) Effect of local alignment on compartmental patterns of knee osteoarthritis, *The Journal of bone and joint surgery. American volume*, **90**, 1961-1969.

Korhonena, R.K., *et al.* (2002) Comparison of the equilibrium response of articular cartilage in unconfined compression, confined compression and indentation., *Journal of biomechanics*, **35**, 903-909.

Kuster, M.S., *et al.* (1997) Joint load considerations in total knee replacement, *The Journal of bone and joint surgery. British volume*, **79**, 109-113.

Kutzner, I., *et al.* (2010) Loading of the knee joint during activities of daily living measured in vivo in five subjects, *Journal of biomechanics*, **43**, 2164-2173.

Kwon, O.R., *et al.* (2014) Biomechanical comparison of fixed- and mobile-bearing for unicomparmental knee arthroplasty using finite element analysis, *Journal of orthopaedic research : official publication of the Orthopaedic Research Society*, **32**, 338-345.

Lanyon, L.E. (1993) Osteocytes, strain detection, bone modeling and remodeling, *Calcified tissue international*, **53 Suppl 1**, S102-106; discussion S106-107.

Leung, S.Y., New, A.M. and Browne, M. (2009) The use of complementary non-destructive evaluation methods to evaluate the integrity of the cement-bone interface, *Proceedings of the Institution of Mechanical Engineers. Part H, Journal of engineering in medicine*, **223**, 75-86.

Lewis, P.L., Brewster, N.T. and Graves, S.E. (1998) The pathogensis of bone loss following total knee arthroplasty, *Orthop Clini North Am*, **29**, 187-197.

Lewold, S., *et al.* (1998) Revision of unicompartmental knee replacement. Outcome in 1,135 cases from the Swedish Knee Arthroplasty study, *Acta Orthop Scand*, **69**, 469-474.

Li, M.G. and Nilsson, K.G. (2000) The effect of the preoperative bone quality on the fixation of the tibial component in total knee arthroplasty, *The Journal of arthroplasty*, **15**, 744-753.

Li, M.G., *et al.* (2006) Mobile vs. fixed bearing unicondylar knee arthroplasty: A randomized study on short term clinical outcomes and knee kinematics, *The Knee*, **13**, 365-370.

Lonner, J.H., *et al.* (2001) Changes in bone density after cemented total knee arthroplasty: influence of stem design, *The Journal of arthroplasty*, **16**, 107-111.

Mancuso, C.A., *et al.* (2001) Patients' expectations of knee surgery, *The Journal of bone and joint surgery. American volume*, **83-A**, 1005-1012.

Mariani, E.M., *et al.* (2007) Early failure of unicompartmental knee arthroplasty, *The Journal of arthroplasty*, **22**, 81-84.

Marti, R.K., *et al.* (2001) Proximal tibial varus osteotomy: indications, technique and five to twenty-one year results, *The Journal of bone and joint surgery. American volume*, **83-A**, 164-170.

Matsuda, S., *et al.* (2004) Anatomical analysis of the femoral condyle in normal and osteoarthritic knees, *Journal of Orthopaedic Research*, **22**, 104-109.

Mavrogordato, M., *et al.* (2011) Real time monitoring of progressive damage during loading of a simplified total hip stem construct using embedded acoustic emission sensors, *Medical engineering & physics*, **33**, 395-406.

McAlindon, T.E., *et al.* (1996) Are risk factors for patellofemoral and tibiofemoral knee osteoarthritis different?, *J Rheumatol*, **23**, 332-337.

Moerman, K.M., *et al.* (2009) Digital image correlation and finite element modelling as a method to determine mechanical properties of human soft tissue in vivo, *Journal of biomechanics*, **42**, 1150-1153.

Morrison, J.B. (1970) The mechanics of the knee joint in relation to normal walking, *Journal of biomechanics*, **3**, 51-61.

Murase, K., *et al.* (1983) An analysis of tibial component design in total knee arthroplasty, *Journal of biomechanics*, **16**, 13-22.

Murray, D.W., *et al.* (2007) The use of the Oxford hip and knee scores, *The Journal of bone and joint surgery. British volume*, **89**, 1010-1014.

Nakagawa, S., *et al.* (2000) Tibiofemoral movement 3: full flexion in the living knee studied by MRI, *The Journal of bone and joint surgery. British volume*, **82-B**, 1199-1200.

Nalla, R.K., *et al.* (2005) Fracture in human cortical bone: local fracture criteria and toughening mechanisms, *Journal of biomechanics*, **38**, 1517-1525.

Newman, J., Pydisetty, R.V. and Ackroyd, C. (2009) Unicompartmental or total knee replacement: the 15-year results of a prospective randomised controlled trial, *The Journal of bone and joint surgery. British volume*, **91-B**, 52-57.

Nicholls, P.J. and Berg, E. (1981) Acoustic emission properties of callus, *Medical & biological engineering & computing*, **19**, 416-418.

Nicolella, D.P., *et al.* (2005) Measurement of microstructural strain in cortical bone, *Eur J Morphol*, **42**, 23-29.

NJR (2012) NJR of England and Wales: 9th Annual Report. In Wales, N.E.a. (ed).

Noble, P.C., *et al.* (2005) Does total knee replacement restore normal knee function?, *Clinical orthopaedics and related research*, 157-165.

None-Listed (2012) Nondestructive Testing Resource Centre: Acoustic Emission. NDT Centre.

Nordin, M. and Frankel, V.H. (2001) *Basic Biomechanics of the Musculoskeletal System*. Lippincott Williams and Wilkins, London.

Norwegian (2010) Annual Report of the Norwegian Arthroplasty Register.

Paley, D. (2002) Chapter 1: Normal limb alignment and joint orientation. In Herzenberg, J.E. (ed), *Principles of Deformity Correction*. Springer, New York, pp. 1-17.

Pandit, H., *et al.* (2010) Minimally invasive Oxford phase 3 unicompartmental knee replacement: results of 1000 cases., *The Journal of bone and joint surgery. British volume*, **93-B**, 198-204.

Pankaj, P. (2013) Patient-specific modelling of bone and bone-implant systems: the challenges, *International journal for numerical methods in biomedical engineering*, **29**, 233-249.

Pankaj, P. and Donaldson, F.E. (2013) Algorithms for a strain-based plasticity criterion for bone, *International journal for numerical methods in biomedical engineering*, **29**, 40-61.

Pearse, A.J., *et al.* (2010) Survival and functional outcome after revision of a unicompartmental to a total knee replacement: the New Zealand National Joint Registry, *The Journal of bone and joint surgery. British volume*, **92**, 508-512.

Pegg, E.C., *et al.* (2013) Evaluation of factors affecting tibial bone strain after unicompartmental knee replacement, *Journal of orthopaedic research : official publication of the Orthopaedic Research Society*, **31**, 821-828.

Pena, E., *et al.* (2006) Why lateral meniscectomy is more dangerous than medial meniscectomy. A finite element study, *Journal of orthopaedic research : official publication of the Orthopaedic Research Society*, **24**, 1001-1010.

Petrie, A. (2006) Statistics in orthopaedic papers, *The Journal of bone and joint surgery. British volume*, **88-B**, 1121-1136.

Prendergast, P.J. and Huiskes, R. (1996) Microdamage and osteocyte-lacuna strain in bone: a microstructural finite element analysis, *Journal of biomechanical engineering*, **118**, 240-246.

Qi, G., Pujol, J. and Fan, Z. (2000) 3-D AE visualization of bone-cement fatigue locations, *J Biomed Mater Res*, **52**, 256-260.

Rawlinson, J.J., *et al.* (2008) Stemmed implants improve stability in augmented constrained condylar knees, *Clinical orthopaedics and related research*, **466**, 2639-2643.

Reilly, D., *et al.* (1982) Effects of tibial components on load transfer in the upper tibia, *Clinical orthopaedics and related research*, 273-282.

Reilly, G.C. (2000) Observations of microdamage around osteocyte lacunae in bone, *Journal of biomechanics*, **33**, 1131-1134.

Richmond, B.I., *et al.* (2013) Proximal Tibial Bone Density Is Preserved After Unicompartmental Knee Arthroplasty, *Clinical orthopaedics and related research*.

Roques, A. (2004) Investigation of fatigue crack growth in acrylic bone cement using the acoustic emission technique, *Biomaterials*, **25**, 769-778.

Rowland, C., Browne, M. and Taylor, A. (2004) Dynamic health monitoring of metal on metal hip prostheses using acoustic emission., *26th European conference on acoustic emission*.

Saenz, C.L., *et al.* (2010) Early failure of a unicompartmental knee arthroplasty design with an all-polyethylene tibial component, *The Knee*, **17**, 53-56.

Sarmah, S.S., *et al.* (2012) The radiological assessment of total and unicompartmental knee replacements, *The Journal of bone and joint surgery. British volume*, **94-B**, 1321-1329.

Sawatari, T., *et al.* (2005) Three-dimensional finite element analysis of unicompartmental knee arthroplasty--the influence of tibial component inclination, *Journal of orthopaedic research : official publication of the Orthopaedic Research Society*, **23**, 549-554.

Schaffler, M.B., Choi, K. and Milgrom, C. (1995) Aging and matrix microdamage accumulation in human compact bone, *Bone*, **17**, 521-525.

Scott, C.E. and Biant, L.C. (2012) The role of the design of tibial components and stems in knee replacement, *The Journal of bone and joint surgery. British volume*, **94**, 1009-1015.

Scott, C.E., *et al.* (2012) Patient expectations of arthroplasty of the hip and knee, *The Journal of bone and joint surgery. British volume*, **94**, 974-981.

Scott, C.E., *et al.* (2014) Five-year survivorship and patient-reported outcome of the Triathlon single-radius total knee arthroplasty, *Knee surgery, sports traumatology, arthroscopy : official journal of the ESSKA*.

Scott, C.E.H., *et al.* (2010) Predicting dissatisfaction following total knee replacement: a prospective study of 1217 patients, *The Journal of bone and joint surgery. British volume*, **92-B**, 1253-1258.

Scott, R.D. (2005) Lateral unicompartmental replacement: a road less traveled., *Orthopedics*, **28**, 983-984.

Servien, E., *et al.* (2008) Lateral versus medial tibial plateau: morphometric analysis and adaptability with current tibial component design, *Knee surgery, sports traumatology, arthroscopy : official journal of the ESSKA*, **16**, 1141-1145.

Sharma, L., *et al.* (2001) The role of knee alignment in disease progression and functional decline in knee osteoarthritis, *JAMA*, **286**, 188-195.

Simpson, D.J., *et al.* (2008) The effect of bearing congruency, thickness and alignment on the stresses in unicompartmental knee replacements, *Clinical biomechanics*, **23**, 1148-1157.

Simpson, D.J., *et al.* (2011) Load transfer in the proximal tibia following implantation with a unicompartmental knee replacement: a static snapshot, *Proceedings of the Institution of Mechanical Engineers, Part H: Journal of Engineering in Medicine*, **225**, 521-529.

Simpson, D.J., *et al.* (2009) Elevated proximal tibial strains following unicompartmental knee replacement--a possible cause of pain, *Medical engineering & physics*, **31**, 752-757.

Small, S.R., *et al.* (2011) Metal backing significantly decreases tibial strains in a medial unicompartmental knee arthroplasty model, *The Journal of arthroplasty*, **26**, 777-782.

Small, S.R., *et al.* (2013) Changes in tibial bone density measured from standard radiographs in cemented and uncemented total knee replacements after ten years' follow-up, *Bone & Joint Journal*, **95-B**, 911-916.

Soininvaara, T.A., *et al.* (2013) Periprosthetic bone mineral density changes after unicondylar knee arthroplasty, *The Knee*, **20**, 120-127.

Squire, M.W., *et al.* (1999) Unicompartmental knee replacement. A minimum 15 year followup study., *Clinical orthopaedics and related research*, **367**, 61.

Steele, R.G., *et al.* (2006) Survivorship of the St Georg Sled medial unicompartmental knee replacement beyond ten years, *The Journal of bone and joint surgery. British volume*, **88**, 1164-1168.

Svärd, U.C.G. and Price, A.J. (2001) Oxford medial unicompartmental knee arthroplasty: A SURVIVAL ANALYSIS OF AN INDEPENDENT SERIES, *Journal of Bone & Joint Surgery, British Volume*, **83-B**, 191-194.

Swedish (2011) The Swedish Knee Arthroplasty Register Annual Report 2011.

Sztefek, P., *et al.* (2010) Using digital image correlation to determine bone surface strains during loading and after adaptation of the mouse tibia, *Journal of biomechanics*, **43**, 599-605.

Taddei, P., *et al.* (2011) Mobile or fixed unicompartmental knee prostheses? In-vitro wear assessments to solve this dilemma, *Journal of the mechanical behavior of biomedical materials*, **4**, 1936-1946.

Terrier, A., *et al.* (2014) Development and experimental validation of a finite element model of total ankle replacement, *Journal of biomechanics*, **47**, 742-745.

Tuncer, M., *et al.* (2013) Validation of multiple subject-specific finite element models of unicompartmental knee replacement, *Medical engineering & physics*, **35**, 1457-1464.

Walker, P.S. and Erkman, M.J. (1975) The role of the menisci in force transmission across the knee, *Clinical orthopaedics and related research*, **109**, 184-192.

Weidow, J. (2006) Lateral osteoarthritis of the knee, *Acta orthopaedica*, **77**, 2-44.

Weidow, J., Mars, I. and Karrholm, J. (2005) Medial and lateral osteoarthritis of the knee is related to variations of hip and pelvic anatomy, *Osteoarthritis and cartilage / OARS, Osteoarthritis Research Society*, **13**, 471-477.

Weidow, J., *et al.* (2006) Hip and knee joint rotations differ between patients with medial and lateral knee osteoarthritis: gait analysis of 30 patients and 15 controls, *Journal of orthopaedic research : official publication of the Orthopaedic Research Society*, **24**, 1890-1899.

Wells, J.G. and Rawlings, R.D. (1985) Acoustic emission and mechanical properties of trabecular bone, *Biomaterials*, **6**, 218-224.

Whittaker, J.P., *et al.* (2010) Does bearing design influence midterm survivorship of unicompartmental arthroplasty?, *Clinical orthopaedics and related research*, **468**, 73-81.

Wise, B.L., *et al.* (2012) Patterns of compartment involvement in tibiofemoral osteoarthritis in men and women and in whites and African Americans, *Arthritis Care Res (Hoboken)*, **64**, 847-852.

Wolf, f.J. (1892) Das Gesetz der Transformation der Knochen.

Yang, N., *et al.* (2010) Effect of frontal plane tibiofemoral angle on the stress and strain at the knee cartilage during the stance phase of gait, *Journal of orthopaedic research : official publication of the Orthopaedic Research Society*, **28**, 1539-1547.

Yang, N.H., *et al.* (2010) Effect of frontal plane tibiofemoral angle on the stress and strain at the knee cartilage during the stance phase of gait, *Journal of orthopaedic research : official publication of the Orthopaedic Research Society*, **28**, 1539-1547.

You, J., *et al.* (2000) Substrate deformation levels associated with routine physical activity are less stimulatory to bone cells relative to loading-induced oscillatory fluid flow, *Journal of biomechanical engineering*, **122**, 387-393.

Yusuf, E., *et al.* (2011) Body mass index and alignment and their interaction as risk factors for progression of knees with radiographic signs of osteoarthritis, *Osteoarthritis and cartilage / OARS, Osteoarthritis Research Society*, **19**, 1117-1122.

Zealand, N. (2010) New Zealand Orthopaedic Association: the New Zealand Joint Registry twelve year report.

Zhao, D., *et al.* (2007) In vivo medial and lateral tibial loads during dynamic and high flexion activities, *Journal of orthopaedic research : official publication of the Orthopaedic Research Society*, **25**, 593-602.

Appendices

1. List of published papers, presentations and prizes related to this work
2. CAD design drawings
3. Reprints of published papers based on this work

7.3 Appendix 1 - Publications

Published Papers

1. **Scott CEH**, Wade FA, Bhattacharya R, MacDonald DJ, Pankaj P, Nutton RW. Changes in bone density in metal backed and all-polyethylene medial unicompartmental knee arthroplasty. *Journal of Arthroplasty* 2015: http://dx.doi.org/10.1016/j.arth.2015.09.046.
2. **Scott CEH**, Eaton MJ, Nutton RW, Wade FA, Pankaj P, Evans SL. Proximal Tibial Strain in Medial Unicompartmental Knee Replacements: A biomechanical study of implant design. *Bone Joint J* 2013; 95-B(10): 1339-47

Oral Presentations

1. Metal Backed *Vs* All-Polyethylene UKA: the effect of implant thickness on tibial bone strain in a validated finite element model. **British Association for Surgery of the Knee (BASK), *Liverpool, UK, March 2016***
2. Proximal tibial strain in medial unicompartmental knee replacements: a biomechanical study of implant design. **British Orthopaedic Association (BOA), *Birmingham, UK, October 2013***
3. Proximal tibial strain in medial unicompartmental knee replacements: a biomechanical study of implant design. **British Association for Surgery of the Knee (BASK), *Leeds, UK, March 2013***
4. A year as the BASK Research Fellow. **British Association for Surgery of the Knee (BASK), *Leeds, UK, March 2013***
5. Proximal tibial strain in medial unicompartmental knee replacements: a radiographic and clinical outcome study of implant design. **British Association for Surgery of the Knee (BASK), *Leeds, UK, March 2013***
6. Subchondral Sclerosis in a Medial Unicompartmental Knee Replacement with an All-Polyethylene Tibial Component: A Cause of "Unexplained Pain" and a New Mode of Failure? **European Federation of Orthopaedics and Traumatology (EFORT), *Copenhagen, Denmark, June 2011***

Poster Presentations

1. Validated finite element analysis of metal backed versus all-polyethylene unicompartmental knee arthroplasty: the effect of implant thickness on proximal tibial strain. **Orthopaedic Research Society (ORS), *Orlando, USA, March 2015***

2. Survivorship and patient satisfaction of a fixed bearing unicompartmental knee replacement incorporating an all polyethylene tibia component. **British Association for Surgery of the Knee (BASK), *Cardiff, UK, March 2011***

Prizes

1. **1st Prize for Oral Presentation, Scottish Committee for Orthopaedics and Trauma (SCOT) Winter Meeting.** Metal Backed *Vs* All-Polyethylene UKA: the effect of implant thickness on tibial bone strain in a validated finite element model. ***Crieff, December 2015***
2. **1st Prize for Oral Presentation Institution of Mechanical Engineers (IMechE) Best Medical Engineering Project (Vicon prize).** Proximal Tibial Strain in Medial Unicompartmental Knee Replacements: A biomechanical study of implant design. ***London, February 2013***

7.4 Appendix 2 – CAD Design Drawings

Please see over page.

7.5 Appendix 3 – Published Papers

Please see over page.